



**COMPARATIVE ANALYSIS OF TWO-STAGE-TO-ORBIT
ROCKET AND AIRBREATHING REUSABLE LAUNCH VEHICLES
FOR MILITARY APPLICATIONS**

THESIS

Joseph M. Hank, Captain, USAF

AFIT/GAE/ENY/06-M12

**DEPARTMENT OF THE AIR FORCE
AIR UNIVERSITY**

AIR FORCE INSTITUTE OF TECHNOLOGY

Wright-Patterson Air Force Base, Ohio

APPROVED FOR PUBLIC RELEASE; DISTRIBUTION UNLIMITED

The views expressed in this thesis are those of the author and do not reflect the official policy or position of the United States Air Force, Department of Defense, or the U.S. Government.

AFIT/GAE/ENY/06-M12

**COMPARATIVE ANALYSIS OF TWO-STAGE-TO-ORBIT
ROCKET AND AIRBREATHING REUSABLE LAUNCH VEHICLES
FOR MILITARY APPLICATIONS**

THESIS

Presented to the Faculty

Department of Aeronautics and Astronautics

Graduate School of Engineering and Management

Air Force Institute of Technology

Air University

Air Education and Training Command

In Partial Fulfillment of the Requirements for the
Degree of Master of Science in Aeronautical Engineering

Joseph M. Hank, BS

Captain, USAF

March 2006

APPROVED FOR PUBLIC RELEASE; DISTRIBUTION UNLIMITED

**COMPARATIVE ANALYSIS OF TWO-STAGE-TO-ORBIT
ROCKET AND AIRBREATHING REUSABLE LAUNCH VEHICLES
FOR MILITARY APPLICATIONS**

Joseph M. Hank, BS

Captain, USAF

Approved:

//SIGNED//
Milton E. Franke (Chairman)

15 Mar 06
Date

//SIGNED//
Ralph A. Anthenien (Member)

14 Mar 06
Date

//SIGNED//
Paul I. King (Member)

14 Mar 06
Date

Abstract

The Department of Defense (DoD) has identified operationally responsive, low-cost access to space as vital to maintaining U.S. military supremacy. Reusable Launch Vehicles (RLVs) will allow the U.S. to keep a technological advantage over our adversaries, and many designs for RLVs have been proposed over the years. In addition, advances in airbreathing propulsion technology have made it feasible for use in space launch vehicles. Using airbreathing propulsion in RLVs has three distinct advantages: better launch, flight, and ground operability than rockets; lower sensitivity to weight growth than rockets; and the potential for large advancements in airbreathing technology when compared to the mature state of rocket technology. This study considers two-stage-to-orbit (TSTO) RLV configurations, each using combinations of propulsion including pure rocket, pure turbine, rocket-based-combined-cycle (RBCC), and turbine-based-combined-cycle (TBCC) for the both stages. The primary figures of merit are vehicle empty mass and vehicle wetted area. Empty mass is an indicator of development and acquisitions cost, and wetted area relates primarily to thermal protection system (TPS) maintenance costs. This study explores the advantages of airbreathing propulsion in those key areas when compared to a baseline configuration. Results show that a vehicle using airbreathing propulsion on the orbiter stage has a lower vehicle empty mass and wetted area than a pure rocket, and allows the RLV to gain the advantages of using airbreathing propulsion. It also has the smallest growth rate with increasing payload. The requirements used for this comparison are: 1) a payload module requirement of 20,000 pounds; 2) a 100x100 nautical mile, 28.5 lat. Easterly orbit and return; 3) use of hydrocarbon fuels (RP-1 and/or JP-7) and liquid hydrogen (LH₂); and 4) use of liquid oxygen and/or air as oxidizers. ASTROX Corporation's Hypersonic System Integrated Design Environment (HySIDE) code is used as the design tool throughout the study.

AFIT/GAE/ENY/06-M12

*To my grandmothers
and my parents*

Acknowledgments

I would like to express my sincere appreciation to my faculty advisor, Dr. Milton Franke, and my sponsors from the Air Force Research Laboratory, Dr. Dean Eklund and Lt Col Doug Decker, for their guidance and support throughout the course of this thesis effort. Their insight and experience were very much appreciated, and their guidance was critical to allowing me to complete this work.

I would also like to thank ASTROX Corporation, particularly Dr. Ajay P. Kothari and V. Raghavan, for their assistance with HySIDE. Their design tool proved invaluable to this study, and their willingness to help me and provide software support made it possible for me to accomplish much more than I imagined possible. I am especially grateful since they provided the program code and went out of their way to answer any questions I had at no expense.

My thanks also go to John Livingston, who was always available to answer questions I had and provide guidance during the course of my study. His vast knowledge in the field of hypersonics is unmatched, and more reliable than any textbook. I hope someday to learn half as much as he knows, and be as willing as he is to share it with others.

I would also like to thank my parents for their support throughout my life and during my time here at AFIT. Without them, I would not be the man I am today, and I am eternally grateful.

Finally, I am grateful to God, through whom all things are possible.

Joe

Table of Contents

	<u>Page</u>
Abstract	iv
Acknowledgments.....	vi
List of Figures	x
List of Tables	xiv
List of Symbols, Subscripts, and Acronyms	xvi
1. Introduction.....	1
1.1 Motivation	1
1.2 Research Objectives	3
1.3 Research Focus	3
1.4 Methodology Overview.....	5
1.5 Assumptions/Limitations.....	5
1.6 Thesis Overview	6
2. Literature Review.....	7
2.1 Reusable Launch Vehicle Background	7
2.2 RLV Basic Design Options	13
2.3 Reusable Launch Vehicle Basic Propulsion Options	15
2.4 Airbreathing Propulsion in Reusable Launch Vehicles.....	21
2.5 Reusable Launch Vehicle Advanced Propulsion Options	24
2.6 Recent Reusable Launch Vehicle Research	26
2.7 Summary.....	30
3. Methodology	31
3.1 TSTO RLV Configurations	32

	<u>Page</u>
3.2 Flight Fundamentals	38
3.3 RLV Design Methodology	42
3.4 Design Assumptions	56
3.5 Mission Descriptions	86
4. Analysis and Results	96
4.1 Baseline RLV Results.....	100
4.2 Payload Sizing Impact Study Results.....	115
4.3 Orbital Rendezvous RLV Results	121
4.4 Global Strike HLV Results.....	135
4.5 Summary.....	146
5. Conclusions and Recommendations	148
5.1 Conclusions and Recommended RLV Configurations.....	148
5.2 Recommendations for Future Research.....	153
5.3 Summary.....	153
Appendix A. Airbreathing Engine Performance Data	155
Appendix B. HySIDE System Element Description.....	157
Appendix C. HySIDE Design Inputs	181
Appendix D. Flyback Lift over Drag Calculations	187
Appendix E. Flyout Lift over Drag Calculations.....	189
Appendix F. Baseline Vehicle Summary	190
Appendix G. Baseline Vehicle Results.....	196
Appendix H. Payload Sizing Impact Study Results.....	200
Appendix I. Orbital Rendezvous Results.....	218
Appendix J. Global Strike Results	222
Bibliography	226

	<u>Page</u>
Vita	231

List of Figures

<u>Figure</u>	<u>Page</u>
Figure 1. Aerojet Corporation's Dyna-Soar concept.....	8
Figure 2. Space Shuttle at liftoff.....	9
Figure 3. National Aerospace Plane concept	11
Figure 4. Artist's rendition of the Hyper-X.....	12
Figure 5. Diagram of liquid- and solid-propellant rocket engines.....	16
Figure 6. Diagram of a turbine engine	18
Figure 7. Diagram of a ramjet engine	19
Figure 8. Diagram of a scramjet engine.....	20
Figure 9. X-51 vehicle with HyTech scramjet engine demonstrator	20
Figure 10. Specific impulse versus Mach number for rocket and airbreathing propulsion	21
Figure 11. Combined-cycle engine flight profile using airbreathing propulsion.....	24
Figure 12. Diagram of vehicle using RBCC propulsion.....	25
Figure 13. Diagram of vehicle using TBCC propulsion	26
Figure 14. Airbreathing vehicle inlet geometry types	30
Figure 15. Thesis model propulsion options overview	33
Figure 16. Basic vehicle propulsion stage types.....	34
Figure 17. Thesis model fueling and takeoff options overview.....	35
Figure 18. Thesis model stages, fuel types, and takeoff types.....	36

	<u>Page</u>
Figure 19. Diagram of vehicle forces	38
Figure 20. Example block diagram of a HySIDE model	43
Figure 21. Example input/output tree of a HySIDE model	43
Figure 22. Diagram of a HySIDE reusable rocket vehicle (hydrocarbon)	47
Figure 23. Diagram of a HySIDE reusable airbreathing vehicle	49
Figure 24. DMSJ I_{sp} variation with Mach number for different fuels	62
Figure 25. DMSJ cutoff EI_{sp} based on Bulk Density Ratio of propellants	64
Figure 26. Drag polar showing flight conditions for maximum Lift-to-Drag Ratio.....	68
Figure 27. Side view of rocket RLV flyback trajectory.....	74
Figure 28. Booster altitude and downrange distance at staging point	76
Figure 29. Top view of airbreathing RLV flyback trajectory	77
Figure 30. Heat transfer rates for vehicle inlet geometry	80
Figure 31. EI_{sp} comparison of 2-D and inward turning vehicles	80
Figure 32. Typical hypersonic vehicle lift-over-drag profile.....	93
Figure 33. Initial velocity required for ballistic range	95
Figure 34. Baseline configuration RLV ascent trajectories	97
Figure 35. Example of how result are presented in this study	99
Figure 36. VTHL baseline vehicle mass comparison	102
Figure 37. Vehicle EI_{sp} comparison between HCRBCC-HCRkt and HCRBCC-HRkt.	105
Figure 38. Vehicle mass change of HCRkt-HCRBCC and HCRkt-HRBCC during ascent	106
Figure 39. VTHL baseline vehicle area comparison	108

	<u>Page</u>
Figure 40. Hydrocarbon Rocket-Hydrocarbon RBCC (HCRkt-HCRBCC Vehicle).....	109
Figure 41. HTHL baseline vehicle mass comparison	111
Figure 42. HTHL baseline vehicle area comparison	113
Figure 43. Hydrocarbon Turbine-Hydrogen RBCC (HCTurb-HRBCC Vehicle)	114
Figure 44. Payload sizing impact study RLV empty mass and wetted area growth rates	118
Figure 45. Number of orbital intercepts with a 1,000 nm (1,852 km) cruise range	128
Figure 46. VTHL orbital rendezvous vehicle mass comparison.....	129
Figure 47. VTHL orbital rendezvous vehicle area comparison.....	131
Figure 48. HTHL orbital rendezvous vehicle mass comparison.....	132
Figure 49. HTHL orbital rendezvous vehicle area comparison.....	134
Figure 50. VTHL global strike vehicle mass comparison	138
Figure 51. Mass breakdown of reusable and expendable stage	140
Figure 52. VTHL global strike vehicle area comparison.....	141
Figure 53. Hydrocarbon rocket-hydrocarbon rocket (HCRkt-HCRkt) global strike vehicle	142
Figure 54. HTHL global strike vehicle mass comparison	143
Figure 55. HTHL global strike vehicle area comparison.....	145
Figure 56. Hydrocarbon Turbine-Hydrocarbon Rocket (HCTurb-HCRkt) global strike vehicle	146
Figure 57. Block diagram and input/output tree of "FreeStream" system element	158
Figure 58. Block diagram and input/output tree of "Rocket" system element	159

	<u>Page</u>
Figure 59. Input/Output tree of "EngineCluster" system element	161
Figure 60. HySIDE reusable rocket vehicle (hydrocarbon).....	165
Figure 61. Block diagram and input/output tree of "HADOVehicleBasic" system element	166
Figure 62. HySIDE reusable airbreathing vehicle	167
Figure 63. Radial Deviation Parameter (RDP) effect	168
Figure 64. Airbreathing vehicle showing placement of a single turbine engine	173
Figure 65. Block diagram and input/output tree of "FixedWeights" system element ...	174
Figure 66. Block diagram and input/output tree of "PropellantUsage" system element	175
Figure 67. Block diagram and input/output tree of "Trajectory" system element	178

List of Tables

<u>Table</u>	<u>Page</u>
Table 1. Properties of rocket fuel.....	15
Table 2. HySIDE “Velocity versus I_{sp} ” table for AFRL turbine accelerator.....	57
Table 3. HySIDE "Velocity versus I_{sp} " table for AFRL HyTech hydrocarbon DMSJ....	59
Table 4. Nominal rocket engine parameters	60
Table 5. Bulk density of rocket and DMSJ propellants	63
Table 6. DMSJ cutoff EI_{sp} for different propellants.....	64
Table 7. Staging velocities and propulsion velocity ranges.....	65
Table 8. Wing sizing inputs	66
Table 9. Best L/D and velocity for flyback.....	71
Table 10. Vehicle ranges and weight fractions.....	78
Table 11. Empty mass comparison of 2-D and inward-turning vehicles.....	81
Table 12. K-factor adjustment	83
Table 13. RLV study empty mass comparison	84
Table 14. Best vehicle range factors for flyout.....	93
Table 15. Baseline RLV empty masses and wetted areas.....	101
Table 16. Payload sizing impact study RLV empty mass and wetted area growth rates	116
Table 17. Orbital Rendezvous RLV empty masses and wetted areas.....	123
Table 18. Payload mass comparisons	124

	<u>Page</u>
Table 19. Vehicle size comparisons.....	125
Table 20. Orbital rendezvous RLV increase in empty mass and wetted area versus baseline RLV.....	135
Table 21. Global strike HLV empty masses and wetted areas	136
Table 22. Rocket wing airfoil characteristics	160

List of Symbols, Subscripts, and Acronyms

<u>Symbol</u>	<u>Description</u>
A_e	Rocket nozzle exit area, ft ² (m ²)
AR	Aspect ratio
BDR	Bulk Density Ratio
BPR	Bypass Ratio
C_D	Drag coefficient
C_{D0}	Zero lift drag coefficient (parasite drag coefficient)
C_f	Flat-plate friction coefficient
C_L	Lift coefficient
c_r	Wing root chord, ft (m)
D	Drag, lbf (N)
d	Vehicle flyback distance, nm (km)
e	Wing Oswald efficiency factor
EI_{sp}	Effective Specific Impulse, sec
g	Local acceleration due to gravity, ft/s ² (m/s ²)
g_0	Standard sea level acceleration due to gravity, 32.16 ft/s ² (9.81 m/s ²)
G_{loss}	Gravity losses, lbf (N)
$GTOM$	Gross takeoff mass, lbm (kg)
$GTOW$	Gross takeoff weight, lbf (N)

H	Height, ft (m)
I_{sp}	Specific Impulse, sec
K	Drag polar parabolic shape factor
$k_{overall}$	HySIDE overall design uncertainty factor
L	Lift, lbf (N); Reynolds number characteristic length, ft (m)
M	Mass, lbm (kg); Mach number
\dot{m}	Mass flow rate, lbm/s (kg/s)
MAC	Mean aerodynamic chord, ft (m)
n	Load factor
P_e	Rocket nozzle exit pressure, psi (Pa)
P_o	Ambient atmospheric pressure, psi (Pa)
q	Dynamic pressure, $\frac{1}{2} \cdot \rho \cdot V^2$, psi (Pa)
R	Radius, ft (m); Breguet range, nm (km)
Re	Reynolds number, $\frac{\rho \cdot V \cdot L}{\mu}$
S_{ref}	Wing trapezoidal reference planform area, ft ² (m ²)
S_{wet}	Vehicle wetted area, ft ² (m ²)
SFC	Specific fuel consumption, lbm/lbf sec (mg/N sec)
t	Time, sec
T	Thrust, lbf (N)
V	Velocity, ft/s (m/s)
V_e	Propellant exhaust velocity, ft/s (m/s)

V_{eq}	Equivalent exhaust velocity, ft/s (m/s)
W	Weight, lbf (N)
y_o	Initial height for parabolic trajectory, nm (km)
α	Angle of attack, deg
ΔV	Change in velocity (delta-V), ft/s (m/s)
γ	Ballistic range factor
λ	Taper ratio
Λ_{LE}	Leading edge sweep angle, deg
μ	Fluid viscosity, lbf sec/ft ² (N sec/m ²); gravitational parameter, 3.986x10 ⁵ km ³ /sec ² (1.407x10 ¹⁶ ft ³ /sec ²)
η	Propellant tank construction efficiency factor
ϕ	Equivalence ratio; bank angle, deg
ρ	Density, lbm/ft ³ (kg/m ³)
σ	Stress, psi (N/m ²)
θ	Angle of rocket vehicle at staging point, deg
ω	Angular velocity, deg/s

Subscript

Description

a	Air
$base$	Base (rear-facing vehicle surface)
$config$	Configuration factor

<i>correl</i>	Correlation factor
<i>cruise</i>	Condition for best cruising range
<i>DP</i>	Design point
<i>e</i>	Exit
<i>Earth</i>	Value relating to the earth
<i>f</i>	Fuel; Final
<i>flyback</i>	Flight back to landing location
<i>i</i>	Inlet; Initial
<i>installed</i>	Value after installation in vehicle
<i>max</i>	Maximum
<i>overall</i>	Applying to whole vehicle
<i>p</i>	Propellant (fuel and oxidizer)
<i>ref</i>	Reference value
<i>Rkt</i>	Rocket
<i>table</i>	Value from a look-up table
<i>tank</i>	Propellant tank
<i>TO</i>	Takeoff
<i>turn</i>	Value relating to RLV turn
<i>uninstalled</i>	Value before installation in vehicle

Acronym

Description

AFRL/PR	Air Force Research Laboratory, Propulsion Directorate
---------	---

AFRL/VA	Air Force Research Laboratory, Air Vehicles Directorate
ASC/XRE	Aeronautical Systems Center, Aerospace Systems Design and Analysis
CAV	Combat aerial vehicle
CG	Center of Gravity
CP	Center of Pressure
DMSJ	Dual-mode scramjet
DoD	Department of Defense
EELV	Evolved Expendable Launch Vehicle, Delta IV and Atlas V
GEO	Geosynchronous earth orbit
H(<i>stage</i>)	Liquid hydrogen-fueled stage
HC(<i>stage</i>)	Liquid hydrocarbon-fueled stage
HADO	Hypersonic Airbreathing Design Optimization
HAVDAC	Hypersonic ASTROX Vehicle Design and Analysis Code
HLV	Hybrid Launch Vehicle
HTHL	Horizontal takeoff, horizontal landing
HySIDE	Hypersonic System Integrated Design Environment
HySTP	Hypersonic Systems Technology Program
HyTech	Hypersonic Technology program
JP-7	Jet Propellant-7, a liquid hydrocarbon fuel
LH ₂	Liquid hydrogen (cryogenic)
LEO	Low earth orbit
LOX	Liquid oxygen (cryogenic)

NASA	National Aeronautics and Space Administration
NASP	National Aerospace Plane
ORS	Operationally Responsive Spacelift
OMS	Orbital maneuvering system
POST	Program to Simulate Trajectories
RBCC	Rocket-based combined-cycle
RCS	Reaction control system
RD-180	Liquid hydrocarbon-fueled engine
RDP	Radial deviation parameter
Rkt	Rocket engine
RLV	Reusable Launch Vehicle
RMLS	Reusable Military Launch System
RP-1	Rocket Propellant-1, a liquid hydrocarbon fuel
RSATS	Responsive Space Advanced Technology Study
SSME	Space shuttle main engine, a liquid hydrogen-fueled engine
SSTO	Single-stage-to-orbit
STS	Space Transportation System, the space shuttle
TAV	Transatmospheric Vehicle
TBCC	Turbine-based combined-cycle
Turb	Turbine engine
TSTO	Two-stage-to-orbit
VTHL	Vertical takeoff, horizontal landing

COMPARATIVE ANALYSIS OF TWO-STAGE-TO-ORBIT ROCKET AND AIRBREATHING REUSABLE LAUNCH VEHICLES FOR MILITARY APPLICATIONS

1. Introduction

1.1 Motivation

In the Defense Planning Guidance published in August 2001, the President directed the Department of Defense (DoD) to begin transforming the U.S. defense posture to maintain a substantial margin of advantage over adversaries in key areas, including space [12:1]. To meet this requirement, Air Force Space Command defined operationally responsive spacelift (ORS) in a mission need statement: “ORS ensures the Air Force has the capability to rapidly put payloads into orbit and maneuver spacecraft to any point in earth-centered space, and to logistically support them on orbit or return them to earth” [12:1]. Current Air Force launch systems are entirely expendable, require years of preparation time, and are custom-tailored for each specific payload. In addition, the current launch cost of \$10,000 per pound to low earth orbit (LEO) is an economic limitation of the number of payloads that can be put in orbit [51]. The current generation of Evolved Expendable Launch Vehicles (EELV) will not meet the needs of the Air Force for responsive space due to cost and unresponsive nature of their design, but reusable launch vehicles (RLVs) have the potential to greatly surpass the abilities of

expendable launch vehicles. RLVs will allow the U.S. to keep the technological advantage over our adversaries as directed by the President [52].

Both the National Aeronautics and Space Administration (NASA) and the U.S. Air Force have studied numerous RLVs since the beginning of spaceflight to find an affordable, routine, and operationally responsive launch system, but no program reached operational capability due to technological hurdles, political opposition, and large program costs. Both agencies, however, still believe RLVs will provide the responsive and inexpensive space access needed to meet U.S. space launch requirements in 2020 and beyond and have renewed their research [9]. It is thought that RLVs are inherently more responsive and capable because they can be designed for aircraft-like operations from existing Air Force bases, especially if propelled by airbreathing engines. Reusability will also reduce the operational costs and, in turn, the life-cycle costs of the system over the costs of expendable vehicles, provided that reusable vehicles can be designed to require maintenance close to aircraft levels. While NASA has recognized the benefits of reusability, it is not pursuing technologies needed to meet the unique requirements of the Air Force [40:27-28].

Space access is a major responsibility of the Air Force, and this responsibility will only increase as the Air Force continues to transition to an air and space force. While expendable vehicles meet current non-responsive requirements, the demands of the future must be addressed today. The United States Air Force Scientific Advisory Board states that “RLVs offer immense potential to meet all the requirements of the future US aerospace force” [40:28]. With NASA focusing on manned space flight, the Air Force

alone must pursue the means to meet its needs for responsive and operable unmanned spacelift, including researching the propulsion technologies necessary [40:28].

1.2 Research Objectives

Previous studies at AFIT have researched two-stage-to-orbit (TSTO) RLVs using advanced propulsion systems [7, 8]. The vehicle empty weight has been the primary criterion used to compare vehicles using different propulsion methods, and the results show that RLVs using airbreathing propulsion are still heavier than RLVs using rockets only. Brock compared RLVs using turbines and rockets for propulsion. His findings were that an all-rocket RLV is the lightest vehicle and that horizontal takeoff is better than vertical takeoff for a turbine powered vehicle [7]. Similarly, Caldwell compared RLVs using turbines, combined-cycle engines, and rockets and found the all-rocket RLV to be the lightest vehicle. However, the all-rocket RLV does not have the flexibility and operability of a RLV using airbreathing propulsion. Of the airbreathing RLVs, Caldwell found the turbine-based combined cycle (TBCC) booster stage and rocket orbiter stage to be the second lightest and recommended investigating the use of a rocket-based combined-cycle (RBCC) orbiter stage [8]. The previous studies did not consider characteristics other than weight or missions other than the baseline launch, which may have neglected the advantages of airbreathing propulsion.

1.3 Research Focus

The baseline vehicles in this study are fully reusable and unmanned, designed to carry a payload of 20,000 lbm (9,071.8 kg) with a volume of 2,800 ft³ (79.3 m³) to a 100

nautical mile (nm) (185.2 km) circular low earth orbit (LEO) at an inclination of 28.5 deg. The launch site for the vehicles is Cape Canaveral AFS, Florida. All inputs were kept the same between vehicles whenever possible, so the results reflect an accurate comparison. Each two-stage vehicle is propelled by turbine (Turb) engines, turbine-based combined cycle (TBCC) engines, rocket-based combined cycle (RBCC) engines, or rocket (Rkt) engines. The fuels used are liquid hydrocarbon, JP-7 or RP-1, and liquid hydrogen, LH₂, with liquid oxygen (LOX) or air used as the oxidizer. Both vertical takeoff, horizontal landing (VTHL) and horizontal takeoff, horizontal landing (HTHL) configurations were considered, for a total of 21 baseline vehicles.

The performance and operability of these vehicles is then measured by three missions: a satellite launch, an orbital rendezvous, and a global strike. For the satellite launch mission, a growth rate for all 21 vehicles determines how sensitive each configuration is to payload mass changes. This is found by having the vehicles launch different payload masses from 0 lbm (no payload) with a volume of 0 ft³ (0 m³) to 30,000 lbm (13,607.8 kg) with a volume of 4,200 ft³ (118.9 m³) in increments of 5,000 lbm (2,268.0 kg) and 700 ft³ (19.8 m³). The orbital rendezvous mission investigates how 17 of the vehicle configurations exploit the advantages of airbreathing propulsions to change the launch trajectory. By flying a set distance prior to accelerating to orbit, the vehicles can change the parameters of their orbit, including expanding the launch window. The global strike mission determines how 14 of the configurations are suited to a hypersonic delivery vehicle for combat aerial vehicles (CAVs). By changing the upper reusable rocket stage to an expendable stage and increasing the payload mass to 40,000

lbm (18,143.7 kg), a new vehicle size can be found. Both the orbital rendezvous vehicle and global strike vehicle can then be compared to the original baseline vehicle.

1.4 Methodology Overview

ASTROX Corporation's Hypersonic System Integrated Design Environment (HySIDE) is used as the design program for all analysis. In the field of hypersonic vehicles, many variables must be considered simultaneously, including vehicle heating, engine performance, vehicle aerodynamic characteristics, system masses, and volume requirements. HySIDE has the flexibility to compute each of these individual variables and integrate them together into a single vehicle; to use many different propulsion types, including turbines, ramjet, scramjets, rockets, or any combination; and to simulate the entire flight trajectory of a vehicle. After the user specifies the vehicle configuration, such as propulsion type, trajectory, and payload, HySIDE calculates vehicle dimensions and performance and iterates until the design is finalized [22].

1.5 Assumptions/Limitations

The U.S. space launch and propulsion industries use English units as the standard measurements for all data. This work gives units in both the English and metric (SI) systems.

In the field of spacecraft design, empty vehicle mass is frequently used as a method to help predict a proposed design's development, acquisition, and operation costs [5:1]. To estimate maintenance costs and man-hours, vehicle wetted area roughly correlates to turn-around time between flights if the maintenance is dominated by the

thermal protection system (TPS) maintenance. For RLVs, the single largest maintenance item is the inspection and refurbishment of the TPS and engines [36]. This study assumes that a RLV with a larger wetted area will cost more and have a longer time between flights than a RLV with a smaller wetted area.

Vehicle gross mass, while given, is not as useful since propellant is a major constituent of this mass and the propellant fraction can vary with different propulsion options. In addition, the cost of the propellant is relatively insignificant compared to the overall system cost [29:3]. However, the vehicle gross mass does provide some insight into overall vehicle parameters such as the vehicle's launch pad and total thrust required, so it is included in this study.

1.6 Thesis Overview

This work consists of five chapters and ten appendices. Chapter 2 provides background information through a literature review of previous RLV programs, RLV propulsion options, and recent research in the field of RLVs. Chapter 3 explains the research methodology, beginning with an explanation of the HySIDE code. The derivation of the mission requirements and other inputs is explained next, along with the assumptions that were made. Chapter 4 presents the results of the study, with an analysis of each configuration's performance of each mission. Finally, Chapter 5 provides conclusions and highlights areas of future study.

2. Literature Review

This chapter begins with the historical background of the U.S. Air Force's research into reusable launch vehicles (RLVs). The next section describes the two basic types of propulsion systems for RLV use: Rocket-based propulsion and airbreathing engine-based propulsion. Rocket-based propulsion has powered all space launches to date, so the third section gives a closer look at airbreathing engine-based propulsion's advantages and disadvantages. The fourth section explores two emerging airbreathing technologies that could power RLVs. Finally, this literature review concludes with descriptions of recent studies into RLVs that are applicable to this study.

2.1 Reusable Launch Vehicle Background

The USAF has researched reusable launch vehicles extensively since the 1950s as a method to provide responsive and inexpensive access to space for military applications. Several past programs and spacecraft are noteworthy: the Dyna-Soar, the space shuttle, the Transatmospheric Vehicle, and the National Aerospace Plane. Currently, the National Aeronautics and Space Administration NASA's Hyper-X program and AFRL's HyTech program are the leading edge of RLV research.

2.1.1 X-20A Dynamic Soarer (Dyna-Soar)

The X-20A Dynamic Soarer, as shown in Figure 1, was a reusable spaceplane developed from the German Silverbird intercontinental skip-glide rocket bomber. The manned upper stage would be rocket-boostered to orbit by an expendable Titan lower stage

and would glide, eventually reentering the atmosphere [46]. The vehicle was designed with a high lift-to-drag ratio to allow it to maneuver during reentry [3:513]. The initial version of the glider developed in Phase I was a basic delta-wing design about 20 ft wide and 35 ft long, massing about 11,000 lbm (4,989.5 kg). Phase II and III versions of it would have fulfilled a variety of military missions: orbital supply, satellite inspection, reconnaissance, research, and even orbital bombing. Nine contractors submitted bids in March 1958, and the first development contract was awarded to Boeing in April 1960. However, controversy over its mission, lack of a strong sponsor, and the politics of potential infringement on the new NASA agency's manned orbital flight mission doomed the X-20A. By the time the program was cancelled in December 1963, over \$410 million had been spent, but critical research and technology developed went into future spacecraft, including the space shuttle [31:133-137].



Figure 1. Aerojet Corporation's Dyna-Soar concept [46]

2.1.2 Space Transportation System (Space Shuttle)

The Space Transportation System (STS), or space shuttle, program began in 1968, with the engine development overseen by the USAF Space Division. Unlike the Dyna-Soar, this program aimed directly for a Phase III solution. In 1970, NASA decided on a two-stage-to-orbit (TSTO), vertical-takeoff-horizontal-landing (VTHL) concept, experimenting with partially-reusable to fully reusable designs. In the budget cutbacks following the moon landing, the Nixon administration threatened to cancel the shuttle program unless NASA could lower development costs and get USAF participation. The Air Force gave political support in return for military use of the shuttle, which led to many design requirements to meet the Air Force's applications. In 1972 and 1973, the external tank, solid rocket boosters (SRBs), and orbiter configuration became the design of choice, reusing only the orbiter portion and SRB casings. Six minor design modifications were made between 1972 and 1974, and the first shuttle, *Enterprise*, was completed in 1976. *Columbia* first lifted off the pad in 1981, as shown in **Error!** **Reference source not found.** [23:431-455].



Figure 2. Space Shuttle at liftoff [42]

NASA planned to achieve routine space access by setting a goal of one shuttle launch per month, using both NASA's Cape Canaveral launch site and the USAF's Vandenberg Air Force Base launch site. The shuttle was supposed to be a cheap, reliable delivery system, but the Space Transportation System failed to meet predictions in several ways. First, the orbiter was 20% heavier than its specified weight and could not lift Air Force payloads into polar orbit from Vandenberg. It also failed to reduce the cost of putting payloads in orbit, mainly due to the fact that it was manned. Finally, NASA was unable to keep a regular launch schedule, managing a maximum of eleven launches in 1985. NASA officials hoped to achieve the goal of twelve launches in 1986, but the *Challenger* failure in January 1986 halted launches for over two years [23:431-455]. While a few military payloads were launched on the shuttle, the Air Force quickly abandoned the shuttle as a launch option and began looking at its own expendable launch systems, which became the Evolved Expendable Launch Vehicles (EELVs) [23:91, 23:146]. The future of the shuttle remains in question following the loss of *Columbia* in 2003 [23:431-455].

2.1.3 Transatmospheric Vehicle

The Transatmospheric Vehicle (TAV) was a classified USAF program that originated in the Advanced Manned Spaceflight Capability program in 1978. Trade studies conducted included different configurations consisting of one or two stages using VTHL and also horizontal-takeoff-horizontal-landing (HTHL). The program reached the test hardware stage consisting of a single-stage-to-orbit (SSTO), rocket-powered, winged vehicle. Interest then shifted to the X-30 National Aerospace Plane concept in 1986 [47].

2.1.4 X-30 National Aerospace Plane

In the 1986 State of the Union address, President Reagan envisioned a “new Orient Express,” that became the X-30 National Aerospace Plane (NASP), an early version of which is shown in Figure 3. Though developed jointly by the Department of Defense and NASA, DoD’s interest in the project was never quite clear. Over the next 8 years, \$3.33 billion dollars produced a concept for a SSTO, airbreathing scramjet-propelled, HTHL RLV. Some scientists believed that the goal of the orbital speed of Mach 25 could be attainable without the use of heavy supplemental rockets. However, as the program progressed, practical considerations and technical difficulties limited the theoretical performance to below Mach 17, with rockets still required to lift the vehicle into orbit. With the projected budget for an operational vehicle for military purposes ballooning to over \$20 billion, support for the NASP slowly died out, though there was never an official program cancellation date. A joint NASA/USAF Hypersonic Systems Technology Program (HySTP) was initiated to continue cataloging the massive amount of technology developed, but when the Air Force ended its participation in January 1995, the NASP program finally ended [48].



Figure 3. National Aerospace Plane concept [50]

2.1.5 X-43 Hyper-X and HyTech

Rocket and NASP's technologies led to the X-33, X-34, and X-43 programs, which each had a slightly different focus. While the X-33 and X-34 programs were cancelled prior to flight, the X-43 Hyper-X program has had two successful flights of the vehicle shown in Figure 4. A joint effort of NASA and the USAF, the Hyper-X used the NASP's hydrogen-fueled scramjet engines to achieve a new world speed record for jet-powered aircraft of Mach 9.6. However, in 2002, a joint study aimed at reducing development costs concluded SSTD vehicles are not yet practical, but TSTD technology is feasible in the short term. NASA further reinforced this by canceling the Hyper-X program following the record-setting flight in November 2004 [54].



Figure 4. Artist's rendition of the Hyper-X [53]

With NASA withdrawing from scramjet research to focus on presidential manned spaceflight directives, the USAF is now leading the way in scramjet research and development. The Hypersonic Technology (HyTech) program, begun at the Air Force

Research Laboratory Propulsion Directorate in 1995, continues to develop hypersonic technologies, focusing on military applications [33:1170]. Quite different from NASA's requirements, current doctrine specifically recommends the Air Force examine RLV technology to meet its need for an operationally responsive spacelift capability to ensure American space superiority [12]. The HyTech program is investigating using a scramjet using conventional hydrocarbon in a TSTO RLV to meet this need by the goal of 2014 [15].

2.2 RLV Basic Design Options

Engineers made many decisions when designing launch vehicles described in the previous section, including staging, fuel type, and propulsion type. This section discusses the staging and fuels used in this study, and section 2.3 describes the propulsion options in detail.

2.2.1 RLV Staging Options

Although future launch vehicles may eventually use only a single stage to reach orbit in order to avoid excessive launch costs, staging does provide many benefits that make it attractive for the immediate future. First and foremost, staging increases the total change in velocity that a system can achieve with a given amount of propellant. It accomplishes this by removing a portion of the vehicle structural mass through staging during the launch trajectory. In SSTO vehicles, energy from the propulsion system is consumed in the acceleration of excess structure no longer needed that could be used for acceleration of the payload. Second, the engines required to accelerate the vehicle at

takeoff may produce high acceleration stresses later in the trajectory when the vehicle has less mass. The original Atlas rocket dropped two of its three rocket engines to reduce mass after they were no longer needed [21]. With staging, the engines on each stage can be sized to match the remaining vehicle mass [19:481]. Finally, if airbreathing propulsion is considered, multi-stage vehicles allow greater potential for pre-launch offset capability due to their much higher fuel efficiencies over rocket-based SSTD vehicles. The NASP program was an ambitious SSTD vehicle, but with the lessons learned from it, a TSTD vehicle seems a more feasible solution than a SSTD vehicle for the near future [9:3-4, 17:3-4].

2.2.2 RLV Fueling Options

Since the majority of the mass and volume of a launch vehicle is propellant, the choice of fuel used can have a major impact on the vehicle's design and ground support requirement. The two most commonly used fuels are liquid hydrogen (LH₂) and hydrocarbon fuels, such as RP-1. Hydrogen fuel releases around 50,133 btu/lbm (116.7 MJ/kg) and has a density of 4.43 lbm/ft³ (71 kg/m³), and RP-1 releases around 18,400 btu/lbm (42.8 MJ/kg) and has a density of 50.56 lbm/ft³ (810 kg/m³) [21:696, 27:1215]. While hydrogen fuel releases a larger amount of energy per unit mass than hydrocarbon fuels, hydrogen fuel has a much smaller density. Thus, hydrocarbon fuel releases more energy per unit volume than hydrogen fuel, as is shown in Table 1. Hydrogen fuel is also cryogenic, which means it must be stored at low temperatures, around 20 K (-424 deg F) to be a liquid [21:696]. Hydrocarbon fuels can be stored over a wide range of temperatures, including room temperature and standard atmospheric pressure. Therefore,

vehicles using hydrogen fuel instead of liquid hydrocarbon fuel require heavier plumbing, larger diameter pipes due to the low density, and insulation to prevent boiling, all of which increases the structural mass of hydrogen fueled vehicles [27:1214].

Table 1. Properties of rocket fuel [27:1215]

Fuel	Mass/Volume density (lbm/ft ³)	Energy/Mass density (btu/lbm)	Energy/Volume density (btu/ft ³)
Liquid H ₂	4.43	50,133	222,090
RP-1	50.56	18,386	929,621

The storage requirements for fuel affect not only vehicle design, but also ground support equipment. Hydrocarbon fuels are much easier to handle than hydrogen and can be stored at room temperatures in normal fuel tanks. Hydrogen fuel is also more expensive than hydrocarbon fuel. The facilities required for hydrogen-fueled vehicles are more extensive and expensive than the facilities for hydrocarbon-fueled vehicles. For responsive military spacelift, hydrocarbon fuels are more practical, and the vehicles are easier to support logistically than hydrogen fuels [27:1214-1215, 33:1170-1171].

2.3 Reusable Launch Vehicle Basic Propulsion Options

A vehicle's propulsion system produces thrust by expelling a fluid at high speeds. This fluid, called the propellant, imparts momentum to the vehicle, propelling the vehicle in the opposite direction from which the propellant is expelled. Two types of propulsion systems used for high-speed vehicles are rocket propulsion and airbreathing propulsion. Rocket propulsion is most commonly used in spacecraft, while airbreathing propulsion is used in aircraft [19:5].

2.3.1 Rocket Propulsion

Rocket propulsion has powered all American spacecraft since the beginning of the space program. Fuel and oxidizer, carried by the rocket, are combined and burned. This combustion converts chemical bond energy to thermal energy, which heats the exhaust gases to high temperatures. As this hot gas is expelled out the rear of the engine through the rocket nozzle, the vehicle gains momentum in the opposite direction. The two types of rocket engines used for launches are solid- and liquid-propellant rocket engines, shown in Figure 5 [19:469].

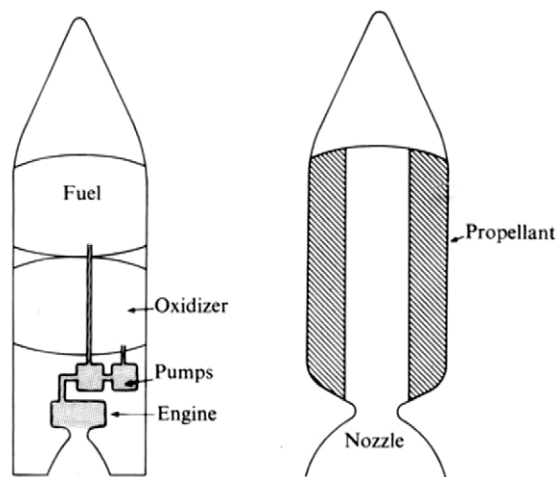


Figure 5. Diagram of liquid- and solid-propellant rocket engines [19:514]

Solid-propellant rocket engines consist of a solid mixture of fuel and oxidizer, whereas liquid-propellant rocket engines mix a liquid fuel and liquid oxidizer, which are stored separately in tanks. In general, solid rocket engines are simpler than liquid-propellant rocket engines, but unless special design elements are included, their operation cannot be interrupted until the propellant is completely burned. In addition, while the

thrust produced by solid rocket engines can be varied, it is determined by the shape in which the mixture is cast and cannot be actively controlled during flight. Liquid rocket engines can be operated intermittently, allowing controllable thrust, and they can even be shut off completely and restarted. However, the liquid fuel and oxidizer are usually cryogenic or toxic and require special handling and fueling methods before launch, whereas solid rocket engines are relatively inexpensive, simple, can be stored for long periods of time, and can be launched quickly. For both types, all of the propellant must be physically lifted off the ground, accelerated, and carried with the spacecraft until the propellant combusts in the engine.

2.3.2 Airbreathing Propulsion

Airbreathing propulsion uses atmospheric air as the oxidizer, drawing it into the engine from outside the vehicle. Only fuel needs to be carried aboard the vehicle, but airbreathing propulsion can be used only where air is available. This type of propulsion can be used to propel a RLV through a portion of the atmosphere before a rocket must be used to reach orbit. Airbreathing propulsion has three characteristics that make it suitable for this application: horizontal launch capability, higher fuel efficiency than rockets, more reliable than rockets, and less maintenance than rockets; potential for lower sensitivity to weight growth than rockets; and the potential for large advancements in airbreathing technology when compared to the mature state of rocket technology [4:2-3]. The three major types of airbreathing propulsion under consideration for RLVs are turbine, ramjet, and scramjet engines.

Turbine engines have been used in aircraft for over 60 years and as such, are well-known and reliable. Capable of supersonic flight to just over Mach 3, they have powered aircraft such as the Concorde up to Mach 2+ and the SR-71 to Mach 3+ [19:166, 55]. In a typical turbine engine shown in Figure 6, incoming air is compressed by rotating compressor blades, and fuel is injected into this compressed air. This mixture is ignited in the combustion chamber, and the hot gas is expelled out the back of the engine nozzle, producing thrust. Extra fuel can be added to this hot exhaust and burned, producing even more thrust. This is called afterburning, but this added thrust comes at the cost of lower fuel efficiency at lower speeds, but with little penalty as speed approaches Mach 3 and above. An afterburning turbine's specific impulse, at 1,800 sec, is approximately 5 times greater than a rocket's specific impulse, at 250 to 450 sec, and is the highest of all propulsion technologies discussed [19:514]. Unfortunately, turbine engines are also about ten times heavier than rocket engines. Turbine engines may be used to reduce the gross takeoff mass of a RLV [38:2].

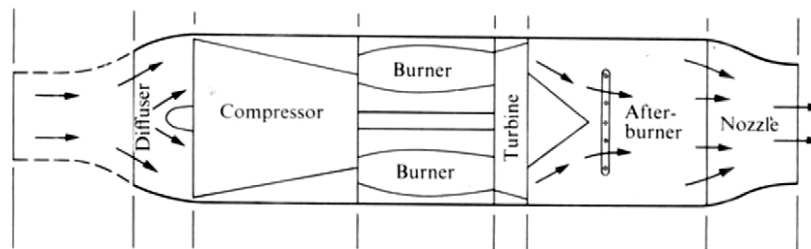


Figure 6. Diagram of a turbine engine [19:164]

Ramjet engines are the simplest airbreathing engines, with no major moving parts, as shown in Figure 7. They use the forward velocity of the vehicle to “ram” the air into

the engine and compress it. Air entering the inlet decelerates to subsonic speeds through a series of shock or compression waves, which compresses the air. The engine injects fuel into the compressed air and ignites it, then expels the products through a nozzle, similar to a turbine engine. Because ramjets rely on the forward motion of the vehicle for compression, they operate efficiently at supersonic velocities, but must be accelerated to supersonic speeds before they will function well. At low speeds, the pressure ratio in the engine is too low for efficient operation, but above Mach 5, the air pressure and temperature is too high after deceleration to subsonic speeds inside the engine, hence the need for supersonic combustion. Ramjet specific impulse is less than that of turbine engines, but still greater than that of rockets [19:155-157].

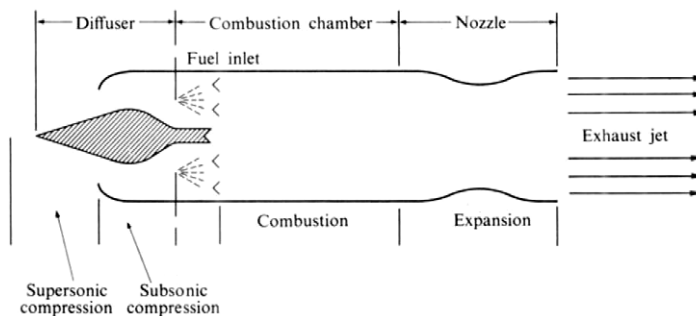


Figure 7. Diagram of a ramjet engine [19:156]

Supersonic combustion ramjets, or scramjets, operate similarly to a ramjet, except that they do not decelerate the incoming air to subsonic speeds. The air only partly decelerates and compresses while remaining supersonic, as shown in Figure 8. This partial compression limits the internal pressures and temperatures, allowing scramjets to operate at speeds above Mach 5. Less compression in the inlet also reduces the

associated losses in the inlet [18:23]. The combustion takes place in air moving at supersonic speeds, but this presents the challenge of properly mixing the fuel and igniting it before the mixture has left the rear of the engine. Scramjets have efficiencies between those of turbines and rockets and should be able to operate up to Mach 15. They will use roughly linearly increasing amounts of fuel with speed, since scramjets fly at constant dynamic pressure paths, along which drag stays about constant [19:263-264]. A combined ramjet-scramjet engine, called dual-mode scramjet (DMSJ), is able to operate over the entire velocity range of both types of engine. The HyTech program is conducting research into hydrocarbon-fuelled DMSJ engines, including the single engine demonstrator used on the X-51 vehicle shown in Figure 9 [33].

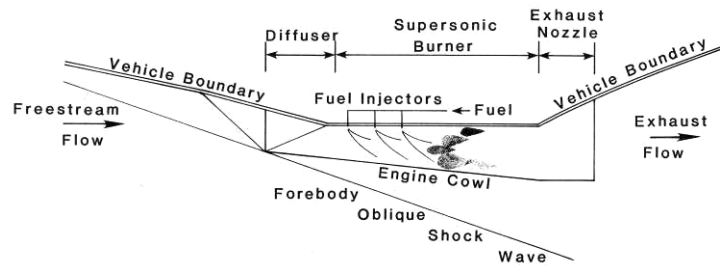


Figure 8. Diagram of a scramjet engine [18:24]



Figure 9. X-51 vehicle with HyTech scramjet engine demonstrator [56]

2.4 Airbreathing Propulsion in Reusable Launch Vehicles

If rockets have been used in space vehicles exclusively in the past, why even consider airbreathing propulsion for a RLV?

2.4.1 Airbreathing Propulsion Advantages

The greatest advantage airbreathing propulsion has over rocket propulsion is the ability to use atmospheric oxygen for combustion, reducing the mass of propellant that must be carried. In conventional rockets, the oxidizer makes up a significant fraction of the vehicle gross mass. The elimination of this mass is apparent in the specific impulse (I_{sp}), which is a measurement of the thrust divided by the weight flow rate of propellant. I_{sp} is a measurement of an engine's fuel efficiency, and has units of seconds. Rockets used for launch typically have an I_{sp} between 250 and 350 sec, while the I_{sp} for airbreathing engines ranges between 1,800 and 3,800 sec, as shown in Figure 10. The higher values of I_{sp} mean airbreathing engines can operate more efficiently than rocket engines by using less carried mass of propellant to produce the same amount of thrust [4:2-3].

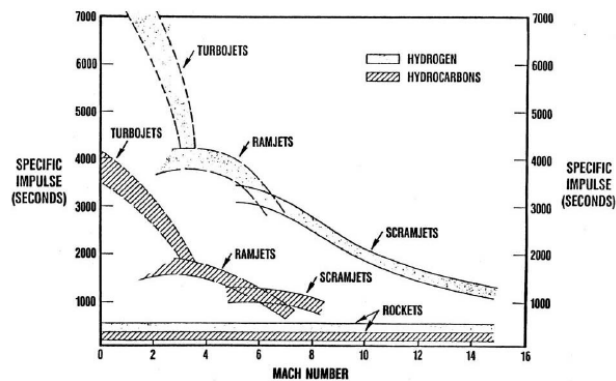


Figure 10. Specific impulse versus Mach number for rocket and airbreathing propulsion [10:18]

Another possible tangible advantage is the flexibility and operability benefits. Airbreathing engines allow a horizontal takeoff because of their smaller propellant requirements. Rather than being confined to a limited number of launch facilities, a RLV propelled by an airbreathing engine could operate from the many existing aircraft runways if oxidizer can be made available at those facilities. Airbreathing engines also allow the RLV to fly back more easily and land if the mission aborts, in addition to the ability to change trajectory in flight. This flexibility may also reduce ground and range support requirements [4:4-6, 17:3-4, 11:1-2].

Airbreathing propulsion systems have a lower operating pressure than rocket-based systems, which may lead to greater reliability and reusability. In recent space launches, the predominant cause of failure has been problems in the propulsion system. This system includes a multitude of parts, including the thrusters, combustion chamber, nozzles, propellant, propellant storage, turbopumps, and feed lines. For vehicles with rocket engines as their sole propulsion source, a failure in the propulsion system usually results in complete loss of the vehicle and payload. Should there be a propulsion system failure in an airbreathing RLV, the flyback mission abort capability makes it easy to return the vehicle with payload and avert a total loss. This also leads to more manageable range safety requirements. [24:1-2, 30:1].

2.4.2 Airbreathing Propulsion Disadvantages

Despite the advantages mentioned above, airbreathing propulsion does have its drawbacks, which explains why it is not currently used in space launches. The most basic is that airbreathing propulsion relies on air, only present in a portion of the flight

path to orbit. Further, no one engine type can operate over the entire range of Mach numbers required to reach orbit, while a single rocket can. Turbine engines cannot operate above Mach 3, ramjets do not operate efficiently below Mach 2-3 or above Mach 6, and scramjets cover Mach 5 to about Mach 15. Even if all three airbreathing engine types are used, a rocket is still needed to reach orbit [32:2].

Empty vehicle mass is commonly used as an indicator of a launch vehicle's cost, and airbreathing propulsion systems used in a RLV have heavier empty masses than a rocket-based system designed for the same mission. Several factors play a role in this. While more propellant efficient, airbreathing engines do not have the large thrust-to-weight ratio that rockets have, meaning an airbreathing engine is heavier than a rocket engine producing the same amount of thrust. Airbreathing engines also require greater thermal protection due to the flight profile. Rockets taking off vertically are quickly able to exit the atmosphere, minimizing the heating of the vehicle due to atmospheric drag at high velocities. However, because an airbreathing engine-based RLV must take off horizontally, it flies through more atmosphere during its ascent, resulting in greater atmospheric heating. Finally, a rocket-based RLV would be shaped similarly to current rockets, long and cylindrical, which allows for efficient and lightweight propellant tank construction. The streamlined vehicle shape required for an airbreather's hypersonic flight create complicated volumes within which to place the fuel tanks. All of these factors increase the empty vehicle mass of a RLV using an airbreathing system, which competes against the mass savings produced by the highest specific impulse [17:2-3].

2.5 Reusable Launch Vehicle Advanced Propulsion Options

While both rocket propulsion and airbreathing propulsion have their advantages and disadvantages, a compromise can be reached between the two by combining both types on the same vehicle. This combination, called combined-cycle engines, would allow a launch system that would be less expensive and weigh less than a pure airbreathing propulsion system, while simultaneously being more flexible than an all-rocket propulsion system. Figure 11 illustrates a possible flight profile using combined-cycle engines.

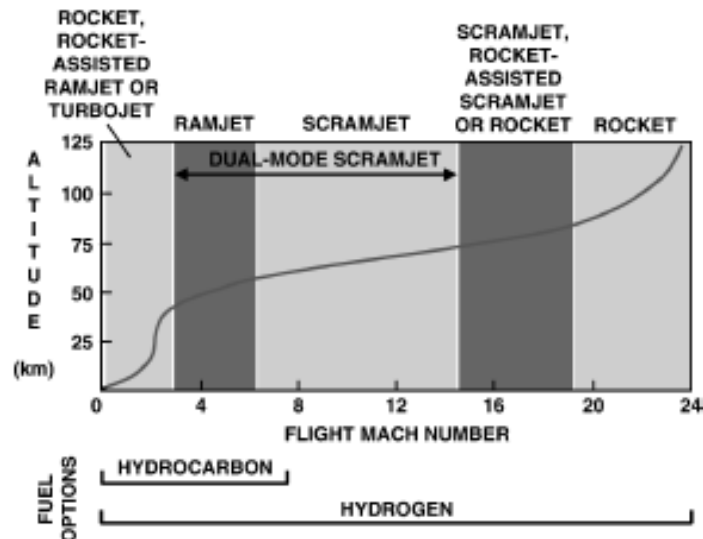


Figure 11. Combined-cycle engine flight profile using airbreathing propulsion [16:32]

2.5.1 Rocket-Based Combined-Cycle Propulsion Systems

Rocket-based combined-cycle (RBCC) propulsion systems use a rocket engine as the foundation and add an airbreathing engine to supplement it, as shown in Figure 12. In order to reduce the mass that must be carried, air-augmented rockets increase propulsive efficiency by using some outside air as the oxidizer, becoming a quasi-airbreathing

engine. While both solid and liquid rocket engines can function this way, the air-augmented engines must eventually revert back to normal rocket propulsion as the vehicle exits the atmosphere [20:630-635]. RBCCs go one step further by using a basic rocket engine or air-augmented rocket engine to propel the craft to ramjet speeds, whereupon a ramjet or scramjet ignites and propels the vehicle through the airbreathing engine's useful range of speeds. The RBCC engine then reverts back to pure rocket for the remainder of the flight profile [17:2].

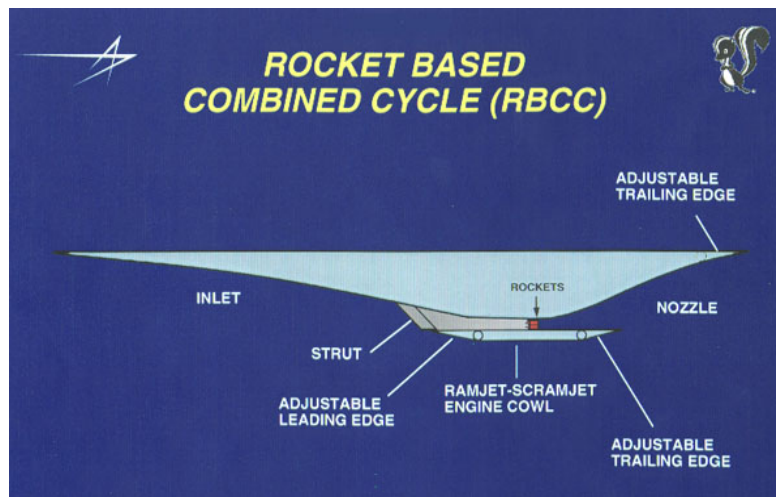


Figure 12. Diagram of vehicle using RBCC propulsion [45]

2.5.2 Turbine-Based Combined-Cycle Propulsion Systems

A turbine engine is used for the basis of a turbine-based combined-cycle (TBCC) engine instead of a rocket engine, as shown in Figure 13. This idea dates back to the 1950s, where the French used a turbo ramjet to power the Griffon II airplane to Mach 2 [16:31]. In a typical TBCC used for space launch, the turbine engine powers the craft from takeoff up to ramjet engine speed, when the RLV switches to ramjets. The ramjets function until the vehicle reaches scramjet speeds, when the scramjets ignite. This allows

the three different airbreathing propulsion types to be used over their functional area of the flight profile. However, a rocket is still required to reach orbit, so TBCC propulsion can only be used in the atmosphere as the first stage of a multiple-stage RLV [20:2].

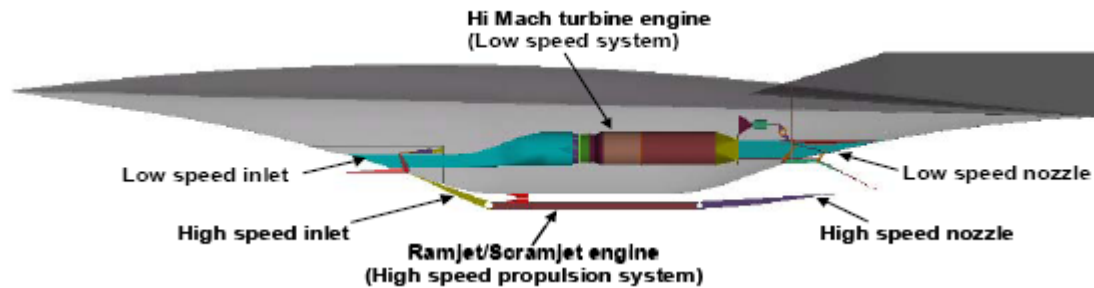


Figure 13. Diagram of vehicle using TBCC propulsion [39]

2.6 Recent Reusable Launch Vehicle Research

In recent years, RLVs have become a popular topic for research. Numerous studies conducted yielded many published papers, with the scope of research ranging from a broad perspective comparison of different designs to a focused study on one particular RLV configuration using advanced propulsion [3]. Five recent research efforts particularly related to this work are summarized. They are the 2004 AFIT RLV study [7], the 2004 ASTROX Corporation RLV study [13], the 2004 SpaceWorks Engineering study [6], the 2005 AFIT RLV weight study [8], and the 2005 University of Maryland study [14].

2.6.1 2004 AFIT Reusable Launch Vehicle Study

This study looked at five different RLV configurations, all TSTO, using rocket engines, turbine engines, and RBCC engines for propulsion [7]. Program to Simulate

Trajectories (POST), a trajectory optimization program, simulated flight profiles of all five RLVs using a fixed takeoff weight of 1 million pounds. Literature of similar RLVs and data from AFRL provided trajectory constraints, mass fractions, engine performance, and aerodynamics. This study concluded the following:

1. Payload and inert weights were the most sensitive to rocket stage inert mass fractions.
2. Horizontal takeoff is better than vertical takeoff for RLVs with turbine first stages. Vertical takeoff with turbines is impractical due to the large number of engines required.
3. RBCC engines should not be used for direct ascent trajectories.
4. An RLV using rockets for both stages has the most potential for future use.

2.6.2 2004 ASTROX Reusable Launch Vehicle Study

ASTROX Corporation used a vehicle design tool they developed, called Hypersonic System Integrated Design Environment (HySIDE), to compare rocket-powered TSTO RLVs to RBCC-powered SSTD RLVs [13]. This program allows a wide range of rocket and airbreathing engines to be modeled throughout the entire flight profile. Each RLV carried a fixed payload of weight of 20,000 pounds, and the figure of merit was the empty vehicle mass. The study compared different fuel combinations, including hydrogen, hydrocarbon, and dual-fuel. For the SSTD, this study found that the VTHL RLV had a lower empty mass than the HTHL RLV, and the dual-fuel RLV had the lightest empty mass. For the rocket-powered TSTO, the dual-fuel RLV also had the lightest empty mass.

2.6.3 2004 SpaceWorks Engineering Reusable Launch Vehicle Study

SpaceWorks Engineering is developing *Quicksat*, a multi-purpose HTHL TSTO launch vehicle capable of lifting a 10,000-lbm (4,535.9 kg) payload into orbit [6]. *Quicksat* is a hybrid vehicle, meaning that the first stage booster is reusable, while the second stage orbiter is expendable. SpaceWorks used a program called ModelCenter to link several industry standard tools within a framework to conduct the analysis. The goal of this study was to minimize the empty vehicle mass. Using a TBCC propulsion system with DMSJ engines from AFRL's HyTech program, *Quicksat* satisfies several possible applications of this research. In addition to the DMSJ engines, six turbine engines are used to initially power the vehicle, along with four tail rockets to boost the vehicle through the transonic velocities [6].

2.6.4 2005 AFIT Reusable Launch Vehicle Weight Study

This study investigated three different areas, using empty weight as the figure of merit and both POST and HySIDE code for the analysis [8]. The first area of study analyzed four different TSTO RLV configurations, using all rocket, RBCC-rocket, TBCC-rocket, and turbine-rocket propulsion. The all-rocket configuration had the lightest weight, with TBCC-rocket coming in second lightest. The second field of study was a sensitivity analysis of hydrocarbon versus hydrogen propellant, similar to the ASTROX study but using all rocket and RBCC-rocket TSTO RLVs. Fuel selection made little difference in VTHL RLVs, but using hydrogen significantly lowered the vehicle weight in HTHL RLVs. Finally, the effect of thrust-to-weight ratio was modeled on TBCC-rocket and turbine-rocket configurations. As expected, increasing the thrust-to-

weight ratio resulted in lower vehicle empty weights, with the largest decrease in the turbine-rocket RLV. The study recommended investigating the use of a RBCC-powered orbiter, since all vehicles in this study used rocket orbiter stages.

2.6.5 2005 University of Maryland Reusable Launch Vehicle Study

This study analyzed several SSTO and TSTO air-breathing vehicles using empty mass, wetted area, and maintenance man-hours as the primary figures of merit [14]. A TSTO rocket-rocket vehicle was used as the baseline vehicle, with both hydrocarbon and hydrogen fuels used. While the hydrocarbon-fueled booster with a hydrogen-fueled orbiter had the lowest vehicle mass, the all hydrocarbon-fueled rocket had a smaller wetted area. The airbreathing vehicles were then compared to this all-rocket vehicle, with both VTHL and HTHL configurations. Two VTHL vehicles, consisting of rocket boosters with RBCC orbiters, compared 2-dimensional (2-D) and inward turning geometries, which are shown in Figure 14. A vehicle with a 2-D inlet produces a wedge-shaped vehicle, while an inward-turning inlet produces a vehicle with a rounded “kidney-bean” shaped cross-section. The inward turning geometry had clear benefits for both empty mass and wetted area. Four HTHL vehicles were studied: a hydrocarbon-fueled turbine booster with a hydrogen-fueled RBCC, a hydrocarbon-fueled TBCC with a hydrogen rocket orbiter, and both hydrocarbon- and hydrogen-fueled RBCC boosters with rocket orbiters. The turbine booster with the RBCC orbiter had the lowest empty mass and smallest wetted area among the HTHL vehicles, but all of the HTHL vehicles had a greater empty mass and larger wetted area than the pure rocket and VTHL vehicles. This study concluded that regardless of the takeoff configuration or booster stage, using

an airbreathing orbiter stage is a superior configuration, for the simple reason that the gross mass of the scramjet upper stage was lighter than the rocket upper stage. This weight is the payload of the first stage, so the savings “ripple down” through the booster as well.

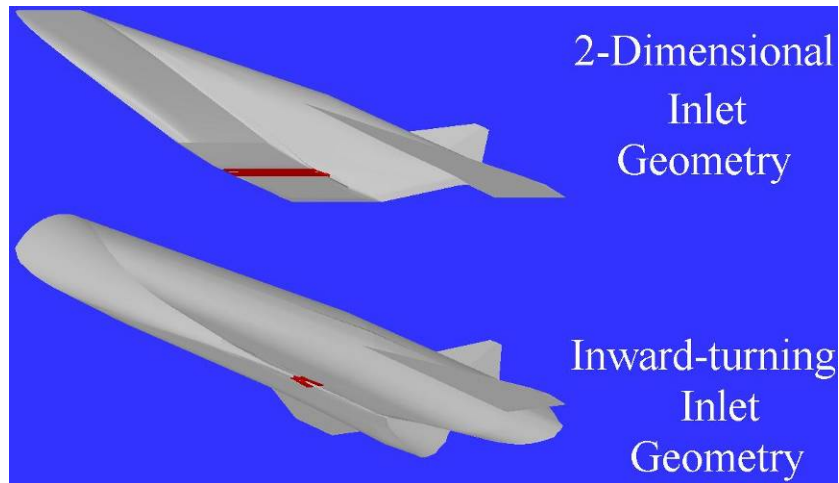


Figure 14. Airbreathing vehicle inlet geometry types

2.7 Summary

The U. S. Air Force has been involved in several RLV programs, some of which used airbreathing propulsion. While some reach operational capability and others did not, much knowledge has been gained through their development. Some clear advantages and disadvantages have been discovered, but much remains to be learned. Just as 50 years ago, the technology for both airbreathing and rocket propulsion was just in its infancy, the research being conducted today will be just as critical when looked back upon from 50 years in the future. While not all ideas from the past became reality, those that have reached operational capability proved that the work being done right now is critical to space access for tomorrow.

3. Methodology

The purpose of this chapter is to describe the methodology used to determine the empty mass and wetted area of different RLV configurations performing distinct missions. Propulsion systems used were turbine engines, dual-mode scramjet (DMSJ) engines, and liquid rocket engines; fuels used were hydrocarbon and hydrogen fuels; and takeoff configurations were vertical takeoff, horizontal landing (VTHL) and horizontal takeoff, horizontal landing (HTHL). ASTROX Corporation's HySIDE code, a vehicle sizing program, was the primary tool used in this study. In the field of hypersonic vehicles, many variables must be considered simultaneously, including vehicle heating, engine performance, vehicle aerodynamic characteristics, system masses, and volume requirements. HySIDE has the flexibility to compute each of these individual variables and integrate them together into a single vehicle [22].

To determine the operability and performance of the various configurations, three distinct military missions were defined. The first mission is a basic payload launch, and the baseline payload module mass used is 20,000 lbm (9,071.8 kg). The first part of this study looked at each vehicle's growth rates for both vehicle empty mass and wetted area dependent on payload mass by sizing vehicles for a varying range of payload masses. The second mission is an orbital rendezvous mission, which involves using airbreathing propulsion to change the vehicle's launch trajectory. The growth of each vehicle over the baseline empty mass and wetted area can be used to determine each one's suitability to trajectory changes. The third mission is a prompt global strike, where each vehicle is

used to deliver combat aerial vehicles (CAVs) worldwide. To accomplish this, each reusable rocket orbiter stage carrying 20,000 lbm (9,071.8 kg) is replaced with an expendable rocket orbiter stage carrying 40,000 lbm (18,143.6 kg), simulating a payload of ten CAVs and the payload bus required to house them. Again, the changes in the figures of merit when compared to the baseline vehicle determine each configuration's suitability to this military application.

3.1 TSTO RLV Configurations

The two-stage-to-orbit (TSTO) reusable launch vehicles in this study use two separate sub-vehicles, or stages, to reach orbit. Each stage contains its own propulsion system and propellant, as well as structure and tank to contain and support them. Reusable vehicles also have extra propellant, as well as a secondary propulsion system if necessary, to return the vehicle to the launch point. Thermal protection systems (TPS), wings, landing gear, and tails are also required for recovery of each sub-vehicle. The booster stage propels the RLV from liftoff to the staging point. At staging, the sub-vehicles separate, and the booster stage returns to land while the orbiter stage propels the RLV from the staging point to orbit. Staging allows a vehicle to discard excess tank and structural mass during the ascent to orbit, decreasing the amount of energy required by the propulsion system to accelerate the payload to orbit [19:481].

The notional RLV flight profile shown in Figure 11 consists of three basic segments, which can be split in several ways between the two stages. The first segment uses a turbine or rocket, the second segment uses a DMSJ, and the third segment uses a rocket. For a TSTO vehicle, the middle segment using the DMSJ can be flown by the

first stage prior to staging, by the second stage after staging, by both stages, or omitted entirely. This results in seven basic methods of propulsion as shown in Figure 15, with the solid dark lines representing the staging point. The boosters are shown in purple and the orbiters in light green. These are the seven basic models used in this study.

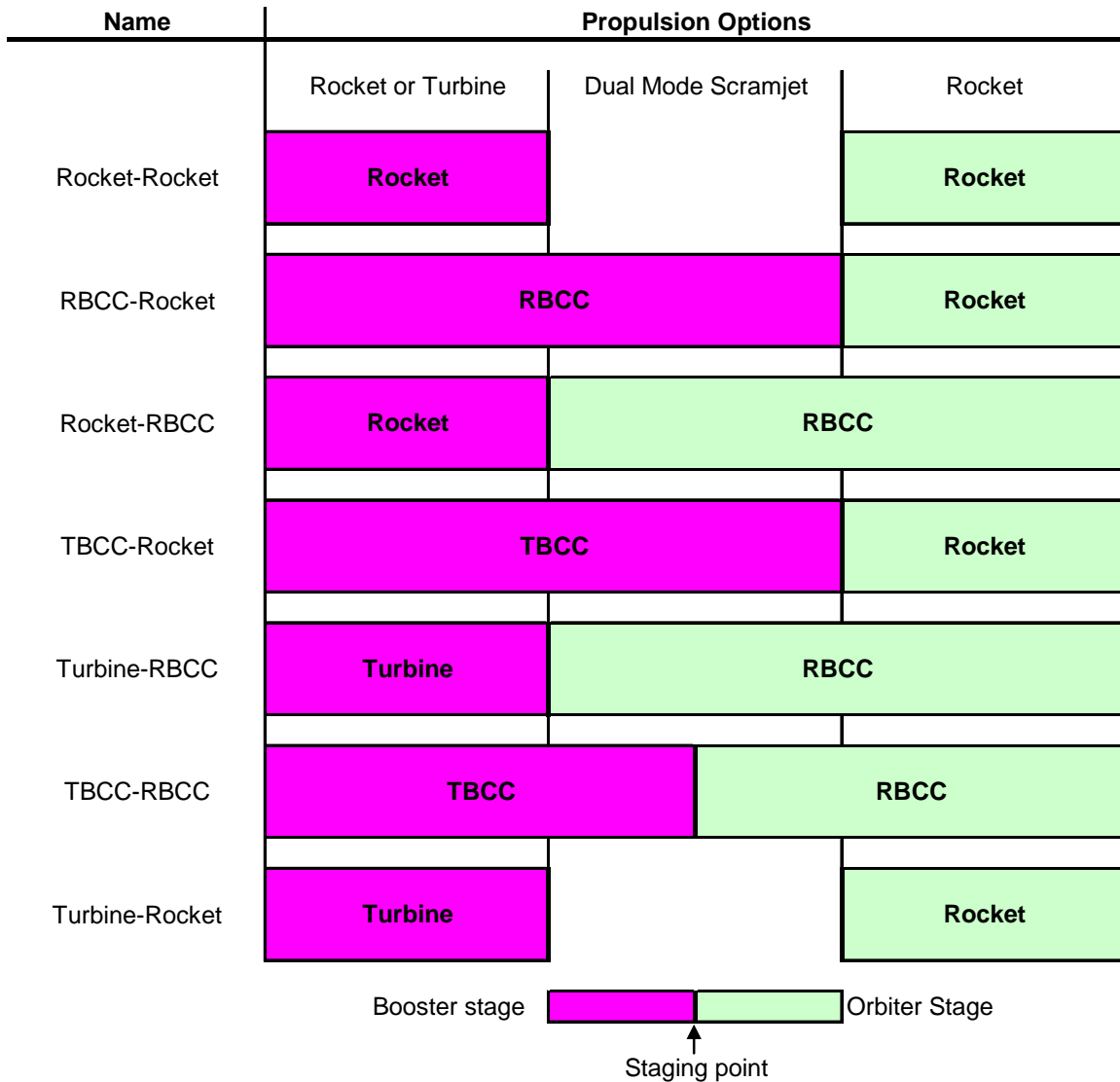


Figure 15. Thesis model propulsion options overview

The boosters in this study are propelled by a pure rocket system (Rkt), a pure turbine system (Turb), a rocket-based combined-cycle (RBCC) system, and turbine-based combined-cycle (TBCC) system. The orbiters are propelled by a pure rocket system (Rkt) or a RBCC system. Rocket engines combined with DMSJ engines are used to model the RBCC propulsion system, and turbine engines combined with DMSJ engines are used to model the TBCC propulsion system. Examples of the four basic stage types used to build the TSTO vehicles are shown in Figure 16. While turbine engines are commonly fueled only by hydrocarbon fuel, DMSJ engines and rocket engines can be fueled by either hydrocarbon fuel or hydrogen fuel. This study did not mix fuel type on the same stage, so the original 7 propulsion combinations are expanded to 19 fueling options as shown in Figure 17.

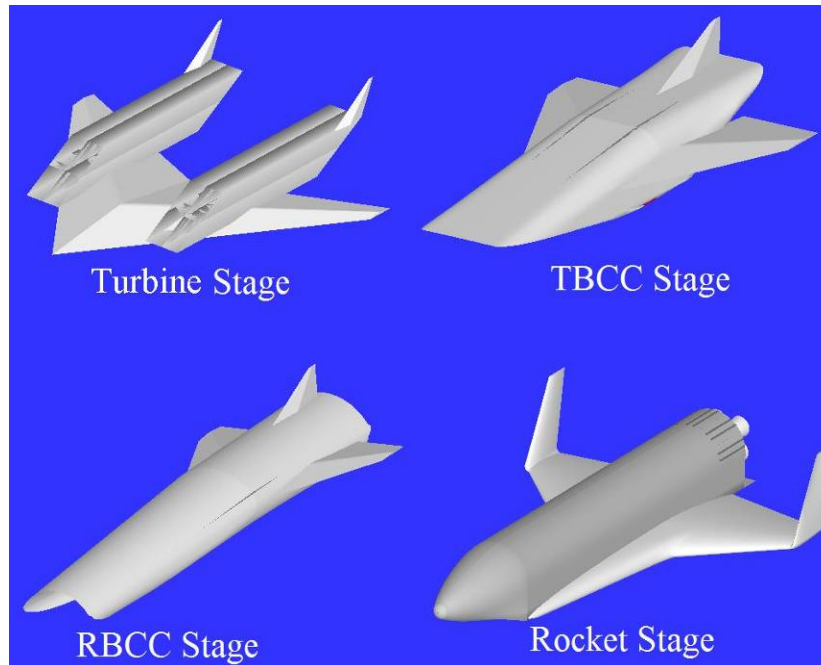


Figure 16. Basic vehicle propulsion stage types

Name	Fuel Options		Takeoff Options
	Booster	Orbiter	
Rocket-Rocket	HC	HC	VTHL
	HC	H	
	H	HC	
	H	H	
RBCC-Rocket	HC	HC	VTHL HTHL
	HC	H	
	H	HC	
	H	H	
Rocket-RBCC	HC	HC	VTHL HTHL
	HC	H	
	H	HC	
	H	H	
TBCC-Rocket	HC	HC	HTHL
	HC	H	
Turbine-RBCC	HC	HC	HTHL
	HC	H	
TBCC-RBCC	HC	H	HTHL
Turbine-Rocket	HC	HC	HTHL
	HC	H	

Figure 17. Thesis model fueling and takeoff options overview

Finally, the takeoff options for each model must be considered. Due to their low thrust-to-weight ratio, a large number of turbines are necessary to lift a RLV vertically off the ground, so turbine and TBCC boosters are best suited to take off horizontally [7]. Rockets, on the other hand, produce sufficient thrust to propel a RLV vertically or horizontally. Horizontal takeoff for a rocket or RBCC only makes sense when an airbreather is used for the second trajectory segment, resulting in the takeoff options as shown in Figure 17.

Due to limitations of the computer code, the hydrocarbon RBCC-Rocket HTHL models could not be included in this study. Therefore, this study includes 21 combinations of fuel options, propulsion options, and takeoff options as shown in Figure 18. These include eight of the models in the 2005 AFIT RLV study and seven of the models in the 2005 University of Maryland study, in addition to nine original models, for a single comprehensive look.

Name	Fuel Options		Takeoff/Landing
	Booster	Orbiter	
Rocket-Rocket	Hydrocarbon Rocket	Hydrocarbon Rocket	VTHL
	Hydrocarbon Rocket	Hydrogen Rocket	VTHL
	Hydrogen Rocket	Hydrocarbon Rocket	VTHL
	Hydrogen Rocket	Hydrogen Rocket	VTHL
RBCC-Rocket	Hydrocarbon RBCC	Hydrocarbon Rocket	VTHL
	Hydrocarbon RBCC	Hydrogen Rocket	VTHL
	Hydrogen RBCC	Hydrocarbon Rocket	VTHL
	Hydrogen RBCC	Hydrogen Rocket	VTHL
	Hydrogen RBCC	Hydrocarbon Rocket	HTHL
	Hydrogen RBCC	Hydrogen Rocket	HTHL
Rocket-RBCC	Hydrocarbon Rocket	Hydrocarbon RBCC	VTHL
	Hydrocarbon Rocket	Hydrogen RBCC	VTHL
	Hydrogen Rocket	Hydrocarbon RBCC	VTHL
	Hydrogen Rocket	Hydrogen RBCC	VTHL
TBCC-Rocket	Hydrocarbon TBCC	Hydrocarbon Rocket	HTHL
	Hydrocarbon TBCC	Hydrogen Rocket	HTHL
Turbine-RBCC	Hydrocarbon Turbine	Hydrocarbon RBCC	HTHL
	Hydrocarbon Turbine	Hydrogen RBCC	HTHL
TBCC-RBCC	Hydrocarbon TBCC	Hydrogen RBCC	HTHL
Turbine-Rocket	Hydrocarbon Turbine	Hydrocarbon Rocket	HTHL
	Hydrocarbon Turbine	Hydrogen Rocket	HTHL

Figure 18. Thesis model stages, fuel types, and takeoff types

The baseline vehicles in this study are unmanned and fully reusable. They are designed to deliver a 20,000 lbm (9,071.8 kg) payload module with a volume of 2,800 ft³

(79.3 m³), or approximately a 12 ft (3.7 m) diameter by 25 ft (7.6 m) length payload bay, launched from Cape Canaveral AFS, Florida. The stages burn serially, where the orbiter stage does not fire until after the booster has completed its burn and separated. After staging, the booster decelerates and flies back to the launch site via turbine engines, while the orbiter continues to a final velocity of 24,503 fps (7,468.5 m/s) earth relative, at an altitude of 303,800 ft, or 50 nm (92.6 km), with an inclination of 28.5 deg. This is the perigee point for a 50 nm (92.6 km) by 100 nm (185.2 km) orbit, and the orbiter circularizes the orbit to a 100 nm (185.2 km) circular orbit via an orbital maneuvering system (OMS) burn at apogee. Following release of the payload in this orbit, the orbiter executes a second OMS burn to de-orbit, reenters the atmosphere, and lands. The 20,000 lbm (9,071.8 kg) payload module includes the satellite, payload support structure, and any upper stage rocket used for final orbital insertion of the satellite.

In the case of airbreathing boosters, the option exists for a mission abort. The boosters are sized to fly back and land with the orbiter stage still attached. Should a mission abort be required, both stages will immediately dump any extra fuel that would have been used to achieve orbit. The mass of the vehicle for flyback consists of the empty booster mass, the empty orbiter mass, the payload mass, and a few residuals including fuel for flyback. The booster is sized to fly back and land with this mass from the maximum range at which staging would have occurred.

3.2 Flight Fundamentals

The motion of any vehicle in the earth's atmosphere, including the RLVs in this study, is determined by the forces acting upon it, which can be divided into body forces and aerodynamic forces. The body force is weight (W), and the aerodynamic forces are lift (L), drag (D), and thrust (T). They are all measured in pounds-force (lbf), and shown in Figure 19.

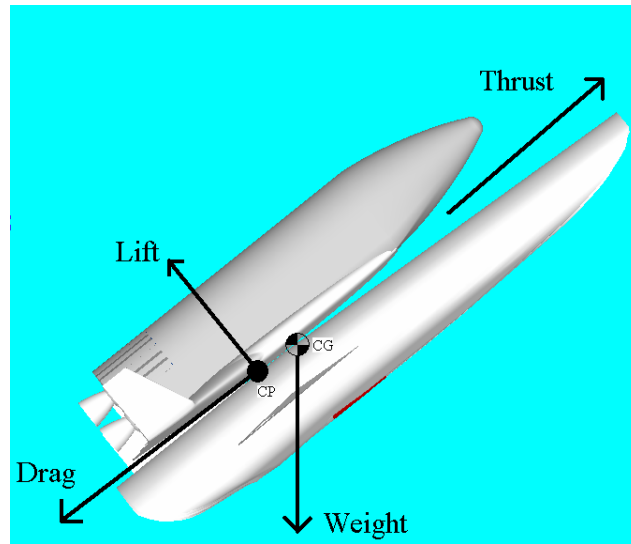


Figure 19. Diagram of vehicle forces

The vehicle mass changes with time as a function of propellant mass flow rate and staging, but the weight at any instant in time is given by

$$W = M \cdot g \quad (1)$$

where M is mass and g is the local acceleration due to gravity [37:113]. This force always acts downwards, towards the center of the earth, through the vehicle's center of gravity (CG). The aerodynamic forces result from breaking a single integrated

aerodynamic force, caused by pressure variations acting through the vehicle's center of pressure (CP) and shear forces acting along the vehicle body, into components for easier analysis. They are oriented with the vehicle itself and can vary direction during flight, unlike weight which always acts in a fixed direction.

Lift is the component of the aerodynamic force that acts perpendicular to the direction of flight. Lift is governed by the following equation:

$$L = C_L \cdot \left(\frac{1}{2} \cdot \rho \cdot V^2 \right) \cdot S_{ref} \quad (2)$$

where C_L is the lift coefficient, ρ is the atmospheric density, V is the vehicle velocity, and S_{ref} is the vehicle reference planform area [2:170]. Drag is the component of the aerodynamic force that acts in the opposite direction from the flight direction and is given by a similar equation to lift:

$$D = C_D \cdot \left(\frac{1}{2} \cdot \rho \cdot V^2 \right) \cdot S_{ref} \quad (3)$$

where C_D is the drag coefficient [2:176]. C_L and C_D are dimensionless quantities that vary depending on angle of attack, vehicle shape, and aerodynamic properties, and are described in further detail in section 3.3.3. The value in parentheses is called the dynamic pressure, q .

In order to accelerate itself to orbital velocity, a vehicle must produce enough thrust to overcome drag and a portion of the weight. A rocket produces this thrust by expelling propellant at a high velocity out the back of the vehicle. The thrust produced is therefore dependent on the rate of propellant expulsion, the velocity at which it is

expelled, plus the difference in pressure between the nozzle exit and the ambient atmospheric pressure. The equation for thrust of a rocket engine is therefore given by

$$T = \dot{m}_p \cdot V_e + (P_e - P_o) \cdot A_e \quad (4)$$

where \dot{m}_p is the propellant mass flow rate, V_e is the rocket propellant exhaust velocity, P_e is the rocket nozzle exit pressure, P_o is the ambient atmospheric pressure, and A_e is the nozzle exit area [21:110].

Since an airbreathing engine uses the air drawn into the engine plus the fuel added to the air as the propellant, thrust is a little more complicated. An additional term must be added to the thrust equation to account for the original momentum of the air, so the equation for thrust becomes

$$T = \dot{m}_e \cdot V_e + (P_e - P_o) \cdot A_e - \dot{m}_a \cdot V \quad (5)$$

where \dot{m}_e is the exit mass flow rate of fuel and air and \dot{m}_a is the air mass flow rate into the engine [19:148].

When evaluating and comparing propulsion systems, two common measures of performance are specific impulse, I_{sp} , and specific fuel consumption, SFC . Specific impulse is commonly used to measure rocket engines and is given by

$$I_{sp} = \frac{V_{eq}}{g} = \frac{T}{\dot{m}_p \cdot g} \quad (6)$$

where V_{eq} is defined as the equivalent exhaust velocity, which is given by

$$V_{eq} = V_e + \left(\frac{P_e - P_o}{\dot{m}_p} \right) \cdot A_e \quad (7)$$

For rocket engines, \dot{m}_p is the mass flow rate of fuel plus oxidizer, but since airbreathing engines use air as the oxidizer, \dot{m}_p for airbreathing engines is the mass flow rate of fuel only [19:471-472]. The division by g is arbitrary, but allows I_{sp} to be expressed in units of seconds, which allows comparison across all common systems of units. The higher the I_{sp} , the more fuel efficient the propulsion system is. For specific fuel consumption, a lower number signifies better fuel efficiency. SFC is given by

$$SFC = \frac{\frac{W_f}{t}}{T} \quad (8)$$

where W_f is the weight of fuel and t is the time [35:23]. SFC is given in units of pounds of fuel per hour per pound of thrust (mg/Ns). Though not expressed as such, the units for SFC is essentially $\frac{1}{hrs}$, so to convert from I_{sp} in sec to SFC in $\frac{1}{hrs}$ and vice-versa, the

following equations are used:

$$I_{sp} = \frac{3600}{SFC} \quad SFC = \frac{3600}{I_{sp}} \quad (9)$$

Specific impulse is more commonly used for comparing rocket engines performance, while specific fuel consumption is more common for airbreathing engines.

3.3 RLV Design Methodology

ASTROX Corporation's Hypersonic System Integrated Design Environment (HySIDE) was used to size each vehicle in this study [22]. Based on a vehicle design code from 1996 called Hypersonic ASTROX Vehicle Design and Analysis Code (HAVDAC), HySIDE is a design environment that allows a user to combine individual modules to build an entire model [26]. This modular design allows the flexibility to study a range of both airbreathing and rocket vehicles throughout their entire flight profile. Using a GUI, shown in Figure 20, the user constructs the vehicle by adding the proper system elements (yellow rectangles) along with inputs (green ovals) and outputs (red ovals) and connecting them appropriately in a block diagram. A collapsible tree, shown in Figure 21, then allows the user to specify individual inputs. Once constructed, the HySIDE design environment then analyzes the constructed vehicles in an integrated fashion, combining engine performance, aerodynamic properties, mass of components, volume requirements, vehicle heating, and propellant usage [22].

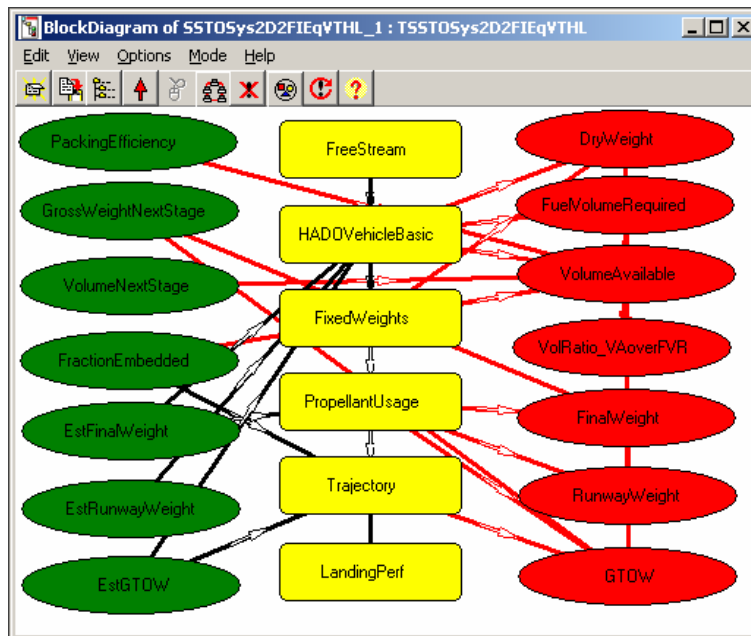


Figure 20. Example block diagram of a HySIDE model

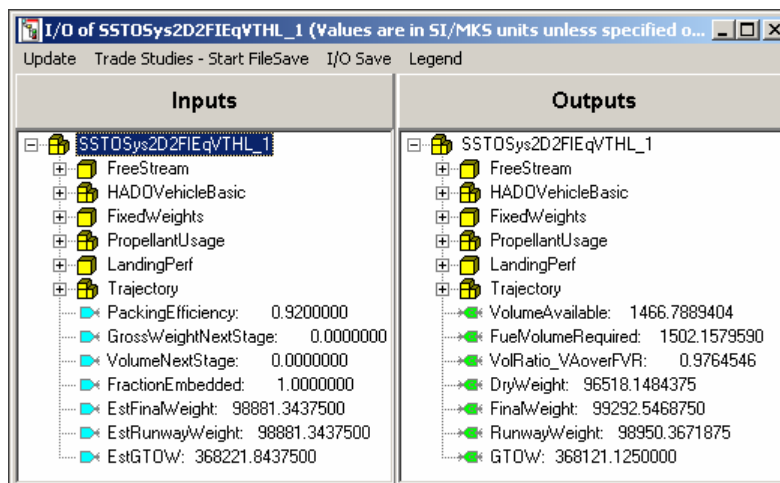


Figure 21. Example input/output tree of a HySIDE model

Using an embedded subroutine, HySIDE estimates a gross takeoff weight (GTOW) based on the user specified RLV dimensions, then “flies” the vehicle through the trajectory and calculates the various masses and volumes of individual components.

The subroutine then calculates a new GTOW and compares this to the estimated GTOW. If the difference is larger than 0.01%, a new GTOW is estimated and the calculations are repeated. When the GTOW has converged, the internal volume required at this GTOW is calculated and compared to the actual internal volume available from the original RLV dimensions. A packing efficiency can also be used as a measure of how well the propellant tank shapes are able to use the volume available. The user can then view the ratio of volume available over volume required based on the original dimensions. The EstGTOW, GTOW, VolumeAvailable, VolumeRequired, and VolRatio can all be seen in Figure 20 and Figure 21 [28].

The user must then attempt to “close” the vehicle by resizing it manually. New dimensions are chosen, and HySIDE rescales all components, repeats the GTOW convergence routine, and calculates a new volume ratio. The user repeats this iterative loop until the volume ratio equals one, a process that can take some time as successive iterations become necessary.

The HySIDE code contains approximately 12,000 lines of code and over 200 subroutines and functions, and is the result of 15 years of analysis and coding [14:23, 29:16]. Industry standard codes, including ENGGEN and Missile DATCOM, have been incorporated into HySIDE for analyses such as aerodynamics and engine performance, and results from the program correlate well to both NASA and Air Force data for many different models [29:16]. Pre-assembled models are included with the software, as well as all of the individual system elements used to construct the models. It has the flexibility to model turbine engines, ramjet/scramjet engines, and rocket engines, so the

user can custom-build a model of just about any space launch vehicle desired [22]. This study depended fully on the results from HySIDE, but this was by necessity, since there is no other such code that can model both rockets and airbreathers in such a short time [29:16].

The following sections give a description of each of the two basic HySIDE vehicles used in this study and the methodology used in each, followed by common system elements. A more detailed description of these system elements and inputs can be found in Appendices B and C. References 8, 14, 22, 25, 26, 28, and 34 were used to compile this section.

3.3.1 HySIDE Rocket Vehicle System Element

The HySIDE rocket vehicle uses the “FreeStream,” “Rocket,” “PropellantUsage,” “FixedWeights,” and “Trajectory” system elements described in Appendix B. The “FreeStream” element allows the user to specify a design point for the vehicle, but is not critical for a rocket. In the “RocketVehicle” system element, the user can change the dimensions of the vehicle to achieve the proper volume ratio. The rocket vehicle’s wings are also sized in this module, based on the landing mass and landing characteristics specified.

The “EngineCluster” system element within “RocketVehicle” sizes the combustion chamber, nozzle, and turbopumps assembly. The user can select pre-loaded parameters for 24 existing rockets, or make changes to the area ratio, fuel used, throttle setting, design altitude, and materials used. The takeoff thrust required is given by

$$T_{To} = \left(\frac{T}{W} \right)_{To} \cdot GTOW \quad (10)$$

where $\left(\frac{T}{W} \right)_{To}$ is the user-input vehicle thrust-to-weight at takeoff. Based on this required takeoff thrust, HySIDE uses the parameters from the existing rocket specified and rubberizes the engines to match. Any changes inputted by the user are then taken into account, and HySIDE individually sizes the thrust chamber, turbopumps, and nozzle to determine the mass of each. “EngineCluster” contains four individual nozzles, combustion chambers, and sets of turbopumps.

The mass of the flyback propulsion and fuel is also calculated for each rocket.

The weight fraction of fuel required is found using the Breguet range equation:

$$\frac{W_f}{W_i} = e^{\frac{-R \cdot SFC}{V \cdot \frac{L}{D}}} \quad (11)$$

where R is the range, $\frac{L}{D}$ is the lift-to-drag ratio, W_f is the weight at the end of the flyback segment, and W_i is the weight at the beginning of the flyback segment [35:21].

Rearranging the exponent in eq. (11) gives the range factor, $\frac{V}{SFC} \frac{L}{D}$, which should be made as large as possible for the farthest range. Two small turbine engines are sized using statistical jet-engine models for non-afterburning engines, given by

$$W_{uninstalled} = 0.084 \cdot \left(\frac{T_{flyback}}{2} \right)^{1.1} e^{-0.045 \cdot BPR} \cdot 0.8 \quad (12)$$

$$L_{uninstalled} = 0.185 \left(\frac{T_{flyback}}{2} \right)^{0.4} \cdot M^{0.2} \cdot 0.8 \quad (13)$$

$$D_{uninstalled} = 0.033 \cdot \left(\frac{T_{flyback}}{2} \right)^{0.5} e^{0.04 \cdot BPR} \cdot 0.9 \quad (14)$$

where the BPR is the bypass ratio, M is the Mach number, and $T_{flyback}$ is found using

$$T_{flyback} = \frac{W_{flyback}}{2 \frac{L}{D}} \quad (15)$$

[35:235]. Weight and lift are directly opposed in straight and level flight, as are thrust and drag, so the thrust required per engine is just the drag divided by the number of engines. A small tank is also sized to contain this fuel.

The entire rocket vehicle, once assembled, is shown in Figure 22.

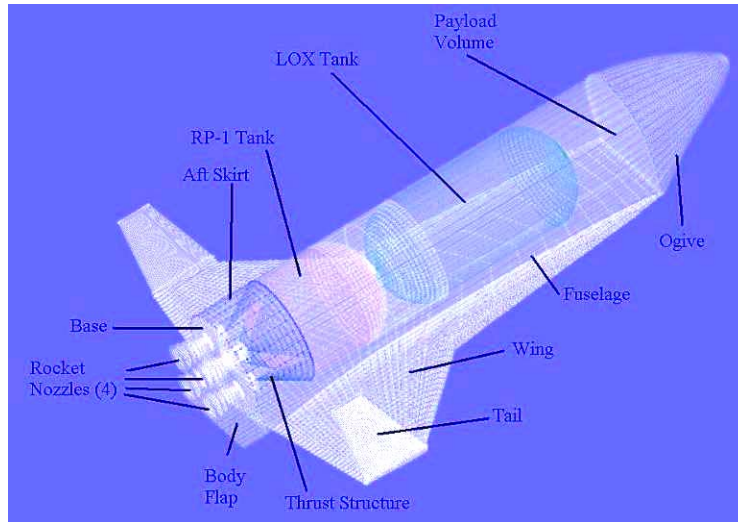


Figure 22. Diagram of a HySIDE reusable rocket vehicle (hydrocarbon)

3.3.2 HySIDE Airbreathing Vehicle System Elements

The HySIDE airbreathing vehicle uses the “FreeStream,” “HADOVehicleBasic,” “PropellantUsage,” “FixedWeights,” “LandingPerf,” and “Trajectory” system elements described in Appendix B.

The user inputs the Mach number and altitude that will be each vehicle’s design point in the “FreeStream” system element, which is critical for proper performance of the DMSJ during its entire operational range of velocities. The entire vehicle’s aerodynamic characteristics are determined from the design point using methods described in section 3.3.3, and the inlet shape affects both drag and vehicle heating. Generally, the best design point is one or two Mach numbers below the maximum DMSJ velocity. If the design Mach number is too close to this maximum velocity, vehicle heating will not be as great at these higher velocities, but the drag will be excessive at the lower end of the DMSJ operational range. If the design Mach number is too low, the opposite will occur. Once the design Mach number has been chosen, the design altitude should then be selected that corresponds with the desired dynamic pressure.

The vehicle body itself is part of the engine, and thus is carefully shaped in the “HADOVehicleBasic” system element depending on the values entered in the “FreeStream” system element. The main parts of the body are the inlet, combustor, isolator, nozzle, and external surface, as shown in Figure 23.

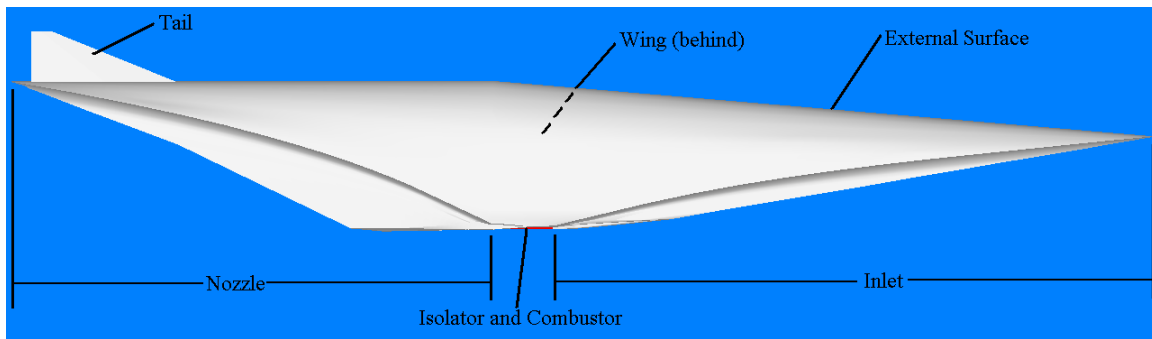


Figure 23. Diagram of a HySIDE reusable airbreathing vehicle

The inlet, combustor, isolator, and nozzle system elements use an inverse design procedure to shape the surface by carving inviscid stream surfaces out of known flow fields at the design point. An axisymmetric method of characteristics is used to find the flow field, streamlines, and all properties throughout. The method of characteristics is a mathematical method of solving partial differential equations by finding characteristic lines in the phase space along which the partial differential equation degenerates into an ordinary differential equation. These ordinary differential equations are easily solved.

The user specifies the leading edge characteristics, which are projected onto the inlet flow field and streamlines traced through it. The inviscid surface geometry is defined by these streamlines, to which viscous flow properties are estimated using a reference temperature method. With the boundary layer properties defined along each streamline, the geometry of the stream surface is altered so as to account for the presence of the boundary layer. The inlet surface itself is then defined, and the surface properties such as lift, drag, moments, and heat transfer can be found. An additional weight function is used to account for sections which are actively and passively cooled, and the

user can specify the maximum actively-cooled and passively-cooled surface temperatures.

The isolator and combustor designs depend of the inlet exit conditions and user inputs such as fuel type, mixing fraction, mixing length, minimum equivalence ratio for the fuel-injector rate, and combustion efficiency. The combustor modeling assumes a quasi-one dimensional combustor design and uniform flow conditions, and combustion is modeled in a two-part process. First, the fuel is accelerated from its stagnation condition to conditions that match the static pressure at the entrance to the combustor, mixing with the air in the fraction specified by the user. This mixture is burned incrementally in ten steps in the downstream direction during the second part of the combustion process. The pressure-area relation, heat release, gas mixture, and flow state are calculated at each of these steps. The inviscid combustor geometry is generated using the shape of the inlet exit and the newly calculated area of each successive combustor hoop. Similar to the inlet design algorithm, viscous properties are generated and the displacement thickness is carved from the surface to account for the boundary layer.

The “Nozzle” system element creates the nozzle geometry using the method of characteristics similar to the inlet design. The last shape of the combustor is used as the initial nozzle shape, and the exit conditions are computed by isentropically expanding the flow to the user specified inlet area to exit area ratio. The method of characteristics is then used to determine the flow field shape, with a user specified nozzle truncation factor that allows for nozzle designs that are not fully expanded. The streamlines from the initial hoop are again traced through the flow field, the inviscid surface defined, a

boundary layer analysis applied, and the nozzle surface determined. The nozzle performance is then determined from the defined shape.

Now that the inlet, combustor, and nozzle have been defined, the vehicle's entire internal flow surface is determined. The "ExtSurf" system element then "wraps" the vehicle from the inlet capture hoop to the nozzle exit hoop to enclose the inner surface and form the external surface. Inviscid properties are then established for this surface, but it is not necessary to carve this displacement thickness out of the surface since it is an external surface.

Wings and tails are sized for the airbreathers based on the takeoff characteristics specified, and are generally thin to reduce drag during airbreathing segments.

3.3.3 Common System Elements

The "PropellantUsage" system element calculates the fuel required by the vehicle throughout the flight. The flight is broken into three trajectory segments per stage as previously described in Figure 11. A SSTO vehicle could use all three segments in a single stage, while a TSTO vehicle only uses one or two of the segments per stage, as shown in Figure 15. The first segment is either a turbine or rocket segment, the second segment is the DMSJ segment, and the third segment is always a rocket segment. The user specifies four velocities corresponding to the start and stop of each segment, and a segment can be omitted by setting the start and stop velocities to be the same. In each segment, the user can also enter a "Velocity vs. I_{sp} " table for the specific method of propulsion used, or select one of many from a drop-down list in HySIDE.

A RLV using the rocket vehicle model uses either the first trajectory segment for a booster or the third trajectory segment for an orbiter. The rocket engines are sized in the “EngineCluster” system element based on the takeoff thrust, which is actually at takeoff for a rocket booster and at the beginning of trajectory segment three for either an all-rocket or RBCC orbiter. “PropellantUsage” calculates the mass flow rate of propellant using

$$\dot{m} = \frac{T_{TO}}{I_{sp} \cdot g} \quad (16)$$

where I_{sp} is given in the user-selected “Velocity vs. I_{sp} ” table and T_{TO} is the takeoff thrust required, as given by eq. (10). For rockets, HySIDE’s default tables assume a basic rocket trajectory and takes into account changes in atmospheric pressure in the “Velocity vs. I_{sp} ” table. The mass flow rate is then held constant for the duration of the rocket trajectory segment. The user must also specify the proper mass ratio between fuel and oxidizer so the proper amounts of each are calculated. The total mass and volume of propellant required for the segment is calculated by integrating the mass flow rate over the time required to complete the segment.

If a turbine is used in the first segment, the mass flow rate of fuel required is given by

$$\dot{m}_f = \dot{m}_a \cdot \phi \cdot FuelStoicRatio \quad (17)$$

where ϕ is the equivalence ratio, *FuelStoicRatio* is the fuel stoichiometric mass ratio, and \dot{m}_f and \dot{m}_a is the fuel and air mass flow rates, respectively. The air mass flow rate is found using

$$\dot{m}_a = \rho \cdot A_{inlet} \cdot V \cdot AreaRatio \quad (18)$$

Where A_{inlet} is the geometric inlet capture area, and $AreaRatio$ is calculated as a function of Mach number. It is a power series equation that gives the ratio of actual area of captured air to the design area of captured air. The user must also set the mass ratio to zero since turbines require no oxidizer to be carried onboard. The total mass of fuel is determined again by integration.

The second trajectory segment is always used for the DMSJ. Since the individual vehicle components have been designed for optimal DMSJ operation based on the FreeStream input, the design point is used to calculate the required mass flow rate. The characteristics of the entire engine flowpath, including pressure forces and viscous forces, are known at every point. The net thrust applied to the vehicle is calculated by integrating the map of these forces to give a value of the design point thrust, T_{DP} . The specific impulse at this design point is found using

$$I_{sp,DP} = \frac{T_{DP}}{\dot{m}_f \cdot g} \quad (19)$$

where m_f is found using eqs. (16) and (17). To calculate I_{sp} at off-design conditions, the values in the “Velocity vs. I_{sp} ” table are used to generate a trend. The difference between the calculated specific impulse at the design point, $I_{sp,DP}$, and the specific impulse in the table, $I_{sp,table}$, is found using

$$\Delta I_{sp} = I_{sp,DP} - I_{sp,table} \quad (20)$$

This difference is I_{sp} at the design point is then applied to all points on the table to find the I_{sp} for all off-design velocities in the DMSJ trajectory using

$$I_{sp} = I_{sp,table} + \Delta I_{sp} \quad (21)$$

Now that the vehicle size, mass, and propulsion system characteristics are known, the “Trajectory” system element combines the variables together to find the forces described in section 3.2, Flight Fundamentals. HySIDE uses the industry-standard code Missile DATCOM to calculate the RLV aerodynamic characteristics. Missile DATCOM uses six-degree of freedom equations to find aerodynamic characteristics at various angles of attack, altitudes, and speeds ranging from subsonic to supersonic.

HySIDE calculates the lift using eq. (2). The wing planform area has already been found in the “Wing” system element, and Missile DATCOM has generated tables for lift coefficient. HySIDE finds the correct angle of attack such that the lift required is equal to the lift available. The drag at this angle of attack is calculated using eq. (3) from the drag coefficient at this angle of attack as calculated by Missile DATCOM. The mass of the vehicle is also known at all points along the flight trajectory. The gravity “losses,” which is the thrust necessary to overcome the force of gravity, is found using

$$G_{loss} = M \cdot g \cdot \frac{\frac{\Delta H}{\Delta t}}{V} \quad (22)$$

where $\frac{\Delta H}{\Delta t}$ is the change in vehicle height over time, or the vertical velocity.

Now that three of the four aerodynamic forces have been found, the only one left is the thrust. The thrust produced by the propulsion system is given by

$$T = \dot{m} \cdot I_{sp} \cdot g \quad (23)$$

where \dot{m} is the mass flow rate of propellant (fuel and oxidizer) for rockets and the mass flow rate of fuel for both turbine and DMSJ engines. However, since drag and gravity losses both oppose the thrust, the net vehicle thrust can also be found. These forces are converted to the effective specific impulse, EI_{sp} , using

$$EI_{sp} = I_{sp} - \frac{D}{\dot{m} \cdot g} - \frac{G_{loss}}{\dot{m} \cdot g} \quad (24)$$

The net vehicle thrust is then found using

$$T_{net} = \dot{m} \cdot EI_{sp} \cdot g \quad (25)$$

The actual flight trajectory can also be manually entered in this system element or selected from a drop-down menu. Different trajectories are used for the first trajectory segment depending on takeoff type, but the second segment trajectory is always determined by path required to maintain a constant dynamic pressure. The third trajectory segment, used only on orbiters in this study, is also different depending on whether the stage is an RBCC or a pure rocket. The position, velocity, and acceleration of the vehicle is calculated at each point along this trajectory, which is used by the “PropellantUsage” system element to calculate the mass of propellant required. A new GTOW is then calculated and HySIDE uses the convergence subroutine described in section 3.3 to repeat the calculations.

3.4 Design Assumptions

3.4.1 Propulsion System

Throughout the design process, assumptions were made to determine the best way to model the performance, masses, and sizes of the various propulsion types used. The engine performance data for both a nominal rocket and turbine are scaled up or down in HySIDE, called “rubberizing,” to meet the required thrust for the vehicle being modeled. The next section describes the nominal engines that were selected.

3.4.1.1 Turbine Engines

The Air Force Research Laboratory, Propulsion Directorate (AFRL/PR), is researching many new advanced propulsion types, including turbines and DMSJs. The turbines in this study was assumed to be capable of propelling a vehicle to at least Mach 4. AFRL/PR provided performance data for their conceptual Mach 4.4 turbine accelerator design for use in this study. The 2004 and 2005 AFIT RLV studies both used this data as well, which is found in Appendix A [7, 8]. From this table, a “Velocity vs. I_{sp} ” table for use in the first segment of “PropellantUsage” was used, as shown in Table 2. A statistical jet-engine model, based on historical data for afterburning engines, is used to determine the uninstalled weight and size. They are given by:

$$W_{uninstalled} = 0.063 \cdot \left(\frac{T_{TO}}{\#of\ turbine\ engines} \right)^{1.1} \cdot M_{max}^{0.25} \cdot e^{-0.081 \cdot BPR} \cdot 0.8 \quad (26)$$

$$L_{uninstalled} = 0.255 \cdot \left(\frac{T_{TO}}{\#of\ turbines\ engines} \right)^{0.4} \cdot M_{max}^{0.2} \cdot 0.8 \quad (27)$$

$$D_{uninstalled} = 0.024 \cdot \left(\frac{T_{TO}}{\#of\ turbines\ engines} \right)^{0.5} \cdot e^{0.04 \cdot BPR} \cdot 0.9 \quad (28)$$

where M_{max} is the maximum Mach number and T_{TO} , the takeoff thrust, is given by eq. (10) [35:235]. The factors of 0.8 and 0.9 on the end of the above three equations are used to reflect technology advancements, since W, L, and D are all based on historical trends and future engines will be lighter and smaller. This study used a bypass ratio of 0.95 to be consistent with the 2004 SpaceWorks study and the 2005 AFIT RLV study [6, 8:46].

Table 2. HySIDE “Velocity versus I_{sp} ” table for AFRL turbine accelerator

V, ft/sec	ISP (sec)
0.000	2122.000
500.000	1963.000
800.000	1776.000
1000.000	1745.000
1500.000	1787.000
2000.000	1780.000
2500.000	1735.000
3000.000	1676.000
3250.000	1630.000
3750.000	1535.000
4000.000	1501.000
4400.000	1453.000
4500.000	0.000
10000.000	0.000
27000.000	0.000

The uninstalled weight calculated from eq. (26) refers only to the engine itself, while the installed weight of an engine includes the equipment necessary for it to function in a vehicle, including inlet and nozzle. HySIDE uses a turbine installation factor, $k_{installed}$, to account for this to calculate the installed turbine weight:

$$W_{installed} = W_{uninstalled} \cdot k_{installed} \cdot k_{overall} \quad (29)$$

The turbines in this study used an installed thrust-to-weight ratio of eight, which is expected to be achievable in the next five to ten years. The thrust table from AFRL was unnecessary, since HySIDE rubberized the engine to match the thrust required.

3.4.1.2 DMSJ Engines

AFRL/PR again provided performance for a hydrocarbon DMSJ engine. Through the U.S. Air Force HyTech program, SpaceWorks Engineering, Inc, performed the 2004 SpaceWorks Engineering Study, as described in Section 2.6.4 [6]. Using SRGULL, a performance prediction code for scramjet engines, SEI derived DMSJ performance data for a 2-D lifting body configuration. This complete table of data is found in Appendix A. The “Velocity vs. I_{sp} ” table used in HySIDE to model this engine is found in Table 3. It consists of the HyTech data up to 8,250 fps (2,514.6 m/s), and values for 8,500 fps (2,590.8 m/s) to 13,000 fps (3,962.4 m/s) extrapolated based on cooling as described in section 3.4.2.1. Due to the integral nature of the DMSJ to the entire vehicle itself, no other sizing data is necessary to model this engine. For hydrogen DMSJ engines, HySIDE’s default “Velocity vs. I_{sp} ” was used to predict engine performance.

Table 3. HySIDE "Velocity versus I_{sp} " table for AFRL HyTech hydrocarbon DMSJ

V, ft/sec	ISP (sec)
0.000	0.000
3500.000	0.000
3750.000	1765.000
4000.000	1628.000
4500.000	1646.000
5000.000	1413.000
6000.000	975.000
7000.000	859.000
8000.000	771.000
8250.000	747.000
8500.000	650.000
9000.000	500.000
11000.000	100.000
13000.000	0.000
27000.000	0.000

3.4.1.3 Rocket Engines

As mentioned in section 3.3.1, rubberized nominal rocket engines were used for rocket engine performance data for this study. RD-180 rocket engines were used for hydrocarbon engine performance data. These engines are manufactured by RD AMROSS, a partnership between Pratt & Whitney in the US and NPO Energomash of Russia, and are currently used on the Atlas III and Atlas V EELV [57], representing the height of hydrocarbon rocket engine technology. Hydrogen rocket engine parameters came from Space Shuttle Main Engines (SSMEs), representing the best hydrogen rocket engine technology, and were rubberized to meet thrust requirements. Table 4 summarizes the nominal rocket parameters used by HySIDE in this study. This same data was used in the studies described in section 2.6: The 2004 AFIT RLV study used the same RD-180 engine data [7], and 2004 ASTROX study [13], 2005 AFIT RLV study

[8], and 2005 University of Maryland study [14] all used the same RD-180 and SSME engine data.

Table 4. Nominal rocket engine parameters

Engine	RD-180	SSME
Parameter		
Fuel	RP-1	H ₂
Oxidizer	LOX	LOX
Mixture Ratio	2.6/1	6.0/1
T/W Ratio (rocket)	80.0	73.3
Nozzle Area Ratio	36.4	77.5
Chamber Pressure (psia)	3,722	3,260
Characteristic Velocity (fps)	5,914	7,684
I _{sp} - Sea Level (s)	311.0	370.8
I _{sp} - Vacuum (s)	337.0	454.4
Average Thrust - Sea Level (lbf)	860,000	418,130
Average Thrust - Vacuum (lbf)	933,000	512,410
Weight (lbf)	11,675	6,990
Length (ft)	13.0	14.0
Diameter (ft)	9.8	8.0

The rocket vehicle calculates the weight of each rocket engine precisely, by sizing the pumps, combustion chamber, and nozzle, but for RBCCs, the thrust-to-weight ratio is used instead. The installed weight of the engines is given by

$$W_{Rkt} = \frac{T_{TO}}{\left(\frac{T}{W}\right)_{Rkt}} \cdot k_{overall} \quad (30)$$

where $\left(\frac{T}{W}\right)_{Rkt}$ is the rocket thrust-to-weight ratio as given in Table 4, and $k_{overall}$ is the overall design uncertainty factor. In order to provide a consistent comparison with previous studies, an overall design uncertainty factor, $k_{overall}$, of 1.25 was used for all vehicles as described in section 3.4.5. In a similar manner to turbine engines, the rocket

engines are not physically placed in the airbreathing vehicle as they are in the rocket vehicle.

3.4.2 Flight Trajectory Assumptions

3.4.2.1 Staging Velocity

For pure rocket vehicles, the staging velocity was chosen to be at 7,000 fps (2,133.6 m/s) based on the literature review and previous studies [7, 8, 14]. For vehicles using a turbine during the first trajectory segment, the turbine was used over its useful operating range, from 0 fps (0 m/s) to 4,000 fps (1,219.2 m/s). If the vehicle had no other propulsion on the first stage, i.e. pure turbine booster, staging occurred at 4,000 fps (1,219.2 m/s). If the stage had a DMSJ for the second segment, i.e. TBCC booster, staging instead occurred at the end of the DMSJ operation. For vehicles using a rocket during the first trajectory segment, the rocket was used only up to the low end of DMSJ operating range, or from 0 fps (0 m/s) to 4,000 fps (1,219.2 m/s). If the vehicle had no other propulsion of the first stage, i.e. pure rocket booster, staging occurred at 4,000 fps (1,219.2 m/s). If the stage had a DMSJ for the second segment, i.e. RBCC booster, staging instead occurred at the end of the DMSJ operation.

The upper velocity for DMSJ cutoff is a little more difficult to fix precisely. As the DMSJ continues to accelerate, the I_{sp} begins to slowly taper off, as shown in Figure 24 by the solid lines. Cooling becomes a significant issue at higher speeds, requiring extra fuel to be dumped into the engine so it does not overheat. This fuel, while unburned, does provide some momentum thrust, but the I_{sp} drops off even more sharply,

as shown by the dashed lines in Figure 24. EI_{sp} follows a similar trend, but with slightly lower values on the y-axis to account for gravity and drag losses.

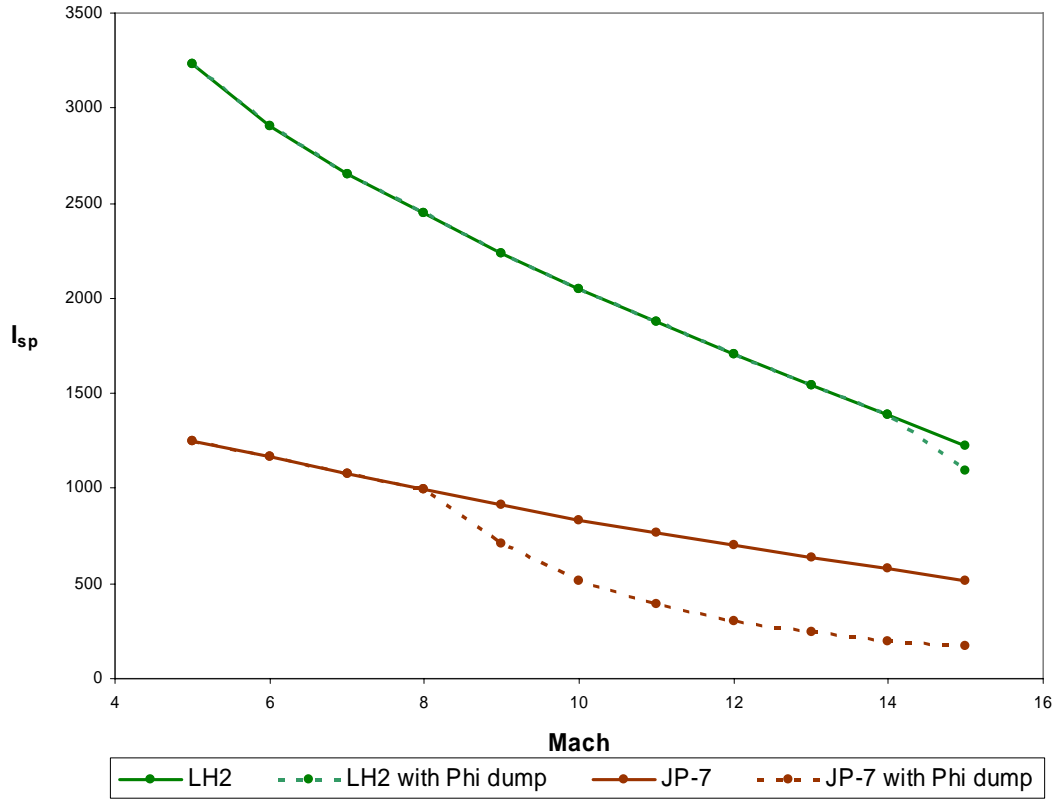


Figure 24. DMSJ I_{sp} variation with Mach number for different fuels [25]

One might think the appropriate velocity for DMSJ cutoff to be when the EI_{sp} of the DMSJ is equal to the I_{sp} of the rocket that will be ignited afterwards. For an RLV using a SSME rocket with an I_{sp} of 455 sec for the final segment, this would mean running the hydrogen DMSJ until the EI_{sp} equals 455 sec, then switching to the rocket. However, there is the factor of propellant bulk density to consider. DMSJ engines use only fuel, while rocket engines use both fuel and oxidizer. This results in different propellant bulk densities as shown in Table 5. Since the combined rocket propellant has

a larger mass for the same volume, a vehicle with a smaller empty mass results if the DMSJ is turned off prior to the EI_{sp} equaling the rocket I_{sp} . This is due to the difference in bulk densities, so the rocket essentially “gets rid of” more mass than the DMSJ does over the same velocity range. The difficult part is finding where the best cutoff point is, and previous studies have found this point for the hydrogen example to be around an EI_{sp} of 700 sec [28]. However, no precise value for this cutoff point exists, nor have any studies been done for other fuels.

Table 5. Bulk density of rocket and DMSJ propellants [19:571]

Propellant	Bulk Density (kg/L)	Bulk Density (lbm/ft ³)
RP-1/LOX	1.03	64.30
JP-7	0.82	51.19
LH ₂ /LOX	0.32	19.98
LH ₂	0.07	4.37

If the bulk density ratio (BDR) of the propellants is equal to one, then DMSJ cutoff should occur when the DMSJ EI_{sp} equals the rocket I_{sp} . If the vehicle begins using the rocket before this point, it is not taking full advantage of the DMSJ, but if the vehicle continues running the DMSJ beyond this point, the I_{sp} drops below that of the rocket and it is not using the most efficient engine for that velocity. For a hydrocarbon DMSJ followed by a hydrocarbon rocket, the bulk density ratio is close to one, but for the hydrogen DMSJ followed by a hydrogen rocket, which has been studied extensively, the ratio is close to seven. Using this data, Figure 25 and Table 6 show the values used in this study for the cutoff EI_{sp} for the DMSJ. This idea used in this study of DMSJ cutoff based on the BDR of propellants has generated interest in the hypersonic design

community, and a study is currently underway at the Aeronautical Systems Center, Aerospace Systems Design and Analysis Group (ASC/XRE) to investigate it further [28].

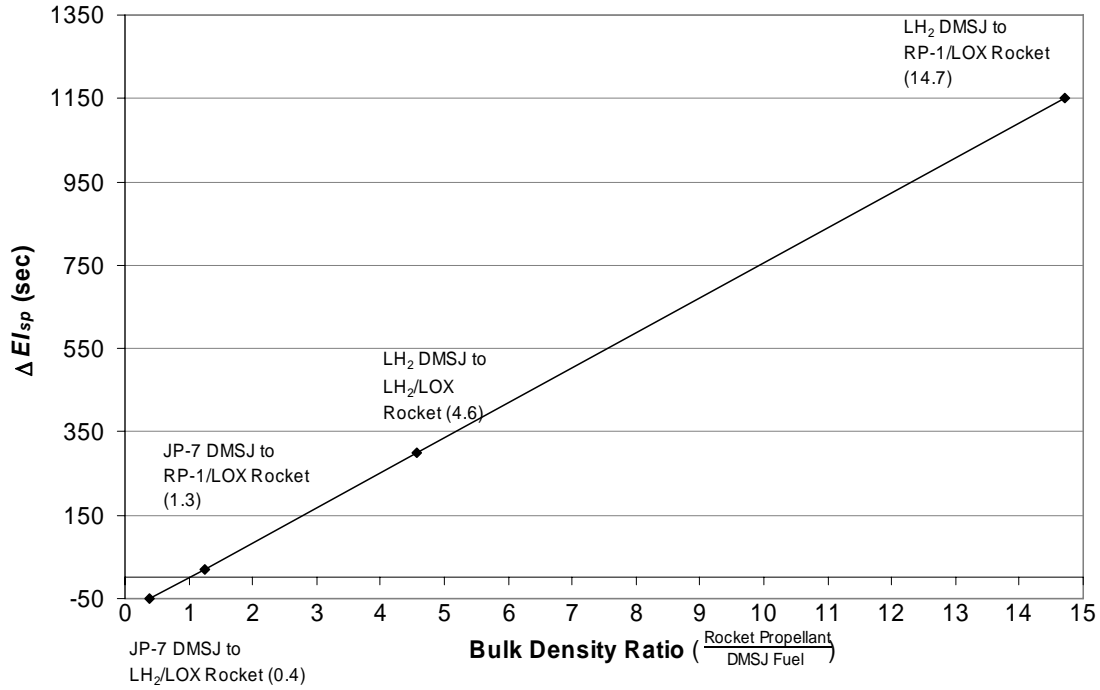


Figure 25. DMSJ cutoff EI_{sp} based on Bulk Density Ratio of propellants

Table 6. DMSJ cutoff EI_{sp} for different propellants

	BDR	ΔEI_{sp} (sec)	Rocket I_{sp} (sec)	DMSJ Cutoff EI_{sp} (sec)
JP-7 DMSJ to LH ₂ /LOX Rocket	0.39	-51	450	399
JP-7 DMSJ to RP-1/LOX Rocket	1.26	22	350	372
LH ₂ DMSJ to LH ₂ /LOX Rocket	4.57	300	450	750
LH ₂ DMSJ to RP-1/LOX Rocket	14.71	1152	350	1502

If the DMSJ is the last propulsion segment for the booster, i.e. TBCC-Rkt or RBCC-Rkt, the vehicle stages at DMSJ cutoff velocity, which is the velocity at which the EI_{sp} is equal to the value found using Table 6. If the DMSJ is on the orbiter, i.e. Rkt-RBCC or Turb-RBCC, then the DMSJ is used until the DMSJ cutoff velocity, then the

rocket is used for final orbital insertion. A summary of the velocity range during which each propulsion type is used is given in Table 7, with VTHL vehicles first and HTHL vehicles listed below the dashed line.

Table 7. Staging velocities and propulsion velocity ranges

Model	Start	Traj Seg 1	End	Start	Traj Seg 2	End	Staging Velocity	Start	Traj Seg 2	End	Start	Traj Seg 3	End
HCRkt-HCRkt	0 fps	HC Rkt	7,000 fps				7,000 fps				7,000 fps	HC Rkt	24,503 fps
HCRkt-HRkt	0 fps	HC Rkt	7,000 fps				7,000 fps				7,000 fps	H Rkt	24,503 fps
HRkt-HCRkt	0 fps	H Rkt	7,000 fps				7,000 fps				7,000 fps	HC Rkt	24,503 fps
HRkt-HRkt	0 fps	H Rkt	7,000 fps				7,000 fps				7,000 fps	H Rkt	24,503 fps
HCRBCC-HCRkt	0 fps	HC Rkt	4,000 fps	4,000 fps	HC DMSJ	8,300 fps	8,300 fps				8,300 fps	HC Rkt	24,503 fps
HCRBCC-HRkt	0 fps	HC Rkt	4,000 fps	4,000 fps	HC DMSJ	8,300 fps	8,300 fps				8,300 fps	H Rkt	24,503 fps
HRBCC-HCRkt	0 fps	H Rkt	4,000 fps	4,000 fps	H DMSJ	10,000 fps	10,000 fps				10,000 fps	HC Rkt	24,503 fps
HRBCC-HRkt	0 fps	H Rkt	4,000 fps	4,000 fps	H DMSJ	9,500 fps	9,500 fps				9,500 fps	H Rkt	24,503 fps
HCRkt-HCRBCC	0 fps	HC Rkt	4,000 fps				4,000 fps	4,000 fps	HC DMSJ	9,000 fps	9,000 fps	HC Rkt	24,503 fps
HCRkt-HRBCC	0 fps	HC Rkt	4,000 fps				4,000 fps	4,000 fps	H DMSJ	15,500 fps	15,500 fps	H Rkt	24,503 fps
HRkt-HCRBCC	0 fps	H Rkt	4,000 fps				4,000 fps	4,000 fps	HC DMSJ	9,000 fps	9,000 fps	HC Rkt	24,503 fps
HRkt-HRBCC	0 fps	H Rkt	4,000 fps				4,000 fps	4,000 fps	H DMSJ	15,500 fps	15,500 fps	H Rkt	24,503 fps
HRBCC-HCRkt	0 fps	H Rkt	4,000 fps	4,000 fps	H DMSJ	10,000 fps	10,000 fps				10,000 fps	HC Rkt	24,503 fps
HRBCC-HRkt	0 fps	H Rkt	4,000 fps	4,000 fps	H DMSJ	9,500 fps	9,500 fps				9,500 fps	H Rkt	24,503 fps
HCTBCC-HCRkt	0 fps	HC Turb	4,000 fps	4,000 fps	HC DMSJ	8,300 fps	8,300 fps				8,300 fps	HC Rkt	24,503 fps
HCTBCC-HRkt	0 fps	HC Turb	4,000 fps	4,000 fps	HC DMSJ	8,300 fps	8,300 fps				8,300 fps	H Rkt	24,503 fps
HCTurb-HCRBCC	0 fps	HC Turb	4,000 fps				4,000 fps	4,000 fps	HC DMSJ	9,000 fps	9,000 fps	HC Rkt	24,503 fps
HCTurb-HRBCC	0 fps	HC Turb	4,000 fps				4,000 fps	4,000 fps	H DMSJ	15,500 fps	15,500 fps	H Rkt	24,503 fps
HCTBCC-HRBCC	0 fps	HC Turb	4,000 fps	4,000 fps	HC DMSJ	8,300 fps	8,300 fps	8,300 fps	H DMSJ	15,500 fps	15,500 fps	H Rkt	24,503 fps
HCTurb-HCRkt	0 fps	HC Turb	4,000 fps				4,000 fps				4,000 fps	HC Rkt	24,503 fps
HCTurb-HRkt	0 fps	HC Turb	4,000 fps				4,000 fps				4,000 fps	H Rkt	24,503 fps

3.4.2.2 Takeoff and Landing Speeds

The trapezoidal “reference” planform wing area, S_{ref} , is calculated by HySIDE for each vehicle, but is found using different inputs if the vehicle is VTHL versus HTHL.

For VTHL, S_{ref} is calculated using the vehicle landing mass, landing velocity, and landing lift coefficient, but for HTHL, S_{ref} is calculated using the vehicle takeoff mass, takeoff velocity, and takeoff lift coefficient. HySIDE then calculates the exact dimensions of the wing based on this area and the specified geometric characteristics. For all models in this study, the takeoff and landing characteristics are given in Table 8.

Table 8. Wing sizing inputs

Stage \ Wing Sizing Input	VTHL Booster All Orbiters	HTHL Booster
Wing Sizing Mass	Final Mass	GTOM
Velocity (knots)	185	225
Lift Coefficient	0.6	0.9

For HTHL vehicles, takeoff speed is one of the primary inputs into wing sizing. The wing area required can be reduced by increasing the takeoff speed, which leads to lighter wings, less TPS area, and smaller drag penalties during the high-speed segments. This study uses a takeoff speed of 225 knots (115.8 m/s) to be consistent with the 2005 AFIT study and 2005 University of Maryland study [8:89, 14:34]. This speed is achievable on standard runways, with enough remaining runway length to allow a RLV to brake to a stop if loss of propulsion occurs during takeoff. This will allow HTHL vehicles to maintain their safety advantage over VTHL vehicles during the takeoff segment. As a comparison, a Boeing 747 has a takeoff speed of 153 knots (79 m/s) and a Concorde has a takeoff speed of 175 knots (90 m/s) [14:34]. For HTHL vehicles, a runway bearing load limit of 1,500,000 lbf (6,672,332.4 N) was assumed, but there is no gross mass limit for VTHL vehicles. This study used a landing velocity of 185 knots (95.2 m/s) for all vehicles, comparable to the space shuttle's landing velocity of 180 knots (92.6 m/s) [23:436].

3.4.2.3 Breguet Range Equation Variables

While HySIDE uses Missile DATCOM for all aerodynamic properties during the ascent, it relies entirely on user inputs for any type of cruise, including the flyback segment of the flight. Therefore, subsonic flight characteristics of each vehicle were calculated for this study to provide accurate inputs for HySIDE.

In order to maximize range with minimum fuel usage, a vehicle should fly at an angle of attack such that the lift and drag coefficients, C_L and C_D , produce a certain lift-to-drag ratio. For every vehicle, a subsonic drag polar can be constructed showing the range of C_L and C_D for every angle of attack, α . From this drag polar, the maximum L/D can be found as the slope of the line from the origin that is just tangent to the drag polar curve. The point of tangency is the value of C_L and C_D for the maximum lift-to-drag ratio, L/D_{max} , as shown in Figure 26. For a jet, the best range for cruising is found by flying at a slightly higher speed [35:27], resulting in a lower L/D as given by

$$\left(\frac{L}{D}\right)_{cruise} = 0.866 \cdot \left(\frac{L}{D}\right)_{max} \quad (31)$$

This results in the best range factor in eq. (11), the Breguet range equation.

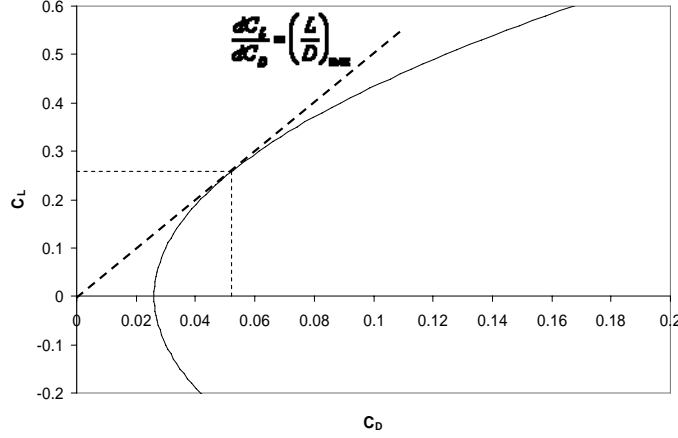


Figure 26. Drag polar showing flight conditions for maximum Lift-to-Drag Ratio

A drag polar is constructed using the relationship between the drag coefficient and lift coefficient, which for an uncambered wing is given by

$$C_D = C_{D0} + K \cdot C_L^2 \quad (32)$$

where C_{D0} is the lift coefficient at zero angle of attack, and K is given by

$$K = \frac{1}{\pi \cdot AR \cdot e} \quad (33)$$

where AR is the aspect ratio and e is the Oswald efficiency factor, which for swept-wing aircraft is given by

$$e = 4.61 \cdot (1 - 0.045 \cdot AR^{0.68}) \cdot (\cos \Lambda_{LE})^{0.15} - 3.1 \quad (34)$$

where Λ_{LE} is the leading edge sweep angle [35:360-361]. The value of C_{D0} , also called the parasite drag, can be found using a component buildup method. This method estimates the subsonic drag of each component using a calculated flat-plate skin-friction drag. The drag of each component is then added together and divided by the planform area:

$$C_{Do} = \frac{\sum \left(\frac{D}{q} \right)_{component}}{S_{ref}} \quad (35)$$

For a flat plate, the value of $\frac{D}{q}$ is found using

$$\frac{D}{q} = C_f \cdot S_{wet} \quad (36)$$

where S_{wet} is the wetted area of that component, and C_f is the flat-plate skin-friction coefficient [35:351]. C_f depends on whether the flow is turbulent or laminar, which can be determined from the Reynolds number as defined as

$$Re = \frac{\rho \cdot V \cdot L}{\mu} \quad (37)$$

where L is the characteristic length of the flat plate and μ is the fluid viscosity [35:343]. For flat plates, a Reynolds number above 500,000 is commonly considered fully turbulent flow. For this study, the flow over the entire vehicle is assumed to be turbulent as indicated by the calculated Reynolds numbers of over 500,000 for each component.

Standard atmospheric tables for density and viscosity at different altitudes are given in reference 2. For airfoils such as the wing and tail, the characteristic length used is the mean aerodynamic chord, MAC , found with

$$MAC = \frac{2}{3} \cdot c_r \frac{(1 + \lambda + \lambda^2)}{(1 + \lambda)} \quad (38)$$

where λ is the taper ratio and c_r is the root chord length [35:56]. For other surfaces such as the RLV exterior surface, inlet, and nozzle, the characteristic length used the length of that component measured in a direction parallel to the airflow over the component. Once

the Reynolds number of the flow over each component is known, the friction coefficient for that component can be found, which for turbulent flow is given by

$$C_f = \frac{0.455}{(\log_{10} \text{Re})^{2.58} (1 + 0.144M^2)^{0.65}} \quad (39)$$

The value of $\frac{D}{q}$ for each component is then found using eq. (36) [35:343].

Another part of the drag that must be considered is the base area drag, which is due to separation of the air flow from any aft-facing flat surface. This becomes particularly important during the flyback portion, when both the rockets and airbreathers are operating on turbine engines and have large flat surfaces facing rearward. The $\frac{D}{q}$ for subsonic base area drag is found using

$$\frac{D}{q} = \left[0.139 + 0.419(M - 0.161)^2 \right] \cdot A_{base} \quad (40)$$

where A_{base} is the area of the aft-facing surface [35:350]. For the rockets, this was the entire base area, while for airbreathers, some spillage was assumed to occur inside the nozzle. The value for base area drag for airbreathers was reduced by a factor of 0.6 to assume 40% spillage occurring in the rearward-facing airbreather nozzles.

After the $\frac{D}{q}$ for each component and the base area drag have been calculated, they are summed and divided by S_{ref} as shown in eq. (35) to find C_{D0} . The drag polar can now be constructed using eq. (32) and L/D_{max} and L/D for best cruising range found. The lift coefficient for best cruise is found using [35:537]:

$$C_{L_{cruise}} = \sqrt{\frac{C_{D0}}{3K}} \quad (41)$$

The corresponding $C_{D, cruise}$ can then be found using eq. (32), and the lift-to-drag ratio for best cruise can be found using

$$\left(\frac{L}{D}\right)_{cruise} = \frac{C_{L_{cruise}}}{C_{D_{cruise}}} \quad (42)$$

The velocity for best cruising range can be found using [35:537]:

$$V_{cruise} = \sqrt{\frac{2 \cdot W}{\rho \cdot S_{ref}}} \sqrt{\frac{3 \cdot K}{C_{D0}}} \quad (43)$$

where W is the vehicle weight at that point in flight. Table 9 shows a summary of the

values of $\left(\frac{L}{D}\right)_{cruise}$ and flyback velocity found for each vehicle, and a sample of the

calculations for a vehicle can be found in Appendix E.

Table 9. Best L/D and velocity for flyback

Vehicle	L/D _{cruise}	V _{flyback} (fps)	Mach _{flyback}	Range Factor (nm)	Change in Range Factor
<i>HySIDE Default Rocket</i>	<i>3.30</i>	<i>250</i>	<i>0.24</i>	<i>611.011</i>	
HCRocket-HCRocket	5.66	551	0.52	2310.315	278.11%
HCRocket-HRocket	5.63	549	0.52	2287.752	274.42%
HRocket-HCRocket	5.11	523	0.49	1979.776	224.02%
HRocket-HRocket	5.13	524	0.50	1993.397	226.25%
HCRocket-HCRBCC	5.48	542	0.51	2198.206	259.77%
HCRocket-HRBCC	5.47	542	0.51	2195.533	259.33%
HRocket-HCRBCC	5.24	530	0.50	2054.566	236.26%
HRocket-HRBCC	5.27	531	0.50	2072.196	239.14%
<i>HySIDE Default TBCC/RBCC</i>	<i>6.60</i>	<i>250</i>	<i>0.24</i>	<i>1222.021</i>	
HCRBCC-HCRocket	4.01	867	0.82	2572.897	110.54%
HCRBCC-HRocket	3.56	851	0.80	2243.752	83.61%
HRBCC-HCRocket	4.28	859	0.81	2723.224	122.85%
HRBCC-HRocket	3.85	842	0.80	2397.221	96.17%
HTHL HRBCC-HCRocket	4.99	827	0.78	3053.849	149.90%
HTHL HRBCC-HRocket	4.64	804	0.76	2762.764	126.08%
HCTBCC-HCRocket	4.43	814	0.77	2138.918	75.03%
HCTBCC-HRocket	4.07	814	0.77	1960.314	60.42%
HCTBCC-HRBCC	3.78	808	0.76	1810.164	48.13%
<i>HySIDE Default Turbine</i>	<i>14.00</i>	<i>250</i>	<i>0.24</i>	<i>2073.733</i>	
HCTurb-HCRBCC	8.39	668	0.63	3322.942	60.24%
HCTurb-HRBCC	6.70	681	0.64	2702.197	30.31%
HCTurb-HCRocket	8.75	667	0.63	3458.736	66.79%
HCTurb-HRocket	7.49	648	0.61	2877.057	38.74%

Table 9 gives the L/D and velocities organized by booster, with the default HySIDE value given first. The default values in HySIDE underestimate the L/D for flyback of rockets by approximately 60%, and overestimate the L/D of airbreathers by 55% for the TBCCs and RBCCs and 75% for the turbines. In addition, the flyback velocities for best range for rockets are over 100% greater than the default, and around 300% greater for TBCCs, RBCCs, and turbines. These new values not only affect the mass of fuel required on all boosters, found by eq. (11), but also the size and weight of the flyback turbine engines that must be added to rocket and RBCC boosters, as found by eqs. (12), (13), and (14). The range factor for each is also shown in Table 9, showing the overall effect of the new flyback values using an assumed SFC of 0.8 or 1 as will be discussed on the following page. The default flyback values in HySIDE are pessimistic, although the range factors for different vehicle types are affected by a different amount. On average, the rockets are a range factor 250% greater than the default, the DMSJ vehicles have a range factor 95% greater, and the turbine boosters have a range factor 65% greater with a RBCC orbiter and 35% greater with a rocket orbiter.

After calculating the L/D for each vehicle, new vehicles were sized using the new L/D. The new dimensions changed the L/D for each vehicle slightly, so a new L/D was calculated. Ideally, this would be an iterative process until both the L/D and vehicle dimensions remained unchanged. However, even after the second L/D calculation, the value for L/D changed by less than 0.2, indicating that the first value calculated was close to what the final value would be. In the interest of time, the calculated L/D from the first vehicle dimensions was used throughout the study for each vehicle.

The only values still unknown in the Breguet range equation, eq. (11), are the range itself and the *SFC* of the engine. For typical jet engines, such as the two small flyback engines in rocket and RBCC vehicles, the *SFC* while cruising at 700-800 fps (213.4-243.8 m/s) is 0.8 lbm/lbf·hr (22.7 mg/Ns), which corresponds to an I_{sp} of 4,500 sec [35:23]. However, the TBCC and turbine vehicles do not have flyback engines, but instead use the large turbines for flyback. These turbine accelerators are designed to accelerate to high Mach numbers, and are not as efficient at cruising subsonically. This study assumed an *SFC* of 1 lbm/lbf·hr (27.24 mg/Ns) or an I_{sp} of 3,600 sec for these engines.

The range is more difficult to find. HySIDE outputs the vehicle distance downrange at staging, but this vehicle is now many thousands of feet in the air, traveling at a speed of up to 10,000 fps (3,048 m/s) away from the landing site. Determining the distance to return it to the takeoff point requires more extensive calculations. This distance is critical since any mass required for a flyback propulsion system is carried through the booster's entire flight starting at takeoff. It is essentially dead mass the booster must lift and accelerate.

At staging, the rocket vehicles are traveling at about a 20 deg angle relative to the horizon and are located at some height above the earth's surface and some distance downrange. The vehicle is essentially on a ballistic trajectory and will eventually fall back to earth. There are two methods of returning the vehicle to the takeoff point so it can be recovered: flyback and boostback. For flyback, the vehicle continues on this ballistic trajectory, decelerates through a high angle of attack decent and atmospheric

“skip,” and turns approximately 180 deg, and flies back to the takeoff point using turbine engines, as shown in Figure 27. For boostback, the booster rotates itself 180 deg after staging and fires its rockets a second time. The vehicle’s velocity changes from downrange to back uprange, towards the starting point. It then glides back to the landing point [28].

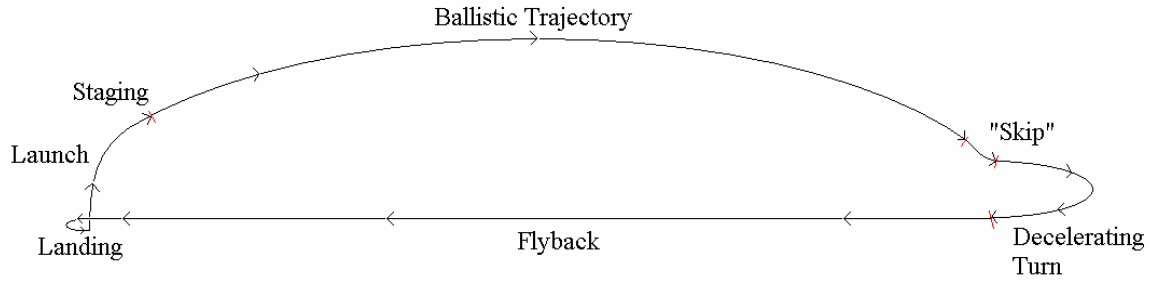


Figure 27. Side view of rocket RLV flyback trajectory

HySIDE is currently able to model flyback returns, provided the proper inputs are provided. To determine the exact distance, the distance the vehicle travels in the ballistic trajectory must be found. The horizontal distance traveled is given by

$$d = \frac{V \cdot \cos \theta}{g} \cdot \left(V \cdot \sin \theta + \sqrt{V^2 \cdot \sin^2 \theta + 2 \cdot g \cdot y_0} \right) \quad (44)$$

where d is the distance the rocket travels from the staging point, θ is the angle at which the rocket is traveling at staging, and y_0 is the height of the rocket at staging [37:79-80]. In addition, the rocket must turn through approximately 180° to change the direction of flight back to the launching point. The radius of this turn is given by

$$R = \frac{V^2}{g \cdot \tan \phi} = \frac{V^2}{g \cdot \sqrt{n^2 - 1}} \quad (45)$$

where R is the turn radius, ϕ is the bank angle and n is the load factor [35:551]. For this study, a bank angle of 60° was used, corresponding to a load factor of two. The rockets were assumed to have decelerated during the ballistic portion of flight and the turn, and the turbine engines were used from the completion of the turn until landing. The total distance for flyback then becomes the total sum of the downrange distance at staging, the horizontal distance traveled during the ballistic trajectory, and a small distance for maneuvering necessary for landing. The horizontal distance required to fly back was most sensitive to the velocity at staging, since this velocity determines the distance traveled during the parabolic trajectory. For rocket boosters staging at 7,000 fps (2,133.6 m/s), the flyback distance is around 300 nm (555.6 km).

The airbreathing vehicles, on the other hand, are traveling nearly horizontal at the staging point, so no ballistic trajectory calculations are necessary. However, at staging, the vehicles are traveling at high speeds and must either continue forward while decelerating, or decelerate through the turn. The radius of this turn can become quite large since it varies with velocity squared, as shown in eq. (45). In addition, the airbreathing segment often takes the vehicle downrange by over 700 nm (1,111.2 km), as shown in Figure 28. These long ranges add extra mass required for the flyback propulsion and fuel to airbreathing boosters.

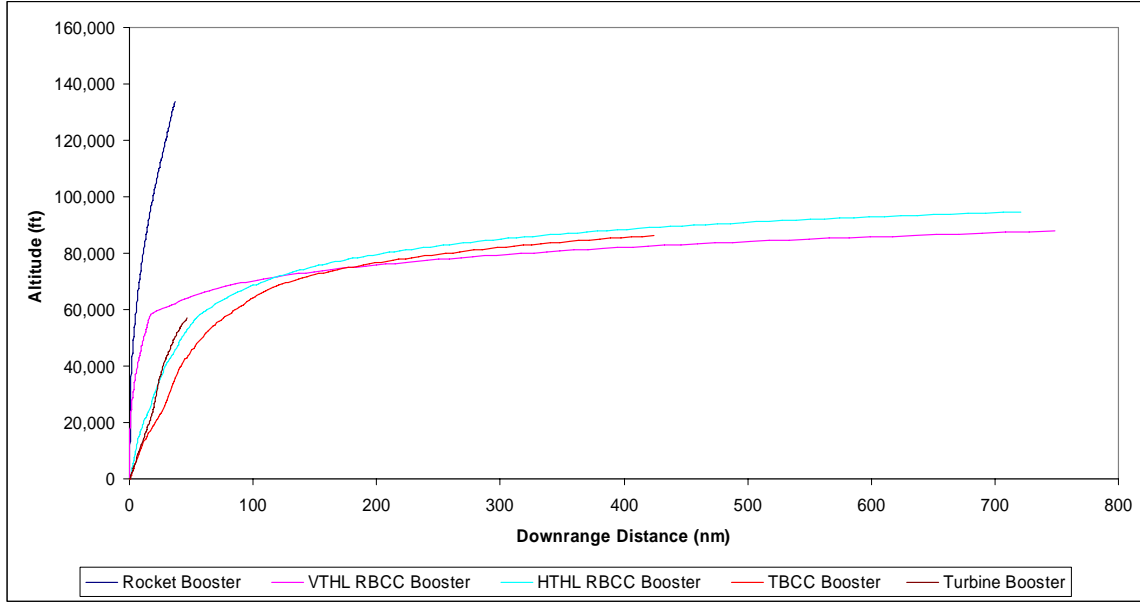


Figure 28. Booster altitude and downrange distance at staging point

To calculate the flyback range, this study assumed the airbreathers decelerate during the turn, reaching the flyback speed at the completion of the turn. This turn carries the vehicle a large distance in a direction perpendicular to the flight, as shown in Figure 29. This study assumed a linear deceleration from the staging velocity to the flyback velocity, and the turn would require an addition 15 deg (0.1π) due to the perpendicular distance, for a total turn of 195 deg (1.1π). The velocity, as a function of the turn angle, θ , is given by

$$V(\theta) = V_{stage} - \frac{V_{stage} - V_{cruise}}{1.1\pi} \theta \quad (46)$$

where V_{stage} is the staging velocity and V_{cruise} is the best velocity for flyback as found with eq. (43), both in feet per second. The radius of the turn, as a function of the turn angle, is given by substituting eq. (46) into eq. (45) as shown:

$$R(\theta) = \frac{\left(V_{stage} - \frac{V_{stage} - V_{cruise}}{1.1\pi} \theta \right)^2}{g \cdot \tan \phi} \quad (47)$$

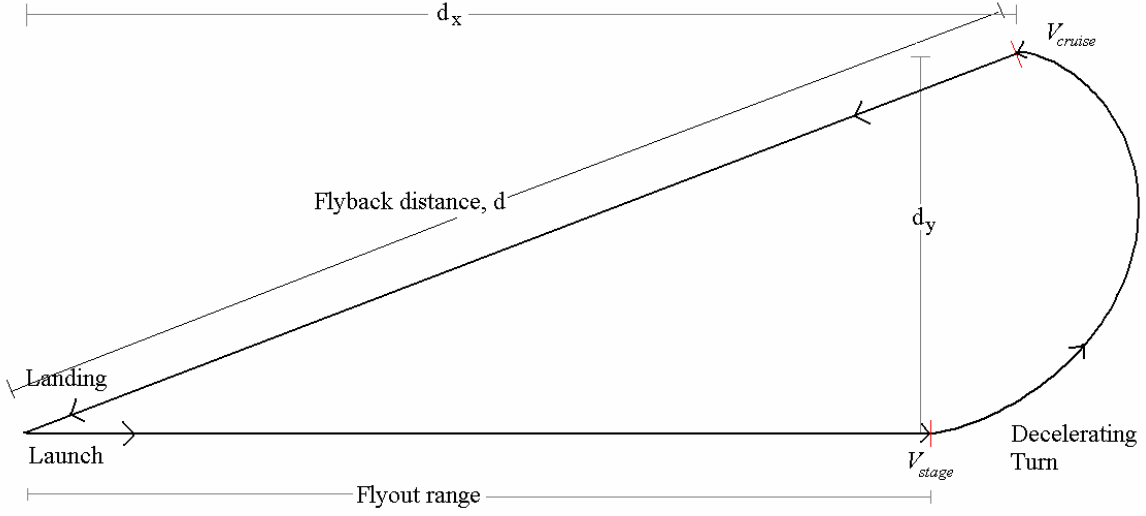


Figure 29. Top view of airbreathing RLV flyback trajectory

The distance at the end of the turn from the starting point can be found in both the x and y directions by integrating each x and y portion of the arc as shown:

$$d_x = \int_0^{1.1\pi} \theta \cdot \cos \theta \cdot \frac{\left(V_{stage} - \frac{V_{stage} - V_{cruise}}{1.1\pi} \theta \right)^2}{g \cdot \tan \phi} d\theta \quad (48)$$

$$d_y = \int_0^{1.1\pi} \theta \cdot \sin \theta \cdot \frac{\left(V_{stage} - \frac{V_{stage} - V_{cruise}}{1.1\pi} \theta \right)^2}{g \cdot \tan \phi} d\theta \quad (49)$$

The total distance an airbreather must travel back is given by the hypotenuse of the triangle shown in Figure 29 is:

$$d = \sqrt{\left(Range + \int_0^{1.1\pi} \theta \cdot \cos \theta \cdot \frac{\left(V_{stage} - \frac{V_{stage} - V_{cruise}}{1.1\pi} \theta \right)^2}{g \cdot \tan \phi} d\theta \right)^2 + \left(\int_0^{1.1\pi} \theta \cdot \sin \theta \cdot \frac{\left(V_{stage} - \frac{V_{stage} - V_{cruise}}{1.1\pi} \theta \right)^2}{g \cdot \tan \phi} d\theta \right)^2} \quad (50)$$

where *Range* is the distance downrange at staging in feet. The approximate distances for flyback and weight fractions can now be found and are given below:

Table 10. Vehicle ranges and weight fractions

Vehicle	Range (nm)	W _f /W _i
<i>HySIDE Default Rocket (example)</i>	<i>250</i>	<i>0.664</i>
HCRocket-HCRocket	300	0.878
HCRocket-HRocket	300	0.877
HRocket-HCRocket	300	0.859
HRocket-HRocket	300	0.860
HCRocket-HCRBCC	120	0.947
HCRocket-HRBCC	120	0.947
HRocket-HCRBCC	120	0.943
HRocket-HRBCC	120	0.944
<i>HySIDE Default TBCC/RBCC (example)</i>	<i>1200</i>	<i>0.375</i>
HCRBCC-HCRocket	865	0.714
HCRBCC-HRocket	850	0.685
HRBCC-HCRocket	860	0.729
HRBCC-HRocket	840	0.704
HTHL HRBCC-HCRocket	825	0.763
HTHL HRBCC-HRocket	805	0.747
HCTBCC-HCRocket	815	0.683
HCTBCC-HRocket	815	0.660
HCTBCC-HRBCC	810	0.639
<i>HySIDE Default Turbine</i>	<i>300</i>	<i>0.865</i>
HCTurb-HCRBCC	100	0.970
HCTurb-HRBCC	105	0.962
HCTurb-HCRocket	100	0.972
HCTurb-HRocket	100	0.966

3.4.3 Inlet Geometry

The inlet geometry can be varied using the RDP variable for airbreathing vehicles, and this inlet geometry affects the entire vehicle geometry. Since the vehicle is

essential to the DMSJ operation, the propulsive force of the engine as well as the aerodynamics, surface area, and volume area all affected by this shape. The two-dimensional “wedge” has been well researched in recent years, including the 2005 AFIT RLV study, which used 2-D geometry for all vehicles [8:89].

Recently, the inward-turning flowfield has become more prominent in research and has several potential gains [14:35-37, 28, 29]. There is less wetted area in the high heat regions in the combustor and adjacent areas in the inlet and nozzle, resulting in a 35% reduction in the active cooling requirement and a 50% reduction in heat transfer over a similar 2-D geometry, as shown in Figure 30 [14:38]. In addition, the single flowpath reduces the complexity in the inward turning geometry over the six to eight flowpaths required in a 2-D vehicle. The 2005 University of Maryland RLV study considered a VTHL RBCC in both a 2-D and inward turning configurations and found significant improvements in aerodynamics as well, as evidenced by the EI_{sp} increase as shown in Figure 31 [14:37]. This also allows the DMSJ to be run to a higher velocity, since the EI_{sp} cutoff does not occur until later, as is easily seen in Figure 31. A trade study conducted during the design of the baseline vehicles in this study confirmed that inward-turning geometry also results in a lower vehicle empty mass. The results for two vehicles are shown in Table 11.

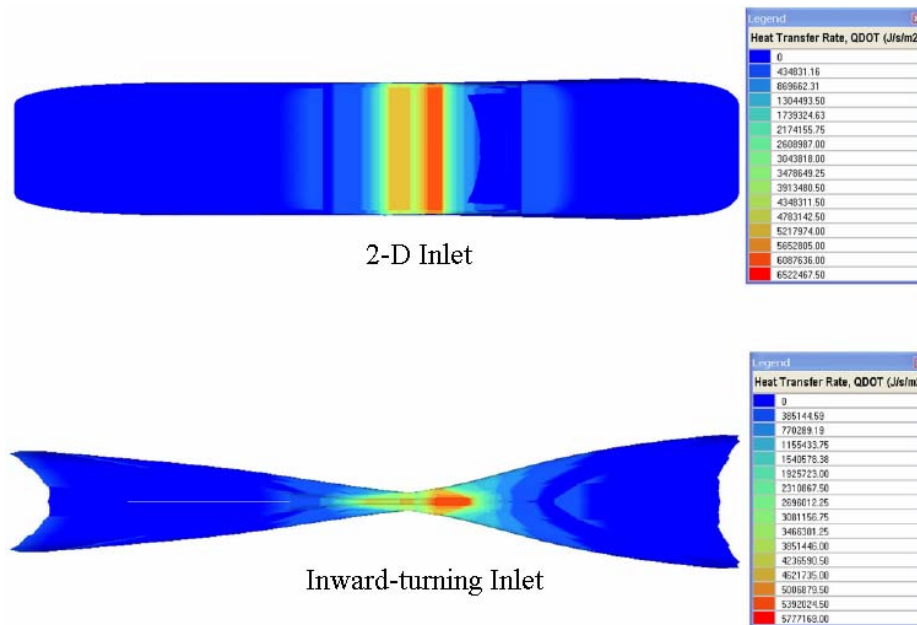


Figure 30. Heat transfer rates for vehicle inlet geometry [14]

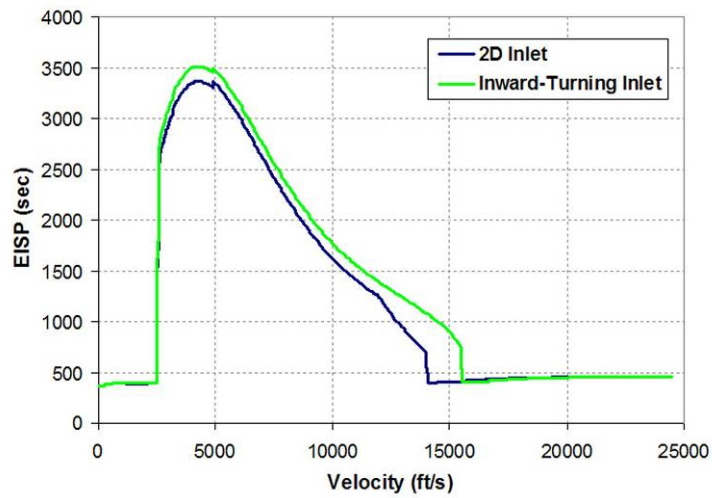


Figure 31. EI_{sp} comparison of 2-D and inward turning vehicles [14]

Table 11. Empty mass comparison of 2-D and inward-turning vehicles

	Inward-Turning HCTurb-HRBCC	2-D HCTurb-HRBCC	Inward-Turning HCRkt-HRBCC	2-D HCRkt-HRBCC
Booster Propellant	65,634	85,154	264,001	347,234
Booster Empty	193,255	240,916	41,509	51,598
Orbiter Propellant	157,713	208,245	230,570	200,716
Orbiter Empty	76,590	101,544	73,375	97,249
Payload	20,000	20,000	20,000	20,000
Gross Mass (lbm)	513,188	655,857	629,452	716,793
Empty Mass (lbm)	269,844	342,461	114,884	148,846

Based on these findings, this study used inward turning geometry for RBCC vehicles. Rockets can be easily integrated into inward turning vehicles. Unfortunately, the integration of turbine engines is difficult to do, even with a 2-D inlet geometry [14:47]. As shown in Figure 13, turbines require a separate flowpath to supply the necessary inlet air, as well as occupying a portion of the vehicle interior volume. This figure only shows a single turbine engine, but the 2005 AFIT RLV study went into great detail as to how the turbine engines were placed within the vehicle interior, and found that as many as 13 turbines may be required [14:56]. Both the volume of the turbines as well as the volume of the inlet and exit flowpaths necessitate sizing up the vehicle to account for the fuel volume that has been displaced [14:48]. The most common method of turbine engine integration used is the “over-under” configuration shown in Figure 13, where the turbine engines are located above the DMSJ [39]. Due to the additional complexities and design challenges involved with properly integrating the flowpath inlets and exits, TBCC vehicles in this study were modeled using 2-D inlet geometry.

3.4.4 Tank Sizing

The “TankStack” system element calculates the mass and volume of the tanks required to hold the fuel and oxidizer for the airbreather. HySIDE uses the NASA CR287, AFRL/VA SP125, and RMLS methods to determine the mass of a cylindrical propellant tank that correlates to the space shuttle external tank [22, 28]. However, the tanks in airbreathers are conformal tanks due to the shape of the vehicle, which will always weigh more than standard cylindrical propellant tanks for the same volume. The exact increase in mass is still unknown, so a mass is calculated using the NASA CR287 method, which is then multiplied by a k-factor. To be consistent with the 2005 University of Maryland study, this study uses a scaling factor of 1.4 applied to all conformal propellant tanks [14:46]. In the rocket vehicle, the tanks are physically placed, but in airbreathers, the tanks are left as abstract mass and volume requirements.

3.4.5 K-Factor Overall ($k_{overall}$)

In light of flyback error corrections (see section 3.4.2.3) consistency checks were made with past studies. This study’s gross and empty masses of the two vehicles common to the 2005 AFIT study [8], the 2005 University of Maryland study [14], and the Reusable Military Launch System (RMLS) [29] and Responsive Space Advanced Technology Study (RSATS) [29] were compared. Using the original flyback model, this study found gross masses and empty masses were within 4% of the vehicles in the other studies, as shown in Table 12, which is as good as can be expected. However, after applying the improved values of flyback as discussed in section 3.4.2.3, the gross mass of the rocket-rocket vehicles dropped by nearly 25% and the empty mass by 15%. These

masses are below what is considered a reasonable launch mass for this type of launch system, indicating that HySIDE models were underestimating mass [28]. Two options were considered: a) Accept the optimistic masses and proceed, or b) Increase the design margin and hence lower the development risks. The latter was chosen to produce more conservative results. Therefore, the design uncertainty factor, $k_{overall}$, for all models in this study was increased from 1.10 to 1.25 for all models to provide a consistently larger design margin and a more conservative estimate for all vehicle masses. This approach maintained more consistency with past studies and current conservative mass estimates. However, the relative comparisons between concepts remains unchanged had either options been chosen. The new masses are shown in the final column of Table 12.

Table 12. K-factor adjustment

HC Rocket- H Rocket	2004 AFIT study	2005 U of M study	This study (default flyback)	This study (new flyback)	This study (new flyback and adjusted k factor)
Gross Mass	1,171,489 lbm	1,207,696 lbm	1,192,305 lbm	894,664 lbm	1,191,491 lbm
Empty Mass	174,683 lbm	160,577 lbm	167,916 lbm	143,096 lbm	167,150 lbm

3.4.6 Validation of Models

The baseline vehicle models in this study were based on several previously used in the 2005 AFIT [8], the 2005 University of Maryland [14], and RSATS [29] studies with several modifications, in addition to many new models. For the systems that could be compared, these differences produced slightly different results, as can be seen in Table 13.

Table 13. RLV study empty mass comparison

	T/O	2005 AFIT				2005 Univ. of Maryland				This Study	
		Gross Mass		Empty Mass		Gross Mass		Empty Mass		Gross Mass	Empty Mass
		(lbm)	Dif	(lbm)	Dif	(lbm)	Dif	(lbm)	Dif	(lbm)	(lbm)
HCRkt-HCRkt	VTHL	1,484,234	1.6%	161,067	5.4%	1,419,856	2.8%	179,737	5.6%	1,460,637	170,215
HCRkt-HRkt	VTHL	1,207,696	1.4%	160,577	3.9%	1,171,489	1.7%	174,683	4.5%	1,191,492	167,150
HRkt-HRkt	VTHL					1,020,968	6.6%	214,596	0.6%	1,093,083	213,372
HCRBCC-HCRkt	VTHL	1,314,218	4.7%	168,105	26.3%					1,255,000	228,225
HCRBCC-HRkt	VTHL	1,131,683	9.7%	172,602	35.1%					1,252,757	266,000
HCRkt-HRBCC	VTHL					524,916	27.3%	109,985	30.2%	721,923	157,574
HRBCC-HRkt	HTHL					1,146,410	24.8%	283,994	4.4%	918,749	297,096
HCTBCC-HCRkt	HTHL	998,384	15.6%	310,861	0.0%					863,587	310,726
HCTBCC-HRkt	HTHL	859,725	5.8%	286,870	9.4%	836,365	3.0%	320,000	1.1%	812,303	316,526
HCTurb-HRBCC	HTHL					629,951	14.5%	301,673	23.7%	550,389	243,779
HCTurb-HCRkt	HTHL	1,464,540	3.6%	426,466	5.3%					1,413,550	450,138
HCTurb-HRkt	HTHL	1,144,101	3.4%	372,863	5.7%					1,106,615	395,304

The significant differences are summarized below:

1. Improved estimates for the lift to drag ratio and flyback velocities were calculated for each individual vehicle. Both previous studies used HySIDE's default values for each, which were lift-to-drag ratios of 3.3 for rockets and 6.6 for airbreathers, and a flyback velocity of 250 fps (76.2 m/s) for all vehicles. This study found rockets had better flyback lift-to-drag ratios of between 5 to 6, while RBCC and TBCC airbreathers had lower ratios of between 3 to 5, and best subsonic flyback speeds between 600 and 800 fps (182.9 and 243.8 m/s). These changes lowered the gross and empty masses of all vehicles and was significant enough to warrant the reexamination of the mass relations used in all of the models. It was decided to increase the design margin k-factor by 15% for all of the vehicles to bring them in line with past studies and add conservatism.

2. All vehicles in this study having an airbreathing booster returned to the launch point with the empty mass of the orbiter stage plus payload mass to simulate an abort. It was assumed that in an abort scenario that the upper stage propellants would be dumped.

The vehicles in both previous studies flew back with the gross mass of the orbiter stage. This change significantly reduced the mass of the flyback propulsion required for the airbreathing vehicles, but had no effect on the rockets.

3. All RBCC vehicles used inward-turning inlets. All RBCCs for the AFIT study were 2-D inlets, while the Maryland study used 2-D inlets for HTHL vehicles and both inward-turning and 2-D inlets for VTHL vehicles. All studies used 2-D inlets for TBCC vehicles. In addition, the mass of several components calculated by HySIDE for RBCC vehicles was thought to be underestimated, particularly for HC RBCCs. This became obvious when an RBCC vehicle using only rocket propulsion to accomplish the same trajectory as a rocket had a smaller empty mass than the rocket vehicle. The packing efficiency, wing weight per unit area, TPS thickness, and masses of components based on volume were adjusted to more conservative levels to remove this logical inconsistency.

4. Turbine boosters for this study were modeled using two turbine engine nacelles as did the Maryland study, while the AFIT study used a single 2-D inlet vehicle. The different modeling approach using nacelles was shown to be logically inconsistent when it was found that a Mach 8 hydrocarbon (HC) TBCC vehicle empty mass was about 20% smaller than the HC turbine booster going to Mach 4 when both were sized to the same liftoff mass. The Mach 4 turbine booster has no fuselage, scramjets or TPS, and should have had a smaller empty mass. Mass inconsistencies in TPS and structure were found and eliminated. The corrected turbine vehicle comes in lighter than the TBCC.

5. Engine data from AFRL was used for the turbines and hydrocarbon DMSJ. The AFIT study used the same data, while the Maryland study used HySIDE's predicted

performance data. The AFIT study used only hydrocarbon Dual Mode Scramjet (DMSJ) engines, while the Maryland study used only hydrogen DMSJ engines. DMSJ shutoff velocity for this study was selected based on the effective specific impulse of each vehicle. All studies used identical rocket engines.

While there were quite a few differences between the vehicles in this study and the previous studies using HySIDE, some changes tended to cancel each other out. As a result, the gross and empty masses of the vehicles in this study differed slightly from the masses of comparable vehicles in other studies. In general this study's models predict vehicles with larger masses than 2005 AFIT [8], and University of Maryland [14] studies but slightly lower masses than the RSATS [29] study. The 2005 AFIT Study and the 2005 University of Maryland study reflected optimistic estimates for vehicle masses, while the RSATS study estimated masses conservatively. Therefore, for the common systems that can be compared, the mass estimates for this study are bracketed by the results of previous studies. This study's refinements improved the existing HySIDE models as well as built entirely new ones. All models used in this study were provided to ASTROX for inclusion in the next release of HySIDE.

3.5 Mission Descriptions

Once the baseline vehicles were designed and data for baseline empty mass and wetted area were obtained, three missions were defined to determine each design's ability to perform different military missions. The next section describes the missions and assumptions made for each.

3.5.1 Payload Sizing Impact Study

In the 2005 University of Maryland RLV study, two of the TSTO vehicles were scaled to launch payloads of 20,000 lbm (9,071.8 kg) to 70,000 lbm (31,751.5 kg) [14:149-161]. Growth rates for each vehicle type were obtained, but no data were gathered for less than 20,000-lbm payloads (9,071.8 kg-payloads). In the future, mini-satellites and micro-satellites will be used increasingly, making the lower end of the payload range equally important. Therefore, the study examined the growth rate of all 21 models using payload masses varying from 0 lbm (no payload) to 30,000 lbm (13,607.8 kg). This will fill the gap in data not covered by the 2005 University of Maryland study but still overlap a portion to assure continuity. In addition, the growth rates of all 21 models can be used to project empty masses and wetted areas for payload larger than 30,000 lbm (13,607.8 kg).

3.5.2 Orbital Rendezvous Mission

In the field of orbital mechanics, trying to get two orbiting objects in close proximity presents unique challenges. There are several reasons for this, including the facts that a launch vehicle cannot launch directly into an orbit of lesser inclination than the launch site's latitude and that two-body motion equations now dictate the results of all maneuvers made by satellites [41:62, 41:78].

Furthermore, any orbital maneuvering that must be made to place a satellite in its desired orbit requires fuel that must also be launched with the satellite as part of the launch vehicle's payload. The amount of fuel required for any orbital maneuver is given by a version of the rocket equation:

$$m_p = m_i \left(1 - e^{\frac{-\Delta V}{V_e}} \right) \quad (51)$$

where m_p is the mass of propellant required, m_i is the mass of the vehicle at the start of the maneuver, and ΔV is the change in velocity required [21:13].

The mission requiring the most critical launch time is the launch of a spacecraft to rendezvous with another object already in orbit. This is done to limit the number of maneuvers required in orbit, which would reduce the useful payload [41:77]. Launch windows, within a few seconds at most, are established to attempt by determining when the desired orbital plane is directly overhead as seen from the launch site [41:79]. If a given inclination or right ascension of the ascending node (RAAN) is desired, the launch is timed so that the payload is released at just the right time to have these orbital characteristics. A launch can also be timed so that a vehicle can rendezvous with another vehicle in the same orbit. However, it is challenging to get the RAAN, inclination, and phasing to all coincide for a direct launch to the orbital rendezvous. The orbital plane may be directly over the launch site, but the satellite or space station that the payload needs to rendezvous with may be on the other side of the earth. In this case, an orbital phasing maneuver is used to bring the satellites together, but can take several days [41:78-80]. Likewise, the target satellite could be at the same argument of latitude as the launch site, but the orbital plane may be currently directly over Europe.

A change in orbital plane, such as an inclination change, is one of the most costly orbital maneuvers to make in terms of fuel required [41:76]. One frequent maneuver made is to change the inclination from the launch inclination, which is equal to the launch

location's latitude, to 0 deg inclination for a geosynchronous orbit. To avoid this change, some countries have placed their launch sites in other countries situated on the equator or even launched from floating platforms located in the ocean at the equator [49, 58]. This has the added benefit of requiring less total ΔV to reach an easterly orbit since the earth's surface rotates fastest at the equator.

For orbital insertion at perigee into a 50 nm (92.6 km) by 100 nm (185.2 km) orbit, the inertial velocity required is 25,841 fps (7,876.3 m/s), as found by

$$V = \sqrt{\frac{2\mu}{a_1} - \frac{2\mu}{a_1 + a_2}} \quad (52)$$

where a_1 is the orbit's semi-major axis, a_2 is the orbit's semi-minor axis, and μ is the gravitational parameter [41:75]. The earth rotates at an angular rate, ω , of 360 deg every 24 hours, so any point on the earth's surface is moving easterly at a velocity, V_s , given by

$$V_s = \omega \cdot R_{earth} \cdot \cos \theta \quad (53)$$

where R_{earth} is the radius of the earth and θ is the latitude of the point [37:280]. Cape Canaveral, at 28.5 deg north latitude, is moving at 1,337 fps (407.6 m/s); Vandenberg AFB, at 34.75 deg north latitude, is moving at 1,250 fps (381.1 m/s); and any point on the equator is moving at 1,521 fps (463.8 m/s). Thus, a rocket launching from Cape Canaveral eastward into a 50 nm (92.6 km) by 100 nm (185.2 km) orbit requires a final earth-relative velocity of 24,503 fps (7,468.5 m/s), while a rocket launching from the equator requires 24,319 fps (7,412.6 m/s). A rocket launching westward from Vandenberg requires a final earth-relative velocity of 27,091 fps (8,257.4 m/s).

The orbiter enters the 50 nm (92.6 km) by 100 nm (185.2 km) orbit at the perigee, and continues to the apogee point. Once there, the orbiter executes an OMS burn of 90.9 fps (27.7 m/s) to circularize the orbit, releases the payload, and executes a second OMS burn to reduce the orbital velocity enough to reenter the atmosphere. This study assumed a launch from Cape Canaveral, so the payload is placed in a 100 nm (185.2 km) circular orbit at a 28.5 deg inclination. To get to a geosynchronous orbit, both the orbital altitude and inclination of the payload's current orbit must be changed, but a payload launched from the equator would only have to change its orbital altitude, increasing the mass of the satellite that can be placed in the final orbit.

A Hohmann transfer can be used to increase the altitude of an orbit. It consists of two ΔV maneuvers, one to place the satellite into an elliptical transfer orbit, and a second to circularize the orbit at the desired altitude. The total change in velocity is given by:

$$\Delta V = (V_{t,p} - V_i) + (V_{geo} - V_{t,a}) \quad (54)$$

where V_{geo} is the velocity of a satellite in geosynchronous orbit, 10,950 fps (3,337.4 m/s), $V_{t,a}$ is the velocity of the satellite at the apogee of the transfer orbit, $V_{t,p}$ is the velocity of the satellite at the perigee of the transfer orbit, and V_i is the velocity of the satellite in its initial circular orbit [41:75]. If an inclination change is made in conjunction with the Hohmann transfer, it is split between the two velocity changes. The total change in velocity for this maneuver is

$$\Delta V = \sqrt{V_i^2 + V_{t,p}^2 - 2 \cdot V_i \cdot V_{t,p} \cdot \cos(\Delta i_1)} + \sqrt{V_{geo}^2 + V_{t,a}^2 - 2 \cdot V_{geo} \cdot V_{t,a} \cdot \cos(i - \Delta i_1)} \quad (55)$$

where i is the total inclination change and Δi_i is the inclination change accomplished during the first Hohmann burn [41:95]. For the ΔV in eq. (54) and (55), the total mass of propellant required to make this change in velocity can be found using eq. (51). This mass of propellant can then be subtracted from the 20,000 lbm (9,071.8 kg) payload to determine the final mass of the satellite that can reach orbit.

With airbreathing propulsion, launch vehicles have the ability to essentially change their launch location by flying to a new location prior to beginning the ascent to orbit. Two potential advantages this could have would be to expand the launch window by allowing the vehicle to intercept the desired orbital plan and to allow the inclination of the initial orbit to be lower than the launch location's latitude. Thus, an airbreather that could fly to the equator with a 20,000 lbm (9,071.8 kg) total payload could place a greater mass satellite in geosynchronous orbit by not having to make the inclination change in orbit that a rocket launched from Cape Canaveral would have to. Another way this could be considered is that for the same final payload mass to geosynchronous orbit from a total 20,000-lbm (9,071.8-kg) payload launched from Cape Canaveral, a vehicle that could fly to the equator would require a total payload of less than 20,000 lbm (9,071.8 kg). To do so, the vehicle would have to fly approximately 1,720 nm (3,185 km) to reach the equator from Cape Canaveral or 2,090 nm (3,870 km) from Vandenberg AFB. A launch from Cape Canaveral would involve overflying South America for several hundred miles at potentially supersonic speeds, turning 90° to head east, and then accelerating over Brazil. This is not practical, but a launch from Vandenberg would fly

and accelerate over the Pacific Ocean. Therefore, an initial distance of 2,090 nm (3,870 km) was selected.

Aerodynamic characteristics for the Breguet range equation were again calculated. For the vehicles with turbines, the subsonic lift over drag calculations are shown in Appendix E for the best range factor, and summarized on Table 14. However, the RBCC vehicles must fly out during the DMSJ portion of the flight. As shown in Figure 24, the I_{sp} for DMSJ engines decrease as velocity increases, but the lift over drag curve is relatively flat in the hypersonic regime, as shown in Figure 32. Therefore, the best range factor occurs at the low end of the DMSJ portion of the flight. The RBCC-Rocket vehicles must cruise prior to staging with the rocket orbiter still attached, while the Rocket-RBCC vehicles can cruise immediately after staging with no second stage. The lift over drag value used for the RBCC-Rocket vehicles was 3, while a value of 3.5 was used for the RBCC orbiter vehicle. Using these values, the initial distance of 2,090 nm (3,870 km) resulted in HTHL vehicles with gross masses that greatly exceeded the assumed runway load limit of 1,500,000 lbf (6,674,612.2 N). As will be explained in Chapter 4, flying to the equator was not feasible. Therefore, a value of 1,000 nm (1,852 km) was chosen for the orbital rendezvous study. While this is not the 2,090 nm (3,870 km) required to fly to the equator, it will give an idea of how each vehicle grows with a required cruise distance. The 1,000 nm (1,852 km) range can still be used to accomplish some degree of inclination change as well as allow the vehicle to launch into the desired orbital plane with an expanded launch window.

Table 14. Best vehicle range factors for flyout

Vehicle	L/D _{cruise}	Turbine			L/D _{cruise}	V _{flyout} (fps)	DMSJ	
		V _{flyout} (fps)	SFC (1/hr)	Range Factor (nm)			SFC (1/hr)	Range Factor (nm)
HCRBCC-HCRkt	-	-	-	-	3	4000	2.2113	3215
HRBCC-HRkt	-	-	-	-	3	4000	0.92	7728
HCRBCC-HCRkt	-	-	-	-	3	4000	2.2113	3215
HRBCC-HRkt	-	-	-	-	3	4000	0.92	7728
HCRkt-HCRBCC	-	-	-	-	3.5	4000	2.2113	3751
HCRkt-HRBCC	-	-	-	-	3.5	4000	0.92	9016
HRkt-HCRBCC	-	-	-	-	3.5	4000	2.2113	3751
HRkt-HRBCC	-	-	-	-	3.5	4000	0.92	9016
HRBCC-HCRkt	-	-	-	-	3	4000	0.92	7728
HRBCC-HRkt	-	-	-	-	3	4000	0.92	7728
HCTBCC-HCRocket	4.13	976	1	2385	3	4000	2.2113	3215
HCTBCC-HRocket	3.91	955	1	2214	3	4000	2.2113	3215
HCTurb-HCRBCC	8.02	880	1	4181	3.5	4000	2.2113	3751
HCTurb-HRBCC	6.57	796	1	3098	3.5	4000	0.92	9016
HCTBCC-HRBCC	3.68	926	1	2022	3	4000	2.2113	3215
HCTurb-HCRocket	8.31	895	1	4406	-	-	-	-
HCTurb-HRocket	7.05	825	1	3442	-	-	-	-

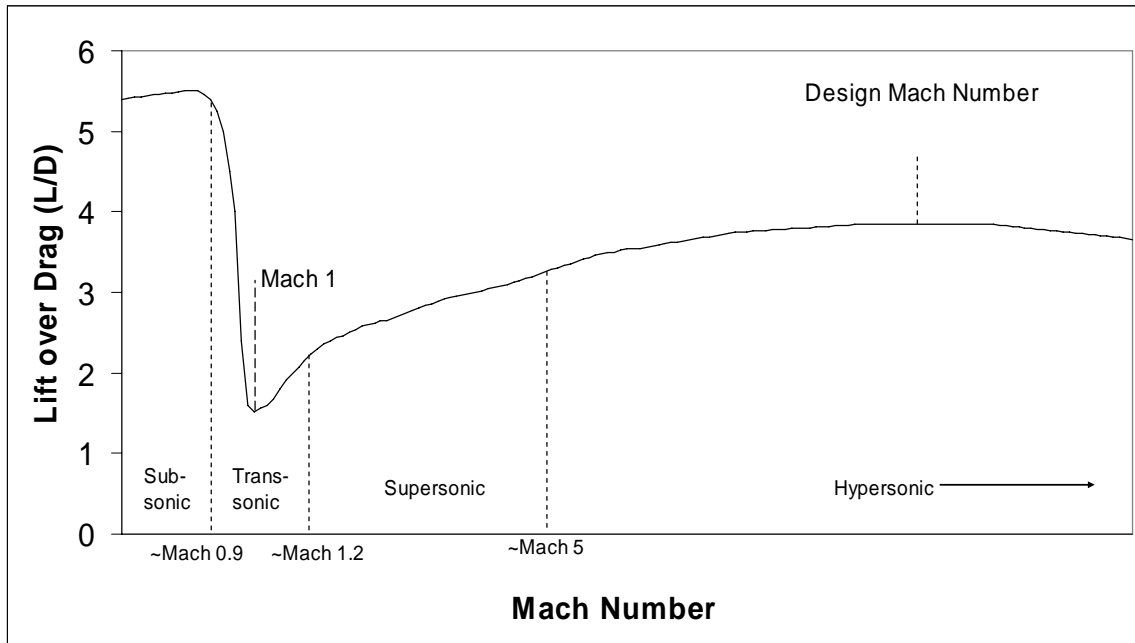


Figure 32. Typical hypersonic vehicle lift-over-drag profile

3.5.3 Prompt Global Strike Mission

For the global strike mission, a suborbital trajectory was chosen. The ballistic range of a projectile is determined by its initial velocity and is given by

$$Range = 2 \cdot R_{earth} \cdot \cos^{-1} \left(\frac{2\sqrt{1-\gamma^2}}{2-\gamma^2} \right) \quad (56)$$

where γ is given by

$$\gamma = \frac{V}{\sqrt{R_{earth} \cdot g_0}} \quad (57)$$

where V is the initial velocity [1:721] and g_0 is the standard sea level acceleration due to gravity. The range can therefore be plotted as a function of the initial velocity, as shown in Figure 33. Based on the current range of the Minuteman III ICBM, which is 6,000+ statute miles, a range of 6,000 statute miles (9,656.1 km) was selected, corresponding to an initial velocity required of 23,500 fps (7,162.8 m/s) [44]. This is only 1,000 fps (304.8 m/s) less than orbital velocity. This is comparable to the space shuttle, which separates from the external tank at a velocity of 725 fps (221 m/s) less than its orbital velocity. Even this small change is enough to place the orbiter in orbit, while the external tank reenters the atmosphere and splashes in the Indian Ocean [23:452]. If maneuvering CAVs with good lift-over-drag characteristics are used, the 6,000 statute mile (9,656.1 km) range can be increased significantly.

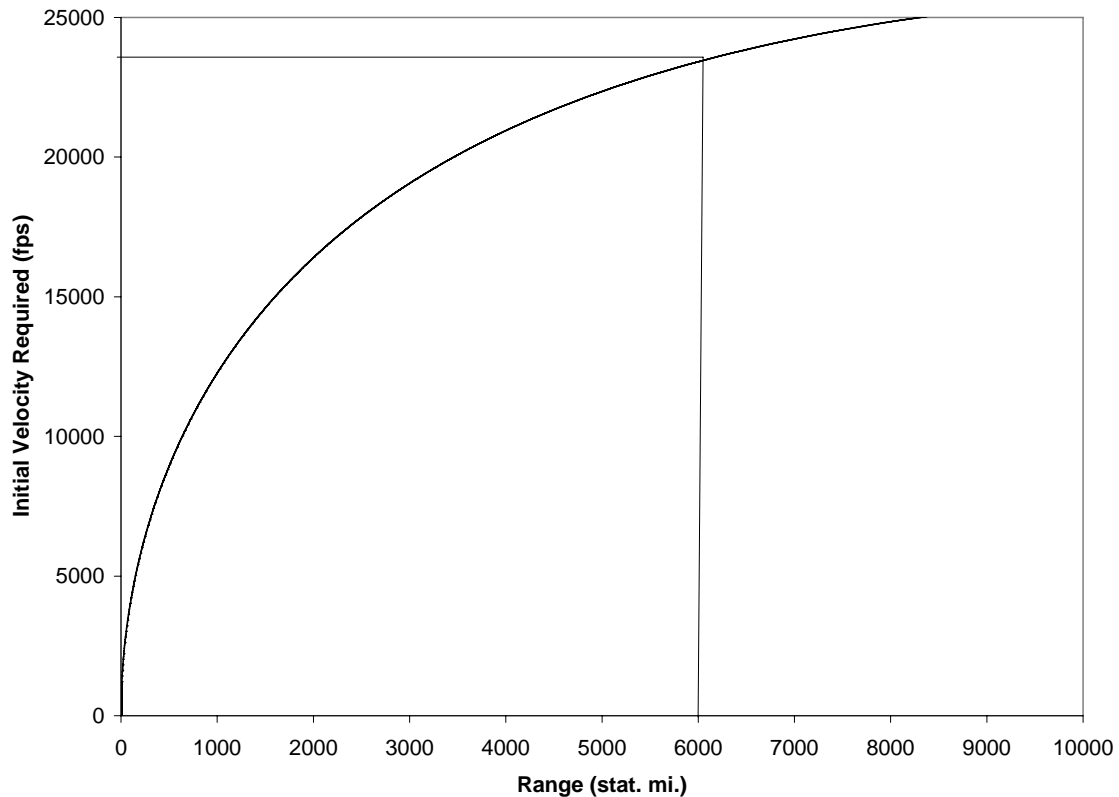


Figure 33. Initial velocity required for ballistic range

Since this is a suborbital trajectory, the orbiter stage cannot complete a complete orbit to return to its launch site. Therefore, the orbiter stages were made expendable for this mission. This eliminated the requirement for wings, TPS, landing gear, OMS, and even RCS. This resulted in a large mass savings for the vehicle, but the payload also dictated unique requirements. Combat aerial vehicles (CAVs) would be most likely to be used for this mission, which would require a payload bus to carry them. The mass of the bus required to carry the CAVs usually doubles the mass of the usable payload [29:2]. Therefore, a payload module mass of 40,000 lbm (18,143.7 kg) was used for this mission.

4. Analysis and Results

This chapter presents and discusses the results of the TSTO RLV study.

ASTROX Corporation's HySIDE code was used to create each model and analyze the performance of each RLV. The baseline vehicles were designed to place a 20,000 lbm (9,071.8 kg) payload module into a 100 nm (185.2 km) circular orbit, with both stages being fully reusable. The turbine engine performance was modeled using performance data and thrust-to-weight ratios provided by AFRL/PR, representing technology achievable in the next 5-10 years [15]. Hydrogen DMSJ engines have been extensively studied, so HySIDE's predicted performance data was used for these engines.

Hydrocarbon DMSJ engine data, also provided by AFRL/PR, represents the state of current research in the HyTech program [15, 33:1170-1171]. Though individual propulsion or takeoff options may have unique requirements, all inputs were kept the same between RLVs whenever possible, and are given in Appendix C. This allows an accurate comparison between vehicles as much as possible, though ascent trajectories vary by several hundred miles of flyout as well as ascent rate, as shown in Figure 34.

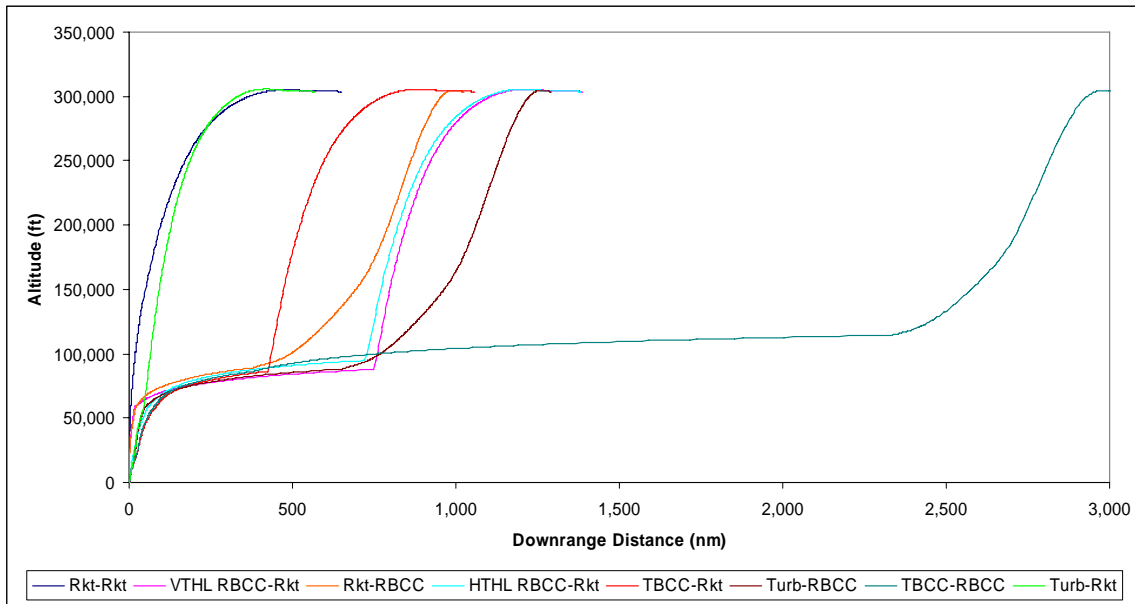


Figure 34. Baseline configuration RLV ascent trajectories

The all of the vehicle trajectories are almost identical up to 50,000 feet (15,240 m), at which point most vehicles have a velocity of 4,000 fps (1,219.2 m/s). The Rkt-Rkt vehicles continue accelerating, stage at 133,000 feet (40,538.4 m), and quickly exit the atmosphere. The Turb-Rkt stages at 4,000 fps (1,219.2 m/s), but the rocket orbiter continues to accelerate and gain altitude rapidly. All of the vehicles with a DMSJ begin this trajectory segment at 4,000 fps (1,219.2 m/s) and follow a path of constant dynamic pressure as they accelerate. This results in a more horizontal path during which they accelerate but do not gain much altitude. At the end of DMSJ operation, the RBCC-Rkt and TBCC-Rkt vehicles stage, and the rocket executes a “pitch-up” maneuver to begin a more vertical trajectory, as seen by the sharp upward turn in the trajectories of the RBCC-Rkt and TBCC-Rkt after the relatively horizontal DSMJ segment. The vehicles with

airbreather upper stages, such as the Rkt-RBCC, Turb-RBCC, and TBCC-RBCC, follow a smoother, curving trajectory to reach orbit. These trajectory differences translate into differences in booster flyback, vehicle heating, and vehicle drag. In particular, the airbreathers are sensitive to drag during the horizontal DMSJ portion of the trajectory.

The first section of this chapter presents the baseline vehicle results for empty mass and wetted area, and gives details about gross masses and active areas. The second section of this chapter discusses the results of the payload study and details how the various vehicle configurations' growth rates change with increasing payload masses. The third section presents the orbital rendezvous vehicle results and describes how each vehicle is able to change the orbital trajectory. The fourth section discusses the results of the global strike study and which vehicles are the most feasible. Finally, the fifth section compares the results of this study with two previous studies that have also used HySIDE as a validation of the results.

Results for the vehicles are given first in a table showing all vehicles ranked by empty mass and wetted area, followed by a more detailed explanation of empty masses and wetted area for each takeoff configuration. The detailed results are given as shown in Figure 35. For the masses, the boosters are shown in purple on the bottom part of the bar, and the orbiters are shown in green in the top part of the bar. For the gross masses, the vehicle empty mass is given in light green or light purple, the propellant mass is given in dark green or dark purple, and the payload is shown in blue. The empty mass chart shows only the vehicle empty masses, the light purple part for boosters and the light green part for boosters. Likewise, the area bar chart shows the total wetted area and

active area of each vehicle, and uses the same colors as the mass charts to denote stages.

The results are given all fueling options of each model shown together, with a dashed line in between different models. The fuel type used on each stage is shown by the “HC” for hydrocarbon (RP-1 or JP-7) or “H” for hydrogen, centered on the bar graph. The velocity listed above each bar is the staging velocity, 8,000 fps (2,438.4 m/s) in this example.

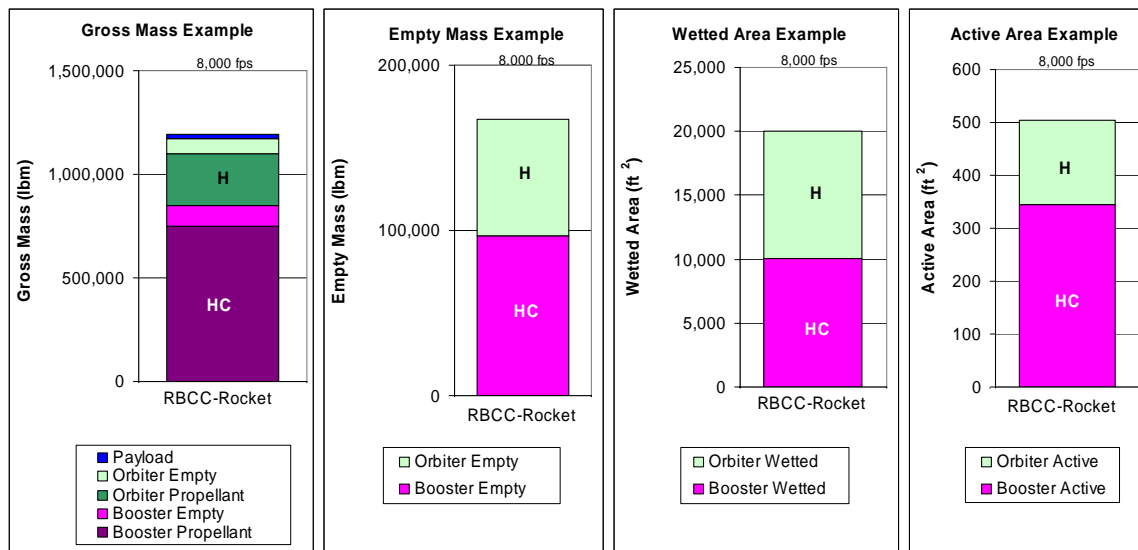


Figure 35. Example of how result are presented in this study

All masses were obtained from HySIDE’s Weight Display outputs. This output gives masses for each individual component, along with each amount of propellant used. The empty mass of each stage includes all structure, TPS, propellant tanks, propulsion systems, landing gear, and ancillary equipment. The propellant mass includes propellant used for launch, cruise (if applicable), RCS, OMS, and flyback. The vehicle gross mass is the sum of both stages’ empty masses, propellant masses, and the payload, while the vehicle empty mass is the sum of both stages’ empty masses. The wetted area is the sum

of wetted areas for both stages, and the active area is the sum of all areas requiring active cooling, provided by the fuel circulated through the panels.

4.1 Baseline RLV Results

For this study, the primary figures of merit are the vehicle empty mass and wetted area. Table 15 lists the 21 baseline RLVs ranked in ascending order for both figures of merit for the baseline payload module mass. These results show that the HCRkt-HCRBCC has the lowest empty mass at 142,846 lbm (64,794 kg) and the smallest wetted area at 15,879 ft² (1,475 m²). The best HTHL vehicle for empty mass is the HCTurb-HRBCC with an empty mass of 243,779 lbm (110,576 kg), and the best HTHL vehicle for wetted area is the HCTBCC-HCRkt with a wetted area of 23,152 ft² (2,151 m²), both of which are not quite double the best VTHL vehicle. The heaviest empty RLV also had the largest wetted area: the HCTurb-HCRkt masses 450,138 lbm (204,179 kg) empty and has a wetted area of 39,502 ft² (3,670 m²). Complete data for the baseline vehicles are given in Appendix G.

Table 15. Baseline RLV empty masses and wetted areas

	T/O	Empty Mass (lbm)		
		Booster	Orbiter	Total
HCRkt-HCRBCC	VTHL	81,799	61,047	142,846
HCRkt-HRBCC	VTHL	63,336	94,239	157,574
HCRkt-HRkt	VTHL	96,923	70,228	167,150
HCRkt-HCRkt	VTHL	114,529	55,685	170,215
HRkt-HCRBCC	VTHL	114,957	61,084	176,041
HRkt-HRBCC	VTHL	88,982	94,146	183,129
HRkt-HCRkt	VTHL	157,497	55,202	212,699
HRkt-HRkt	VTHL	139,547	73,825	213,372
HCRBCC-HCRkt	VTHL	178,447	49,778	228,225
HCTurb-HRBCC	HTHL	133,256	110,522	243,779
HCTBCC-HRBCC	HTHL	179,997	76,658	256,655
HCRBCC-HRkt	VTHL	201,204	64,795	266,000
HRBCC-HCRkt	VTHL	241,507	45,438	286,945
HRBCC-HCRkt	HTHL	251,526	42,767	294,293
HRBCC-HRkt	HTHL	242,265	54,831	297,096
HCTBCC-HCRkt	HTHL	261,055	49,671	310,726
HRBCC-HRkt	VTHL	253,220	59,555	312,775
HCTBCC-HRkt	HTHL	250,901	65,625	316,526
HCTurb-HCRBCC	HTHL	266,099	73,145	339,244
HCTurb-HRkt	HTHL	278,595	116,708	395,304
HCTurb-HCRkt	HTHL	360,534	89,603	450,138

	T/O	Wetted Area (ft ²)		
		Booster	Orbiter	Total
HCRkt-HCRBCC	VTHL	7,978	7,901	15,879
HCRkt-HCRkt	VTHL	11,763	7,765	19,527
HCRkt-HRkt	VTHL	10,064	9,926	19,991
HCRBCC-HCRkt	VTHL	13,233	7,059	20,292
HCRkt-HRBCC	VTHL	6,446	14,577	21,023
HRkt-HCRBCC	VTHL	13,217	7,912	21,129
HCTBCC-HCRkt	HTHL	16,185	6,967	23,152
HCRBCC-HRkt	VTHL	14,387	9,581	23,968
HCTBCC-HRBCC	HTHL	11,776	12,711	24,487
HRkt-HRBCC	VTHL	10,811	14,534	25,344
HCTBCC-HRkt	HTHL	15,966	9,676	25,642
HRkt-HCRkt	VTHL	18,546	7,584	26,130
HRkt-HRkt	VTHL	16,830	10,794	27,624
HCTurb-HRBCC	HTHL	10,747	16,899	27,646
HRBCC-HCRkt	HTHL	22,596	6,158	28,754
HRBCC-HRkt	HTHL	21,594	7,899	29,493
HRBCC-HCRkt	VTHL	23,027	6,701	29,728
HCTurb-HCRBCC	HTHL	20,231	9,522	29,753
HRBCC-HRkt	VTHL	23,335	8,889	32,224
HCTurb-HRkt	HTHL	21,103	16,922	38,025
HCTurb-HCRkt	HTHL	26,741	12,761	39,502

4.1.1 Baseline VTHL RLV Detailed Mass Analysis

The gross masses and empty masses of the VTHL vehicles are shown in Figure 36. The gross masses of the vehicles follow a similar trend based on the fuel used on each stage. The hydrocarbon-hydrocarbon vehicles have the highest gross mass, while the hydrogen-hydrogen vehicles have the lowest gross mass. A vehicle's propellant typically makes up about 80% of a RLV's gross mass, and for the same required ΔV , a hydrogen-fuelled vehicle requires less fuel than a hydrocarbon-fuelled vehicle.

Therefore, the gross masses of the RLVs are driven by the fuel used.



Figure 36. VTHL baseline vehicle mass comparison

The gross mass of the orbiter stage is essentially the payload of the booster stage, so any mass savings achieved on the orbiter stage “trickles down” to additional mass savings on the booster stage. This is evidenced by the lower gross mass of a vehicle using a hydrogen orbiter compared to a vehicle, using the identical booster type, with a hydrocarbon orbiter. This is apparent in the Rkt-Rkt vehicles and the Rkt-RBCC vehicles, but for the RBCC-Rkt vehicles, there is little difference, so another factors must be considered. Looking again at Figure 34, the RBCC-Rkt vehicle operates on the DMSJ as a two-stage vehicle for a large portion of the trajectory, while the Rkt-Rkt quickly exits the atmosphere and the Rkt-RBCC operates on the DMSJ as only the orbiter stage. The drag on the vehicle, therefore, also affects the vehicle gross mass. Hydrogen fuel has a lower density than hydrocarbon fuel, and thus requires a larger volume to contain it. For

the RBCC-Rkt vehicles, the larger volume of the hydrogen orbiter causes more drag which counters the effects of the gross mass savings.

The VTHL vehicle empty masses, however, do not follow any common trend among configurations, but the effects of the orbiter gross masses do produce a few noticeable effects. For the same booster configuration, the empty mass of a hydrocarbon orbiter is less than that of a hydrogen orbiter for every case. This is mostly easily seen in the bottom graph of Figure 36 by comparing the height of just the green portion of the bar between a hydrocarbon orbiter and the hydrogen orbiter to its right. This is due to the smaller volume required to contain the denser hydrocarbon fuel. However, as mentioned previously, the propellant makes up the largest fraction of the orbiter's mass, so the empty mass savings of hydrocarbon orbiters is not enough to make up for the larger fuel mass savings of hydrogen orbiters. The gross mass of hydrogen orbiters is therefore about 15-20% less than that of hydrocarbon orbiters, though this is difficult to see in the gross mass graph at the top of Figure 36. This effect is noticeable in the empty mass of the booster, as can be seen in the height of the purple bars in the bottom graph of Figure 36. A booster lifting a hydrogen orbiter requires less propellant and has a lower empty mass than a booster lifting a hydrocarbon orbiter. The effect of increased orbiter empty mass but decreased booster empty mass with hydrogen versus decreased orbiter empty mass but increased booster empty mass with hydrocarbon becomes a delicate balance, with each offsetting the other. In Rkt-Rkt vehicles, this balance works out in favor of the hydrogen orbiter, with the HCRkt-HRkt vehicle having the smallest empty mass.

However, this does not hold true for airbreathing vehicles. Airbreathing vehicles spend a significant portion of their trajectory flying through the air, as was shown in Figure 34. A RBCC-Rkt vehicle with a larger hydrogen orbiter has a higher drag than a RBCC-Rkt with the smaller hydrocarbon vehicle, but the hydrogen orbiter is 15-20% less massive than the hydrocarbon orbiter. Both the drag, driven by vehicle size, and gravity loss, driven by vehicle mass, are variables in a vehicle's EI_{sp} , as given by eq. (24), which is the propulsive efficiency of a whole vehicle, not just the propulsion system. Figure 37 shows the EI_{sp} for both the HCRBCC-HCRkt and HCRBCC-HRkt, and shows that the vehicle with a hydrocarbon orbiter has a higher EI_{sp} . The I_{sp} of both vehicles' propulsion systems is the same, but after the drag and gravity losses have been subtracted, the HCRBCC-HCRkt vehicle as a whole has a higher EI_{sp} than the HCRBCC-HRkt vehicle. This indicates that the drag increase with hydrogen rocket orbiters has a larger effect on EI_{sp} than the decreased mass of the hydrogen rocket orbiter. The lower EI_{sp} means that more fuel is required to produce the same amount of thrust, so the HCRBCC-HRkt uses more fuel and thus has a higher empty mass than the HCRBCC-HRkt, as can be seen in Figure 36. This trend with the orbiters also holds true for the HRBCC-HCRkt and HRBCC-HRkt vehicles, but the drag for the hydrogen boosters is greater than that for the hydrocarbon boosters, resulting in the vehicles with HRBCC boosters having greater empty masses than the vehicles with HCRBCC boosters.

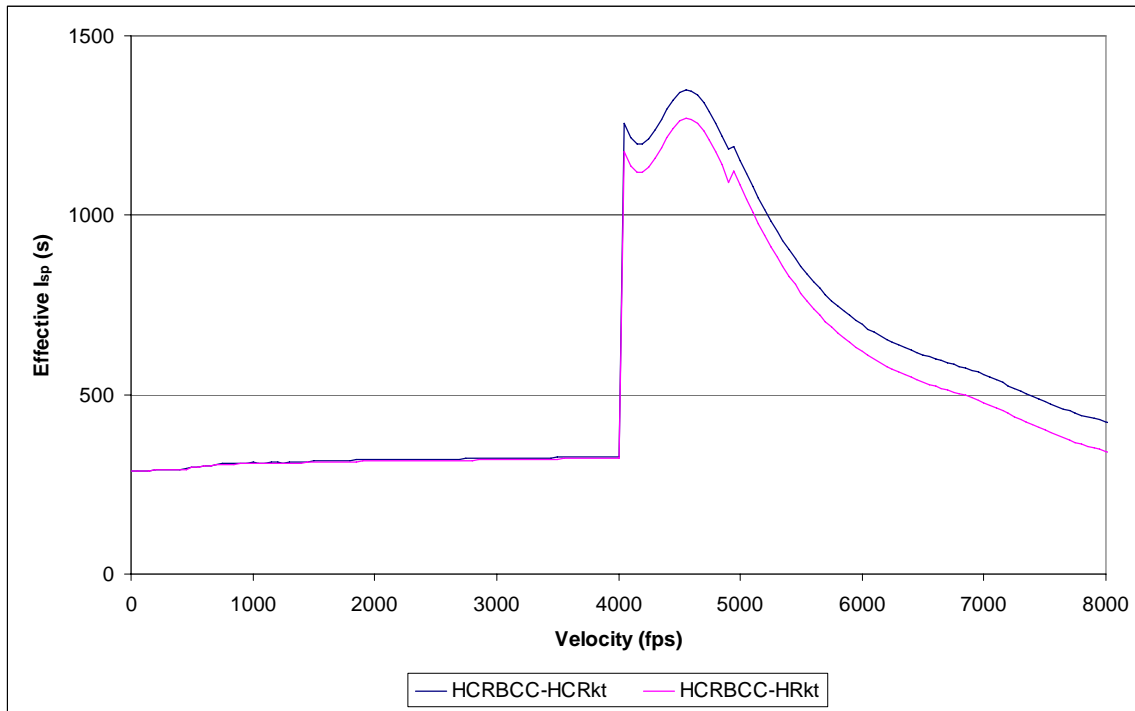


Figure 37. Vehicle EI_{sp} comparison between HCRBCC-HCRkt and HCRBCC-HRkt

For Rkt-RBCC vehicles, a different trend develops. The booster is a rocket, so it does not have an airbreathing portion. Thus, its empty mass is driven almost entirely by the gross mass of the second stage, so once again the vehicles with hydrogen orbiters have boosters with smaller empty masses. With the airbreather on the second stage, drag once again becomes a factor, so the hydrocarbon orbiters have the lightest empty mass. Again, it becomes a balancing act as with the Rkt-Rkt vehicles, but the effect is more pronounced. The HCRkt-HCRBCC starts out with a larger gross mass than the HCRkt-HRBCC, but ends up with a smaller empty mass.

This trend is interesting to observe when tracking the change in vehicle masses throughout the flight trajectory. Figure 38 shows the HCRkt-HCRBCC vehicle, which

has the lightest empty mass, compared with the HCRkt-HRBCC vehicle, which starts with a lighter gross mass. The difference between masses slowly decreases as booster fuel is expended. At staging at 4,000 fps (1,219.2 m/s), both vehicles' masses drop as the booster is detached, with the hydrocarbon-hydrocarbon vehicle losing slightly more mass than the hydrocarbon-hydrogen vehicle. Through the orbiter trajectory, the vehicles are now expending different types of fuel, with the hydrocarbon-fueled vehicle requiring larger masses of fuel for the same ΔV due to lower I_{sp} . The mass of the hydrocarbon orbiter eventually drops below the mass of the hydrogen orbiter, finally arriving at the vehicle empty mass plus payload mass at the far right of the graph.

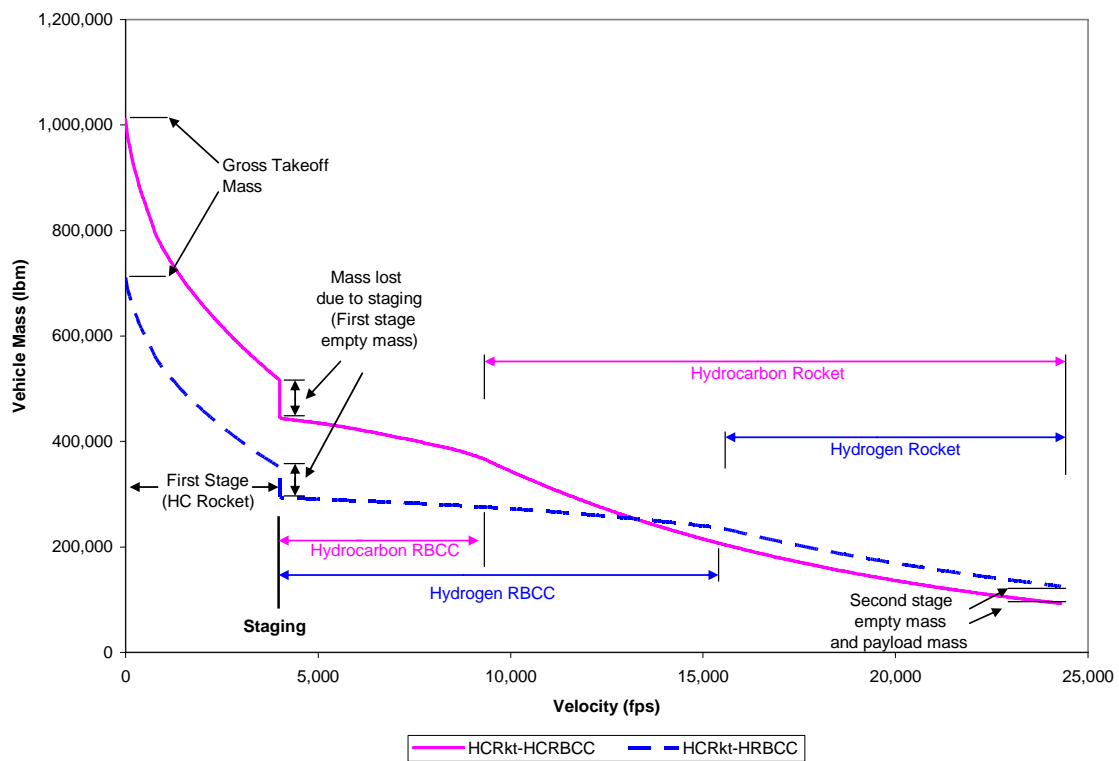


Figure 38. Vehicle mass change of HCRkt-HCRBCC and HCRkt-HRBCC during ascent

The effect of using airbreathing propulsion on the orbiter stage also becomes apparent from Figure 36. While the required vehicle geometry and equipment required for a DMSJ does increase the empty mass of the vehicle, both empty mass savings and gross mass savings are achieved by not requiring oxidizer. For boosters, the gross mass savings has little effect, as the empty mass increase due to the DMSJ and empty mass decrease due to no longer requiring LOX balance each other out or actually cause the empty mass to increase as in the RBCC-Rkt case. However, the gross mass decrease of airbreather orbiters affects the booster as well as the orbiter, resulting in empty mass savings on both stages. This savings is enough to overcome the mass penalty associated with airbreathing propulsion, resulting in the lightest vehicles. The HCRkt-HCRBCC vehicle has the smallest empty mass, even less than that of any Rkt-Rkt vehicle.

4.1.2 Baseline VTHL RLV Detailed Wetted Area Analysis

The effect of using low density hydrogen fuel becomes even more apparent in larger wetted areas of VTHL vehicles using this fuel, as shown in Figure 39. In all the vehicle types, the all-hydrocarbon fueling option has the least wetted area, while the all-hydrogen vehicles have the largest wetted areas. For mixed fuels on the same vehicle, both the Rkt-Rkt and RBCC-Rkt vehicles have smaller wetted areas when the denser hydrocarbon is used for the booster and hydrogen is used for the orbiter. For the Rkt-RBCC, the opposite is true, with the HCRkt-HRBCC having a higher wetted area than the HRkt-HCRBCC. The HRBCC requires a high design Mach number for proper operation of the DMSJ, resulting in a long, thin vehicle with a large wetted area. The HCRBCC is a more compact vehicle and has a much smaller wetted area. This is

noticeable regardless of whether the RBCC is used as an orbiter or booster. Among the VTHL vehicles, the HCRkt-HCRBCC has the smallest wetted area, even less than that of a HCRkt-HCRkt. With most scramjet research focusing on hydrogen, this vehicle configuration, shown in Figure 40, has not been given serious consideration in the past. However, as shown in this study, it ranks higher than the Rkt-Rkt for both figures of merit and is worth a closer look in the future.



Figure 39. VTHL baseline vehicle area comparison

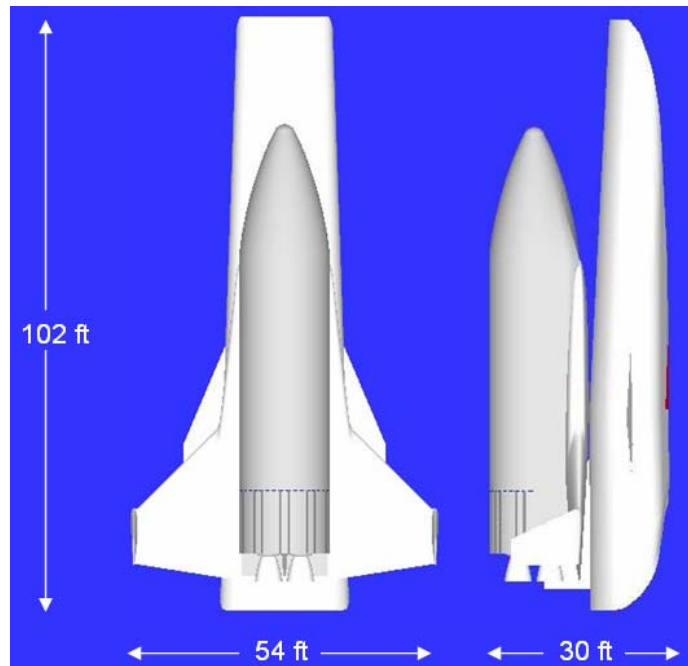


Figure 40. Hydrocarbon Rocket-Hydrocarbon RBCC (HCRkt-HCRBCC Vehicle)

Using airbreathing propulsion on the booster stage does not produce the large increase in wetted area as it does to vehicle empty mass. The wetted area of a Rkt-Rkt vehicle is nearly the slightly smaller than that of the RBCC-Rkt vehicle with the same fueling option. However, with the Rkt-RBCC vehicles, the wetted area begins to spread out more. As a whole, however, the vehicles using airbreathing propulsion on the orbiter stage have less wetted area than Rkt-Rkt vehicles, indicating a shorter turnaround time for the Rkt-RBCC configuration.

Areas requiring active cooling are exposed to the highest temperatures and therefore require more care during inspection between flights. As shown in Figure 39, the use of airbreathing propulsion increases the amount of active area greatly. For pure rocket vehicles, active cooling is used on the rocket nozzles only, which can be easily

inspected and replaced if necessary. However, airbreathing vehicles require cooling on many surfaces, including the portions of the inlet, combustor, and nozzle, which are a part of the vehicle's body. This large amount of complicated cooling required would greatly increase the turnaround time due to the more rigorous inspection procedures that might be required.

4.1.3 Baseline HTHL RLV Detailed Mass Analysis

The HTHL vehicles in this study have gross masses and empty masses as shown in Figure 41. The gross masses of all of the configurations decreased when the orbiter fuel was changed from hydrocarbon to hydrogen, but this trend did not extend to the empty masses. For the RBCC-Rkt and TBCC-Rkt vehicles, the vehicle empty mass actually increased slightly. The change in empty mass is different from the findings in the 2005 AFIT study for the TBCC-Rkt, which found that using a hydrogen orbiter stage resulted in a smaller empty mass than using a hydrocarbon orbiter stage. This is could be due to differences in the flyback model used. The 2005 AFIT study calculated the flyback fuel and turbine size using the gross mass of the orbiter stage, while this study used the empty mass of the orbiter stage for flyback. Hydrocarbon orbiters have a larger gross mass but a smaller empty mass, while hydrogen orbiters have a smaller gross mass but a larger empty mass. These opposing trends produced the difference in results. For both the RBCC-Rkt and TBCC-Rkt, the booster empty mass is less for a hydrogen orbiter than a hydrocarbon orbiter, but the hydrogen orbiter empty mass is much larger than the hydrocarbon orbiter empty mass. For the turbine boosters, the hydrogen orbiters significantly decrease the empty mass of the booster, but the turbine vehicles consistently

have the highest empty mass of the HTHL vehicles, both of which are consistent with the 2005 AFIT study.

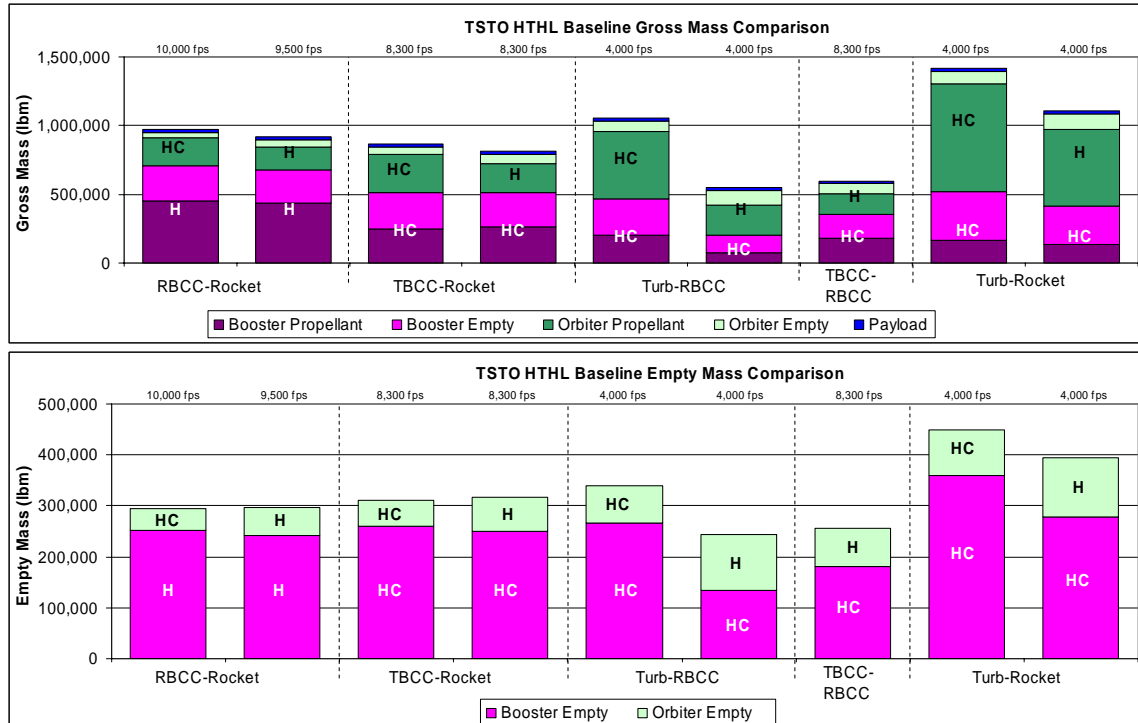


Figure 41. HTHL baseline vehicle mass comparison

The potential advantages of using airbreathers on the orbiter stage is immediately apparent for HTHL vehicles. The turbine vehicles using RBCC orbiters have a significantly smaller empty mass than the turbine vehicles using rocket orbiters, and the HCTurb-HRBCC vehicle has a smaller empty mass than either of the TBCC-Rkt vehicles, including the HCTBCC-HRkt. Indeed, the HCTurb-HRBCC vehicle had the smallest empty mass of all vehicles. Though the HCTBCC-HRBCC vehicle has an empty mass almost the same as the HCTurb-HRBCC, several other factors must be considered beyond the simple empty mass figure of merit. First, the HCTBCC-HRBCC

will be a complicated vehicle, and may not be feasible. It uses all three propulsion options and includes two DMSJs on the vehicle, one integrated with the turbines and one integrated with a rocket. In addition, it has the largest downrange distance, as shown in Figure 34, indicating the vehicle will be subjected to heating for a long period of time, which could cause quicker wear on the TPS. Lastly, this vehicle will require both hydrocarbon and hydrogen fuel. All of these considerations are not accounted for by the simple empty mass figure of merit, but may make the vehicle more costly than another HTHL configuration. The HCTurb-HRBCC, on the other hand, has a simple turbine booster lower stage.

When only the Turb-RBCC and Turb-Rkt vehicles are considered, the use of airbreathing propulsion on the upper stage results in a decrease in the vehicle empty mass, similar to the VTHL vehicle results. Though the adding a DMSJ to the orbiter adds some empty mass to the orbiter, the overall vehicle empty mass decreases since the RBCC does not require LOX during the DMSJ portion of its trajectory. The Turb-Rkt vehicle, on the other hand, must use a rocket to accelerate from the staging velocity, 4,000 fps (1,219.2 m/s), to orbit, which requires a large amount of propellant. This volume of propellant requires a tank to contain it, which adds a large amount of empty mass. Combined with the large mass of the turbines on the booster stage, the Turb-Rkt vehicles have the largest empty mass of all HTHL vehicles.

4.1.4 Baseline HTHL RLV Detailed Wetted Area Analysis

Wetted areas and active areas are given for the HTHL vehicles in Figure 42. The HTHL vehicle wetted areas varied more than the empty masses. The TBCC vehicles,

which have a 2-D inlet geometry, have smaller wetted areas than the inward-turning RBCCs. As with the VTHL vehicles, the HTHL vehicles using hydrogen orbiters have larger wetted areas than their counterparts using hydrocarbon orbiters. The difference in empty mass between TBCC and RBCC booster vehicles using different orbiter fuels is not very large, but the difference in wetted areas is much larger. The wetted area results for vehicles with turbine boosters are the same as the empty mass results, as explained in the previous section. The hydrogen orbiters have larger wetted areas than the hydrocarbon orbiters, but for the vehicles with turbine boosters, the turbine booster has a much smaller wetted area, give an overall smaller wetted area for turbine vehicles with hydrogen orbiters. For the vehicles with TBCC and RBCC boosters, the use of a hydrogen-fuelled orbiter results in an overall larger wetted area than the use of a hydrocarbon-orbiter.

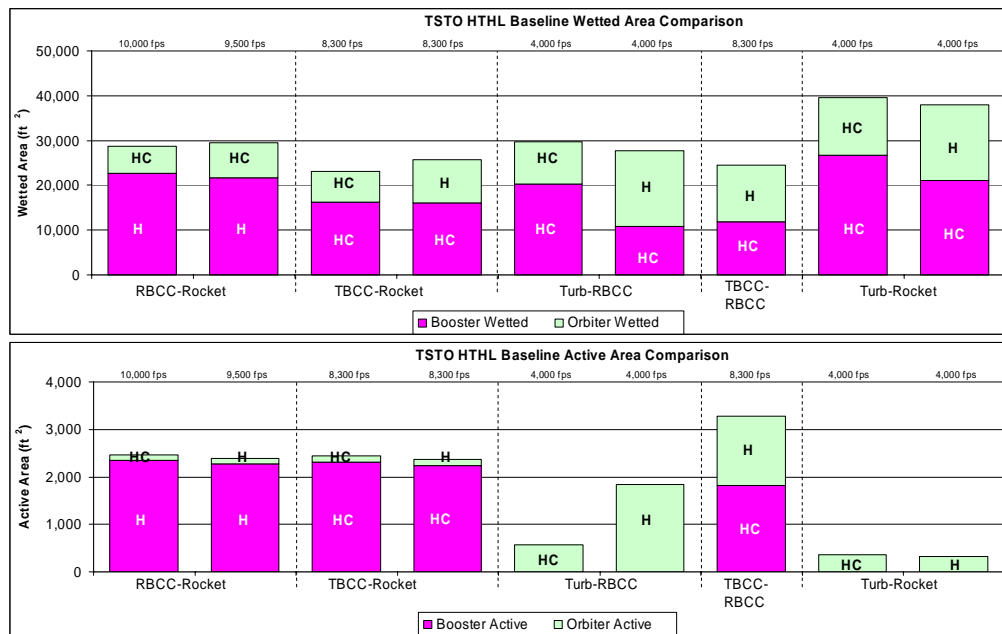


Figure 42. HTHL baseline vehicle area comparison

The vehicle with the smallest wetted area is the HCTBCC-HCRkt, though the HCTurb-HRBCC's wetted area is not much larger. Based on the significantly lower empty mass of the HCTurb-HRBCC vehicle shown in Figure 43, is it the best performer among the HTHL vehicles based on the figures of merit of this study. Again comparing the Turb-RBCC and Turb-Rkt vehicles, the vehicles with airbreather orbiters have smaller wetted areas than vehicles with rocket orbiters. The large ΔV required for orbiters with turbine boosters makes airbreathing propulsion for orbiters a better option than pure rocket propulsion due to the large orbiter gross mass savings that can be achieved by not having to carry LOX and the mass of the tank to contain it.

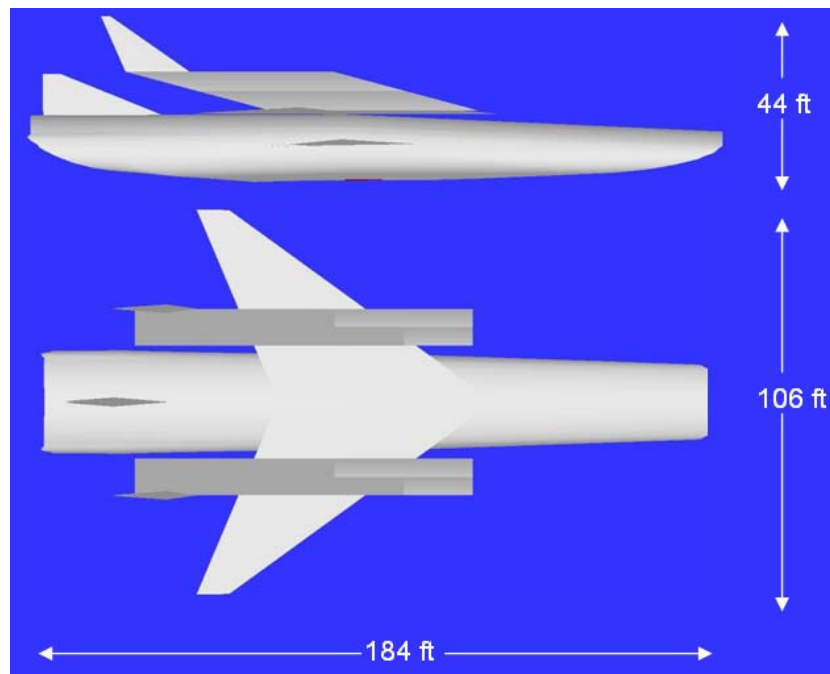


Figure 43. Hydrocarbon Turbine-Hydrogen RBCC (HCTurb-HRBCC Vehicle)

The active areas for HTHL vehicles produced interesting results. The turbine boosters required no active cooling, so for those vehicles, only the orbiters have any

active area. This could potentially reduce the turnaround time for those vehicles. The RBCC and TBCC boosters have nearly the same active area, despite the geometry differences. This is understandable since the TBCC has a smaller wetted area than the RBCC, but a larger fraction of active cooling area required. The TBCC-RBCC, which has the second smallest wetted area, requires the largest amount of active cooling area, further indicating the complexity of the vehicle. This vehicle may not have a lower turnaround time if extensive inspection time is required for the larger active area.

4.2 Payload Sizing Impact Study Results

For the payload study, each of the 21 vehicles was scaled up or down to find the vehicle size required for payloads varying between 0 lbm (no payload) and 30,000 lbm (13,607 kg) in 5,000 lbm (2,268 kg) increments. The empty mass and wetted area of each configuration was recorded for a given payload, resulting in seven data points for each vehicle. The points formed a linear growth trend for both empty mass and wetted area, so a linear equation was found to approximate the seven individual data points for each vehicle. These equations give the base empty mass and base wetted area, along with the linear growth rate of each from this base point. Table 16 lists the growth rates of the RLVs found in the payload study ranked in ascending order for both the empty mass and wetted area figures of merit, and complete data for the 21 vehicles in the payload study are given in Appendix H. These results show that the HCRkt-HCRBCC has the lowest growth rate for both empty mass and wetted area. The empty mass of the HCRkt-HCRBCC increases by 3.26 lbm per lbm of payload mass and the wetted area increases by 0.38 ft² per lbm of payload mass. The HTHL vehicles do not have a clear best choice,

as two different vehicles ranked highest for the two figures of merit. The HCTBCC-HRBCC has a growth rate of 7.22 lbm of empty mass per lbm of payload mass, while the HCTurb-HCRBCC wetted area increased by 0.60 ft² per lbm of payload mass. The vehicle with the highest growth rate for empty mass also had the largest growth rate for wetted area: The HTHL HRBCC-HCRkt has growth rates of 13.556 lbm of empty mass per lbm of payload mass and 1.14 ft² per lbm of payload mass.

Table 16. Payload sizing impact study RLV empty mass and wetted area growth rates

		Empty Mass				Wetted Area	
		Base Empty Mass	Growth Rate			Base Wetted Area	Growth Rate
	T/O	lbm EM	lbm EM/lbm Payload		T/O	ft ²	ft ² /lbm Payload
HCRkt-HCRBCC	VTHL	27888	3.260	HCRkt-HCRBCC	VTHL	4538	0.3818
HCRkt-HRBCC	VTHL	42421	3.602	HCRkt-HRBCC	VTHL	6567	0.4615
HRkt-HCRBCC	VTHL	43465	3.936	HRkt-HCRBCC	VTHL	7188	0.4687
HRkt-HRBCC	VTHL	64037	3.952	HCRkt-HRkt	VTHL	10210	0.4872
HCRkt-HRkt	VTHL	79476	4.219	HCRBCC-HRkt	VTHL	12150	0.5053
HRkt-HRkt	VTHL	108889	4.626	HRkt-HRBCC	VTHL	10496	0.5182
HCRkt-HCRkt	VTHL	67928	5.043	HCRkt-HCRkt	VTHL	8527	0.552
HCRBCC-HRkt	VTHL	89046	5.427	HRkt-HRkt	VTHL	14455	0.5654
HRkt-HCRkt	VTHL	89832	5.975	HCTurb-HCRBCC	HTHL	8019	0.6004
HCRBCC-HCRkt	VTHL	67354	6.927	HCTBCC-HRkt	HTHL	14267	0.6011
HCTBCC-HRBCC	HTHL	38492	7.224	HCRBCC-HCRkt	VTHL	8894	0.6113
HCTurb-HRBCC	HTHL	89323	7.853	HCTBCC-HRBCC	HTHL	6372	0.6691
HCTurb-HCRBCC	HTHL	118934	7.932	HRkt-HCRkt	VTHL	11850	0.6886
HCTBCC-HRkt	HTHL	139271	8.044	HCTBCC-HCRkt	HTHL	10496	0.7068
HRBCC-HRkt	VTHL	107801	8.490	HCTurb-HRBCC	HTHL	7395	0.731
HCTBCC-HCRkt	HTHL	105206	10.071	HCTurb-HRkt	HTHL	23048	0.767
HRBCC-HCRkt	VTHL	79415	10.137	HRBCC-HRkt	VTHL	15886	0.8626
HCTurb-HRkt	HTHL	296241	10.424	HCTurb-HCRkt	HTHL	26187	0.8983
HRBCC-HRkt	HTHL	78903	12.054	HRBCC-HCRkt	VTHL	12140	0.9674
HCTurb-HCRkt	HTHL	368426	13.319	HRBCC-HRkt	HTHL	11336	1.0744
HRBCC-HCRkt	HTHL	73382	13.556	HRBCC-HCRkt	HTHL	10746	1.1426

The growth rates in Table 16 have been extended to payload masses of 100,000 lbm (45,359.2 kg) and several are plotted in Figure 44. Due to the large number of lines this would cause on a single graph, only the vehicles discussed in the following sections are shown, but the plot for all vehicles can be found in Appendix H. The solid lines represent VTHL vehicles, while the dashed lines are HTHL vehicles. This plot shows that despite the differences in base empty mass and base wetted area, there are only a few instances of cross-over, so the growth rate is the most important factor to consider for

large payload masses. In general, the vehicles with the largest base empty mass and base wetted area also have the largest growth rates. Another trend that is noticeable is that, in general, the VTHL vehicles have lower growth rates than the HTHL vehicles. In fact, all of the HTHL vehicles were ranked in the bottom half of the empty mass growth rate table, and the best HTHL vehicle for wetted area growth rate ranks lower than eight other VTHL vehicles. These high growth rates are due to the fact that the wings and landing gear on HTHL vehicles are sized based on takeoff mass, and are thus sensitive to increases in the vehicle gross mass. The wings and landing gear on VTHL vehicles are sized based on the landing mass, which does not increase as much as the gross mass does with increasing payloads. These large wings also produce a large amount of drag during the DMSJ trajectory segment, so a vehicle with large wings requires more propellant for the same change in velocity as a vehicle with small wings.

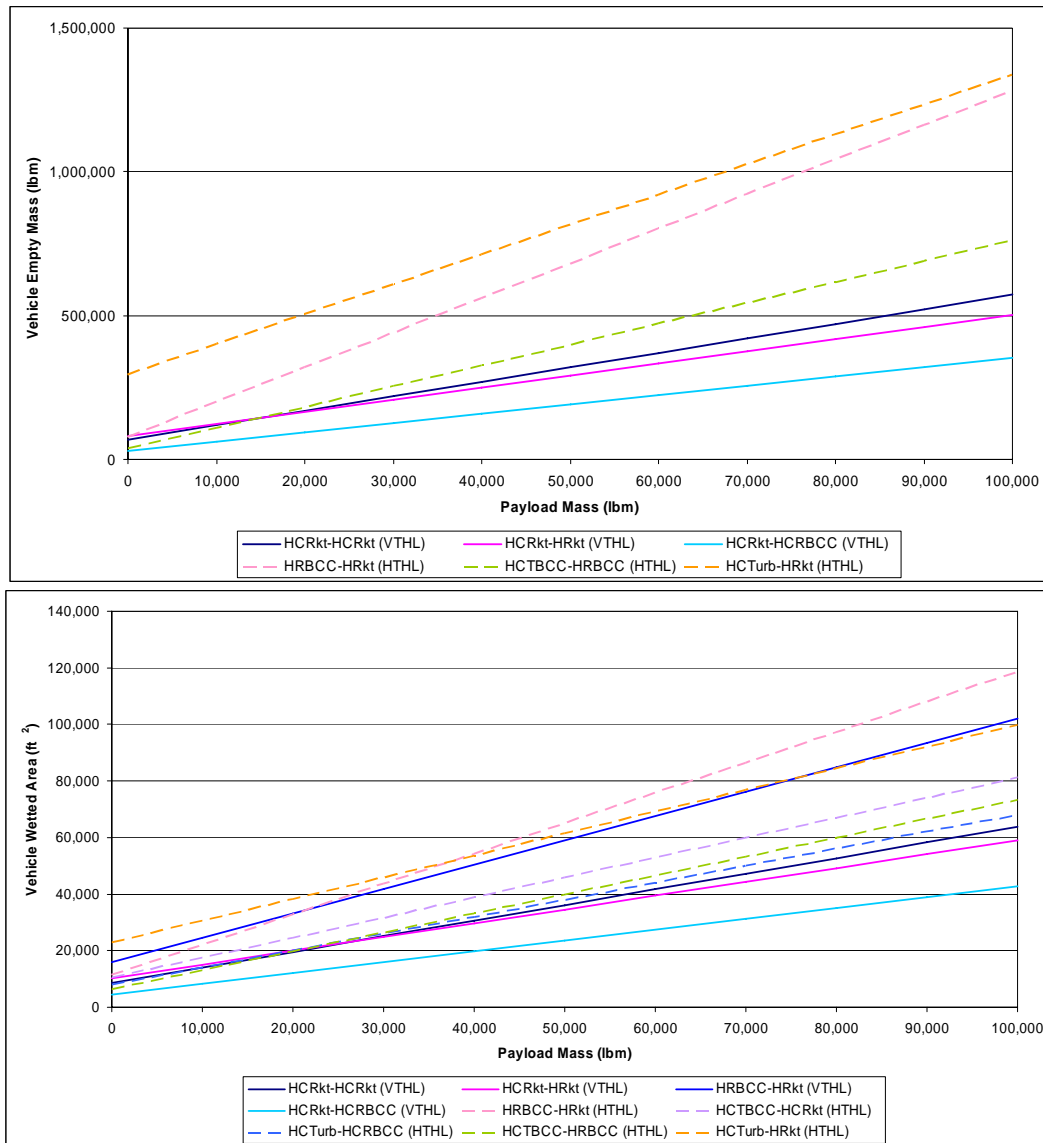


Figure 44. Payload sizing impact study RLV empty mass and wetted area growth rates

4.2.1 Payload Sizing Impact Study RLV Detailed Mass Growth Analysis

The overall configuration with the best empty mass growth rates is the Rkt-RBCC configuration. This model is the least sensitive to increases in the payload mass, and the HCRkt-HCRBCC vehicle has the smallest growth rate of all the vehicles. The baseline HCRkt-HCRBCC had the smallest empty mass for the baseline payload mass of 20,000

lbm (9,071.8 kg), and the payload study shows that it also has the smallest empty mass for all payload masses from 0 lbm (0 kg) to 30,000 lbm (13,607.7 kg). The rocket-rocket vehicles have the second smallest empty mass growth rates. The HCRocket-HRocket, which had the lightest empty mass of the baseline rocket-rocket vehicles, also has the smallest growth rate, indicating that the close empty mass difference between it and the HCRocket-HCRocket vehicle at the baseline payload weight will become larger for more massive payloads.

The HTHL vehicle with the smallest empty mass growth rate is the HCTBCC-HRBCC vehicle. Though at the baseline payload mass of 20,000 lbm (9,071.8 kg) the HCTurb-HRBCC has a smaller empty mass, the HCTurb-HRBCC has a higher growth rate. When the growth rate is projected out to a payload mass of 100,000 lbm (45,359.2 kg), the empty mass of the HCTBCC-HRBCC vehicle is the smallest of all HTHL vehicles. For reasons discussed in section 4.1.3, this vehicle may not be feasible.

The HTHL RBCC-Rkt vehicles and Turb-Rkt vehicles have the highest growth rate of all vehicles in this study. Since the RBCC-Rkt vehicles start with smaller base empty masses than the Turb-Rkt vehicles, the payload mass has to become large before the RBCC-Rkt empty masses become larger than the Turb-Rkt empty masses. In addition to the HTHL vehicles, the VTHL vehicles with hydrogen RBCC boosters also had high empty mass growth rates, while the hydrocarbon RBCC boosters ranked just under the Rkt-Rkt vehicles. The high growth rates of the hydrogen RBCC booster, regardless of takeoff configuration, and the Turb-Rkt vehicles show that both

configurations are poor choices for launch vehicles if medium to heavy payloads are required.

4.2.2 Payload Sizing Impact Study RLV Detailed Wetted Area Growth

Analysis

For wetted area growth rates, the Rkt-RBCC and Rkt-Rkt vehicles remain the best choices. As with the empty mass, the HCRkt-HCRBCC has the smallest wetted area growth rate of any vehicle, while the HCRkt-HRkt had the smallest wetted area growth rate of the rocket-rocket vehicles. The HCRkt-HRkt wetted area growth rate was less than that of the HCRkt-HCRkt. For the baseline vehicles, the HCRkt-HCRkt had a slightly smaller wetted area than the HCRkt-HRkt, but the smaller wetted area growth rate of the HCRkt-HRkt indicates that the HCRkt-HRkt will have a smaller wetted area at higher payloads. Figure 44 shows that the HCRkt-HRkt has both a lower empty mass and smaller wetted area than the HCRkt-HCRkt for payloads above 25,000 lbm (11,339.8 kg). The HCTurb-HCRBCC had the best rate of wetted area growth of all the HTHL vehicles, and when projected to a payload of 100,000 lbm (45,359.2 kg), has the smallest wetted area of the HTHL vehicles. The HCTBCC-HCRkt, which had a smaller wetted area than the HCTurb-HCRBCC at a payload of 20,000 lbm (9,071.8 kg), has a higher wetted area growth rate and has a larger wetted area than the HCTurb-HCRBCC vehicle.

The vehicles with the highest wetted area growth rates are the RBCC-Rkt with hydrogen boosters, regardless of takeoff configuration. The Turb-Rkt vehicles also experience high rates of wetted area growth, though not as large as the hydrogen RBCC boosters. The baseline vehicles indicated that the Turb-Rkt vehicles had higher empty

masses than the HTHL RBCC-Rkt vehicles, but for a 100,000 lbm (45,359.2 kg) payload, the wetted areas of the HTHL RBCC-Rkt vehicles are greater than the Turb-Rkt vehicles. In addition, as the baseline vehicle results showed, both the VTHL RBCC-Rkt and HTHL Turb-Rkt configurations are poor choices for a 20,000 lbm (9,071.8 kg) payload and continue to be so for heavier payloads as well.

4.3 Orbital Rendezvous RLV Results

As discussed in section 3.5.2, the airbreathing propulsion allows the initial inclination to be changed or the launch window to be expanded. The lowest inclination is 0 degrees, and only launches at the equator can launch directly into this inclination. To reach the equator, a vehicle launched from Cape Canaveral would have to fly 1,712 nm (3,170.6 km) and a vehicle launched from Vandenberg would have to fly 2,090 nm (3,870 km). Either of these distances resulted in HTHL vehicles whose gross takeoff masses would produce weights exceeding the assumed runway load limit of 1,500,000 lbf (6,674,612.2 N). However, a flight distance of 1,000 nm (1,852 km) still allowed over half of the HTHL vehicles to remain near the load limit while still resulted in vehicles with some ability to change their trajectory.

For the Turb-Rkt vehicles, which only have a turbine, this study used that turbine to perform the cruise; likewise, vehicles with only a DMSJ cruised on the DMSJ. However, if the vehicle has both, such as a TBCC, either propulsion system could be used. The vehicle should cruise at the velocity for best range factor, as shown in Table 14. The lift over drag and velocity for best range each configuration using the turbine are shown in the left side, and the right side of the table summarizes the DMSJ values, and

range factors are calculated for each. For the TBCC vehicles, the range factor is greater for the DMSJ, which is the best propulsion system to use for the cruise. This has two benefits: a) the larger range factor means the fuel fraction will be closer to 1, indicating less fuel required, and b) The weight of the vehicle will be smaller at this point, so the weight fraction will be based on a smaller vehicle weight. The turbine vehicles cruise at subsonic velocities immediately after takeoff, so they cruised on almost the entire GTOM, while the vehicles using DMSJ propulsion for the cruise not longer carried the mass of fuel required to reach DMSJ operating velocity. For this reason, in addition to the fact that the booster stage mass could be removed, the HCTurb-HCRBCC cruised on the DMSJ after staging, despite the fact that the turbine had a slightly higher range factor than the RBCC.

For the flight distance of 1,000 nm (1,852 km), Table 17 lists the 17 orbital rendezvous RLVs ranked in ascending order for the figures of merit. The HCRkt-HCRBCC again has the lowest empty mass and smallest wetted area of all vehicles considered. It has an empty mass of 229,984 lbm (104,273 kg) and a wetted area of 23,777 ft² (2,209 m²). For the HTHL vehicles, two different configurations ranked highest: HRBCC-HCRkt had the smallest empty mass of 457,349 lbm (207,450 kg) and the HCTBCC-HRBCC had the smallest wetted area of 37,676 ft² (3,500 m²). The poorest performer in both figures of merit is the hydrocarbon turbine-hydrocarbon rocket, massing 1,043,655 lbm (454,161 kg) empty and having a wetted area of 67,680 ft² (6,288 m²). Complete data for the orbital rendezvous vehicles are given in Appendix I.

Table 17. Orbital Rendezvous RLV empty masses and wetted areas

	T/O	Empty Mass (lbm)				T/O	Wetted Area (ft ²)		
		Booster	Orbiter	Total			Booster	Orbiter	Total
HCRkt-HCRBCC	VTHL	133,460	96,424	229,884	HCRkt-HCRBCC	VTHL	12,222	11,555	23,777
HRkt-HCRBCC	VTHL	184,407	96,424	280,831	HCRBCC-HCRkt	VTHL	19,365	7,068	26,433
HCRBCC-HCRkt	VTHL	264,325	50,054	314,379	HCRBCC-HRkt	VTHL	21,786	9,581	31,367
HCRBCC-HRkt	VTHL	310,857	64,795	375,653	HRkt-HCRBCC	VTHL	19,826	11,555	31,381
HCRkt-HRBCC	VTHL	129,235	271,952	401,186	HCTBCC-HRBCC	HTHL	24,897	12,779	37,676
HRkt-HRBCC	VTHL	182,657	265,817	448,474	HCTBCC-HCRkt	HTHL	33,724	7,107	40,831
HRBCC-HRkt	HTHL	402,840	54,509	457,349	HCTurb-HCRBCC	HTHL	29,817	13,201	43,018
HRBCC-HCRkt	HTHL	421,123	42,573	463,696	HRBCC-HRkt	HTHL	35,662	7,897	43,560
HCTBCC-HRBCC	HTHL	417,494	77,502	494,996	HRBCC-HCRkt	HTHL	37,465	6,156	43,621
HRBCC-HCRkt	VTHL	465,958	45,438	511,395	HCRkt-HRBCC	VTHL	11,653	32,733	44,386
HCTurb-HCRBCC	HTHL	406,083	106,548	512,632	HCTBCC-HRkt	HTHL	35,275	9,895	45,169
HRBCC-HRkt	VTHL	487,934	59,555	547,489	HRBCC-HCRkt	VTHL	42,723	6,701	49,424
HCTurb-HRkt	HTHL	497,276	117,440	614,715	HRkt-HRBCC	VTHL	19,834	32,135	51,969
HCTBCC-HCRkt	HTHL	594,203	50,590	644,793	HRBCC-HRkt	VTHL	43,422	8,889	52,311
HCTurb-HCRkt	HTHL	559,095	89,563	648,658	HCTurb-HRkt	HTHL	35,694	16,934	52,629
HCTBCC-HRkt	HTHL	620,052	67,150	687,202	HCTurb-HCRkt	HTHL	40,678	12,750	53,428
HCTurb-HRBCC	HTHL	682,685	212,578	1,001,254	HCTurb-HRBCC	HTHL	30,616	37,065	67,680

4.3.1 Orbital Rendezvous Flexibility

4.3.1.1 Inclination Changes

The total payload module mass of 20,000 lbm (9,071.8 kg) includes the structure required to support the useful payload, the propulsion and fuel used to move the useful payload to its final orbit, and the useful payload itself. The payload structure and fairing typically makes up about 20% of the payload module mass for internal payloads to 33% of the payload module mass for external payloads [28]. This study uses internal payloads and assumed the total payload module mass consisted of 25% payload structure, leaving 15,000 lbm (6,803.9 kg) left for useful payload and propellant. The weight fraction of useful payload for a required ΔV can be found using the rocket equation, eq. (51). All calculations in this study assumed an I_{sp} of 300 sec for the propulsion system used to move the useful payload to its final orbit.

Table 18 shows two comparisons to a baseline launch, Case 1. All of the baseline vehicles in section 4.2 place a 20,000 lbm (9,071.8 kg) payload module in a 100 nm

(185.2 km) circular orbit at 28.5 deg inclination. Case 1 shows the useful payload mass that can be placed in orbit from this inclination. The required change in velocity to accomplish the Hohmann transfer from 3,498 nm (6,478.2 km) to 19,323 nm (35,786 km) and an inclination change from 28.5 deg to 0 deg is 13,867 fps (4,226.5 m/s). This results a useful payload mass to geosynchronous orbit of 3,570 lbm (1,619.3 kg).

Table 18. Payload mass comparisons

Case	Initial Payload Mass (lbm)	Payload without Structure (lbm)	Initial Inclination (deg)	ΔV to GEO (fps)	Propellant Mass (lbm)	Useful Payload Mass to GEO (lbm)
1	20,000	15,000	28.5	13,867	11,430	3,570
2	20,000	15,000	0	12,530	10,900	4,100
3	22,969	17,227	28.5	13,867	13,127	4,100

Case	Useful Payload Mass to GEO (lbm)	Initial Inclination (deg)	ΔV to GEO (fps)	Propellant Mass (lbf)	Payload without Structure (lbm)	Initial Payload Mass (lbm)
1	3,570	28.5	13,867	10,297	15,000	20,000
4	3,570	0	12,530	9,491	13,061	17,415

Case 2 considers the increase in useful payload if the vehicle flew to the equator so an inclination change is not required. The change in velocity is only 12,530 fps (3,819.1 m/s), so the useful payload to geosynchronous orbit is increased by 530 lbm (240.4 kg) to 4,100 lbm (1,859.7 kg). This is a 15% increase in useful payload. Case 4 considers the total payload that would be required flown to the equator to place the same payload as was delivered in Case 1. The change in velocity is the same as Case 2, so the total payload required is 17,415 lbm (7,899.3 kg). This is a 13% reduction in total payload mass, and based on the payload growth rates from the first part of this study, would not have a large effect on the overall sizing of the vehicle. The all of the orbital rendezvous vehicles grow large flying even 1,000 nm (1,852 km), so the small decrease in gross mass that would result from launching the 17,415 lbm (7,899.3 kg) would still

result in large vehicles required to accomplish the flight. Therefore, the empty masses and wetted areas of the vehicles would still be larger than the baseline vehicles.

These results show that while airbreathing propulsion can be used to change the inclination, it is best done while in orbit. Even the 1,000 nm (1,852 km) cruise results in only a 16.6 degree inclination change. Case 2 shows that the useful payload mass to geosynchronous orbit increases by only 15% when the same mass is launched from the equator, but requires enormous amounts of propellant and results in vehicles of impractical size. Case 3 shows that the reduction in total payload mass to place the same useful payload in geosynchronous orbit is not enough to significantly reduce the enormous amounts of propellant required and still results in impractical vehicles. Table 19 shows a vehicle size comparison of Cases 2 and 3, both of which place 4,100 lbm (1,859.7 kg) in GEO. The HCRkt-HCRBCC vehicle in Case 2 has been resized to fly 1,720 nm (3,185.4 km) to the equator with a 20,000 lbm (9,071.8 kg) payload, while the HCRkt-HCRBCC vehicle in Case 3 has been resized to launch from Cape Canaveral with a 23,000 lbm (1,043.3 kg) payload. The vehicle that must fly to the equator has over twice the empty mass and twice the wetted area of the vehicle that launches from Cape Canaveral with a more massive payload.

Table 19. Vehicle size comparisons

HCRkt-HCRBCC	Case 2	Empty Mass	369,259	lbm
	(Fly to Equator with 20,000 lbm)	Wetted Area	37,084	ft ²
	Case 3	Empty Mass	152,525	lbm
	(Launch from CC with 23,000 lbm)	Wetted area	17,013	ft ²

4.3.1.2 Launch Window Expansion

As mentioned in section 3.5.2, vehicles that are going to rendezvous with another object already in orbit are launched when the target's orbit passes over the launch location, but there is no way to ensure that the target is at the correct position within that orbital plane for an immediate rendezvous [41:79]. Instead of waiting until the desired orbital plane is overhead, the airbreathers could instead fly east from Cape Canaveral or west from Vandenberg, or even north or south, to intercept the plane over a larger window of time, which may allow the payload to rendezvous directly with the target. Using the 1,000 nm (1,852 km) range and the flyout speed, the exact time by which the window is expanded can be found. While airbreathers do already fly up to 600 nm (1,111.2 km) for a normal launch, this distance is not included in the launch window expansion since they will always fly this same distance.

Orbital planes stay stationary in inertial space, while the earth is rotating underneath the plane at an angular rate of 360 deg per 24 hr, or 0.0000727 rad/s. The airbreather can fly along the earth's surface at the same latitude as the launch site, and accelerate to orbit at the proper location to end the trajectory in the desired orbital plane. For an east coast launch from Cape Canaveral, an orbital plane is moving westward at a speed of 1,337 fps (407.5 m/s), or 0.22 nm/s along the 28.5 deg N parallel. An RLV launching eastward must launch early to reach the orbit before it cross over Cape Canaveral. The time the launch window is expanded by is equal to the time it takes the earth to rotate through 1,000 nm (1,852 km) along the 28.5 deg N parallel at a rate of 0.22 nm/s (407.5 m/s). This comes to 4,545 sec, or 1 hr, 15 min, 45 sec. For a west coast

launch from Vandenberg, the orbital plane is moving westward at a speed of 1,250 fps (351.1 m/s), or 0.21 nm/s along the 34.75 deg N parallel. A RLV launching westward from Vandenberg must be traveling at least this fast to catch up to an orbital plane.

If the airbreather is traveling subsonically, the orbital plane is moving faster than the airbreather can travel. Therefore, the subsonic airbreather can launch westward early and fly westward while the orbital plane catches up to the vehicle. Most turbine boosters fly out at approximately 850 fps (259.1 m/s), so it takes 7,200 sec to fly 1,000 nm (1,852 km). During that time, the orbital plane is moving westward at 0.21 nm/s for a total of 1,471 nm (2,724.2 km). The airbreather then launched when the orbital plane was 471 nm (872.2 km) eastward along the 34.75 parallel from Vandenberg. It takes the orbital plane a time of 2,289 sec to travel the 471 nm (872.2 km), for a launch window expansion of 38 min, 9 sec.

If the airbreather is traveling on the DMSJ at 4,000 fps (1219.2 m/s), the airbreather is moving faster than the orbital plane and can catch up to it. It takes 1,519 sec to fly 1,000 nm (1,852 km), during which the plane has traveled 313 nm (578.9 km). The airbreather can launch when the plane is as far as 687 nm (1,273.1 km) past Vandenberg. Since the plane travels at 0.21 nm/s, the launch window is expanded by 3,340 sec, or 55 min, 40 sec. This is the only case where the vehicle can launch after the normal launch window if it is unable to launch at the correct time.

With the flyout capability, airbreathers can expand the launch window by the amounts given above. Thus, if the target satellite is crossing the 28.5 deg N latitude at a certain time, but the orbital plane will not pass over the correct place for an airbreather

direct launch to orbit for another 30 minutes, an airbreather could launch early, fly out for the correct distance, and then accelerate to orbit. The payload could rendezvous with the target immediately after launch without having to accomplish a phasing maneuver taking several days. If the RLV flies in a direction other than east from Cape Canaveral, the orbital rendezvous options are increased even further, as shown in Figure 45. A 1,000 nm (1,852 km) cruise range allows interception of up to 7 consecutive orbits during which an orbital rendezvous could be accomplished. In the case of a station resupply or an emergency evacuation of a manned space station, the time saved could be critical.

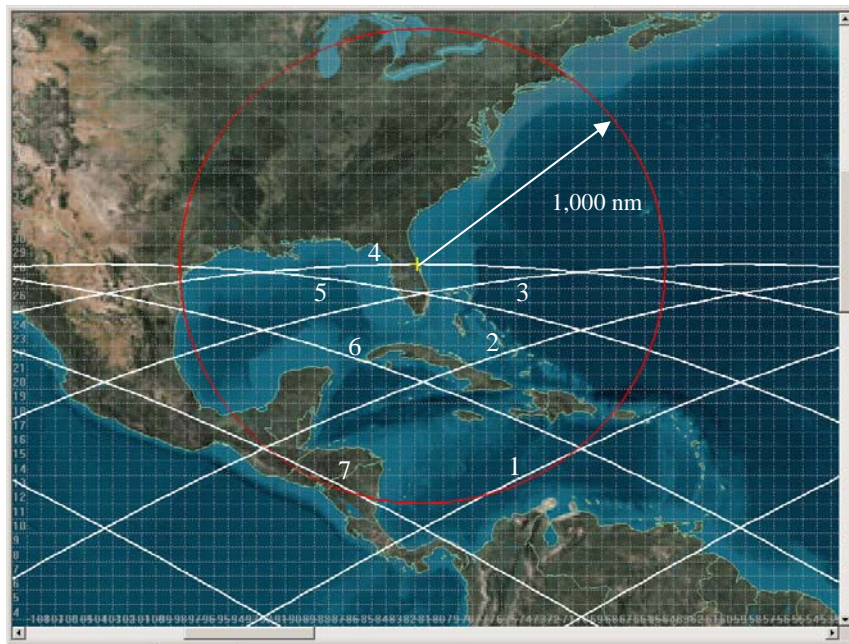


Figure 45. Number of orbital intercepts with a 1,000 nm (1,852 km) cruise range

4.3.2 Orbital Rendezvous VTHL RLV Detailed Mass Analysis

Among the VTHL vehicles, empty mass and wetted area depended highly on the fuel used for the cruise, with the vehicles cruising on hydrocarbon fuels being better for

both figures of merit, regardless of propulsion configuration. The RBCC-Rkt vehicles cruised 1,000 nm (1,852 km) at a velocity of 4,000 fps (1,219.2 m/s) on the DMSJ with the orbiter attached, which resulted in boosters with large empty masses. Figure 46 shows the gross and empty masses of the orbital rendezvous vehicles. In particular, the hydrogen RBCC vehicles had high empty masses due to the large volume of hydrogen required to accomplish this cruise. When switching from a hydrocarbon orbiter to a hydrogen orbiter, the booster empty mass became larger, due to the decreased EI_{sp} as explained previously. The RBCC-Rkt vehicles are poor cruisers since they must cruise carrying the rocket orbiter and also fly the entire distance back to the launch location after staging.

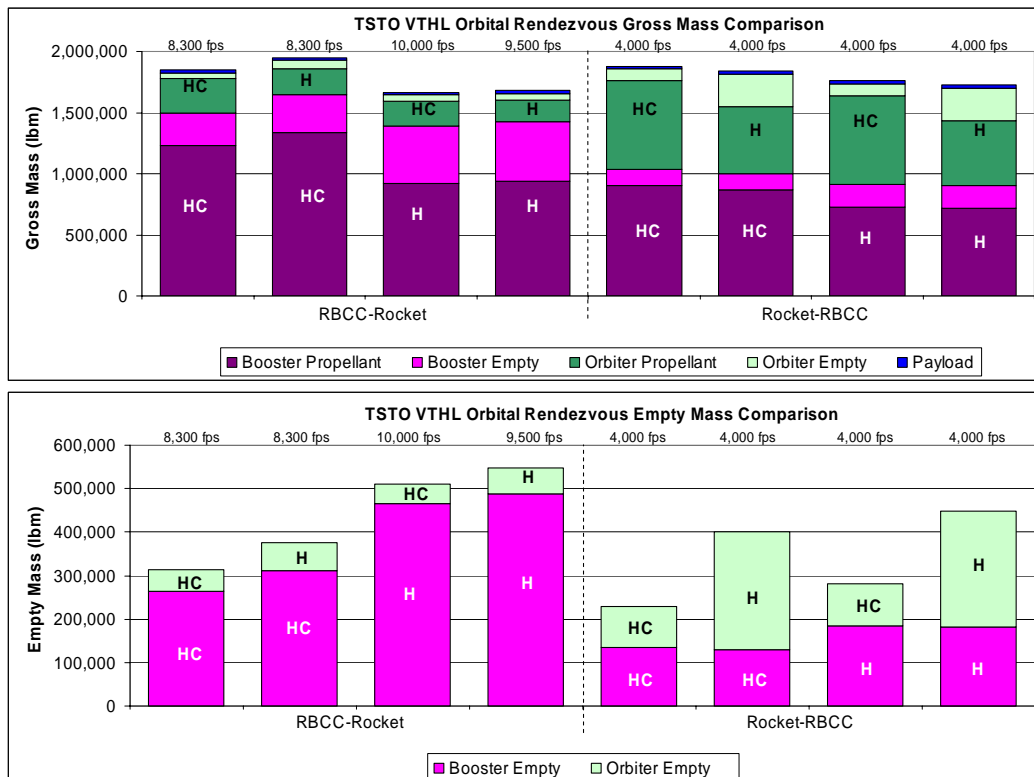


Figure 46. VTHL orbital rendezvous vehicle mass comparison

The Rkt-RBCC vehicles cruise the same distance at the same velocity, but do so after staging. The rocket booster is discarded once the cruise speed was reached, so the Rkt-RBCC vehicles are able to cruise without this extra mass and without the extra drag. The gross mass of the orbiter stage increases greatly, as can be seen in Figure 46 by the larger green bars for the Rkt-RBCC vehicles, but the large boosters of the RBCC-Rkt vehicles make the RBCC-Rkt vehicles have an overall larger empty mass. The hydrogen RBCCs remain poor cruisers, even when as an orbiter, but the vehicles with hydrocarbon RBCC orbiters have empty masses less than any of the other VTHL vehicles. Furthermore, all of the vehicles cruising on hydrocarbon fuel have smaller vehicle empty masses than any of the vehicles cruising on hydrogen fuel. Hydrocarbon fuel is clearly the best fuel to use to cruise a VTHL vehicle due to its higher density compared to hydrogen fuel, and cruising with just the orbiter stage is the best way to accomplish this. This makes the HCRkt-HCRBCC the best vehicle to accomplish an orbital rendezvous, and it may have the capability to fly all the way to the equator from either Cape Canaveral or Vandenberg without an excessive vehicle gross takeoff mass, though this is not a large concern for VTHL vehicles.

4.3.3 Orbital Rendezvous VTHL RLV Detailed Wetted Area Analysis

The wetted area results shown in Figure 47 indicate the same relative rankings as the empty masses, with all vehicles using hydrocarbon fuel to cruise have smaller wetted areas than any of the vehicles using hydrogen fuel. This division becomes even clearer in the amount of active area required for hydrogen RBCCs, whether used as a booster or orbiter. The fuel used for the DMSJ engine is the clear driver of the amount of active

area required, and divides the active area into two groups: The vehicles with hydrocarbon RBCCs require 1,600 ft² (148.6 m²) of active area, while the hydrogen RBCCs have active areas of around 3,000 ft² (278.8 m²) and even 4,500 ft² (418.1 m²). The results from the wetted area analysis again supports the use of hydrocarbon fuel for VTHL vehicles required to cruise a distance. The HCRkt-HCRBCC vehicle has the smallest wetted area of all VTHL orbital rendezvous vehicles for the same reasons mentioned in the empty mass analysis: It cruises using high density hydrocarbon fuel and it cruises without an upper stage to produce drag and the dead mass that must be carried.

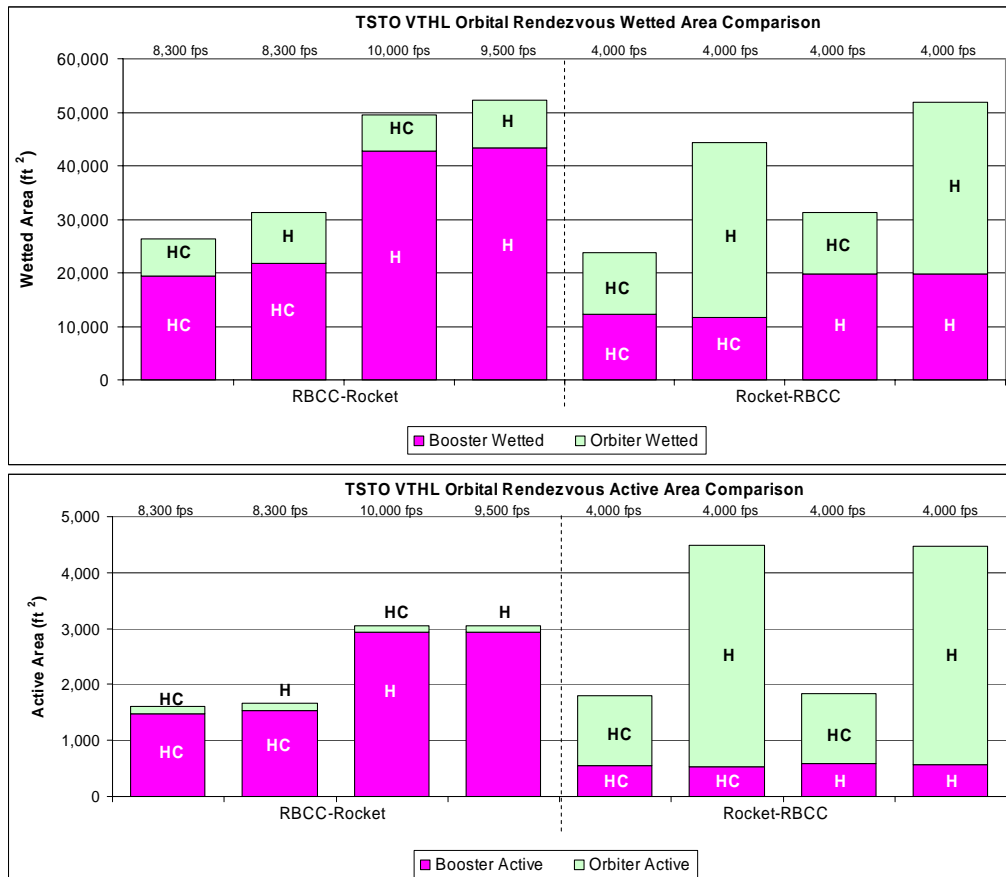


Figure 47. VTHL orbital rendezvous vehicle area comparison

4.3.4 Orbital Rendezvous HTHL RLV Detailed Mass Analysis

The gross masses of the vehicles in Figure 48 indicate that some of the vehicles have weights that will exceed the 1,500,000 lbf (6,674,612.2 N) assumed runway bearing load limit, even when flying only 1,000 nm (1,852 km). The TBCC-Rkt and Turb-Rkt vehicles in particular exceed the load limit substantially, grossing around 2,000,000 lbfm (907,184.7 kg). These vehicles would be limited to operating from runways able to support the large gross mass. However, these four vehicles also have the largest empty mass of the HTHL vehicles considered, and are therefore likely to have the largest development and production costs in addition to potentially requiring reinforced runways.

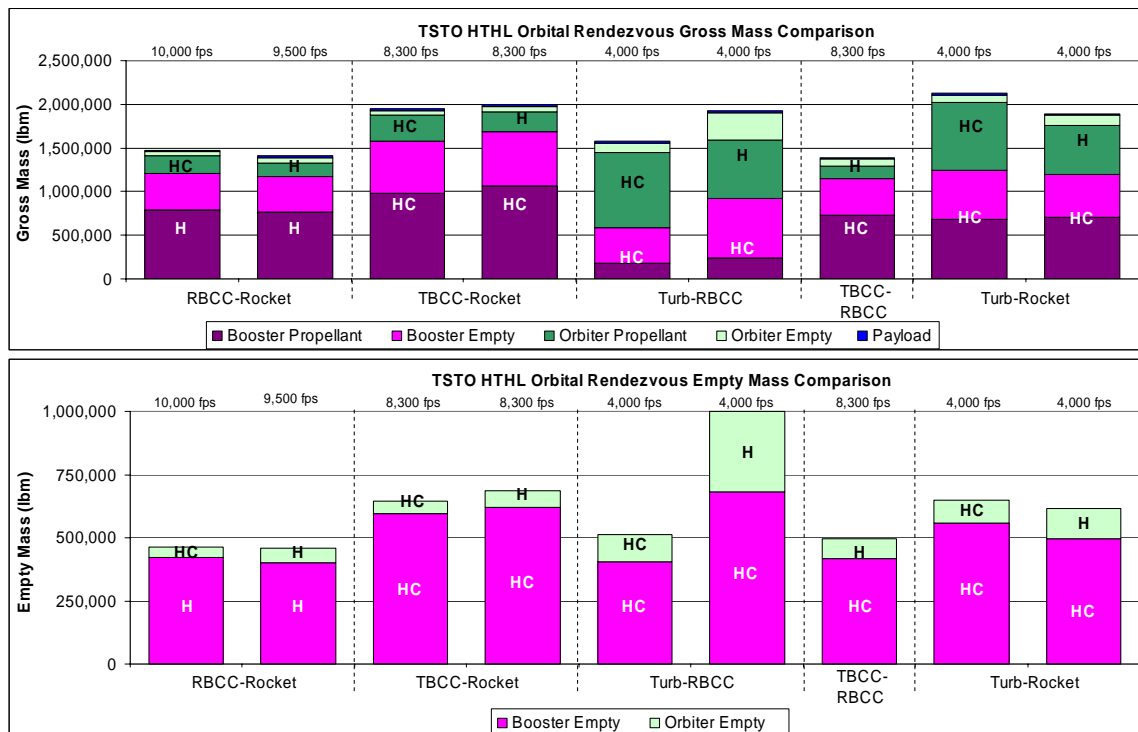


Figure 48. HTHL orbital rendezvous vehicle mass comparison

Of the remaining vehicles, the RBCC-Rkt vehicles did not grow much, as compared to the TBCC and turbine vehicles in particular. This is due mainly to the high range factors for each vehicle, as given in Table 14, and the lower gross mass used for the Breguet range equation. The HTHL RBCC-Rkt vehicle range factors, at 7,728 nm (14,312.3 km), are approximately double the TBCC booster vehicle range factors, at 3,215 nm (5,954.2 km), and the turbine booster vehicle range factors, which varied between 3,100 nm (5,741.2 km) and 4,400 nm (8,148.8 km). Thus, for the given range of 1,000 nm (1,852 km), the RBCC-Rkt vehicles have a smaller weight fraction for the cruise segment. This is apparent in Figure 48, in which the RBCC-Rkt vehicles have the lowest empty mass.

The other vehicles remaining near the runway load limit are Turb-RBCC and TBCC-RBCC configurations. The HCTurb-HRBCC has a much larger empty mass, due mainly to the orbiter which uses hydrogen fuel. However, both the HCTurb-HCRBCC and HCTBCC-HRBCC remained close in empty mass.

4.3.5 Orbital Rendezvous HTHL RLV Detailed Area Analysis

The vehicle wetted areas shown in Figure 49 indicates that the RBCC-Rkt vehicles, the HCTurb-HCRBCC, and HCTBCC-HRBCC vehicles all have similar wetted areas. The HCTBCC-HRBCC has the smallest wetted area, but has a larger active area than the other vehicles. The vehicle with the second smallest wetted area is the HCTBCC-HCRkt, although its gross mass of nearly 2,000,000 lbm (907,184.7 kg) exceeds the runway load limit. The HCTurb-HCRBCC has the third smallest wetted area, though the RBCC-Rkt vehicles are close.

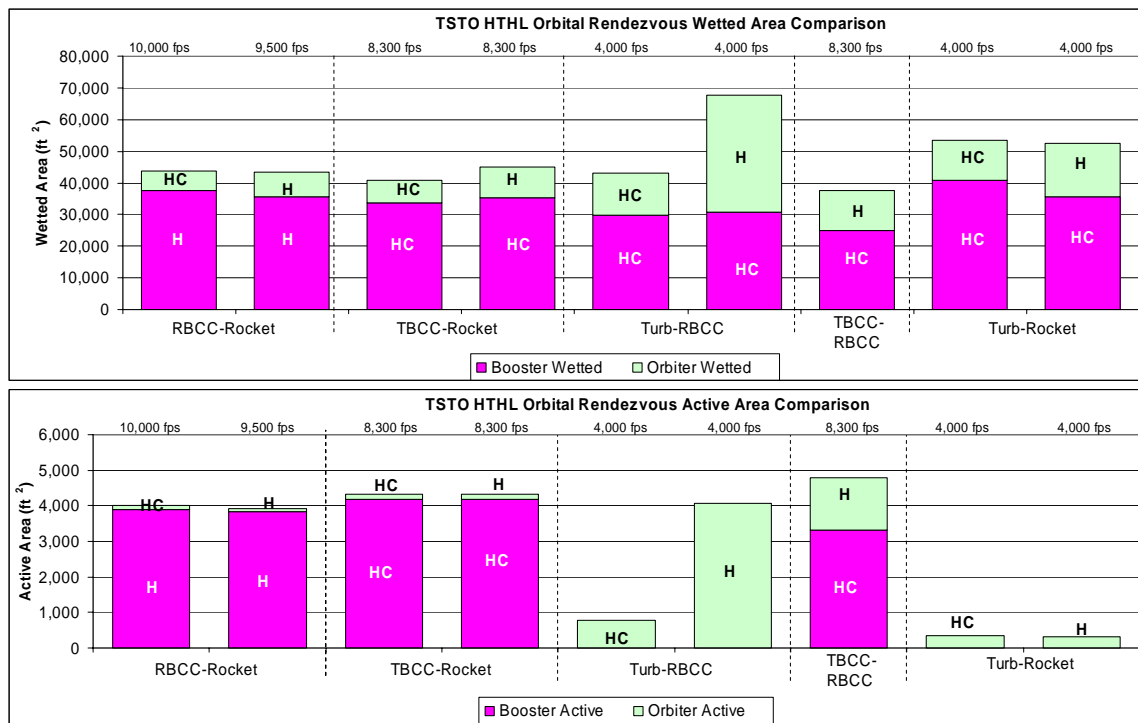


Figure 49. HTHL orbital rendezvous vehicle area comparison

The active area table shows the HCTurb-HCRBCC vehicle has significantly smaller active areas than the RBCC-Rkt vehicles, and so would have even less turnaround time than the RBCC-Rkt vehicles. In addition, the all hydrocarbon HCTurb-HCRBCC uses a single, non-cryogenic fuel and would require less extensive ground facilities. In addition, Table 20 shows the relative mass and wetted area increases of the orbital rendezvous vehicles compared to the baseline vehicles. The orbital rendezvous HCTurb-HCRBCC has the smallest increase in both empty mass and wetted area, indicating that it would have the smallest relative increase in empty mass and wetted area for distances even farther than 1,000 nm (1,852 km). The HRBCC-HRkt vehicle ranks immediately below the HCTurb-HCRBCC vehicle, but would require facilities for the

cryogenic hydrogen. Though a close call, the all-hydrocarbon turbine-RBCC is the best HTHL vehicle to provide trajectory flexibility by flying a distance prior to beginning the vertical ascent.

Table 20. Orbital rendezvous RLV increase in empty mass and wetted area versus baseline RLV

Empty Weight			Wetted Area		
HCRBCC-HCRkt	VTHL	37.75%	HCRBCC-HCRkt	VTHL	30.26%
HCRBCC-HRkt	VTHL	41.22%	HCRBCC-HRkt	VTHL	30.87%
HCTurb-HCRkt	HTHL	44.10%	HCTurb-HCRkt	HTHL	35.25%
HCTurb-HCRBCC	HTHL	51.11%	HCTurb-HRkt	HTHL	38.41%
HRBCC-HRkt	HTHL	53.94%	HCTurb-HCRBCC	HTHL	44.58%
HCTurb-HRkt	HTHL	55.50%	HRBCC-HRkt	HTHL	47.69%
HRBCC-HCRkt	HTHL	57.56%	HRkt-HCRBCC	VTHL	48.52%
HRkt-HCRBCC	VTHL	59.53%	HCRkt-HCRBCC	VTHL	49.73%
HCRkt-HCRBCC	VTHL	60.93%	HRBCC-HCRkt	HTHL	51.70%
HRBCC-HRkt	VTHL	75.04%	HCTBCC-HRBCC	HTHL	53.86%
HRBCC-HCRkt	VTHL	78.22%	HRBCC-HRkt	VTHL	62.34%
HCTBCC-HRBCC	HTHL	92.86%	HRBCC-HCRkt	VTHL	66.26%
HCTBCC-HCRkt	HTHL	107.51%	HCTBCC-HRkt	HTHL	76.15%
HCTBCC-HRkt	HTHL	117.11%	HCTBCC-HCRkt	HTHL	76.36%
HRkt-HRBCC	VTHL	144.90%	HRkt-HRBCC	VTHL	105.05%
HCRkt-HRBCC	VTHL	154.60%	HCRkt-HRBCC	VTHL	111.13%
HCTurb-HRBCC	HTHL	328.12%	HCTurb-HRBCC	HTHL	144.81%

4.4 Global Strike HLV Results

The vehicles in this study were hybrid launch vehicles (HLVs), with a reusable booster stage and an expendable orbiter stage. When selecting the best vehicle configuration with a hybrid vehicle, empty mass is still used as the primary figure of merit, but each stage must be considered separately. The empty mass of the orbiter stage is throwaway mass, so the least expensive vehicle over a large number of launches is the vehicle with the smallest orbiter empty mass. The empty mass of the booster stage is still of concern, but a slightly more expensive booster used with a cheaper expendable orbiter will end up paying for itself over a number of launches in savings. A new orbiter must be

purchased for every launch, so for a large number of hybrid vehicle launches, the empty mass of the orbiter stage correlates best to the overall system cost.

Likewise, vehicle wetted areas are still useful as a figure of merit, but also must be considered differently. The wetted area of the expendable upper stage is of no interest since it is not reused. Only the booster stage will require maintenance and inspection prior to reuse, so the wetted area figure of merit for hybrid vehicles considers only the wetted area of the reusable stage.

Table 21 lists the empty masses and wetted areas of the 14 HLVs in this study ranked in ascending order. Though neither the lowest overall vehicle empty mass nor lowest orbiter empty mass, the HCRkt-HCRkt vehicle is the best choice for VTHL vehicles, with an orbiter empty mass of 30,032 lbm (13,622 kg) and vehicle empty mass of 129,377 lbm (56,399.2 kg) and wetted area of 10,506 ft² (976 m²). The best HTHL vehicle is the HCTurb-HCRkt with an empty mass of 265,282 lbm (120,330 kg) and a wetted area of 17,398 ft² (1,616.3 m²). Complete data for the global strike vehicles are given in Appendix J.

Table 21. Global strike HLV empty masses and wetted areas

	T/O	Empty Mass (lbm)			T/O	Wetted Area (ft ²)	
		Booster	Orbiter	Total		Booster	
HCRkt-HRkt	VTHL	84,291	40,048	124,339	HCRkt-HRkt	VTHL	9,044
HCRkt-HCRkt	VTHL	99,345	30,032	129,377	HCRkt-HCRkt	VTHL	10,506
HRkt-HRkt	VTHL	115,038	37,984	153,022	HCRBCC-HCRkt	VTHL	12,325
HRkt-HCRkt	VTHL	139,084	31,066	170,150	HCTurb-HRkt	HTHL	13,319
HCRBCC-HCRkt	VTHL	162,091	27,516	189,607	HCTBCC-HRkt	HTHL	14,022
HCTurb-HRkt	HTHL	169,070	52,872	221,942	HCRBCC-HRkt	VTHL	14,214
HCRBCC-HRkt	VTHL	191,779	35,248	227,026	HRkt-HRkt	VTHL	14,309
HRBCC-HCRkt	VTHL	218,326	23,648	241,975	HCTBCC-HCRkt	HTHL	14,896
HCTBCC-HRkt	HTHL	214,669	36,505	251,174	HRkt-HCRkt	VTHL	16,470
HCTBCC-HCRkt	HTHL	235,803	28,402	264,205	HCTurb-HCRkt	HTHL	17,398
HCTurb-HCRkt	HTHL	224,257	41,025	265,282	HRBCC-HCRkt	VTHL	21,181
HRBCC-HCRkt	HTHL	242,833	23,643	266,476	HRBCC-HRkt	HTHL	21,533
HRBCC-HRkt	HTHL	237,573	32,136	269,709	HRBCC-HCRkt	HTHL	22,084
HRBCC-HRkt	VTHL	251,840	30,365	282,204	HRBCC-HRkt	VTHL	23,785

Despite the fact that the payload mass was doubled, the expendable orbiter empty masses and wetted areas are less than those of the equivalent reusable orbiter. The elimination of the wings did remove some of the volume available for required components, but also decreased the vehicle empty mass and wetted area. This decreased the orbiter gross mass and thus decreased the size of the booster as well. Furthermore, the drag on the wingless expendable orbiters was less than that of the winged reusable orbiters, which led to further reductions in the size of the boosters. These decreases in empty mass and wetted area were not only able to account for the increases due to the larger payload, but provide savings on the empty mass and wetted areas of the global strike vehicles.

In dealing with a hybrid vehicle, as the global strike vehicles are, the takeoff option becomes significant. Similar to the current ICBM fleet, each VTHL vehicle would require its own launch pad or silo to launch from. If 50 CAVs are required for a strike mission, then each of the 5 VTHL vehicles would require its own launch pad with the associated ground support equipment. HTHL vehicles, on the other hand, could share the same runway, and launch in quick succession, similar to bomber strike missions. In addition, until the staging point, the HTHL vehicles can return to the launch point should it be necessary to abort the strike mission. The entire vehicle, including CAVs can be recovered and reused. However, since the VTHL vehicles rely on stage separation, boostback, and each stage landing separately for recovery, only the booster of the VTHL strike vehicles can be recovered. Once launched, the VTHL orbiter stage and all CAVs cannot be recovered, even if the mission is aborted.

4.4.1 Global Strike VTHL HLV Detailed Mass Analysis

Since airbreathers cannot be used on the orbiter stage, there are only eight global strike vehicles, and their masses are shown in Figure 50. The results look similar to the baseline vehicle results. For the Rkt-Rkt vehicles, using a hydrogen orbiter instead of a hydrocarbon orbiter decreased the mass of the booster and the overall empty mass of the vehicle. For the RBCC-Rkt vehicles, the hydrogen orbiters increased the mass of the booster over the hydrocarbon orbiter, identical to the baseline vehicles. However, since the Rkt-RBCC vehicles were not considered for this mission since they have an airbreather orbiter stage, the Rkt-Rkt vehicles have the smallest overall empty mass.

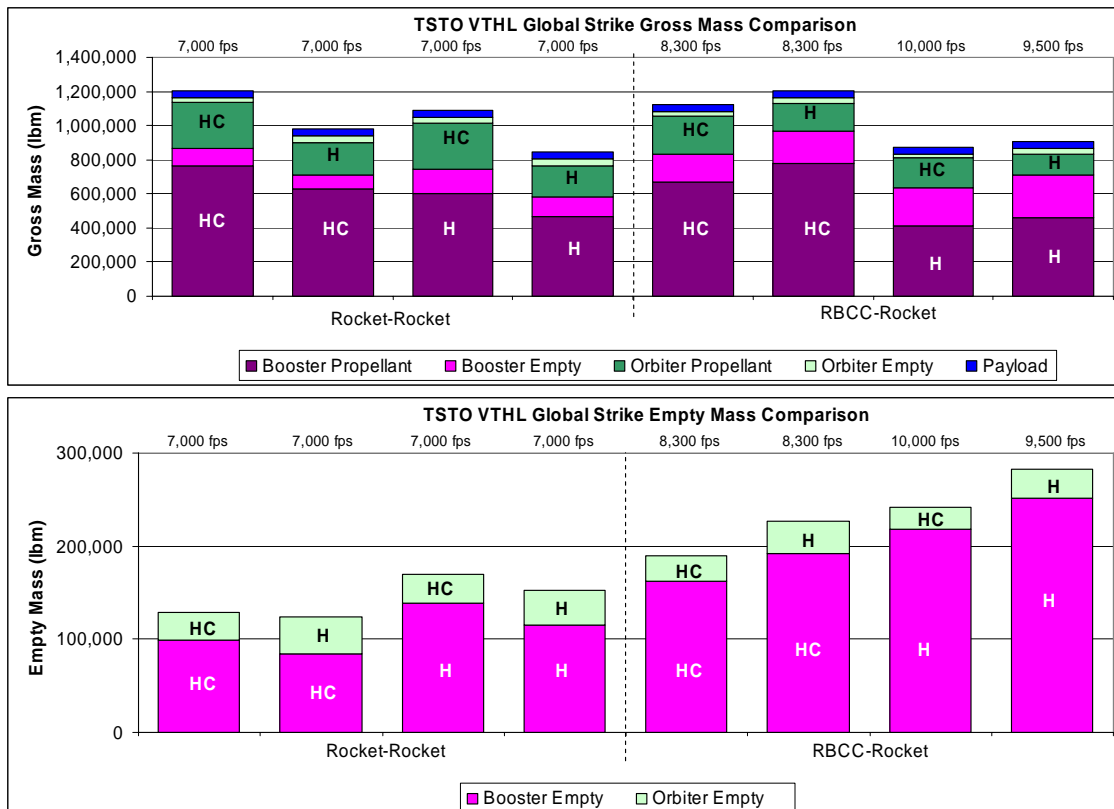


Figure 50. VTHL global strike vehicle mass comparison

The hydrocarbon orbiters, which will be thrown away, have smaller empty masses than hydrogen orbiters, so the best orbiter stage to use is a hydrocarbon-fueled orbiter. Of the two Rkt-Rkt vehicles with hydrocarbon orbiters, the HCRkt-HCRkt has both the smallest orbiter empty mass and overall vehicle empty mass. In addition, the use of the single fuel for both stages makes both the vehicle itself and the ground support facilities less complex than a mixed fueling option would. This makes the HCRkt-HCRkt the best choice for a VTHL global strike vehicle, despite the fact that it has neither the lowest vehicle empty mass nor lowest orbiter empty mass. Rather, it has a good compromise of both.

Figure 50 also illustrates the relatively small empty masses of the expendable orbiters when compared to the reusable boosters. When compared to Figure 36, it immediately becomes apparent that the orbiters make up a smaller fraction of the overall vehicle empty mass. This demonstrates the empty mass penalty that reusable vehicles incur over expendable vehicles; even orbiters which do not need to have any type of flyback propulsion. While the global strike vehicles do have a total ΔV of 1,000 fps (304.8 m/s) less than the baseline vehicles, it is primarily the removal of the extra mass required for the wings, landing gear, and thermal protection system that accounts for the lighter empty masses. This is shown in Figure 51, an empty mass breakdown of a reusable stage versus an expendable stage.

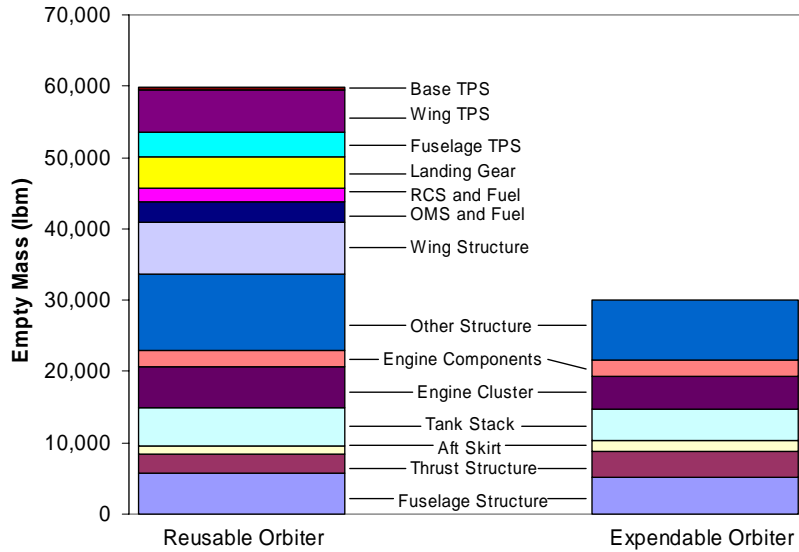


Figure 51. Mass breakdown of reusable and expendable stage

4.4.2 Global Strike VTHL HLV Detailed Area Analysis

The wetted areas and active areas of the global strike vehicles are shown in Figure 52, and are given for the reusable boosters only. The orbiter stage wetted area is not considered for this figure of merit, but the orbiter fuel type is given in parentheses above the bar as a reference. Since only the wetted and active areas of the booster are considered, the results for this study differed from the baseline vehicles. The use of hydrogen in the booster stage results in larger wetted areas. In fact, every hydrogen booster has a larger wetted area than any hydrocarbon booster. This makes the hydrocarbon boosters the logical choice for a strike vehicle, since they would have the shortest turnaround time between launches in addition to requiring ground support equipment for only one fuel type. Thus, the HCRkt-HCRkt, while ranked second for wetted area, is still the best choice for a global strike vehicle, though it does not have the

ability to return with the orbiter stage should an abort be necessary after launch. This vehicle is shown in Figure 53.

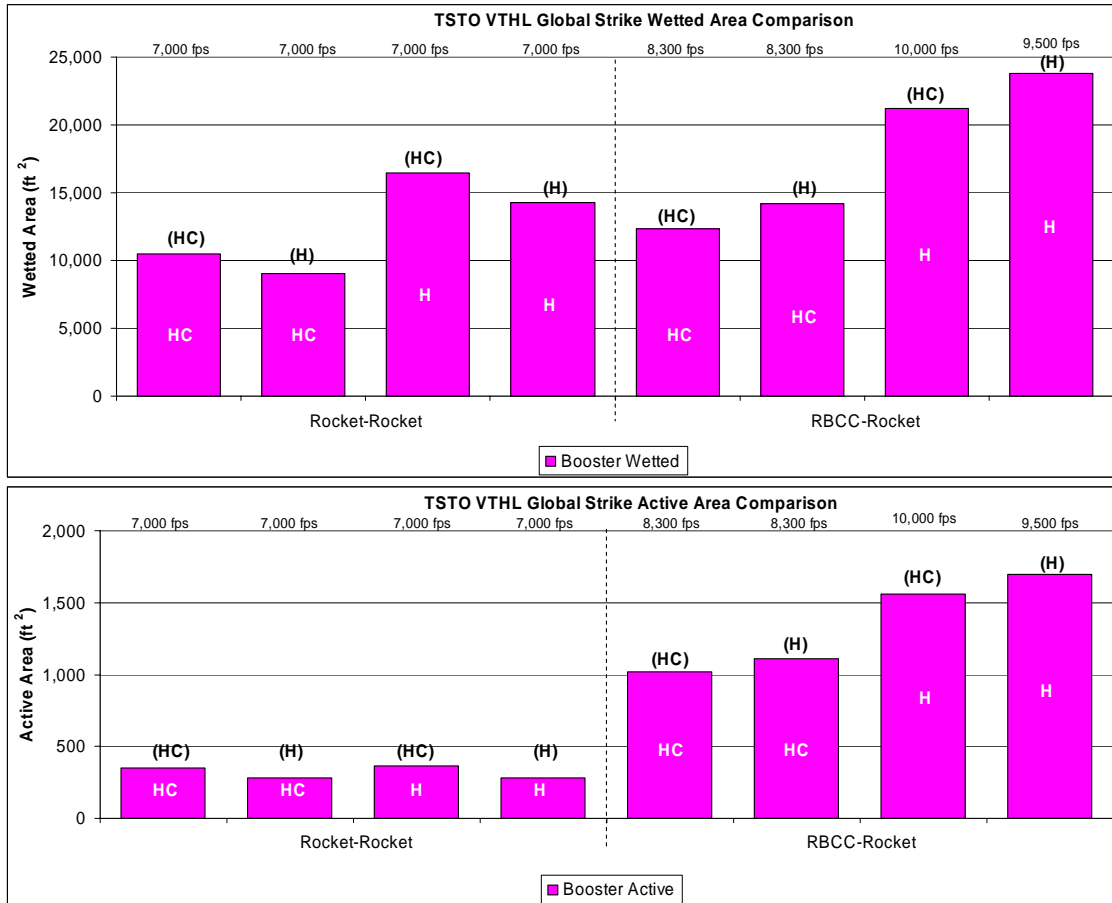


Figure 52. VTHL global strike vehicle area comparison

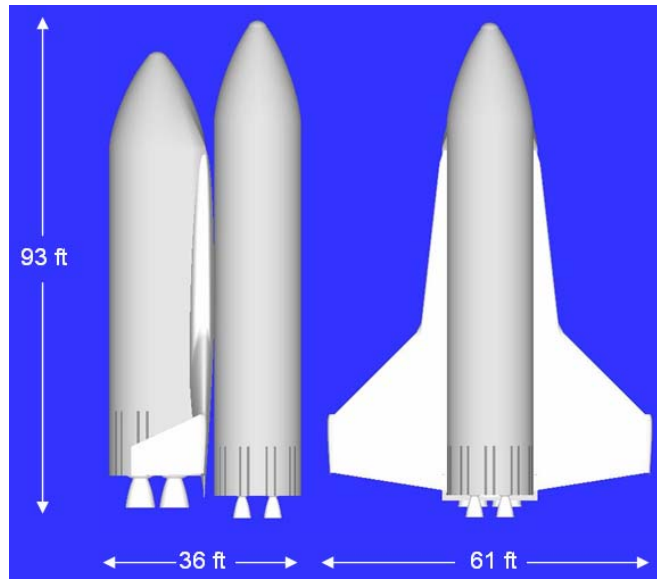


Figure 53. Hydrocarbon rocket-hydrocarbon rocket (HCRkt-HCRkt) global strike vehicle

The active area graph further demonstrates the suitability of Rkt-Rkt vehicles to this application. The rocket vehicles require active cooling on the rocket nozzles, which results in a small active area that can be easily inspected and the entire engine replaced if necessary. The RBCC boosters require at least three times the active cooling area for hydrocarbon DMSJ engines and about five times the active cooling for hydrogen DMSJ engines. The RBCC boosters would require a much larger number of man-hours required for refurbishing. However, the RBCC vehicles would be able to return the expendable orbiter stage and the payload of CAVs to the launch site in the case of a mission abort. The orbiter of a rocket booster vehicle would be lost, along with the CAVs, in the case of a mission abort.

4.4.3 Global Strike HTHL HLV Detailed Mass Analysis

The empty masses shown in Figure 54 reveal that the HCTurb-HRkt has the lowest vehicle empty mass, but the HCTurb-HCRkt has the smallest orbiter empty mass. The HCTurb-HCRkt, both RBCC-Rkt vehicles, and both TBCC-Rkt vehicles have almost the same overall empty masses. In all cases, the hydrocarbon orbiter again has a smaller empty mass than the equivalent hydrogen orbiter, making it the best choice for the orbiter stage. Though the HCTurb-HCRkt has an orbiter stage with greater empty mass than either the HRBCC-HCRkt or HCTBCC-HCRkt, it is a simpler vehicle than either of those. It has the additional advantage over the HRBCC-HCRkt of only requiring a single fuel. This makes the HCTurb-HCRkt the best choice for the HTHL global strike vehicle.

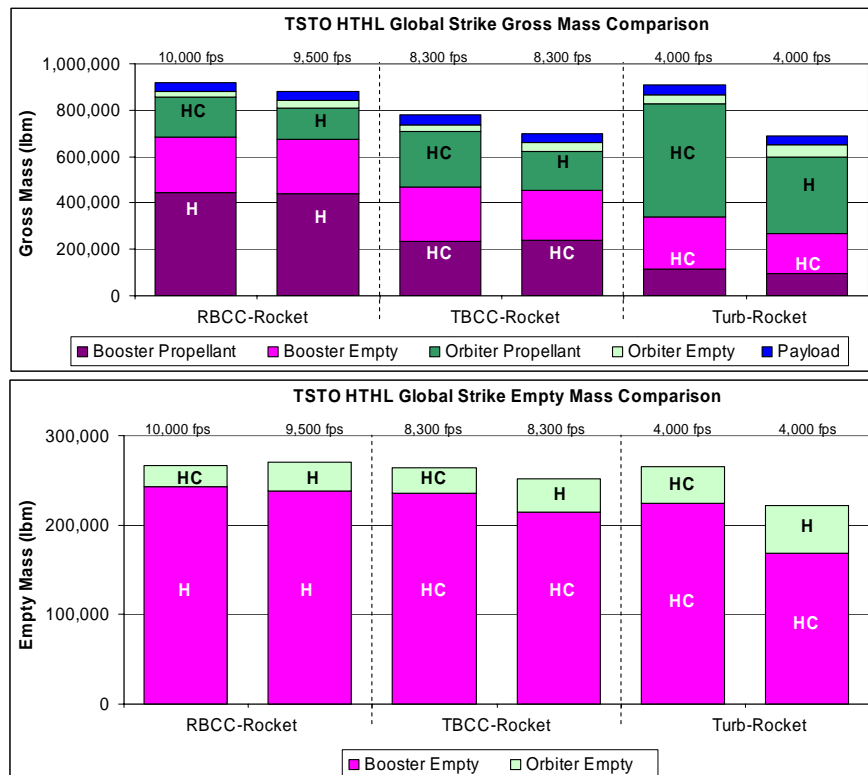


Figure 54. HTHL global strike vehicle mass comparison

A close look also shows the HCTurb-HRkt vehicle and HCTBCC-HRkt vehicle have nearly the same gross masses, but much different empty masses. The turbine booster has a smaller empty mass than the TBCC booster, as expected, since it does not have a DSMJ and only accelerates to 4,000 fps (1,219.2 m/s), after which the hydrogen rocket orbiter continues to 23,500 fps (7,162.8 m/s). However, it does have a hydrogen rocket orbiter with a slightly larger empty mass than the TBCC's hydrogen orbiter, since the TBCC's hydrogen orbiter only has to accelerate from 8,000 fps (2,438.4 m/s) to 23,500 fps (7,162.8 m/s). Overall, the smaller booster mass of the HCTurb-HRkt results in an overall smaller empty mass for the HCTurb-HRkt, making it the second best choice for a HTHL global strike vehicle. The third choice would be the HRBCC-HCRkt vehicle, due to its small orbiter empty mass.

When comparing the RBCC and TBCC vehicles, the RBCC vehicles require oxidizer for the first trajectory segment and a large volume of hydrogen, so the RBCC vehicles require larger propellant tanks than the TBCC vehicles. However, the turbines on the TBCC vehicles are more massive than the rockets on the RBCC vehicles. The gross masses of the RBCC vehicles are also higher than those of the TBCC vehicles, indicating that the RBCCs have larger wings than the TBCCs. The final result of these competing factors is that the empty masses end up about even. The choice of hydrogen over hydrocarbon for orbiter propellant decreases the booster empty mass but increases the orbiter empty mass. These trends again seem to balance each other out, so the empty masses remain within 20,000 lbm (9,071.8 kg).

4.4.4 Global Strike HTHL HLV Detailed Area Analysis

The wetted area of the HCTurb-HCRkt vehicle is not the smallest of the HTHL vehicles, as shown in Figure 55. However, the turbine vehicles require no active cooling area, indicating their turnaround time may be the shortest of all HTHL vehicles. Coupled with the hydrocarbon orbiter with a smaller empty mass, the HCTurb-HCRkt vehicle is the best choice for a HTHL global strike vehicle. However, its empty mass of 265,282 lbm (120,330 kg) is double that of the HCRkt-HCRkt's empty mass of 129,377 lbm (56,399.2 kg) and it has 7,000 ft² (650.3 m²) more wetted area. It does have two significant advantages over the HCRkt-HCRkt: a) It can return with the orbiter and CAVs in case of abort, and b) Multiple Turb-Rkt vehicles can be surged from the same runway in a short amount of time.



Figure 55. HTHL global strike vehicle area comparison

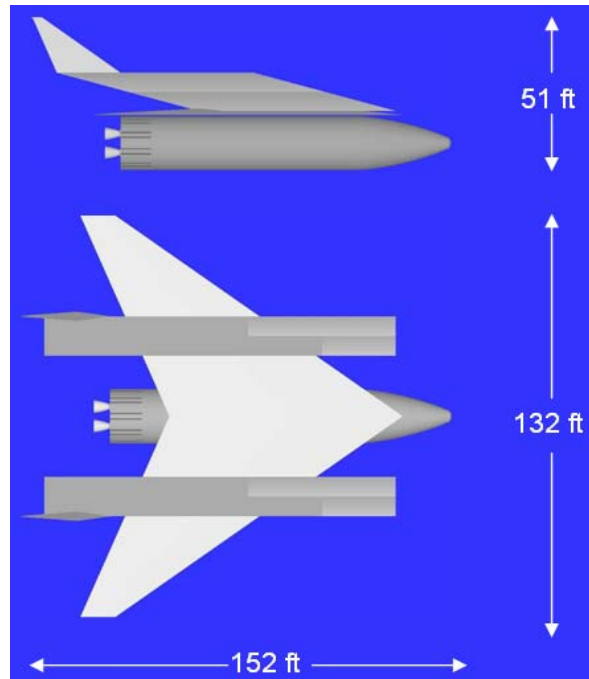


Figure 56. Hydrocarbon Turbine-Hydrocarbon Rocket (HCTurb-HCRkt) global strike vehicle

Of the remaining HTHL vehicles, the inward turning geometry and larger wings of the RBCC vehicles cause their wetted areas to be higher than those of the 2-D TBCC vehicles. For the TBCC vehicles, the wetted areas of the orbiters are no longer a factor, so the smaller booster with the hydrogen orbiter has less wetted area than its counterpart with a hydrocarbon orbiter. The active areas of the RBCC-Rkt and TBCC-Rkt vehicles remain nearly the same, since the 2-D vehicles, despite having a lesser wetted area in this case, require more active cooling than inward turning vehicles.

4.5 Summary

This study showed that there was no single design that fulfilled all of the missions and consistently had the smallest empty mass and wetted area. The hydrocarbon rocket

booster with a hydrocarbon RBCC orbiter proved to have the smallest empty mass and wetted area for the baseline payload launch of 20,000 lbm (9,071.8 kg), and the growth rates from the payload study showed this configuration would remain the best vehicle for these figures of merit. In addition, this vehicle's empty mass and wetted area remained below the other vehicles' empty masses and wetted areas when flown 1,000 nm (1,852 km) to accomplish an orbital rendezvous. However, this vehicle proved to be unsuitable for the global strike mission since the RBCC orbiter would be unable to be recovered. The hydrocarbon rocket booster with a hydrocarbon rocket orbiter proved to be the best choice for the global strike mission. In general, the VTHL vehicles had lighter empty masses and smaller wetted areas than the HTHL vehicles, regardless of fueling options.

5. Conclusions and Recommendations

This research effort was sponsored by the AFRL Propulsion Directorate to investigate potential solutions to the DoD requirements for responsive and low-cost space launch for military applications. Extensive research has been conducted using vehicles propelled by hydrogen-fueled scramjet engines, but little research has been done regarding the use of hydrocarbon-fueled scramjet engines for space launch. The U.S. Air Force HyTech program is investigating this area due to practical and operational benefits hydrocarbon fuels provide, so engine performance data from this program was used to model both TBCC and RBCC propulsion systems.

5.1 Conclusions and Recommended RLV Configurations

5.1.1 Baseline Space Launch Mission

1. For the baseline space launch mission, the recommended VTHL system is the HCRkt-HCRBCC. This configuration had both the lowest empty mass and the smallest wetted area, both of which were smaller than even the Rkt-Rkt vehicle. It does however require over twice as much actively cooled area as the rocket system. Since many researchers correlate a launch vehicle's empty mass with the total acquisition and operational cost and the wetted area with the turn-around time and man-hours required between flights, these results indicate the Rkt-RBCC could be the better VTHL configuration in both respects. In addition, the use of a single, non-cryogenic fuel makes it the easiest to support logistically. The recommended HTHL vehicle is the HCTurb-HRBCC configuration. This configuration again had the lowest empty mass and nearly

the smallest wetted area of all baseline HTHL vehicles, though not nearly as low as the VTHL HCRkt-HCRBCC vehicle. The HCTurb-HRBCC uses air for its oxidizer for over 60% of the total velocity range, including the use of an airbreather on the orbiter stage.

2. Using airbreathing propulsion on the orbiter stage results in empty mass and wetted area savings in the entire vehicle despite the increase in orbiter empty mass and wetted area. As mentioned before, the orbiter stage gross mass is the payload of the booster stage, so the gross mass of the orbiter has the largest impact on the gross mass of the booster and thus the booster's empty mass and wetted area. By using airbreathing propulsion on the orbiter, the empty mass of the orbiter increases by a small amount due to the complex geometry and high fineness ratio required, but this is offset by the large amount of stage gross mass saved since less LOX is required. The orbiter stage gross mass savings leads to a smaller booster stage gross and empty mass and more than makes up for the small increase in orbiter empty mass.

3. A two stage system using an airbreathing orbiter with hydrogen fuel has a little smaller overall empty mass, but a much larger wetted area than a similar rocket vehicle, but using hydrocarbon fuel results in a substantial reduction in both empty mass and wetted area relative to a hydrocarbon rocket.

5.1.2 Payload Sizing Impact Study

1. For the payload size impact study, VTHL vehicles in general had smaller growth rates with increasing payloads than the HTHL vehicles. The Rkt-RBCC configurations had the smallest growth rates among VTHL vehicles, while the RBCC-Rkt configurations had the highest growth rates, again confirming the advantages of using

airbreathers on the second stage. The vehicle with the smallest growth rate for empty mass was again the HCRkt-HCRBCC, indicating its suitability for increasing payload masses beyond the baseline payload mass. For the HTHL configurations, the airbreathing orbiters had smaller growth rates in general than those of the rocket orbiters.

2. As previously mentioned, VTHL vehicles in general had smaller growth rates than the HTHL vehicles. Though this growth is not very apparent in the 0-30,000 lbm (0-13,607.8 kg) range, this trend becomes clear as the payload mass is extended to 100,000 lbm (45,359.2 kg). This is due to the heavier wings and landing gear associated with horizontal takeoff, since these systems are sized based on the gross takeoff mass. Vertical takeoff vehicles have wings and landing gear sized based on the landing mass, which is significantly less than the gross takeoff mass. HTHL vehicles are burdened with large wings and heavy gear which causes them to grow faster than the VTHL systems.

5.1.3 Orbital Rendezvous Mission

1. For the orbital rendezvous study, the Rkt-Rkt vehicles were not considered, since they cannot cruise unless additional propulsion is added to the vehicle. The remaining 17 systems were sized with a 1,000 nm (1,852 km) radius prior to accelerating to orbit. The HCRkt-HCRBCC vehicle is the best VTHL vehicle for the mission, and the HCTJ-HCRBCC is the best HTHL vehicles. Both of these vehicles are able to cruise after dropping the empty mass of the first stage and cruise using dense hydrocarbon fuel.

2. Airbreathers have more trajectory flexibility than rockets. Launch windows can be expanded by flying an offset radius when launch timing and placement is critical for rendezvous missions. This study showed that without refueling, the vehicle growth

limits this radius to about 1,000 nm (1,852 km). Again, the advantage of this amount of orbital trajectory flexibility must be weighed against the required 40%-150% increase system empty mass and wetted area. The HCRkt-HCRBCC was the lightest system for both this and the baseline missions and showed about a 55% increase in empty mass and wetted area to obtain the 1,000 nm (1,852 km) radius. Low density liquid hydrogen fuel used for the cruise resulted in large increases in vehicle empty mass and wetted area, with high-density hydrocarbon being the best fuel for this mission.

5.1.4 Hybrid Global Strike Mission

1. For the global strike mission, the same figures of merit are used, but the vehicles are evaluated differently, with more emphasis on the empty weight of the expendable orbiter. Additionally, only the wetted area of the reusable booster is considered. Among all vehicles, the HCRkt-HCRkt has one of the lightest empty mass, and second smallest wetted area of the global strike vehicles, but it has the least massive and simplest expendable upper stage, making it the best choice for this mission. For the HTHL vehicles, the HCTurb-HCRkt vehicle is the best choice for similar reasons. Both stages are simple vehicles, the expendable hydrocarbon orbiter has a small empty mass, and both stages use hydrocarbon fuel.

2. The VTHL Rkt-Rkt vehicle has the smallest empty mass and wetted area, but will require an individual launch pad per vehicle or an hour or more delay between launches from the same pad. The HTHL Turb-Rkt vehicle, by far the best of the HTHL systems for this mission, has double the empty mass and 150% the wetted area of the VTHL rocket system, but many of these vehicles could share the same runway with

takeoff spacing of a couple of minutes. This would allow a large number of CAVs to be rapidly launched from a single runway without requiring large numbers of launch pads. The HTHL vehicle could also be recalled up until the staging point and return with the entire orbiter stage and payload. This would not be possible with Rkt-Rkt vehicles.

5.1.5 Other Findings

1. The fly-back lift to drag ratio for hypersonic vehicles has a significant effect on the flyback propulsion, therefore it is important to use an accurate value. These vehicles typically have a subsonic L/D of less than 5 when carrying the second stage. This results in poor flyback performance. Airbreathing boosters must fly back to the launch site with the second stage still attached in the case of a mission abort, but the mass of the orbiter flown back affects the empty mass of the booster. Significant empty mass savings can be achieved by dumping the propellant of the second stage to allow the booster to fly back with the empty orbiter plus payload rather than the entire gross mass of the second stage.

2. The cutoff velocity for the DMSJ should not remain a fixed number for a given fuel. The effective specific impulse of the vehicle and bulk density ratio of the propellants used for the DMSJ and rocket will determine the optimum velocity to switch propulsion systems. Until the ASC/XRE study is completed, a linear trend can be used to find the proper cutoff point rather than a lengthy trial-and-error method to minimize empty mass.

5.2 Recommendations for Future Research

1. The vehicles using a scramjet for the orbiter stage had less empty mass and wetted areas than systems with rocket orbiter stages. Furthermore, for all VTHL systems, the hydrocarbon RBCC orbiters were better than the LH_2 orbiters in both figures of merit. A sensitivity study of the Rkt-RBCC, Turb-RBCC, and TBCC-RBCC configurations using different hydrocarbon fuels, including JP-7, methane, and ethane, would seem to be needed to flush out the detailed trades. The differences in specific impulses, heating values, and densities of each fuel could produce a vehicle of even less empty mass and smaller wetted area.

2. This study considered only two-stage vehicles, which will be technologically feasible in an estimated 10 to 15 years, as discussed in section 2.2. Single-stage-to-orbit vehicles may be possible in 15 to 20 years, so it is not too early to consider these configurations. Such a vehicle could use bi-propellants, with a single fuel and oxidizer, or tripropellant, with two different fuels and a single oxidizer. A study of SSTD configurations is a logical next step beyond the analysis performed in this study, but a conservative approach should be taken to avoid problems plaguing early SSTD designs such as NASP.

3. Further studies should be done to determine the optimum amount of offset radius and the best cruise conditions for rendezvous missions.

5.3 Summary

This study provided a comprehensive look at 21 alternative launch systems, extending the work done in several previous studies by exploring different launch,

propulsion and fuel options. The HCRkt-HCRBCC configuration, which had not been previously studied, proved to be one of the best performers for both empty mass and wetted area despite relatively conservative mass estimates. This study explored growth rates for varying payload masses, as well as defining two additional missions and determined their impact on alternative system sizes. The HCRkt-HCRBCC vehicle has the smallest growth rates for both figures of merit and also proved to be the best vehicle to make an orbital trajectory change. Finally, the global strike mission explored the use of hybrid vehicles, and the HCRkt-HCRkt hybrid vehicle ranked highest. Benefits were identified for horizontal launch for this mission. Hopefully the conclusions of this study will prove useful in the emerging field of airbreathing propulsion in RLVs.

Appendix A. Airbreathing Engine Performance Data

AFRL Turbine Accelerator Engine Thrust (lbf)

Mach #	0	0.5	0.8	1.0	1.5	2.0	2.5	3.0	3.25	3.75	4.0	4.4
Altitude (ft)												
0	51,621.0	54,326.0	51,785.0	53,721.0	74,073.0	0	0	0	0	0	0	0
5,000	0	47,598.0	39,940.0	45,774.0	65,959.0	0	0	0	0	0	0	0
10,000	0	0	33,160.0	38,853.0	58,108.0	81,412.0	127,578.0	0	0	0	0	0
20,000	0	0	22,508.0	26,583.0	42,066.0	65,315.0	100,391.0	146,736.0	0	0	0	0
30,000	0	0	14,923.0	17,615.0	29,340.0	48,284.0	71,157.0	100,641.0	0	0	0	0
40,000	0	0	9,584.4	11,293.0	19,106.0	31,506.0	46,397.0	65,463.0	74,388.0	92,791.0	103,912.0	119,178.0
42,000	0	0	0	10,254.0	17,324.0	28,618.0	42,120.0	59,417.0	67,514.0	84,201.0	94,279.0	108,120.0
50,000	0	0	0	6,966.7	11,778.0	19,448.0	28,620.0	40,321.0	45,834.0	57,072.0	63,871.0	73,190.0
60,000	0	0	0	4,295.0	7,270.1	11,984.0	17,650.0	24,826.0	28,208.0	35,084.0	39,236.0	44,908.0
70,000	0	0	0	2,638.8	4,479.5	7,362.4	10,815.0	15,206.0	17,256.0	21,419.0	23,971.0	27,422.0
72,000	0	0	0	2,391.9	4,063.7	6,669.8	9,792.5	13,770.0	15,619.0	19,403.0	21,696.0	24,808.0
80,000	0	0	0	1,620.7	2,748.4	4,502.2	6,610.1	9,293.5	10,525.0	13,053.0	14,604.0	16,683.0
90,000	0	0	0	1,005.0	1,700.8	2,780.2	4,071.7	5,719.5	6,468.0	8,007.4	8,954.3	10,234.0
100,000	0	0	0	627.4	1,058.2	1,727.3	2,526.8	3,548.0	4,003.0	4,945.4	5,535.9	6,309.4

AFRL Turbine Accelerator Engine ISP (sec)

Mach #	0	0.5	0.8	1.0	1.5	2.0	2.5	3.0	3.25	3.75	4.0	4.4
Altitude (ft)												
0	2122.1	1957.1	1765.5	1719.4	1605.4	0	0	0	0	0	0	0
5,000	0	1963.6	1776.4	1731.2	1640.8	0	0	0	0	0	0	0
10,000	0	0	1759.1	1745.2	1674.3	1558.7	1563.0	0	0	0	0	0
20,000	0	0	1732.6	1731.0	1719.8	1671.2	1652.7	1605.6	0	0	0	0
30,000	0	0	1717.3	1716.2	1765.1	1751.7	1708.5	1649.0	0	0	0	0
40,000	0	0	1721.4	1718.3	1786.9	1780.2	1734.7	1676.4	1630.0	1534.9	1501.1	1453.0
42,000	0	0	0	1717.6	1783.6	1779.4	1733.7	1675.1	1628.0	1533.4	1499.4	1451.1
50,000	0	0	0	1714.2	1780.9	1776.4	1729.8	1669.8	1623.0	1526.7	1492.1	1442.8
60,000	0	0	0	1708.9	1777.6	1769.5	1724.5	1662.6	1615.0	1517.6	1482.3	1431.5
70,000	0	0	0	1702.6	1775.0	1763.2	1714.0	1650.8	1602.0	1502.7	1467.6	1415.5
72,000	0	0	0	1701.0	1773.8	1760.2	1710.8	1647.3	1598.0	1498.9	1463.7	1411.0
80,000	0	0	0	1694.4	1764.8	1747.3	1698.0	1633.3	1582.0	1481.5	1446.8	1393.2
90,000	0	0	0	1688.3	1756.2	1734.4	1681.9	1615.5	1563.0	1459.6	1424.3	1370.6
100,000	0	0	0	1681.8	1745.7	1720.3	1666.4	1598.1	1543.0	1437.9	1402.5	1347.0

AFRL HyTech DMSJ Engine Performance Data

Flight Path Angle = 0 deg			
Mach Number	Q (psf)	Thrust Coefficient	ISP (sec)
3.5	0	0	0
	250	0	0
	500	0	0
	1000	0	0
	2000	0	0
3.75	0	0	0
	250	0.546	1310.13
	500	0.728	1746.84
	1000	0.741	1759.93
	2000	0.745	1765.23
4.0	0	0	0
	250	0.632	1212.62
	500	0.843	1616.82
	1000	0.817	1621.24
	2000	0.822	1628.02
4.5	0	0	0
	250	0.586	1222.44
	500	0.782	1629.92
	1000	0.794	1639.12
	2000	0.805	1645.86
5.0	0	0	0
	250	0.666	1051.40
	500	0.888	1401.87
	1000	0.901	1408.23
	2000	0.909	1412.73
6.0	0	0	0
	250	0.419	701.00
	500	0.559	934.66
	1000	0.578	956.39
	2000	0.595	975.34
7.0	0	0	0
	250	0.346	605.15
	500	0.461	806.87
	1000	0.489	838.25
	2000	0.506	859.19
8.0	0	0	0
	250	0.284	532.38
	500	0.379	709.84
	1000	0.409	747.77
	2000	0.427	771.15
8.25	0	0	0
	250	0.270	514.30
	500	0.360	685.73
	1000	0.390	724.26
	2000	0.407	747.43

Flight Path Angle = 4 deg			
Mach Number	Q (psf)	Thrust Coefficient	ISP (sec)
3.5	0	0	0
	250	0	0
	500	0	0
	1000	0	0
	2000	0	0
3.75	0	0	0
	250	0.674	1344.75
	500	0.899	1793.00
	1000	0.914	1804.57
	2000	0.914	1800.45
4.0	0	0	0
	250	0.744	1218.96
	500	0.992	1625.28
	1000	1.014	1643.38
	2000	1.020	1648.68
4.5	0	0	0
	250	0.722	1225.07
	500	0.962	1633.43
	1000	0.977	1642.76
	2000	0.990	1649.38
5.0	0	0	0
	250	0.832	1050.79
	500	1.109	1401.05
	1000	1.127	1405.80
	2000	1.144	1409.60
6.0	0	0	0
	250	0.545	709.48
	500	0.727	945.97
	1000	0.751	964.88
	2000	0.772	981.51
7.0	0	0	0
	250	0.460	616.26
	500	0.613	821.68
	1000	0.649	849.72
	2000	0.671	868.22
8.0	0	0	0
	250	0.401	545.00
	500	0.534	726.66
	1000	0.573	760.93
	2000	0.597	782.85
8.25	0	0	0
	250	0.385	525.84
	500	0.513	701.12
	1000	0.553	736.59
	2000	0.577	758.03

Appendix B. HySIDE System Element Description

The following references were used to compile this appendix: 8, 14, 22, 25, 26, 28, and 34

B.1 “FreeStream” System Element

The user inputs the Mach number and altitude that will be each vehicle’s design point in the FreeStream system element, shown in Figure 57. This is critical for an airbreathing design, but not as important for a rocket. For a rocket, the staging point is a good choice for the booster stage, while the midpoint of the orbiter stage’s trajectory is an appropriate choice for the orbiter. For an airbreathing vehicle, the design point is critical for proper performance of the DMSJ during its entire operational range of velocities. The entire vehicle’s aerodynamic characteristics are determined from the design point using methods described in section B.5 of this appendix, and the inlet shape affects both drag and vehicle heating. Generally, it is best to choose a design point one or two Mach numbers below the maximum DMSJ velocity. If the design Mach number is too close to this maximum velocity, vehicle heating will not be as great at these higher velocities, but the drag will be excessive at the lower end of the DMSJ operational range. If the design Mach number is too low, the opposite will occur. Once the design Mach number has been chosen, the design altitude should then be selected that corresponds with the desired dynamic pressure.

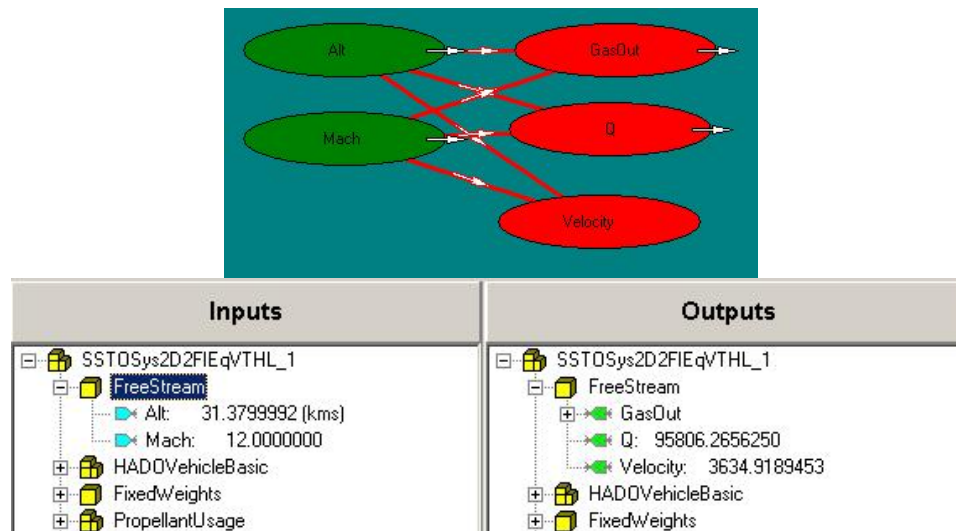


Figure 57. Block diagram and input/output tree of "FreeStream" system element

B.2 Vehicle System Elements

The system elements for an airbreathing vehicle and a rocket vehicle differ significantly, and are described separately in the sections below.

B.2.1 “Rocket” Vehicle System Element

The rocket vehicle system element, as shown in Figure 58, consists of all the modules necessary to build a rocket vehicle. The “RocketFuselage” system element allows the user to input the desired cylindrical radius of the vehicle, the length of the fuselage, and the length of the ogive. These dimensions are used in all future calculations, and the user modifies these to achieve the desired volume available over volume required ratio. In addition, the user can specify a few other geometrical properties of the fuselage, such as the body flap length. The “AftSkirt,” “Base,” and “ThrustStructure” system elements are linked to the “RocketFuselage” system element for overall vehicle dimensions, with inputs for a few other geometrical properties as well.

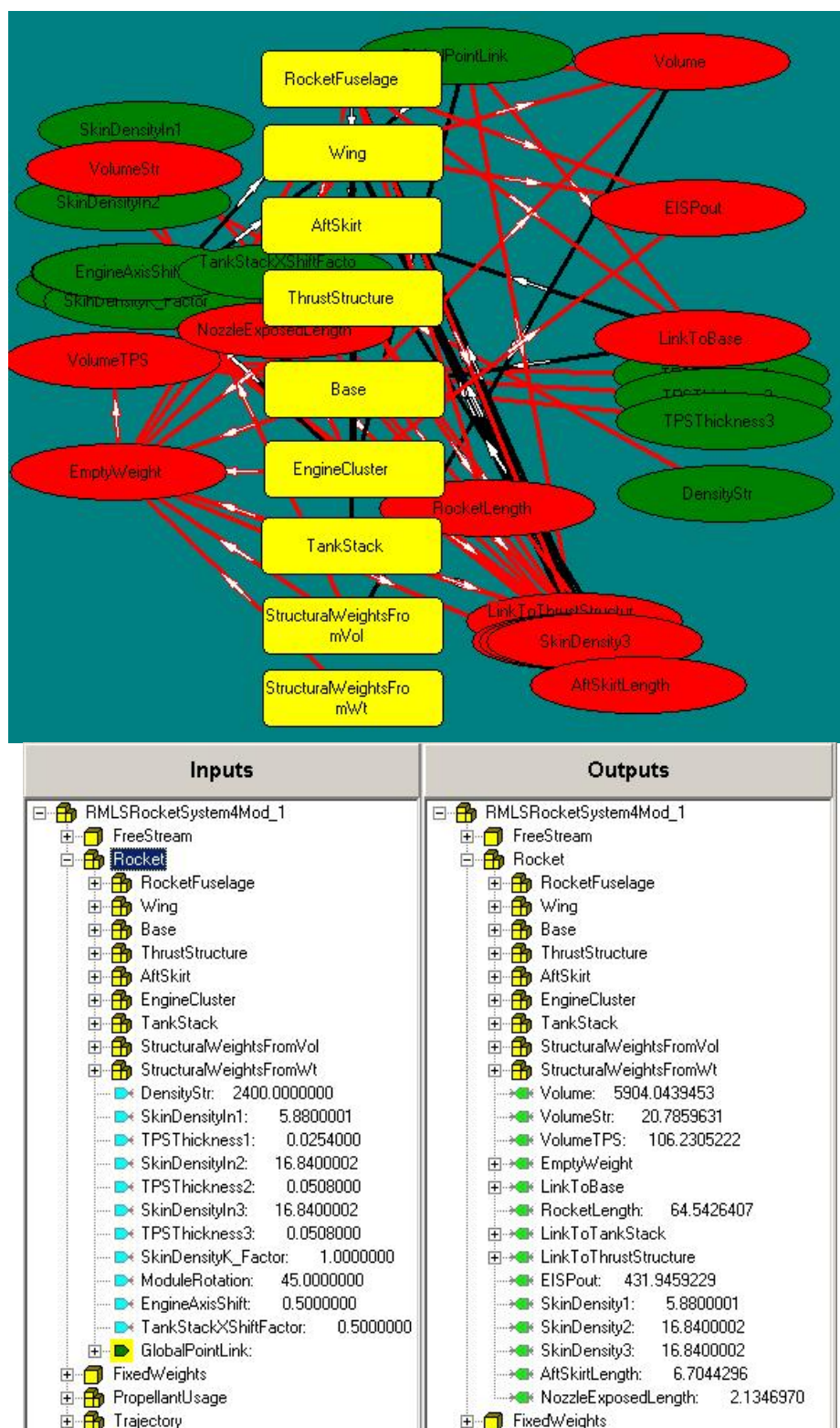


Figure 58. Block diagram and input/output tree of "Rocket" system element

The “Wing” system element contains the inputs for the airfoil geometric characteristics, including aspect ratio, taper ratio, and leading edge sweep. The trapezoidal “reference” planform wing area (S_{ref}) is calculated in this module. Since rockets in HySIDE are VTHL, S_{ref} is calculated using the vehicle landing mass and landing velocity, for both boosters and orbiters. HySIDE then calculates the exact dimensions of the wing based on this area and the specified geometric characteristics. The default airfoil characteristics for HySIDE are listed in Table 22. This module also sizes the tail based on a fraction of the wing planform area and uses similar airfoil characteristic inputs as the wing.

Table 22. Rocket wing airfoil characteristics

Airfoil Characteristic	Value
NACA Series	2412
Thickness-to-Chord Ratio	0.07
Taper Ratio	0.18
Leading Edge Sweep (Deg)	45
Aspect Ratio	2.4

The “EngineCluster” system element, shown in Figure 59 is a detailed model that sizes the combustion chamber, nozzle, and turbopumps assembly. The user can select pre-loaded parameters for 24 existing rockets, or make changes to the area ratio, fuel used, throttle setting, design altitude, and materials used. The takeoff thrust required is given by

$$T_{TO} = \left(\frac{T}{W} \right)_{TO} \cdot GTOW \quad (58)$$

where $\left(\frac{T}{W} \right)_{TO}$ is the user-inputted vehicle thrust-to-weight at takeoff. Based on this required takeoff thrust, HySIDE uses the parameters from the existing rocket specified and rubberizes the engines to match. Any changes inputted by the user are then taken into account, and HySIDE individually sizes the thrust chamber, turbopumps, and nozzle to determine the mass of each. “EngineCluster” contains four individual nozzles, combustion chambers, and sets of turbopumps.

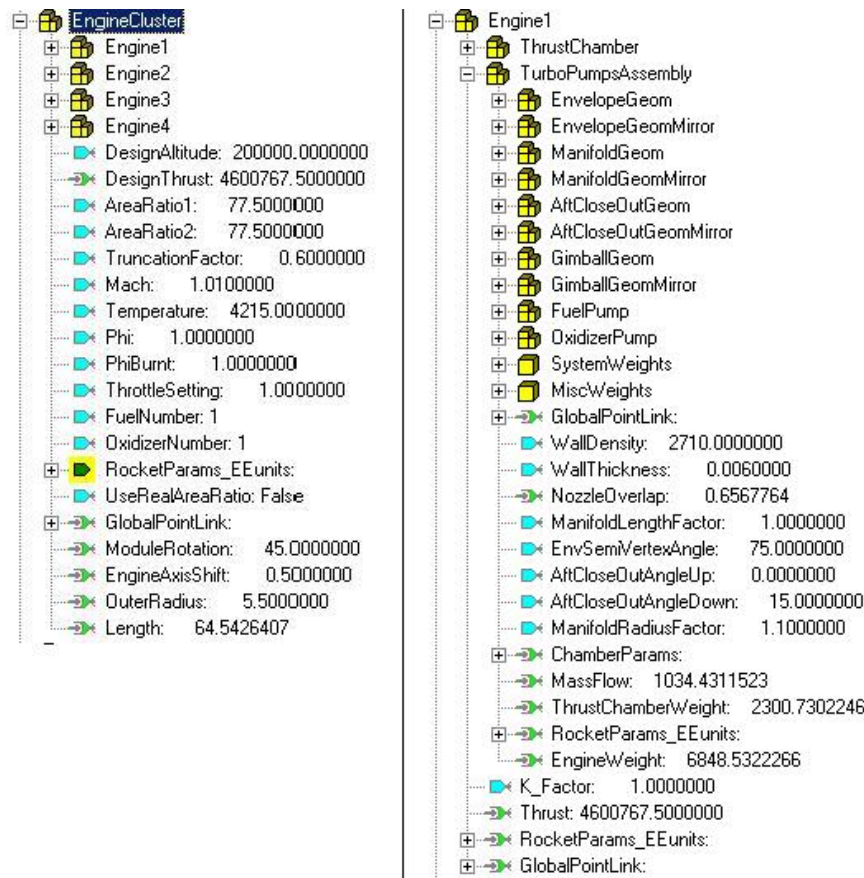


Figure 59. Input/Output tree of "EngineCluster" system element

The “TankStack” system element calculates the mass and volume of the fuel and oxidizer tanks. The tanks are modeled as standard cylindrical propellant tanks with ellipsoidal end caps, which there is a great deal of experience in designing. The tank geometry and mass are based on NASA’s CR287 method; Air Force Research Laboratory, Air Vehicle Directorate’s (AFRL/VA’s) SP125 method; and Aeronautical System Center’s (ASC’s) Reusable Military Launch System (RMLS) work. The tank weight is found using

$$W_{tank} = \frac{k_{correl} \cdot k_{\rho_p} \cdot C_{config} \cdot P_p \cdot Vol \cdot \rho_{tank}}{\eta \cdot \sigma_{max}} \quad (59)$$

where k_{correl} is a correlation factor to the space shuttle external tank, k_{ρ_p} is a factor based on the density of the propellant, C_{config} is the configuration factor based on a cylindrical tank, P_p is the pressure required by the propellant, Vol is the volume of the propellant, ρ_{tank} is the density of the tank material, η is the construction efficiency factor, and σ_{max} is the maximum stress allowable by the tank material. The user can specify most of these inputs, a safety factor, and ullage fraction, as well as a k-factor for uncertainty.

“TankStack” uses these inputs and the total amount of propellant, which is calculated by the “PropellantUsage” system element, to size the tanks and place them within the user-defined fuselage dimensions.

The final two system elements use the total vehicle mass and volume, along with design factors, to account for the additional mass of various necessary components from trend curves. “StructuralWeightsFromVol” adds mass due to miscellaneous components that have trends as a function of vehicle volume. These items include: structural

provisions, such as access doors, gear door seals, and crew cabin insulation; equipment, such as avionics and hydraulics; fuselage structures, such as bulkhead insulation and tank mounts; engine components, such as propellant feed lines, actuators, and controls; and other miscellaneous components. The mass of any component that is not used in a particular model, such as crew-related items in this study, can be eliminated by using a design factor of zero, or setting the k-factor to zero if a whole group is not needed. None of these components is physically placed in the vehicle, but the total mass and volume requirement of each component is tabulated.

The “StructuralWeightsFromWeight” system element calculates additional masses that have trend curves as a function of vehicle mass. Since the vehicle mass varies at different points in the flight trajectory, each component may have a different mass linked to it depending on the configuration. For example, the mass of the nose and main landing gear is calculated by this module, using either the landing mass for VTHL vehicles, or the GTOM for HTHL vehicles. The mass of the takeoff propulsion system element calculates the mass of the rocket or turbine engine required for takeoff. The mass calculation in this system element is not used in the rocket vehicle, since the “EngineCluster” system element calculates precise masses for the rocket engines rather than relying on a trend. However, the turbine engine inputs entered here are used in sizing the flyback turbine engines as explained later. The mass of the reaction control system (RCS) and orbital maneuvering system (OMS) and fuel for each is calculated based on a ΔV inputted by the user and the mass of the vehicle at the end of the flight trajectory. For an orbiter stage, the ΔV necessary to circularize the 50 nm (92.6 km) by

100 nm (185.2 km) orbit as well as the ΔV necessary to de-orbit are entered here. The mass of the linkage structure between stages of multiple stage vehicles is also calculated here. For this study, orbiter mass was used to find the linkage mass, and the linkage weight was added to the booster stage.

The final mass in “StucturalWeightsFromWeight” is the mass of the flyback propulsion and fuel. The weight fraction of fuel required is found using the Breguet range equation:

$$\frac{W_f}{W_i} = e^{\frac{-R \cdot SFC}{v \cdot \frac{L}{D}}} \quad (60)$$

where R is the range, $\frac{L}{D}$ is the lift-to-drag ratio, W_f is the weight at the end of the flyback segment, and W_i is the weight at the beginning of the flyback segment [35:21].

Rearranging this equation gives the range factor, $\frac{V}{SFC} \frac{L}{D}$, which should be made as large as possible for the farthest range. Two small turbine engines are sized using the turbine inputs from the “MassOfTakeoffPropulsion” using statistical jet-engine models for non-afterburning engines, given by

$$W_{uninstalled} = 0.084 \cdot \left(\frac{T_{flyback}}{2} \right)^{1.1} e^{-0.045 \cdot BPR} \cdot 0.8 \quad (61)$$

$$L_{uninstalled} = 0.185 \left(\frac{T_{flyback}}{2} \right)^{0.4} \cdot M^{0.2} \cdot 0.8 \quad (62)$$

$$D_{uninstalled} = 0.033 \cdot \left(\frac{T_{flyback}}{2} \right)^{0.5} e^{0.04 \cdot BPR} \cdot 0.9 \quad (63)$$

where the BPR is the bypass ratio, M is the Mach number, and $T_{flyback}$ is found using

$$T_{flyback} = \frac{W_{flyback}}{2 \frac{L}{D}} \quad (64)$$

Weight and lift are directly opposed in straight and level flight, as are thrust and drag, so the thrust required per engine is just the drag divide by the number of engines, two. A small tank is also sized to contain this fuel.

The entire rocket vehicle, once assembled, is shown in Figure 60.

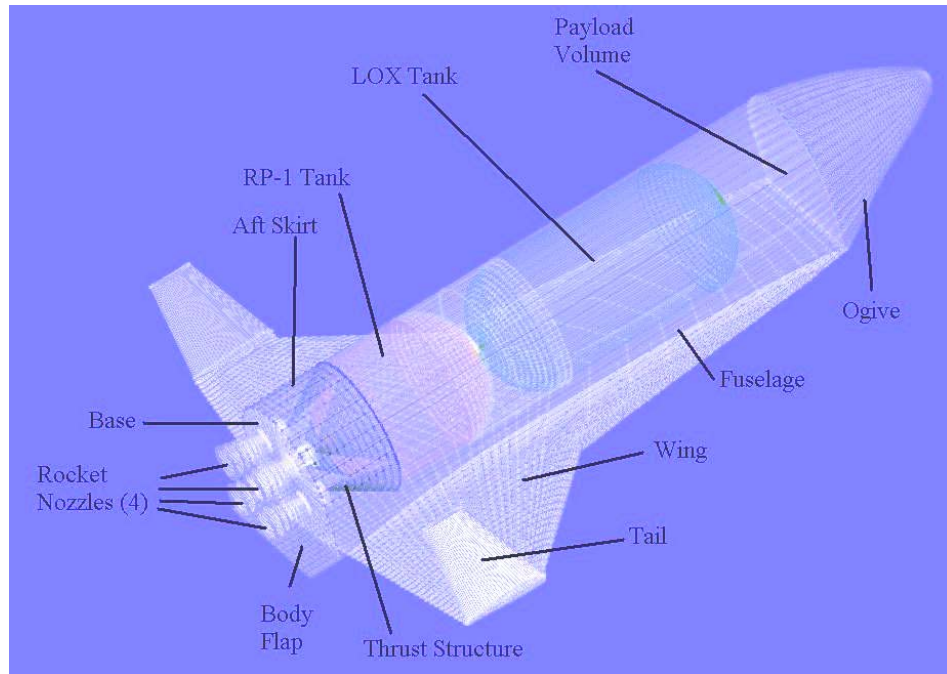


Figure 60. HySIDE reusable rocket vehicle (hydrocarbon)

B.2.2 Hypersonic Airbreathing Design Optimization (HADO) Vehicle System Element

The airbreathing vehicle system element is called Hypersonic Airbreathing Design Optimization (HADO), as shown in Figure 61, and is more complicated than the rocket vehicle. Some of the system elements within it are the same as a rocket, but most are different. The vehicle body itself is part of the engine, and thus is carefully shaped. The main parts of the body are the inlet, combustor, isolator, nozzle, and external surface, as shown in Figure 62.

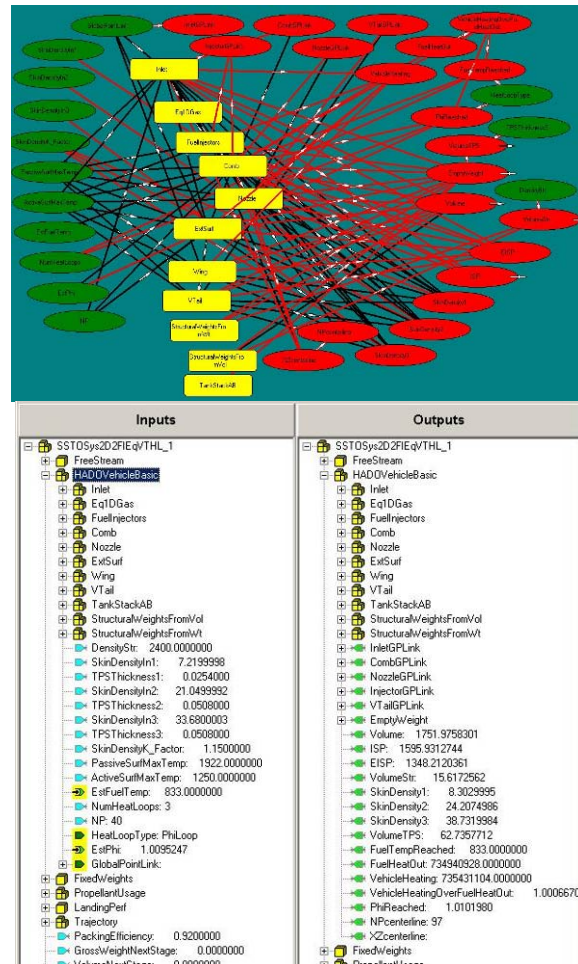


Figure 61. Block diagram and input/output tree of "HADOVehicleBasic" system element

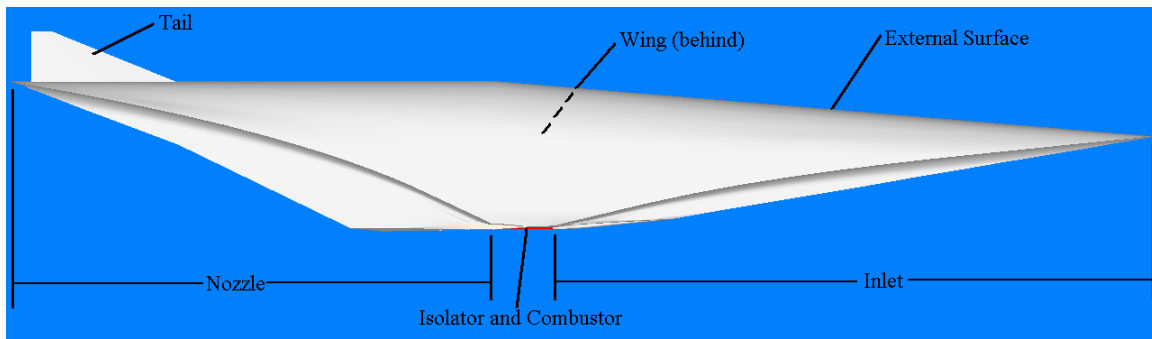


Figure 62. HySIDE reusable airbreathing vehicle

The inlet system element uses an inverse design procedure to shape the surface by carving inviscid stream surfaces out of known flow fields. The vehicle is designed to be flown at a known flight condition, which is specified in the “FreeStream” system element, so the flow field at this known design point is generated using an axisymmetric method of characteristics. The method of characteristics is a mathematical method of solving partial differential equations by finding characteristic lines in the phase space along which the partial differential equation degenerates into an ordinary differential equation. These ordinary differential equations are easily solved.

HySIDE generates the inlet surface based on six key inputs in addition to the design point. The first is the geometric capture area, which determines the overall vehicle size. The user increases or decreases the inlet capture area to obtain the desired volume available over volume required ratio of 1. The next three inputs, the radial deviation parameter (RDP), the initial bow shock strength, and the inlet exit pressure, are used to find the solution of the inlet generating flow field. The RDP value changes the inlet shape and varies from -1 (outward turning “spike” inlet) to 1 (inward turning inlet). A RDP value of 0 produces a 2-dimensional inlet, as shown in Figure 63. These three

inputs are used to create the flow field, with the assumptions of a straight initial shock with isentropic flow behind it, thermally perfect air flow, and a uniform inlet exit condition. The final two inputs, RcH and LH, are then used to create an array of points defining the leading edge cross section. The LH parameter is the ratio of the outer arc length of the inlet cross section to the height of the cross section at the centerline. For inward turning inlets, a value of π corresponds to a semicircle, while 2π would be an enclosed circular inlet. For 2-D inlets, it roughly corresponds to a width to height ratio. The RcH parameter is used to introduce sweep into the inlet shape. A value of 0 produces a squared-off inlet, while higher values give swept leading edges and more pointed geometries. The geometry used in this study is discussed in section 3.4.3.

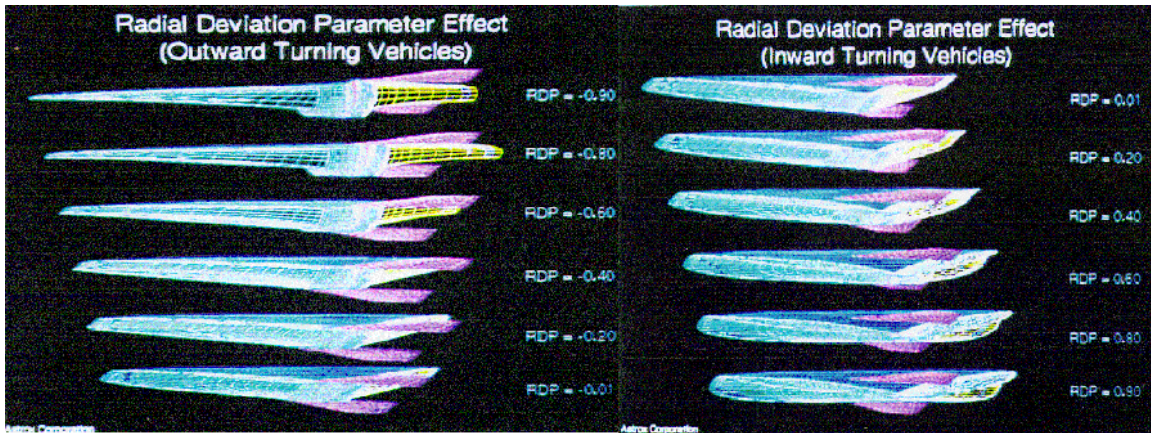


Figure 63. Radial Deviation Parameter (RDP) effect [26]

Once the leading edge points are found, they are projected onto the inlet flow field and streamlines traced through it. The inviscid surface geometry is defined by these streamlines, to which viscous flow properties are estimated using a reference temperature method. With the boundary layer properties defined along each streamline, the geometry

of the stream surface is altered so as to account for the presence of the boundary layer. The inlet surface itself is then defined, and the surface properties such as lift, drag, moments, and heat transfer can be found. An additional weight function is used to account for sections which are actively and passively cooled, and the user can specify the maximum actively-cooled and passively-cooled surface temperatures.

The isolator and combustor designs depend of the inlet exit conditions and user inputs such as fuel type, mixing fraction, mixing length, minimum equivalence ratio for the fuel-injector rate, and combustion efficiency. The combustor modeling assumes a quasi-one dimensional combustor design and uniform flow conditions, with mixing fraction and burning efficiency specified by the user. Combustion is modeled in a two-part process. First, the fuel is accelerated from its stagnation condition to conditions that match the static pressure at the entrance to the combustor, mixing with the air in the fraction specified by the user. This mixture is burned incrementally in ten steps in the downstream direction during the second part of the combustion process. The pressure-area relation, heat release, gas mixture, and flow state are calculated at each of these steps. The inviscid combustor geometry is generated using the shape of the inlet exit and the newly calculated area of each successive combustor hoop. Similar to the inlet design algorithm, viscous properties are generated and the displacement thickness is carved from the surface to account for the boundary layer.

The nozzle system element creates the nozzle geometry using the method of characteristics similar to the inlet design. The last shape of the combustor is used as the initial nozzle shape, and the exit conditions are computed by isentropically expanding the

flow to the user specified inlet area to exit area ratio. The method of characteristics is then used to determine the flow field shape, with a user specified nozzle truncation factor that allows for nozzle designs that are not fully expanded. The streamlines from the initial hoop are again traced through the flow field, the inviscid surface defined, a boundary layer analysis applied, and the nozzle surface determined. The nozzle performance is then determined from the defined shape.

Now that the inlet, combustor, and nozzle have been defined, the vehicle's entire internal flow surface is determined. The "ExtSurf" system element then "wraps" the vehicle from the inlet capture hoop to the nozzle exit hoop to enclose the inner surface and form the external surface. Inviscid properties are then established for this surface, but it is not necessary to carve this displacement thickness out of the surface since it is an external surface.

The Wing system element for airbreathing vehicles contains the inputs for the airfoil geometric characteristics, including aspect ratio, taper ratio, and leading edge sweep. The trapezoidal "reference" planform wing area, S_{ref} , is calculated in this module, but is found using different inputs if the vehicle is VTHL versus HTHL. For VTHL, S_{ref} is calculated using the vehicle landing mass, landing velocity, and landing lift coefficient, but for HTHL, S_{ref} is calculated using the vehicle takeoff mass, takeoff velocity, and takeoff lift coefficient. HySIDE then calculates the exact dimensions of the wing based on this area and the specified geometric characteristics. For HTHL vehicles, takeoff speed is one of the primary inputs into wing sizing. The wing area required can be reduced by increasing the takeoff speed, which leads to lighter wings, less TPS, and

smaller drag penalties during the high-speed segments. As a comparison, a Boeing 747 has a takeoff speed of 153 knots (79 m/s) and a Concorde has a takeoff speed of 175 knots (90 m/s).

The airbreather has a single vertical tail, which is sized as a fraction of the wing planform, S_{ref} . The user can also input the leading edge sweep, thickness to chord ratio, and taper ratio, to determine the tail dimensions.

The “TankStackAB” system element calculates the mass and volume of the tanks required to hold the fuel and oxidizer for the airbreather. However, the tanks in airbreathers are conformal tanks due to the shape of the vehicle, which will always weigh more than standard cylindrical propellant tanks for the same volume. The exact increase in mass is still unknown, so HySIDE uses the same NASA CR287, AFRL/VA SP125, and RMLS methods used in rockets, which is then multiplied by a k-factor. HySIDE uses a scaling factor of 1.4 applied to all conformal propellant tanks. As with the rocket, the user can input the wall thickness, safety factor, ullage fraction, as well as an additional k-factor for uncertainty. “TankStackAB” uses these inputs and the total amount of propellant, which is calculated by the “PropellantUsage” system element described in this appendix, to size the tanks. Unlike the rocket vehicle, the tanks are not actually placed within the vehicle, but rather left as abstract mass and volume requirements, similar to the method used for “StructuralWeightsFromVol” and “StructuralWeightsFromWt.”

The “StructuralWeightsFromVol” and “StructuralWeightsFromWt” system elements are identical to those in the rocket; however, the “StructuralWeightsFromWt”

system element is used to calculate the mass of the takeoff propulsion system in airbreathers. The takeoff propulsion can be either a turbine or a rocket, and are sized as described below.

The “TurbineCluster” system element sizes the turbines used for takeoff. A statistical jet-engine model, based on historical data for afterburning engines, is used to determine the uninstalled weight and size. They are given by:

$$W_{uninstalled} = 0.063 \cdot \left(\frac{T_{TO}}{\# \text{ of turbine engines}} \right)^{1.1} \cdot M_{\max}^{0.25} \cdot e^{-0.081 \cdot BPR} \cdot 0.8 \quad (65)$$

$$L_{uninstalled} = 0.255 \cdot \left(\frac{T_{TO}}{\# \text{ of turbine engines}} \right)^{0.4} \cdot M_{\max}^{0.2} \cdot 0.8 \quad (66)$$

$$D_{uninstalled} = 0.024 \cdot \left(\frac{T_{TO}}{\# \text{ of turbine engines}} \right)^{0.5} \cdot e^{0.04 \cdot BPR} \cdot 0.9 \quad (67)$$

where M_{\max} is the maximum Mach number and T_{TO} , the takeoff thrust, is given by eq. (58). The factors of 0.8 and 0.9 on the end of the above three equations are used to reflect technology advancements, since W, L, and D are all based on historical trends and future engines will be lighter and smaller.

The uninstalled weight calculated from eq. (65) refers only to the engine itself, while the installed weight of an engine includes the equipment necessary for it to function in a vehicle, including inlet and nozzle. HySIDE uses a turbine installation factor, $k_{installed}$, to account for this to calculate the installed turbine weight:

$$W_{installed} = W_{uninstalled} \cdot k_{installed} \cdot k_{overall} \quad (68)$$

These turbines are not actually placed, but a single turbine is shown in the physical model as a reference, as shown in Figure 64. The turbines sized for takeoff area also used for the flyback propulsion, so only the mass and volume of the flyback fuel and tank are calculated for these boosters.

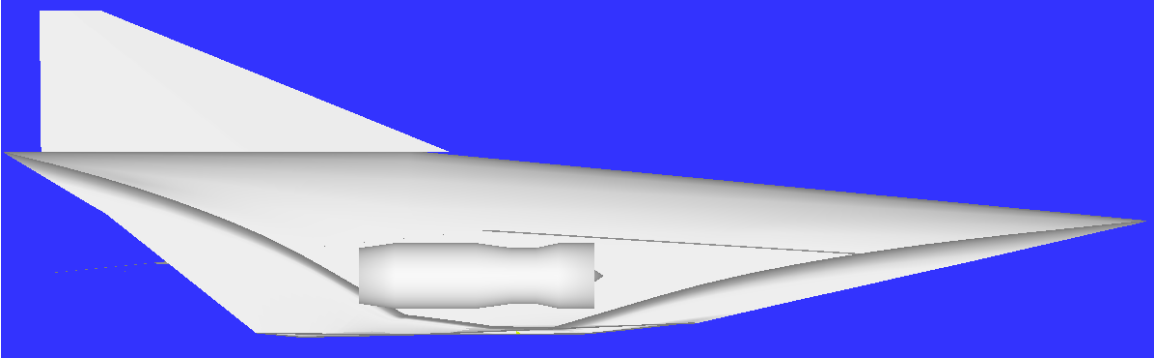


Figure 64. Airbreathing vehicle showing placement of a single turbine engine

If rockets are used for takeoff, the installed weight of rocket engines is determined directly from the rocket thrust-to-weight ratio. The equation is

$$W_{Rkt} = \frac{T_{TO}}{\left(\frac{T}{W}\right)_{Rkt}} \cdot k_{overall} \quad (69)$$

where $\left(\frac{T}{W}\right)_{Rkt}$ is the rocket thrust-to-weight ratio as given in (58), and $k_{overall}$ is the overall design uncertainty factor. In a similar manner to turbine engines, the rocket engines are not physically placed in the airbreathing vehicle as they are in the rocket vehicle.

B.3. Fixed Weights System Element

The user inputs any payload mass, mass of crew and equipment, and extra volume requirements in the “FixedWeights” system element, shown in Figure 65. The masses entered here are added to the overall vehicle mass, and the volume entered is added to the overall volume required. For a booster stage, all the inputs are set to zero, but for the orbiter stage, the mass and volume of the payload are specified here.

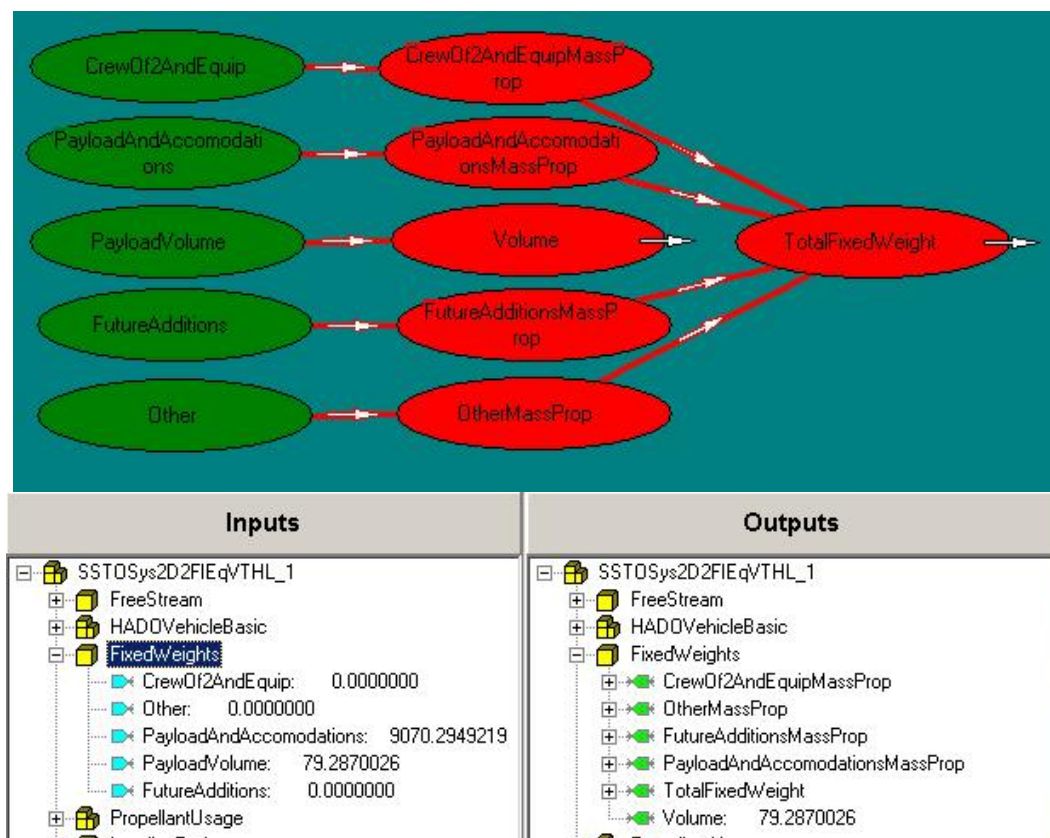


Figure 65. Block diagram and input/output tree of “FixedWeights” system element

B.4. “PropellantUsage” System Element

The “PropellantUsage” system element, shown in Figure 66, calculates the fuel required by the vehicle throughout the flight. The flight is broken into three trajectory

segments per stage as previously described in Figure 11. A SSTO vehicle could use all three segments in a single stage, while a TSTO vehicle only uses one or two of the segments per stage, as shown in Figure 15. The first segment is either a turbine or rocket segment, the second segment is the DMSJ segment, and the third segment is always a rocket. The user specifies four velocities corresponding to the start and stop of each segment, and a segment can be omitted by setting the start and stop velocities to be the same. In each segment, the user can also enter a “Velocity vs. I_{sp} ” table for the specific method of propulsion used, or select one of many from a drop-down list in HySIDE.

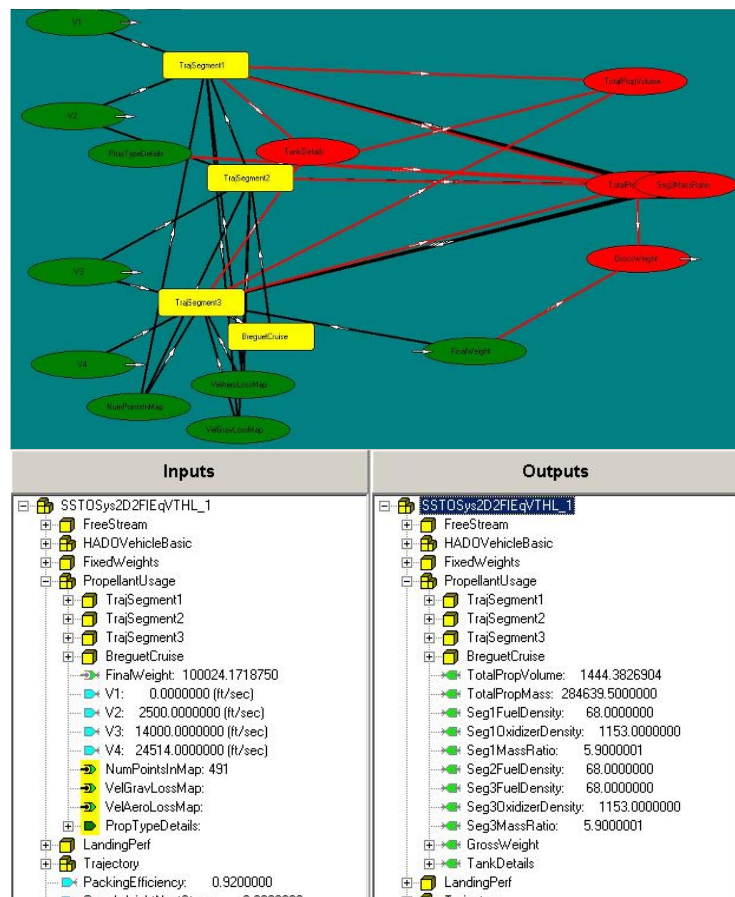


Figure 66. Block diagram and input/output tree of "PropellantUsage" system element

A RLV using the rocket vehicle model uses either the first trajectory segment for a booster or the third trajectory segment for an orbiter. The rocket engines are sized in the “EngineCluster” system element based on the takeoff thrust, which is actually at takeoff for a rocket booster and at the beginning of trajectory segment three for either an all-rocket or RBCC orbiter. “PropellantUsage” calculates the mass flow rate of propellant using

$$\dot{m} = \frac{T_{TO}}{I_{sp} \cdot g} \quad (70)$$

where I_{sp} is given in the user-selected “Velocity vs. I_{sp} ” table and T_{TO} is the takeoff thrust required, as given by eq. (58). For rockets, HySIDE’s default tables assume a basic rocket trajectory and takes into account changes in atmospheric pressure in the “Velocity vs. I_{sp} ” table. The mass flow rate is then held constant for the duration of the rocket trajectory segment. The user must also specify the proper mass ratio between fuel and oxidizer so the proper amounts of each are calculated. The total mass and volume of propellant required for the segment is calculated by integrating the mass flow rate over the time required to complete the segment.

If a turbine is used in the first segment, the mass flow rate of fuel required is given by

$$\dot{m}_f = \dot{m}_a \cdot \phi \cdot FuelStoicRatio \quad (71)$$

where ϕ is the equivalence ratio, *FuelStoicRatio* is the fuel stoichiometric mass ratio, and \dot{m}_f and \dot{m}_a is the fuel and air mass flow rates, respectively. The air mass flow rate is found using

$$\dot{m}_a = \rho \cdot A_{inlet} \cdot V \cdot AreaRatio \quad (72)$$

Where A_{inlet} is the geometric inlet capture area, and $AreaRatio$ is calculated as a function of Mach number. It is a power series equation that gives the ratio of actual area of captured air to the design area of captured air. The user must also set the mass ratio to zero since turbines require no oxidizer to be carried onboard. The total mass of fuel is determined again by integration.

The second trajectory segment is always used for the DMSJ. Since the individual vehicle components have been designed for optimal DMSJ operation based on the FreeStream input, the design point is used to calculate the required mass flow rate. The characteristics of the entire engine flowpath, including pressure forces and viscous forces, are known at every point. The net thrust applied to the vehicle is calculated by integrating the map of these forces to give a value of the design point thrust, T_{DP} . The specific impulse at this design point is found using

$$I_{sp,DP} = \frac{T_{DP}}{\dot{m}_f \cdot g} \quad (73)$$

where m_f is found using eqs. (70) and (71). To calculate I_{sp} at off-design conditions, the values in the “Velocity vs. I_{sp} ” table are used to generate a trend. The difference between the calculated specific impulse at the design point, $I_{sp,DP}$, and the specific impulse in the table, $I_{sp,table}$, is found using

$$\Delta I_{sp} = I_{sp,DP} - I_{sp,table} \quad (74)$$

This difference is I_{sp} at the design point is then applied to all points on the table to find the I_{sp} for all off-design velocities in the DMSJ trajectory using

for lift coefficient. HySIDE finds the correct angle of attack such that the lift required is equal to the lift available. The drag at this angle of attack is calculated using eq. (3) from the drag coefficient at this angle of attack as calculated by Missile DATCOM. The mass of the vehicle is also known at all points along the flight trajectory. The gravity losses, which is the thrust necessary to overcome the force of gravity, is found using

$$G_{loss} = M \cdot g \cdot \frac{\frac{\Delta H}{\Delta t}}{V} \quad (76)$$

where $\frac{\Delta H}{\Delta t}$ is the change in vehicle height over time, or the vertical velocity.

Now that three of the four aerodynamic forces have been found, the only one left is the thrust. The thrust produced by the propulsion system is given by

$$T = \dot{m} \cdot I_{sp} \cdot g \quad (77)$$

where \dot{m} is the mass flow rate of propellant (fuel and oxidizer) for rockets and the mass flow rate of fuel for both turbine and DMSJ engines. However, since drag and gravity losses both oppose the thrust, the net vehicle thrust can also be found. These forces are converted to the effective specific impulse, EI_{sp} , using

$$EI_{sp} = I_{sp} - \frac{D}{\dot{m} \cdot g} - \frac{G_{loss}}{\dot{m} \cdot g} \quad (78)$$

The net vehicle thrust is then found using

$$T_{net} = \dot{m} \cdot EI_{sp} \cdot g \quad (79)$$

The actual flight trajectory can also be manually entered in this system element or selected from a drop-down menu. Different trajectories are used for the first trajectory segment depending on takeoff type, but the second segment trajectory is always determined by path required to maintain a constant dynamic pressure. The third trajectory segment, used only on orbiters in this study, is also different depending on whether the stage is an RBCC or a pure rocket. The position, velocity, and acceleration of the vehicle is calculated at each point along this trajectory, which is used by the “PropellantUsage” system element to calculate the mass of propellant required. A new GTOW is then calculated and HySIDE uses the convergence subroutine described in section 3.3 to repeat the calculations.

Appendix C. HySIDE Design Inputs

Rocket Inputs

SysEl: RMLSRocketSystem4Mod

Inputs:

FreeStream		
Alt		Not critical for rockets, these two values are used by airbreathers to set the constant Q value to fly at.
Mach		
Rocket		
RocketFuselage		
RadiusMax		These values change the fuselage radius, conical nose section length and cylindrical fuselage length. Vary these to get the right volume ratio False for boosters, True for orbiters
LengthOgive		
LengthCylinder		
Reentry:		
Wing		
WingUpperSurf		
Reentry:		False for boosters, True for orbiters
WingLowerSurf		
Reentry:		False for boosters, True for orbiters
Origin		Varies (Dependent on Fuselage Length)
LaunchMachNo		Used for landing speed
LaunchCL		Used for landing lift coefficient
EngineCluster		
Engine1/2/3/4		
DesignAltitude		Set for midway along path
AreaRatio1/2		Usually between 50-100
FuelNumber		6 for JP-7, 1 for H ₂
RocketParams_EEunits		2 for RD-180, 1 for SSME
TankStack		
StructuralWeightsFromVol		
StructuralWeightsFromWt		
MassOfTakeOffPropulsion		
TurbineCluster		
Turbine		
ThrustToWeightAtTakeoff		VTHL: 1.4, HTHL: 0.7, Orbiter/E: 1.0
RocketEngine_ToverW_Inst		HC: 80.000, H: 73.50000
K_Factor		0.00000 (Uses EngineCluster for sizing)
Turbine		False
FlybackPropulsion		
TurbineTooverW		3.00 for booster, 0.00 for orbiter
AvgEISP		4500.00000
CruiseVel		Varies
Range		Booster: Varies (around 300 nm), Orbiter: 0
L_over_D		Varies
FuelDensity		805.00
GlobalPointLink		Change this to move the vehicles around
Fixed Weights		
PayloadAndAccommodations		Booster: 0.000, Orbiter: 9071.85 kg
PayloadVolume		Booster: 0.000, Orbiter: 79.29 m ³

PropellantUsage		
TrajSegment1		
V_Lo		Sourced Input
V_Hi		Sourced Input
VelISPMMap		LHC Rocket or LH2 Rocket
TrappedUnusableFraction		Set to 0.005 if this segment is used, else 0.0
ReserveFraction		Set to 0.010 if this segment is used, else, 0.0
StartupTime		Set to 3.00 if this is the booster
TrajSegment2		
TrappedUnusableFraction		0.0 (This segment not used for rockets)
ReserveFraction		0.0 (This segment not used for rockets)
StartupTime		0.0 (This segment not used for rockets)
TrajSegment3		
VelISPMMap		LHC Rocket or LH2 Rocket
TrappedUnusableFraction		Set to 0.005 if this segment is used, else 0.0
ReserveFraction		Set to 0.010 if this segment is used, else, 0.0
StartupTime		0.00
V1		Beginning of Seg1
V2		End of Seg1, Beginning of Seg2
V3		End of Seg2, Beginning of Seg3
V4		End of Seg3, Beginning of Seg4
PropTypeDetails:	HC Booster:	Traj1: Fuel 2 (RP-1)/Oxidizer 1 (LOX) MR: 2.580 Traj2: Fuel 1 (LH ₂) Traj3: Fuel 1 (LH ₂)/Oxidizer 1 (LOX) MR: 5.900
	H Booster:	Traj1: Fuel 1 (LH ₂)/Oxidizer 1 (LOX) MR: 5.900 Traj2: Fuel 1 (LH ₂) Traj3: Fuel 1 (LH ₂)/Oxidizer 1 (LOX) MR: 5.900
	HC Orbiter:	Traj1: Fuel 1 (LH ₂)/Oxidizer 1 (LOX) MR: 5.900 Traj2: Fuel 1 (LH ₂) Traj3: Fuel 2 (RP-1)/Oxidizer 1 (LOX) MR: 2.600
	H Orbiter:	Traj1: Fuel 1 (LH ₂)/Oxidizer 1 (LOX) MR: 5.900 Traj2: Fuel 1 (LH ₂) Traj3: Fuel 1 (LH ₂)/Oxidizer 1 (LOX) MR: 5.900
Trajectory		
VelAltMap		
RocketDrag		Used if this stage is a rocket
RocketDragNextStage		Used if next stage is a rocket (not used for orbiter stage)
WingDrag		Always used
FuselageDragNextStage		Used if next stage is an airbreather (not used for orbiter stage)
ExtModDrag		Used if an external pod is used
TrajStageName		Booster: stFirstStage,Orbiter: stSecondStage
ThirdSegInitialHeight		Booster: 133718.00, Orbiter: Input
HeightFinal		Booster: Input, Orbiter: 303805.77
VelAltMapSeg1		RMLS Vertical Rocket staging @ 7000
VelAltMapSeg3		JWL Vertical Rocket (7K)
FuelStoichMassRatio		HCB/HCO/HO/HB/E: 0.0288000
OrbitInclination		Change if a inclination change is desired
ExtModUsed		Change if external pod is used
WingUsed		True
PackingEfficiency		Booster: 0.880000, Orbiter: 0.96000
GrossWeightNextStage		Booster: Sourced Input, Orbiter: 0.000000
VolumeNextStage		Booster: Sourced Input, Orbiter: 0.000000
ThrustToWeightAtTakeoff		Booster: 1.4, Orbiter: 1.000

TBCC/RBCC Inputs

RBCC SysEl: TSSTOSys2D2FIEqVTHL

TBCC SysEl: THCTurbine Stage

Inputs:

FreeStream		
Alt		Not critical for rockets, these two values are used by
Mach		airbreathers to set the constant Q value to fly at.
HADOVehicleBasic		
Inlet		
	InletGeom	
	InletMirrorGeom	
	RDP	0.99 for inward-turning, 0.01 for 2-D
	LH	Width/height ratio
	VehCapArea	Use this to size the vehicle
Comb		
	CombFlag	1
	FuelNumber	7 for JP-7 (Endo), 1 for LH2
	FuelTempMax	833 for Hydrogen, about 650 for Hydrocarbon
Wing		
	Origin	Use this to move the wing around
	WingStrWtPerUnitArea	80.000
	LaunchMachNo	VTHL: Landing spd, HTHL: Takeoff spd
	LaunchCL	VTHL: Lnding lift coeff, HTHL: T/O coeff
VTail		
	PlanformScaleFactor	0.1000000
TankStackAB		
	LH2Tank	
	K_Factor	1.4 for conformal tanks
	RP1Tank	
	K_Factor	1.4 for conformal tanks
	JP1Tank	
	K_Factor	1.4 for conformal tanks
	LOXTank	
	K_Factor	1.4 for conformal tanks
StructuralWeightsFromVol		
StructuralWeightsFromWt		
	MassOfTakeOffPropulsion	
	TurbineCluster	
	Turbine	
	TurbineGeom	
	TurbineGeomMirror	
	MMax	2.50
	ByPassRatio	0.950
	VolInstK_Factor	Set these to get good T/W
	WtInstK_Factor	installed value in outputs
	Afterburning	True
	Origin	Use this to move the single turbine
	NumberOfTurbines	Vary this for more turbines
	ThrustToWeightAtTakeoff	VTHL Booster: 1.4
		HTHL Booster: 0.7, Orbiter: 1.000
	RocketEngine_ToverW_Inst	HC: 80.00, LH2: 73.50

	TurbineEngine_ToverW_Inst	8.0000
	Turbine:	RBCC: False, TBCC: True
	FlybackPropulsion	
	Engine1	
	Engine2	
	TurbineToverW	RBCC Booster: 3.000, RBCC Orbiter: 0.000
		TBCC: 0.0 (Uses TurbineCluster turbine)
	AvgEISP	4500.00000
	CruiseVel	Varies
	Range	Booster: Varies, Orbiter: 0.000 (nm)
	L_over_D	Varies
	HeatLoopType	Use PhiTempLoop if FuelTempReached (in ouputs) exceeds FuelTempMax specified
	GlobalPointLink	Use this to move vehicle around in viewer
Fixed Weights		
	PayloadAndAccomodations	Booster: 0.000, Orbiter: 9071.85 kg
	PayloadVolume	Booster: 0.000, Orbiter: 79.29 m ³
PropellantUsage		
	TrajSegment1	
	V_Lo	Sourced Input
	V_Hi	Sourced Input
	VelISPMMap	LHC Rocket or LH2 Rocket, or Turbine
	TrappedUnusableFraction	Set to 0.005 if this segment is used, else 0.0
	ReserveFraction	Set to 0.010 if this segment is used, else, 0.0
	StartupTime	Set to 3.00 if this is the booster
	TrajSegment2	
	V_Lo	Sourced Input
	V_Hi	Sourced Input
	VelISPMMap	HC Ram-Scram or LH2 Ram-Scram New
	VBegin	HC: 8000, H: 12000 (Temp at which fuel dump begins for cooling)
		Set to 0.005 if this segment is used, else 0.0
	TrappedUnusableFraction	Set to 0.010 if this segment is used, else, 0.0
	ReserveFraction	
	TrajSegment3	
	VelISPMMap	LHC Rocket or LH2 Rocket
	TrappedUnusableFraction	Set to 0.005 if this segment is used, else 0.0
	ReserveFraction	Set to 0.010 if this segment is used, else, 0.0
	StartupTime	0.00
	V1	Beginning of Seg1
	V2	End of Seg1, Beginning of Seg2
	V3	End of Seg2, Beginning of Seg3
	V4	End of Seg3, Beginning of Seg4
PropTypeDetails: RBCC HC Booster:		Traj1: Fuel 2 (RP1)/Oxidizer 1 (LOX) MR: 2.580
		Traj2: Fuel 3 (JP1)
		Traj3: Fuel 1 (LH2)/Oxidizer 1 (LOX) MR: 5.900
RBCC H Booster:		Traj1: Fuel 2 (LH2)/Oxidizer 1 (LOX) MR: 5.900
		Traj2: Fuel 3 (LH2)
		Traj3: Fuel 1 (LH2)/Oxidizer 1 (LOX) MR: 5.900
RBCC HC Orbiter:		Traj1: Fuel 1 (LH2)/Oxidizer 1 (LOX) MR: 5.900
		Traj2: Fuel 3 (JP1)
		Traj3: Fuel 2 (RP1)/Oxidizer 1 (LOX) MR: 2.600
RBCC H Orbiter:		Traj1: Fuel 1 (LH2)/Oxidizer 1 (LOX) MR: 5.900
		Traj2: Fuel 1 (LH2)

TBCC HC Booster:	Traj3: Fuel 1 (LH2)/Oxidizer 1 (LOX) MR: 5.900
	Traj1: Fuel 3 (JP1)/Oxidizer 1 (LOX) MR: 0.00
	Traj2: Fuel 3 (JP1)
	Traj3: Fuel 1 (LH2)/Oxidizer 1 (LOX) MR: 5.900

Trajectory

RocketDrag	(Used if next stage is a rocket)
FuselageDrag	(Always used)
WingDrag	(Always used)
FuselageDragNextStage	(Used if next stage is an airbreather)
HeightInitial	0.000000 (ft)
ThirdSegHeightInitial	86000
HeightFinal	303805 (ft)
VelAltMapSeg1	VTHL: RMLS Vertical Rocket @ 7000
	HTHL: Default horizontal takeoff
	Horizontal Rocket
VelAltMapSeg3	0.0673000
FuelStoichRatioSeg1Turbine	HC: 0.067300 LH2: 0.0291000
FuelStoichRatioSeg2RamScram	RBCC: False, TBCC: True
Turbine	True
UseFuselageDrag	True if next stage is airbreather,
UseFuselageDragNextStage	False if next stage rocket or no next stage
	True if next stage is rocket,
	False if next stage is airbreather no next stg
UseRocketDragNextStage	0.85
PackingEfficiency	Booster: Sourced Input, Orbiter: 0.0000
GrossWeightNextStage	Booster: Sourced Input, Orbiter: 0.0000
VolumeNextStage	

Turbine Inputs

SysEI: DualQuadTurboSystem

Inputs:

FreeStream	
Alt	Not critical for turbines, these two values are used by
Mach	airbreathers to set the constant Q value to fly at.
HADOVehicleBasic	
Wing	
WingStrWtPerUnitArea	50.000
LaunchMachNo	Used for landing speed
LaunchCL	Used for landing lift coefficient
VTail(1/2)	
EngineStack	
EngineStackMirror	
TankStackAB	
LH2Tank	
K_Factor	1.4 for conformal tanks
RP1Tank	
K_Factor	1.4 for conformal tanks
JP1Tank	
K_Factor	1.4 for conformal tanks
LOXTank	
K_Factor	1.4 for conformal tanks

StructuralWeightsFromVol	
StructuralWeightsFromWt	
MassOfTakeOffPropulsion	
TurbineCluster	
Turbine	
MMax	2.500000
ByPassRatio	0.950000
VolInstK_Factor	0.000000
WtInstK_Factor	1.40000
Afterburning	True
NumberOfTurbines	8
ThrustToWeightAtTakeoff	0.7000000
RocketEngine_ToverW_Inst	0.0000000
TurbineEngine_ToverW_Inst	8.00000
Turbine:	True
FlybackPropulsion	
TurbineToverW	0.000000 (Uses TurbineCluster)
AvgEISP	4500.00000
CruiseVel	Varies
Range	Varies
L_over_D	Varies
GlobalPointLink	Use this to move vehicle
Fixed Weights	
PayloadAndAccommodations	0.0000000
PayloadVolume	0.0000000
PropellantUsage	
TrajSegment1	
VelISPMMap	Turbine
TrappedUnusableFraction	0.0050000
ReserveFraction	0.0300000
StartupTime	3.0000000
TrajSegment2	(Not used)
TrajSegment3	(Not used)
V1	0.00000 ft/sec
V2	End of turbine segment
V3	Same as V2
V4	Same as V3
PropTypeDetails	Traj1: Fuel 3 (JP1)/Oxidizer 1 (LOX) MR: 0.000 Traj2: Fuel 1 (LH2)
Trajectory	
RocketDrag	Used if next stage is a rocket
FuselageDrag	Not used
WingDrag	Used to calculate drag
FuselageDragNextStage	Used if next stage is an airbreather
HeightInitial	0.000000 (ft)
ThirdSegInitialHeight	57008.0000 (ft)
HeightFinal	303805.7700 (ft)
VelAltMapSeg1	Default Horizontal Takeoff
FuelStoichRatioSeg1Turbine	0.0673000
UseFuselageDrag	False
UseFuselageDragNextStage	True for airbreather 2 nd stage, else False
UseRocketDragNextStage	True for rocket 2 nd stage, else False
PackingEfficiency	0.6

Appendix D. Flyback Lift over Drag Calculations

Sample calculation showing single rocket stage flyback:

HCRocket-HCRocket Flyback Lift over Drag

	fps	Mach	m/s
Flyback Speed (Booster Stage):	418	0.395331681	127.4228026
Booster Rocket Planform Area:	160.9240875		
Booster Rocket Wing Leading Edge Sweep:	45		Altitude: 15000
Booster Rocket Wing Taper Ratio:	0.18		
Booster Rocket Wing Aspect Ratio:	2.4		Flyback Weight: 54603.60938 kg
Booster Rocket Wing Root Chord:	13.8788309		Wing Loading: 69.49918955 lbf/ft ²

Flyback (Booster Stage):

Part	Length/MAC (m)	Reynolds number	C_l	S_{wet} (m ²)	D/Q (m ²)
Booster Rocket Fuselage	25.2679863	1.51E+08	0.001980973	467.22	0.92555
Booster Rocket Wing	9.506607109	5.69E+07	0.002272994	394.25	0.896128
Booster Rocket Aft Skirt	3.7915592	2.27E+07	0.002605042	66.7	0.173756

Booster Rocket Base Area: 27.9444638

Factor: 1

4.527223

Booster C_{do} : 0.040533

Booster Rocket Oswald Efficiency: 0.919293181

K: 0.144273

$L/D_{max, booster}$: 6.538465635

$L/D_{cruise, booster}$: 5.662477

$C_{L \text{ max } L/D, booster}$: 0.530040813

$C_{L \text{ cruise } L/D, booster}$: 0.306019

$C_{D \text{ max } L/D, booster}$: 0.081065015

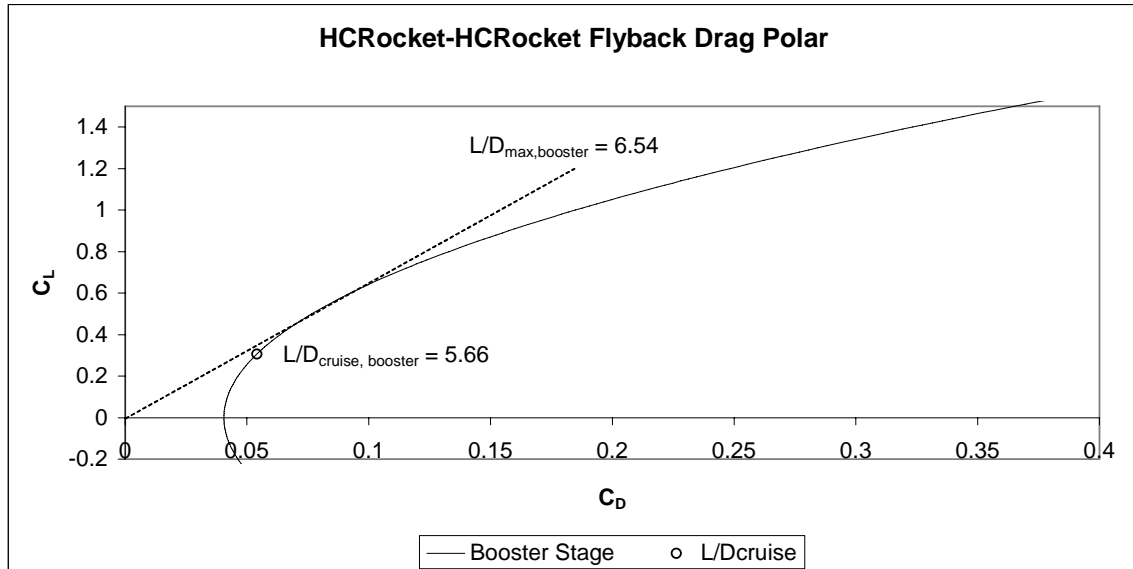
$C_{D \text{ max } L/D, booster}$: 0.054043

$V_{max \text{ } L/D, booster}$: 127.6027701

$V_{cruise \text{ } L/D, booster}$: 167.9347 m/s

$V_{cruise \text{ } L/D, booster}$: 550.8963 fps

$M_{cruise \text{ } L/D, booster}$: 0.521021



Sample calculation showing airbreather flyback with rocket second stage attached:

HTHL HRBCC-HCRocket Flyback Lift over Drag

	fps	Mach	m/s
Speed:	628	0.593943292	191.4390431
RBCC Planform Area:	735.9074707		
RBCC Wing Leading Edge Sweep:	68		Altitude: 15000
RBCC Wing Taper Ratio:	0.15		
RBCC Wing Aspect Ratio:	1.2		Flyback Weight: 234704.5801
RBCC Wing Root Chord:	43.0678444		
RBCC Tail Leading Edge Sweep:	68		Wing Loading: 65.32475613 lbf/ft ²
RBCC Tail Taper Ratio:	0.15		
RBCC Tail Root Chord:	19.2605247		
Rocket Planform Area:	87.0218353		
Rocket Wing Leading Edge Sweep:	45		
Rocket Wing Taper Ratio:	0.18		
Rocket Wing Aspect Ratio:	2.4		
Rocket Wing Root Chord:	10.2060213		

Flyback (Both Stages):

Part	Length/MAC (m)	Reynolds number	C_f	S_{wet} (m ²)	D/Q (m ²)
RBCC Inlet	30.536747	2.75E+08	0.001795725	274.55	0.493016
RBCC Combustor	3.0064468	2.70E+07	0.002492238	14.67	0.036561
RBCC Nozzle	21.5777169	1.94E+08	0.00188125	293.2	0.551582
RBCC Ext Surface	55.0841713	4.95E+08	0.001662369	1087.19	1.807311
RBCC Wing	29.27365076	2.63E+08	0.001805837	699.07	1.262406
RBCC Tail	13.09157404	1.18E+08	0.002014544	142.79	0.287657
Rocket Fuselage	23.1081772	2.08E+08	0.001863933	297.06	0.5537
Rocket Wing	6.990836285	6.29E+07	0.002201184	228.97	0.504005
Rocket Aft Skirt	2.1765366	1.96E+07	0.002617836	24.61	0.064425

RBCC Base Area: 46.4400063

Factor: 0.6

6.061461

Rocket Base Area: 11.5484934

Factor: 1

2.512228

Both C_{do} : 0.019207

RBCC Oswald Efficiency: 0.67599211

K: 0.392398

$L/D_{max, both}$: 5.759436796

$L/D_{cruise, both}$: **4.987819**

$C_{L, max L/D, both}$: 0.221239533

$C_{L, cruise L/D, both}$: 0.127733

$C_{D, max L/D, both}$: 0.038413397

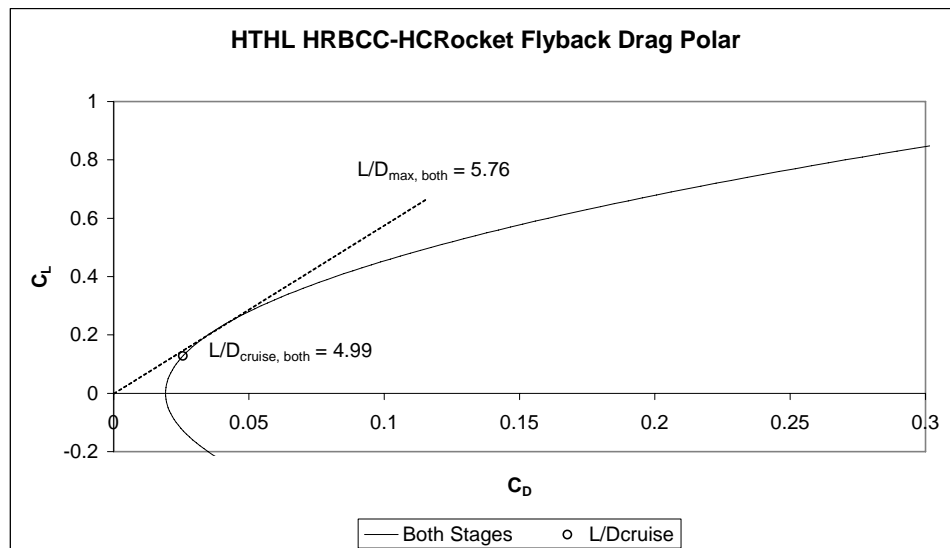
$C_{D, cruise L/D, both}$: 0.025609

$V_{max L/D, both}$: 191.4839687

$V_{cruise L/D, both}$: 252.0071 m/s

$V_{cruise L/D, both}$: **826.6891** fps

$M_{cruise L/D, both}$: 0.781857



Appendix E. Flyout Lift over Drag Calculations

Sample calculation showing airbreather flyout with rocket second stage attached:

HTHL HCTBCC-HCRocket Flyout Lift over Drag

Speed:	fps	Mach	m/s
	788	0.72095151	240.2133216
TBCC Planform Area:	569.8891602		
TBCC Wing Leading Edge Sweep:	68		Altitude: 6000
TBCC Wing Taper Ratio:	0.15		
TBCC Wing Aspect Ratio:	1.2		Takeoff Weight: 425097.893
TBCC Wing Root Chord:	37.8997841		Flyout Weight: 406159.7819
TBCC Tail Leading Edge Sweep:	68		
TBCC Tail Taper Ratio:	0.15		Wing Loading: 145.9775146 lbf/ft ²
TBCC Tail Root Chord:	11.9849634		
Rocket Planform Area:	102.5951157		
Rocket Wing Leading Edge Sweep:	45		
Rocket Wing Taper Ratio:	0.18		
Rocket Wing Aspect Ratio:	2.4		
Rocket Wing Root Chord:	11.0816822		

Flyout (Both Stages):

Part	Length/MAC (m)	Reynolds number	C_l	S_{wet} (m ²)	D/Q (m ²)
TBCC Inlet	16.623558	2.39E+08	0.001802672	219.07	0.394911
TBCC Combustor	4.0203324	5.78E+07	0.002195595	81.82	0.179644
TBCC Nozzle	11.2731457	1.62E+08	0.001899791	191.06	0.362974
TBCC Ext Surface	31.906992	4.58E+08	0.001654524	596.21	0.986444
TBCC Wing	25.76086774	3.70E+08	0.001701216	472.57	0.803943
TBCC Tail	8.14630121	1.17E+08	0.001986687	55.29	0.109844
Rocket Fuselage	25.0278912	3.60E+08	0.001707654	313.05	0.534581
Rocket Wing	7.590639265	1.09E+08	0.002006312	299.13	0.600148
Rocket Aft Skirt	2.39888	3.45E+07	0.002368114	30.14	0.071375
TBCC Base Area: 49.9139977		Factor: 0.6			8.097318
Rocket Base Area: 14.2573776		Factor: 1			3.854848

Both C_{do} : 0.028069

TBCC Oswald Efficiency: 0.67599211

K: 0.392398

$L/D_{max, both}$: 4.764260252

$L/D_{cruise, both}$: **4.12597**

$C_{L max L/D, both}$: 0.267452876

$C_{L cruise L/D, both}$: 0.154414

$C_{D max L/D, both}$: 0.056137336

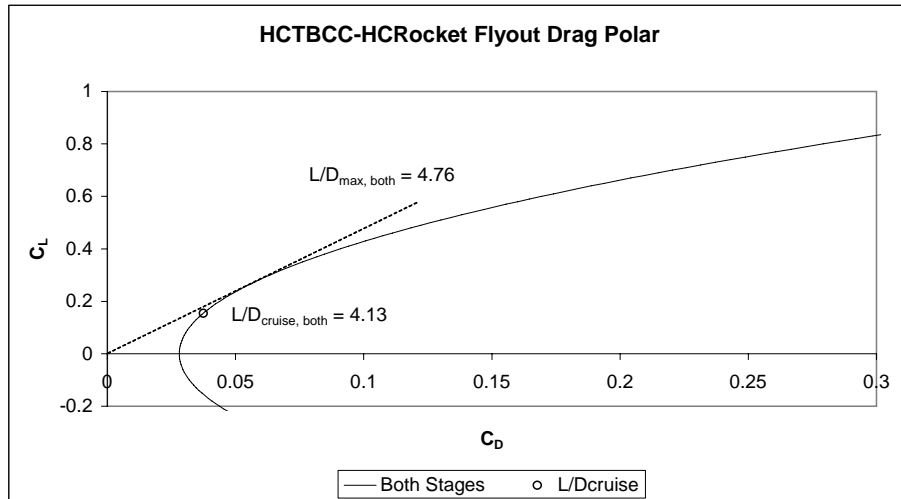
$C_{D max L/D, both}$: 0.037425

$V_{max L/D, both}$: 225.9612239

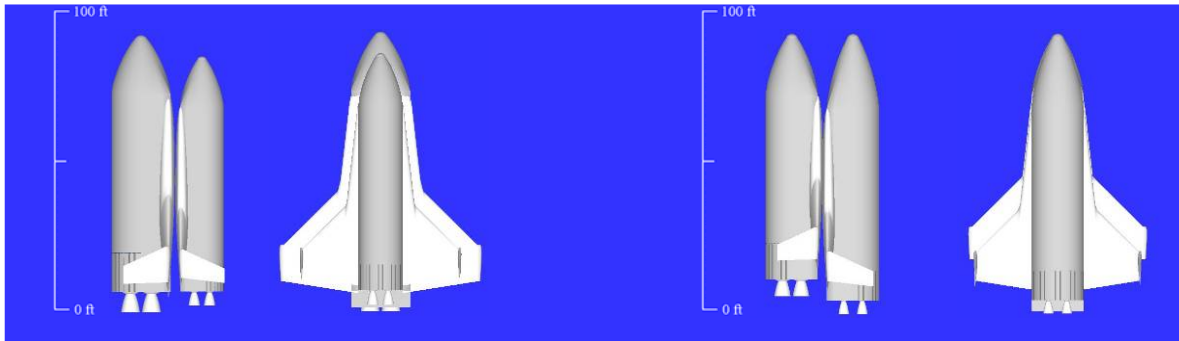
$V_{cruise L/D, both}$: 297.3817 m/s

$V_{cruise L/D, both}$: **975.5369** fps

$M_{cruise L/D, both}$: 0.892531



Appendix F. Baseline Vehicle Summary



Hydrocarbon Rocket Booster Hydrocarbon Rocket Orbiter

Length: 90.32 ft (27.53 m)
Width: 65.17 ft (19.86 m)
Height: 36.59 ft (11.15 m)

Booster Design Mach: 7
Rocket: 0-7000 fps, Propellant: RP-1/LOX

Staging Velocity: 7000 fps

Orbiter Design Mach: 20
Rocket: 7000-24500 fps, Propellant: RP-1/LOX

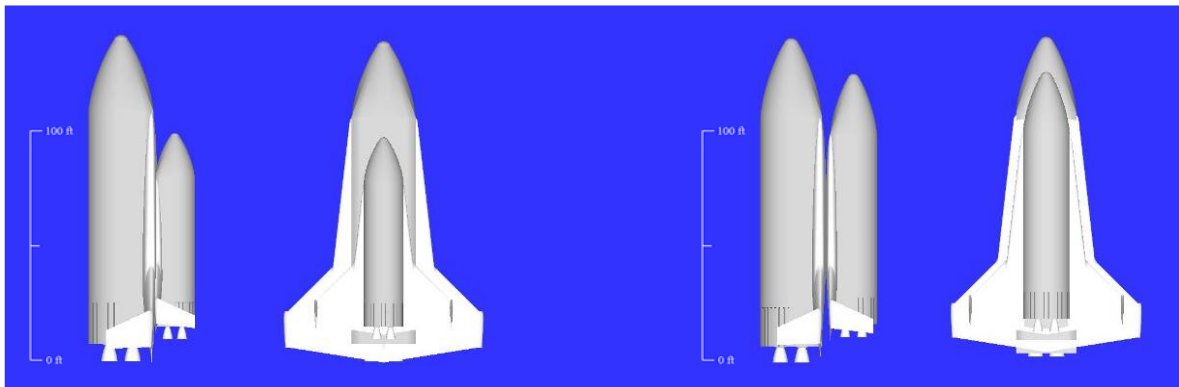
Hydrocarbon Rocket Booster Hydrogen Rocket Orbiter

Length: 93.84 ft (28.60 m)
Width: 59.85 ft (11.24 m)
Height: 37.73 ft (11.50 m)

Booster Design Mach: 7
Rocket: 0-7000 fps, Propellant: RP-1/LOX

Staging Velocity: 7000 fps

Orbiter Design Mach: 20
Rocket: 7000-24500 fps, Propellant: H₂/LOX



Hydrogen Rocket Booster Hydrocarbon Rocket Orbiter

Length: 120.67 ft (36.78 m)
Width: 74.94 ft (22.84 m)
Height: 39.04 ft (11.90 m)

Booster Design Mach: 7
Rocket: 0-7000 fps, Propellant: H₂/LOX

Staging Velocity: 7000 fps

Orbiter Design Mach: 20
Rocket: 7000-24500 fps, Propellant: RP-1/LOX

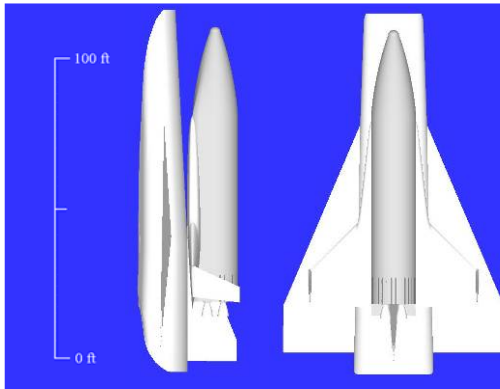
Hydrogen Rocket Booster Hydrogen Rocket Orbiter

Length: 123.67 ft (37.69 m)
Width: 70.43 ft (21.47 m)
Height: 42.08 ft (12.83 m)

Booster Design Mach: 7
Rocket: 0-7000 fps, Propellant: H₂/LOX

Staging Velocity: 7000 fps

Orbiter Design Mach: 20
Rocket: 7000-24500 fps, Propellant: H₂/LOX



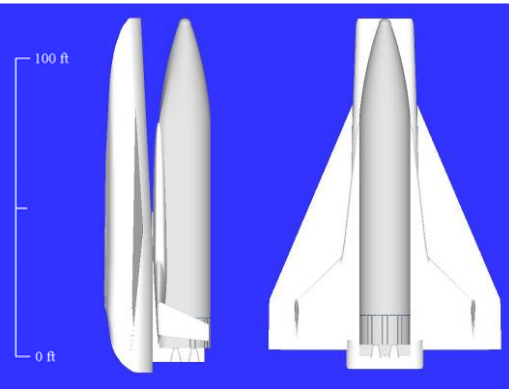
**Hydrocarbon RBCC Booster
Hydrocarbon Rocket Orbiter**

Length: 111.31 ft (33.93 m)
Width: 70.75 ft (21.57 m)
Height: 30.93 ft (9.43 m)

Booster Design Mach: 7
Rocket: 0-4000 fps, Propellant: RP-1/LOX
HC DMSJ: 4000-8300 fps, Propellant: JP-7

Staging Velocity: 8300 fps

Orbiter Design Mach: 20
Rocket: 8300-24500 fps, Propellant: RP-1/LOX



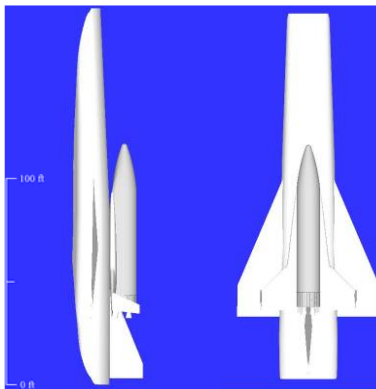
**Hydrocarbon RBCC Booster
Hydrogen Rocket Orbiter**

Length: 111.72 ft (34.05 m)
Width: 76.64 ft (23.36 m)
Height: 32.55 ft (9.92 m)

Booster Design Mach: 7
Rocket: 0-4000 fps, Propellant: RP-1/LOX
HC DMSJ: 4000-8300 fps, Propellant: JP-7

Staging Velocity: 8300 fps

Orbiter Design Mach: 20
Rocket: 8300-24500 fps, Propellant: H₂/LOX



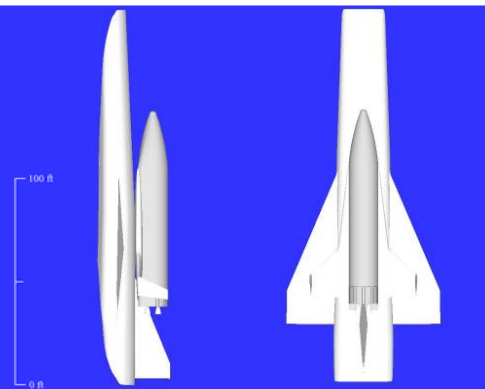
**Hydrogen RBCC Booster
Hydrocarbon Rocket Orbiter**

Length: 189.19 ft (57.67 m)
Width: 75.87 ft (23.13 m)
Height: 36.53 ft (11.13 m)

Booster Design Mach: 8
Rocket: 0-4000 fps, Propellant: H₂/LOX
H₂ DMSJ: 4000-10000 fps, Propellant: H₂

Staging Velocity: 10000 fps

Orbiter Design Mach: 20
Rocket: 10000-24500 fps, Propellant: RP-1/LOX



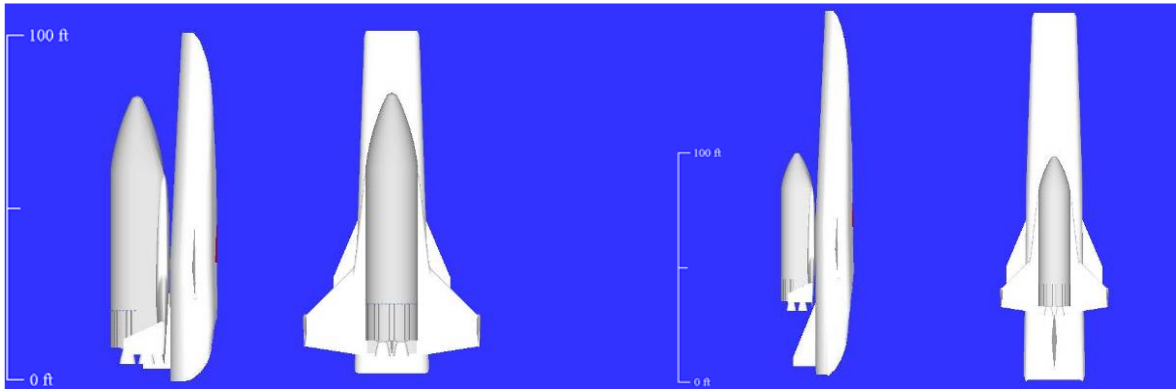
**Hydrogen RBCC Booster
Hydrogen Rocket Orbiter**

Length: 187.25 ft (57.08 m)
Width: 79.18 ft (24.13 m)
Height: 36.99 ft (11.28 m)

Booster Design Mach: 8
Rocket: 0-4000 fps, Propellant: H₂/LOX
H₂ DMSJ: 4000-9500 fps, Propellant: H₂

Staging Velocity: 9500 fps

Orbiter Design Mach: 20
Rocket: 9500-24500 fps, Propellant: H₂/LOX



**Hydrocarbon Rocket Booster
Hydrocarbon RBCC Orbiter**

Length: 101.53 ft (30.95 m)
Width: 53.78 ft (16.39 m)
Height: 29.76 ft (9.07 m)

Booster Design Mach: 4
Rocket: 0-4000 fps, Propellant: RP-1/LOX

Staging Velocity: 4000 fps

Orbiter Design Mach: 7
HC DMSJ: 4000-8500 fps, Propellant: JP-7
Rocket: 8500-24500 fps, Propellant: RP-1/LOX

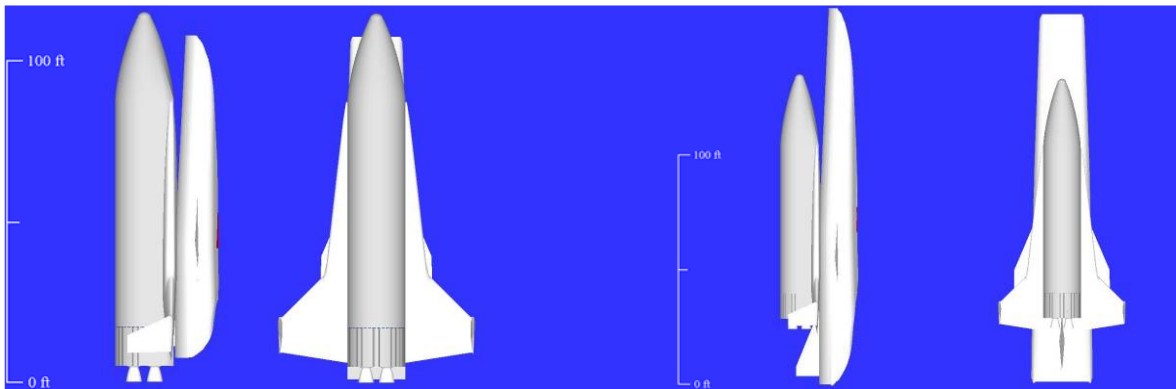
**Hydrocarbon Rocket Booster
Hydrogen RBCC Orbiter**

Length: 165.55 ft (54.93 m)
Width: 47.22 ft (15.80 m)
Height: 31.34 ft (10.07 m)

Booster Design Mach: 4
Rocket: 0-4000 fps, Propellant: RP-1/LOX

Staging Velocity: 4000 fps

Orbiter Design Mach: 12
H₂ DMSJ: 4000-15500 fps, Propellant: H₂
Rocket: 15500-24500 fps, Propellant: H₂/LOX



**Hydrogen Rocket Booster
Hydrocarbon RBCC Orbiter**

Length: 112.50 ft (34.29 m)
Width: 62.70 ft (19.11 m)
Height: 31.34 ft (9.55 m)

Booster Design Mach: 4
Rocket: 0-4000 fps, Propellant: H₂/LOX

Staging Velocity: 4000 fps

Orbiter Design Mach: 7
HC DMSJ: 4000-8500 fps, Propellant: JP-7
Rocket: 8500-24500 fps, Propellant: RP-1/LOX

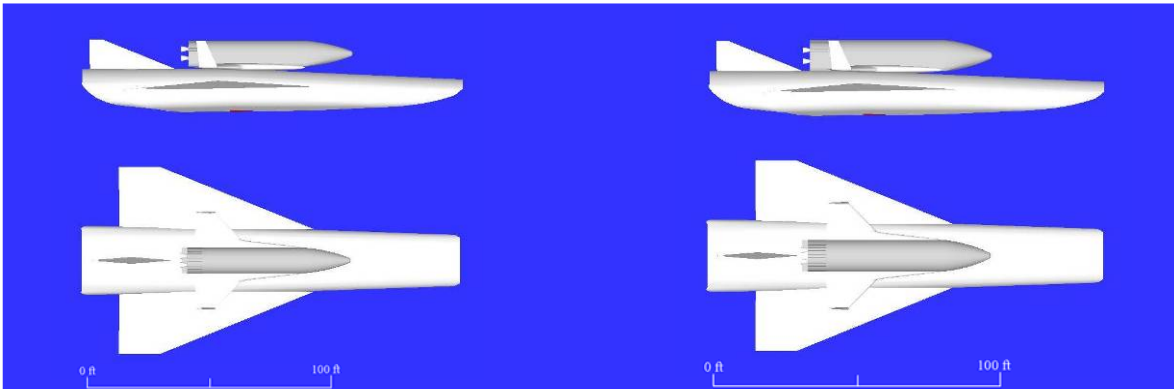
**Hydrogen Rocket Booster
Hydrogen RBCC Orbiter**

Length: 166.07 ft (50.62 m)
Width: 55.05 ft (16.78 m)
Height: 32.50 ft (9.91 m)

Booster Design Mach: 4
Rocket: 0-4000 fps, Propellant: H₂/LOX

Staging Velocity: 4000 fps

Orbiter Design Mach: 12
H₂ DMSJ: 4000-15500 fps, Propellant: H₂
Rocket: 15500-24500 fps, Propellant: H₂/LOX



**Hydrogen RBCC Booster
Hydrocarbon Rocket Orbiter**

Length: 158.66 ft (48.36 m)
Width: 86.58 ft (26.39 m)
Height: 39.74 ft (12.11 m)

Booster Design Mach: 8
Rocket: 0-4000 fps, Propellant: H₂/LOX
H₂ DMSJ: 4000-10000 fps, Propellant: H₂

Staging Velocity: 10000 fps

Orbiter Design Mach: 20
Rocket: 10000-24500 fps, Propellant: RP-1/LOX

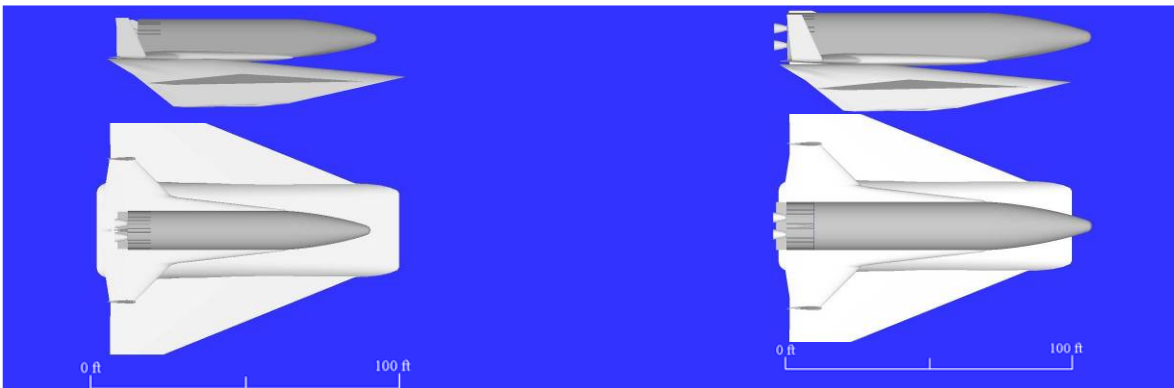
**Hydrogen RBCC Booster
Hydrogen Rocket Orbiter**

Length: 155.51 ft (47.40 m)
Width: 84.24 ft (25.68 m)
Height: 38.92 ft (11.86 m)

Booster Design Mach: 8
Rocket: 0-4000 fps, Propellant: H₂/LOX
H₂ DMSJ: 4000-10000 fps, Propellant: H₂

Staging Velocity: 9500 fps

Orbiter Design Mach: 20
Rocket: 10000-24500, Propellant: H₂/LOX



**Hydrocarbon TBCC Booster
Hydrocarbon Rocket Orbiter**

Length: 101.65 ft (30.98 m)
Width: 81.80 ft (24.93 m)
Height: 30.60 ft (9.33 m)

Booster Design Mach: 7
Turbine: 0-4000 fps, Propellant: JP-7
HC DMSJ: 4000-8300 fps, Propellant: JP-7

Staging Velocity: 8300 fps

Orbiter Design Mach: 20
Rocket: 8300-24500 fps, Propellant: RP-1/LOX

**Hydrocarbon TBCC Booster
Hydrogen Rocket Orbiter**

Length: 106.31 ft (32.40 m)
Width: 79.37 ft (24.19 m)
Height: 33.88 ft (10.33 m)

Booster Design Mach: 7
Turbine: 0-4000 fps, Propellant: JP-7
HC DMSJ: 4000-8300 fps, Propellant: JP-7

Staging Velocity: 8300 fps

Orbiter Design Mach: 20
Rocket: 8300-24500 fps, Propellant: H₂/LOX



**Hydrocarbon Turbine Booster
Hydrocarbon RBCC Orbiter**

Length: 163.60 ft (49.87 m)
Width: 143.07 ft (43.61 m)
Height: 48.10 ft (14.66 m)

Booster Design Mach: 4
Turbine: 0-4000 fps, Propellant: JP-7

Staging Velocity: 4000 fps

Orbiter Design Mach: 7
HC DMSJ: 4000-8300 fps, Propellant: JP-7
Rocket: 8300-24500 fps, Propellant: RP-1/LOX

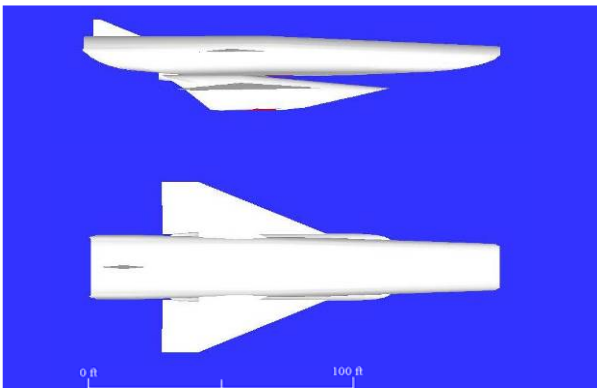
**Hydrocarbon Turbine Booster
Hydrogen RBCC Orbiter**

Length: 183.87 ft (56.04 m)
Width: 106.24 ft (32.38 m)
Height: 44.10 ft (13.44 m)

Booster Design Mach: 4
Turbine: 0-4000 fps, Propellant: JP-7

Staging Velocity: 4000 fps

Orbiter Design Mach: 12
H₂ DMSJ: 4000-15500 fps, Propellant: H₂
Rocket 15500-24500 fps, Propellant: H₂/LOX



**Hydrocarbon TBCC Booster
Hydrogen RBCC Orbiter**

Length: 159.38 ft (48.58 m)
Width: 68.21 ft (20.79 m)
Height: 36.87 ft (11.24 m)

Booster Design Mach: 7
Turbine: 0-4000 fps, Propellant: JP-7
HC DMSJ: 4000-8300 fps, Propellant: JP-7

Staging Velocity: 8300 fps

Orbiter Design Mach: 12
H₂ DMSJ: 8300-15500 fps, Propellant: H₂
Rocket: 15500-24500 fps, Propellant: H₂/LOX



**Hydrocarbon Turbine Booster
Hydrocarbon Rocket Orbiter**

Length: 186.69 ft (56.90 m)
Width: 165.31 ft (50.39 m)
Height: 58.17 ft (17.73 m)

Booster Design Mach: 4
Turbine: 0-4000 fps, Propellant: JP-7

Staging Velocity: 4000 fps

Orbiter Design Mach: 20
Rocket: 4000-24500 fps, Propellant: RP-1/LOX

**Hydrocarbon Turbine Booster
Hydrogen Rocket Orbiter**

Length: 167.02 ft (50.91 m)
Width: 146.35 ft (44.61 m)
Height: 58.38 ft (17.80 m)

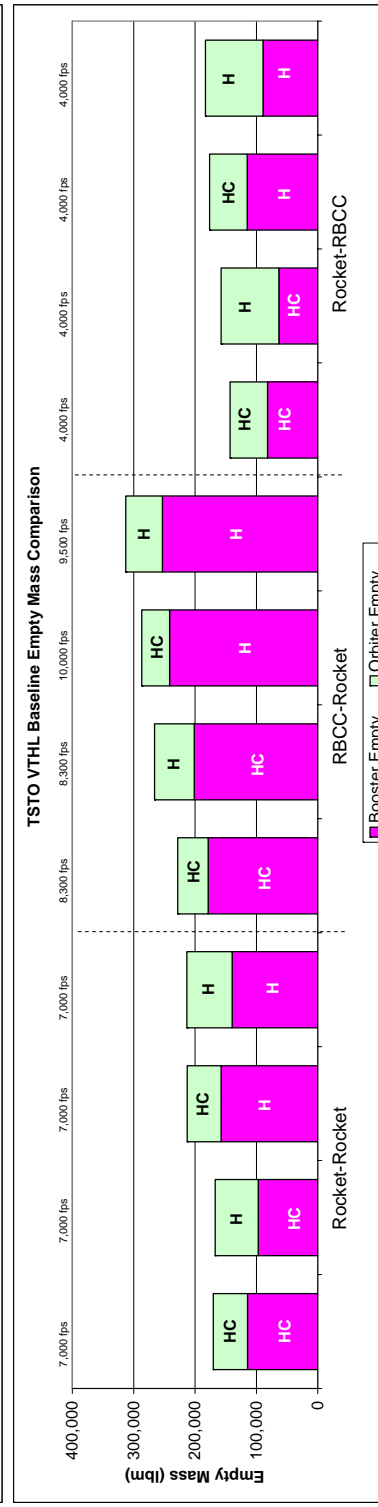
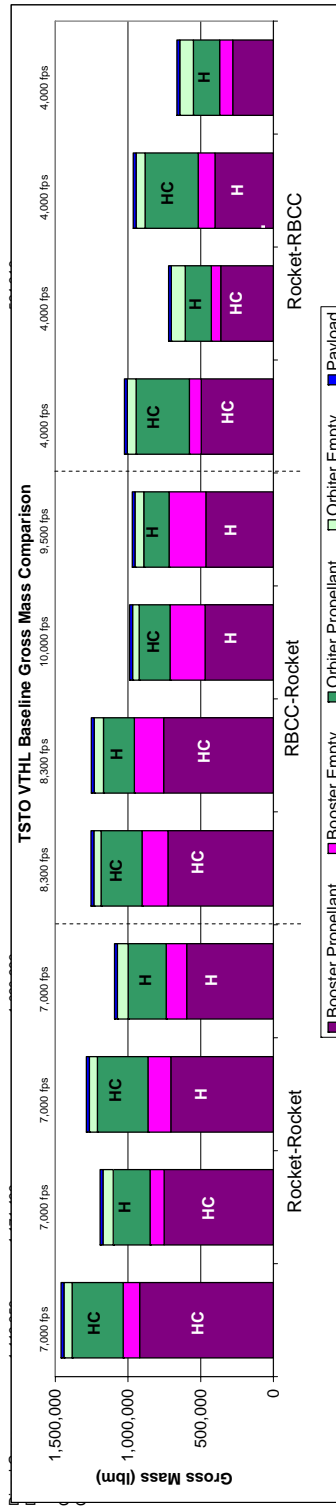
Booster Design Mach: 4
Turbine: 0-4000 fps, Propellant: JP-7

Staging Velocity: 4000 fps

Orbiter Design Mach: 20
Rocket: 4000-24500 fps, Propellant: H₂/LOX

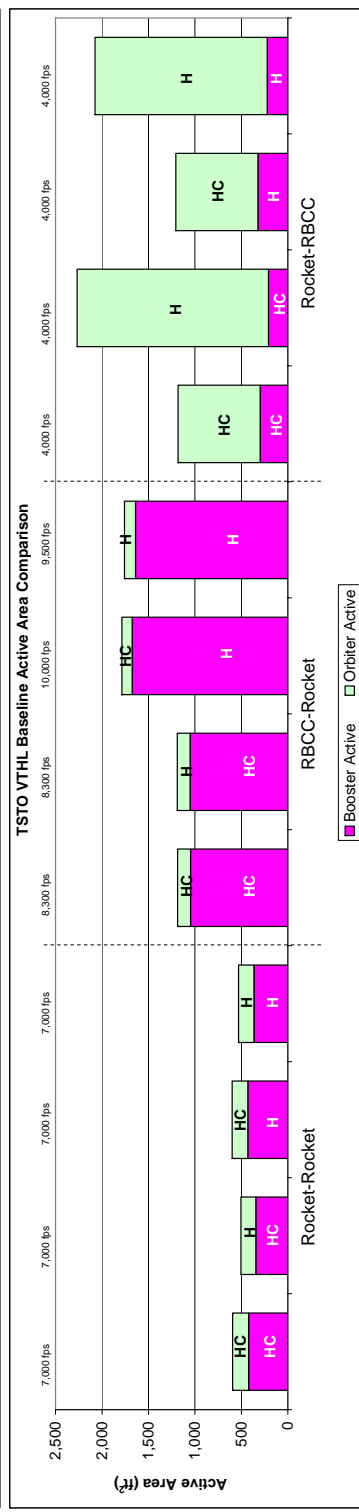
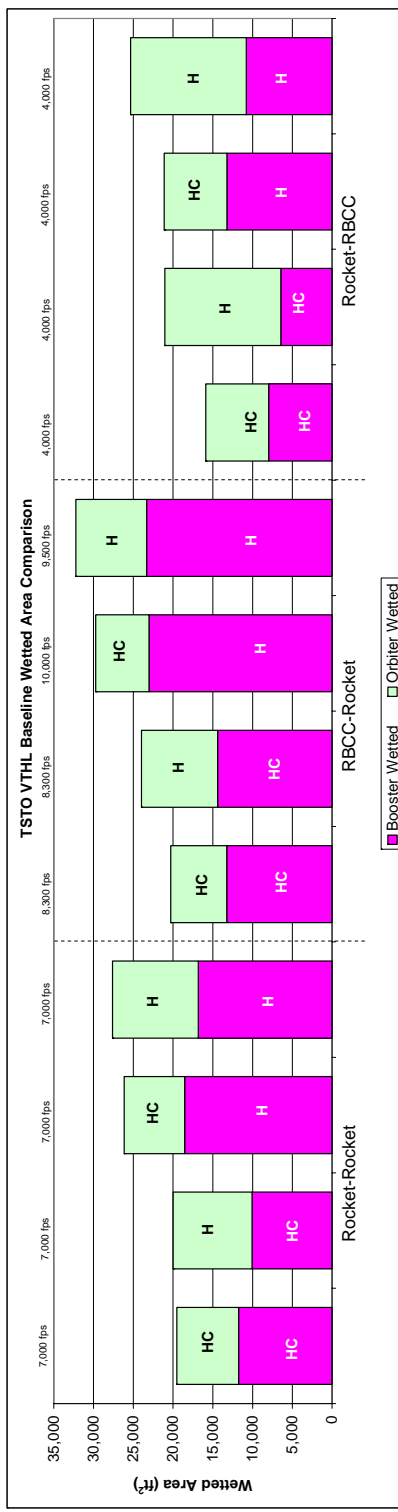
Appendix G. Baseline Vehicle Results

Baseline VTHL Models

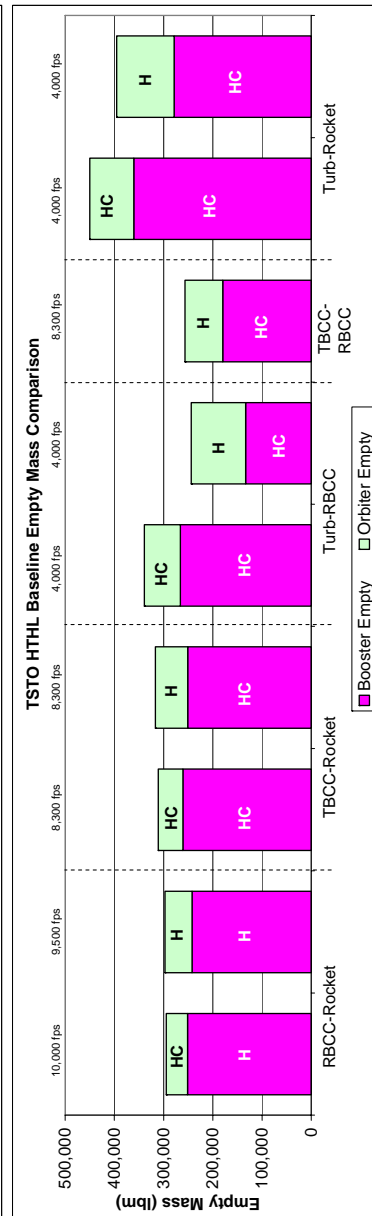
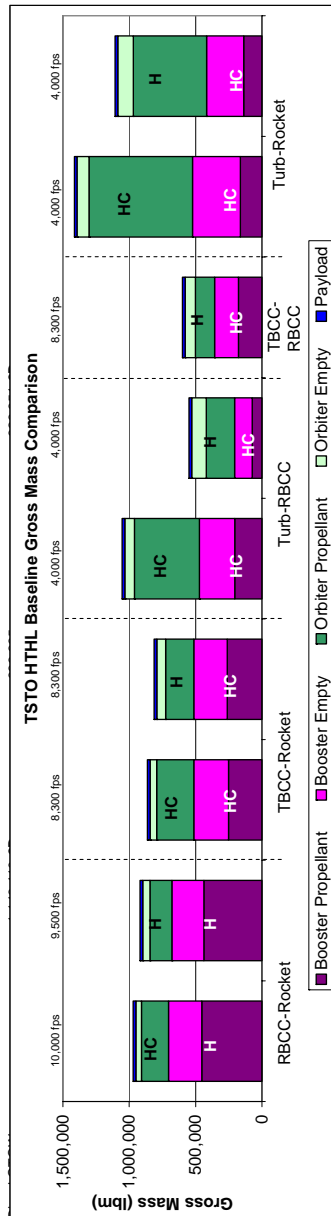
[illegible]

Baseline VTHL Models

Design Mach #	HCRL-HCRk1	HCRL-HRk1	HRk-HCRk1	HRk-HRk1	HCRCBCC-HCRk1	HCRCBCC-HRk1	HRBCC-HCRk1	HRBCC-HRk1	HCRL-HCRBCC	HCRL-HRBCC	HRk-HCRBCC
Staging Velocity	M7/M20	M7/M20	M7/M20	M7/M20	M7/M20	M7/M20	M7/M20	M7/M20	M4/M7	M4/M7	M4/M7
Metric (SI)											
Orbiter Wetted	721.34 m ²	922.14 m ²	704.55 m ²	1,002.79 m ²	665.78 m ²	890.11 m ²	622.52 m ²	825.78 m ²	1,354.18 m ²	735.07 m ²	1,350.17 m ²
Orbiter Active	15.86 m ²	14.78 m ²	15.77 m ²	15.36 m ²	13.06 m ²	12.78 m ²	10.32 m ²	10.94 m ²	82.05 m ²	82.05 m ²	172.09 m ²
Booster Wetted	1,092.75 m ²	934.99 m ²	1,722.96 m ²	1,563.52 m ²	1,229.39 m ²	1,336.55 m ²	2,139.21 m ²	2,167.80 m ²	598.84 m ²	1,227.85 m ²	1,004.31 m ²
Booster Active	39.34 m ²	32.11 m ²	39.96 m ²	33.98 m ²	97.29 m ²	97.79 m ²	155.68 m ²	152.33 m ²	19.48 m ²	30.02 m ²	20.67 m ²
Wetted Area	1,814 m ²	1,857 m ²	2,428 m ²	2,566 m ²	1,885 m ²	2,227 m ²	2,762 m ²	2,994 m ²	1,953 m ²	1,963 m ²	2,354 m ²
Active Area	55 m ²	47 m ²	56 m ²	49 m ²	110 m ²	111 m ²	166 m ²	163 m ²	211 m ²	112 m ²	183 m ²
Metric (English)											
Orbiter Wetted	7,765 ft ²	9,928 ft ²	7,584 ft ²	10,784 ft ²	7,069 ft ²	9,581 ft ²	6,701 ft ²	8,889 ft ²	14,577 ft ²	7,912 ft ²	14,534 ft ²
Orbiter Active	171 ft ²	159 ft ²	170 ft ²	165 ft ²	141 ft ²	138 ft ²	111 ft ²	118 ft ²	883 ft ²	883 ft ²	1,852 ft ²
Booster Wetted	11,763 ft ²	10,064 ft ²	18,546 ft ²	16,830 ft ²	13,233 ft ²	14,387 ft ²	23,027 ft ²	23,335 ft ²	6,446 ft ²	13,217 ft ²	10,811 ft ²
Booster Active	423 ft ²	346 ft ²	430 ft ²	366 ft ²	1,047 ft ²	1,053 ft ²	1,676 ft ²	1,640 ft ²	210 ft ²	323 ft ²	222 ft ²
Wetted Area	19,527 ft ²	19,991 ft ²	26,130 ft ²	27,624 ft ²	20,292 ft ²	23,968 ft ²	29,728 ft ²	32,224 ft ²	21,023 ft ²	21,129 ft ²	25,344 ft ²
Active Area	594 ft ²	505 ft ²	600 ft ²	531 ft ²	1,188 ft ²	1,190 ft ²	1,787 ft ²	1,757 ft ²	2,287 ft ²	1,206 ft ²	2,075 ft ²

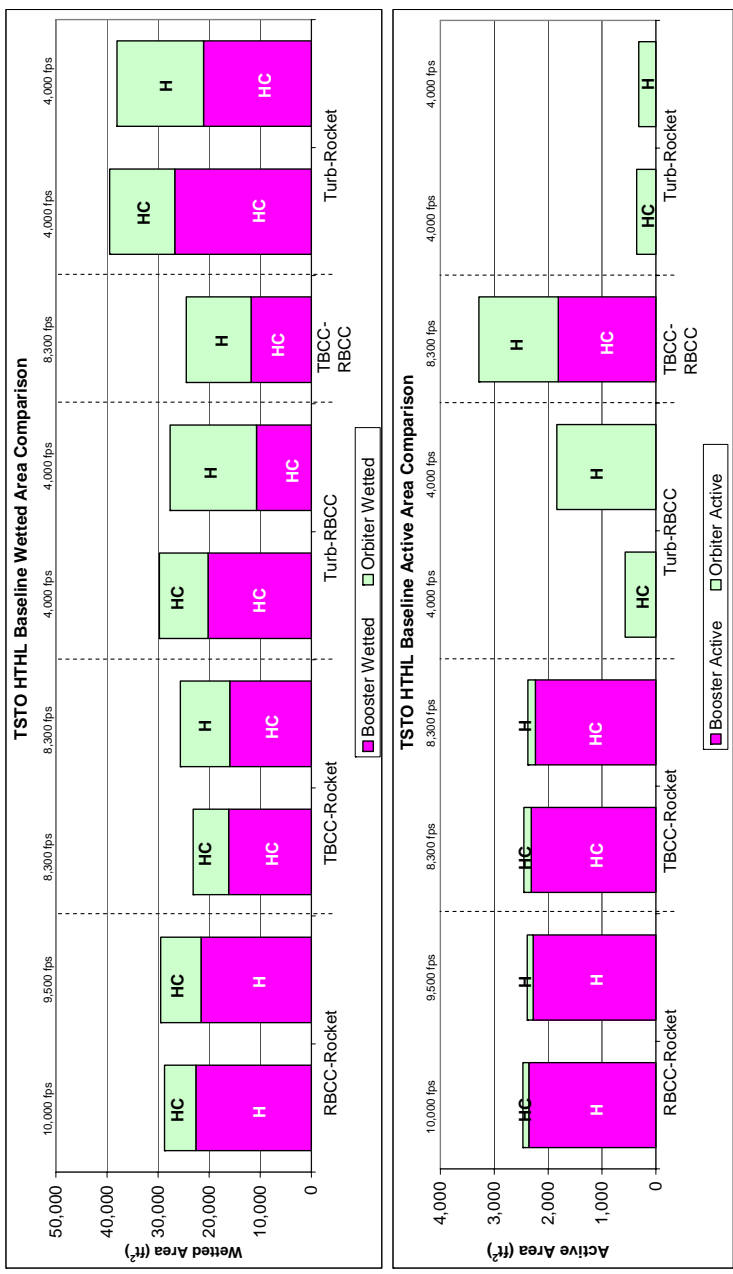


Design Mech #	Staging Velocity	Metric (SI)				English			
		HRBCC-HCRkt	HRBCC-HCRkt	HRBCC-HCRkt	HRBCC-HCRkt	HRBCC-HCRkt	HRBCC-HCRkt	HRBCC-HCRkt	HRBCC-HCRkt
M4M20	10,000 fps	92,232.19 kg	74,521.06 kg	127,285.45 kg	96,956.64 kg	222,128.28 kg	96,526.52 kg	50,334.13 kg	250,845.62 kg
M4M20	9,500 fps	19,338.74 kg	22,530.51 kg	29,677.12 kg	29,677.12 kg	33,178.04 kg	50,334.13 kg	40,643.32 kg	52,938.03 kg
M4M20	9,000 fps	205,676.55 kg	198,384.08 kg	114,416.28 kg	118,852.06 kg	12,982.93 kg	87,661.68 kg	74,083.53 kg	62,728.14 kg
M4M20	8,500 fps	114,090.47 kg	118,412.57 kg	113,806.76 kg	120,700.51 kg	60,444.10 kg	81,645.38 kg	163,638.63 kg	126,368.63 kg
M4M20	8,000 fps	9,071.85 kg	9,071.85 kg	9,071.85 kg	9,071.85 kg	9,071.85 kg	9,071.85 kg	9,071.85 kg	9,071.85 kg
M4M20	7,500 fps	44,040.70 kg	416,737 kg	391,717 kg	388,454 kg	249,652 kg	271,782 kg	601,176 kg	501,352 kg
M4M20	7,000 fps	133,489 kg	134,760 kg	140,943 kg	143,574 kg	153,879 kg	110,576 kg	204,179 kg	179,307 kg
Design Mech #	Staging Velocity	Metric (SI)				English			
		HRBCC-HCRkt	HRBCC-HCRkt	HRBCC-HCRkt	HRBCC-HCRkt	HRBCC-HCRkt	HRBCC-HCRkt	HRBCC-HCRkt	HRBCC-HCRkt
M4M20	10,000 fps	203,337 kg	164,291 lb	280,616 lb	213,753 lb	489,709 lb	212,805 lb	144,782 lb	553,020 lb
M4M20	9,500 fps	42,767 lb	54,831 lb	49,671 lb	65,625 lb	73,145 lb	110,522 lb	76,658 lb	116,708 lb
M4M20	9,000 fps	453,439 lb	437,362 lb	252,245 lb	282,024 lb	204,992 lb	73,806 lb	163,326 lb	138,292 lb
M4M20	8,500 fps	251,526 lb	242,265 lb	261,055 lb	250,901 lb	266,099 lb	133,256 lb	360,534 lb	278,595 lb
M4M20	8,000 fps	20,000 lb	20,000 lb	20,000 lb	20,000 lb	20,000 lb	20,000 lb	20,000 lb	20,000 lb
M4M20	7,500 fps	971,749 lb	863,587 lb	812,303 lb	1,053,945 lb	599,176 lb	550,389 lb	1,413,550 lb	1,106,615 lb
M4M20	7,000 fps	294,023 lb	307,096 lb	310,726 lb	316,526 lb	339,244 lb	243,779 lb	450,138 lb	395,304 lb

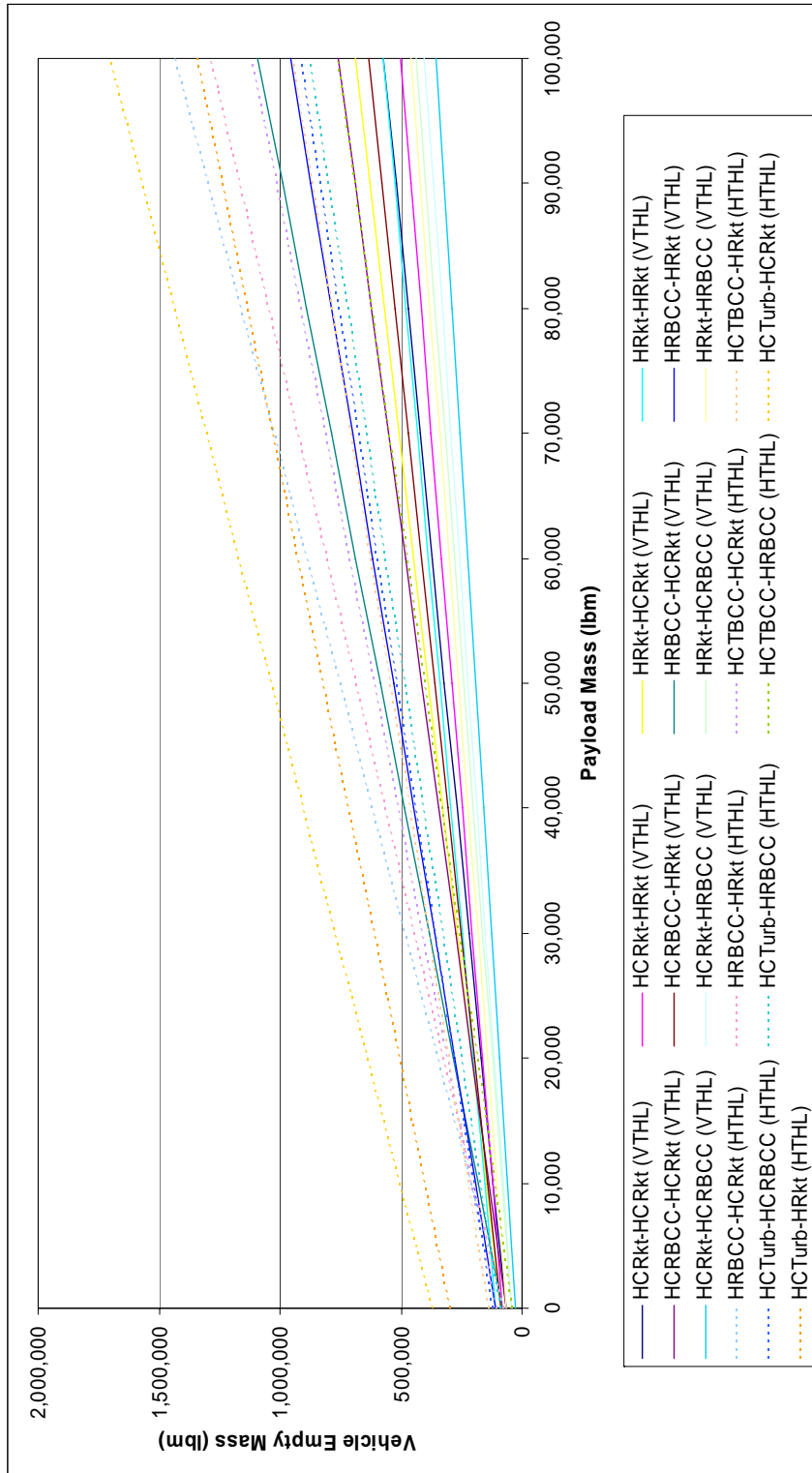


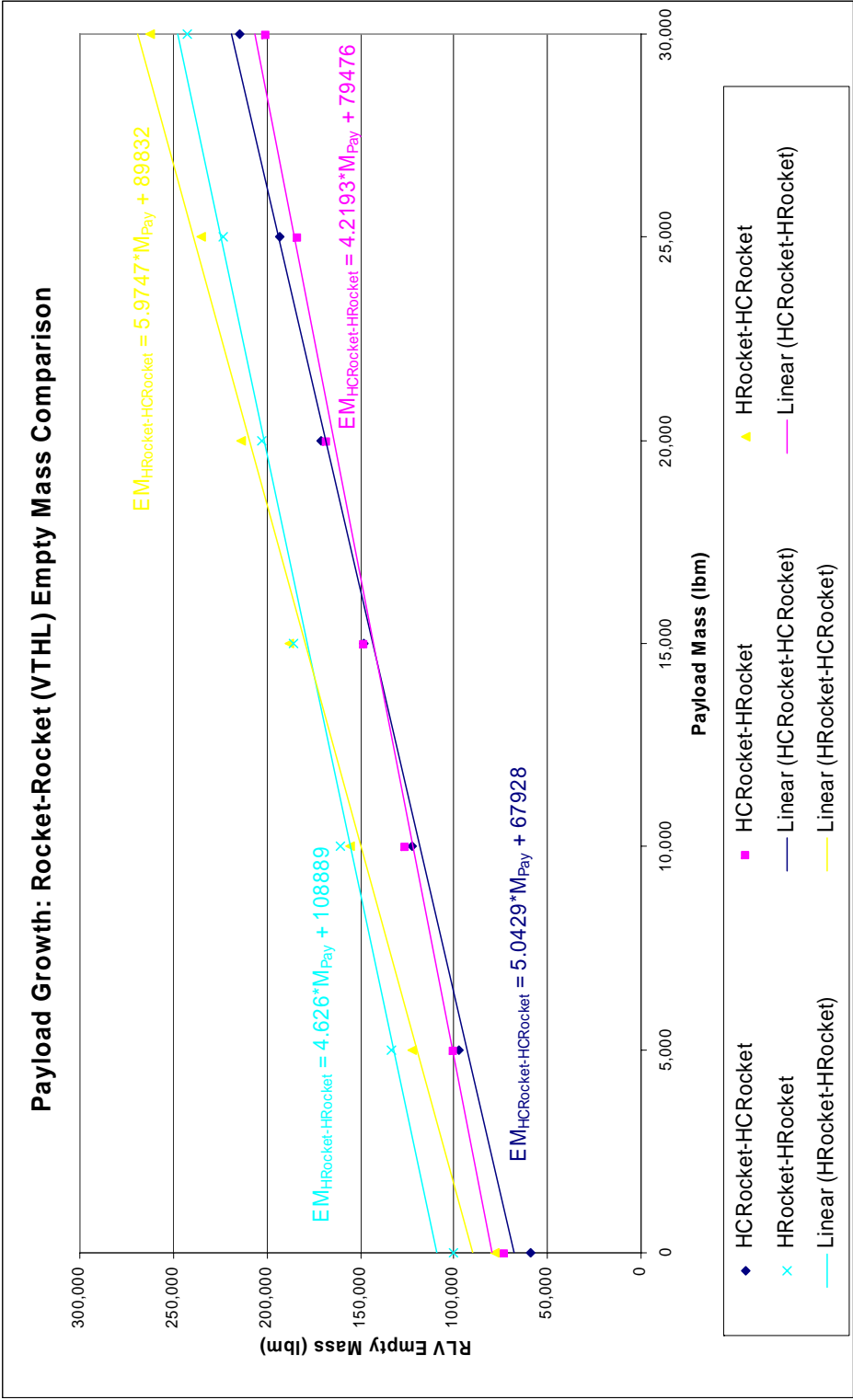
Baseline HTHL Models

Design Mach #	HRBCC-HCRkt	HRBCC-HRkt	M7M20	HCTBCC-HCRkt	HCTBCC-HRkt	M7M20	HCTub-HCRBCC	HCTub-HCRkt	M4M12	HCTub-HRBCC	HCTBCC-HRBCC	HCTub-HCRkt	M4M20	HCTub-HCRkt
Staging Velocity	10,000 fps	9,500 fps	8,300 fps	4,000 fps	4,000 fps	8,300 fps	4,000 fps	4,000 fps	4,000 fps	4,000 fps	8,300 fps	4,000 fps	4,000 fps	4,000 fps
Metric (SI)														
Orbiter Wetted	572.11 m ²	733.85 m ²	647.21 m ²	884.58 m ²	898.93 m ²	1,569.90 m ²	1,180.86 m ²	1,185.47 m ²	1,185.47 m ²	1,185.47 m ²	1,185.47 m ²	1,185.47 m ²	1,185.47 m ²	1,572.04 m ²
Orbiter Active	9.91 m ²	10.31 m ²	13.04 m ²	12.91 m ²	12.91 m ²	170.68 m ²	136.9 m ²	33.12 m ²	33.12 m ²	33.12 m ²	33.12 m ²	33.12 m ²	33.12 m ²	29.73 m ²
Booster Wetted	2,099.14 m ²	2,006.08 m ²	1,503.61 m ²	1,879.49 m ²	1,483.25 m ²	998.41 m ²	1,093.98 m ²	2,484.26 m ²	2,484.26 m ²	2,484.26 m ²	2,484.26 m ²	2,484.26 m ²	2,484.26 m ²	1,960.47 m ²
Booster Active	219.17 m ²	211.5 m ²	214.74 m ²	207.87 m ²	207.87 m ²	0 m ²	0 m ²	0 m ²	0 m ²	0 m ²	0 m ²	0 m ²	0 m ²	0 m ²
Wetted Area	2,671 m ²	2,740 m ²	2,151 m ²	2,382 m ²	2,382 m ²	2,764 m ²	2,568 m ²	3,670 m ²	3,670 m ²	3,670 m ²	3,670 m ²	3,670 m ²	3,670 m ²	3,533 m ²
Active Area	229 m ²	222 m ²	228 m ²	221 m ²	221 m ²	53 m ²	171 m ²	33 m ²	33 m ²	33 m ²	33 m ²	33 m ²	33 m ²	30 m ²
English														
Orbiter Wetted	6,158 ft ²	7,899 ft ²	6,967 ft ²	9,676 ft ²	9,676 ft ²	16,889 ft ²	12,711 ft ²	12,761 ft ²	12,761 ft ²	12,761 ft ²	12,761 ft ²	12,761 ft ²	12,761 ft ²	16,922 ft ²
Orbiter Active	107 ft ²	111 ft ²	140 ft ²	139 ft ²	139 ft ²	1,837 ft ²	1,474 ft ²	357 ft ²	357 ft ²	357 ft ²	357 ft ²	357 ft ²	357 ft ²	320 ft ²
Booster Wetted	22,596 ft ²	21,594 ft ²	16,185 ft ²	20,231 ft ²	15,966 ft ²	10,747 ft ²	11,776 ft ²	26,741 ft ²	26,741 ft ²	26,741 ft ²	26,741 ft ²	26,741 ft ²	26,741 ft ²	21,103 ft ²
Booster Active	2,359 ft ²	2,277 ft ²	2,312 ft ²	2,238 ft ²	2,238 ft ²	0 ft ²	0 ft ²	0 ft ²	0 ft ²	0 ft ²	0 ft ²	0 ft ²	0 ft ²	0 ft ²
Wetted Area	28,754 ft ²	29,493 ft ²	23,152 ft ²	25,642 ft ²	25,642 ft ²	27,646 ft ²	24,487 ft ²	39,502 ft ²	39,502 ft ²	39,502 ft ²	39,502 ft ²	39,502 ft ²	39,502 ft ²	38,025 ft ²
Active Area	2,466 ft ²	2,388 ft ²	2,452 ft ²	2,377 ft ²	2,377 ft ²	1,837 ft ²	3,285 ft ²	357 ft ²	357 ft ²	357 ft ²	357 ft ²	357 ft ²	357 ft ²	320 ft ²



Appendix H. Payload Sizing Impact Study Results

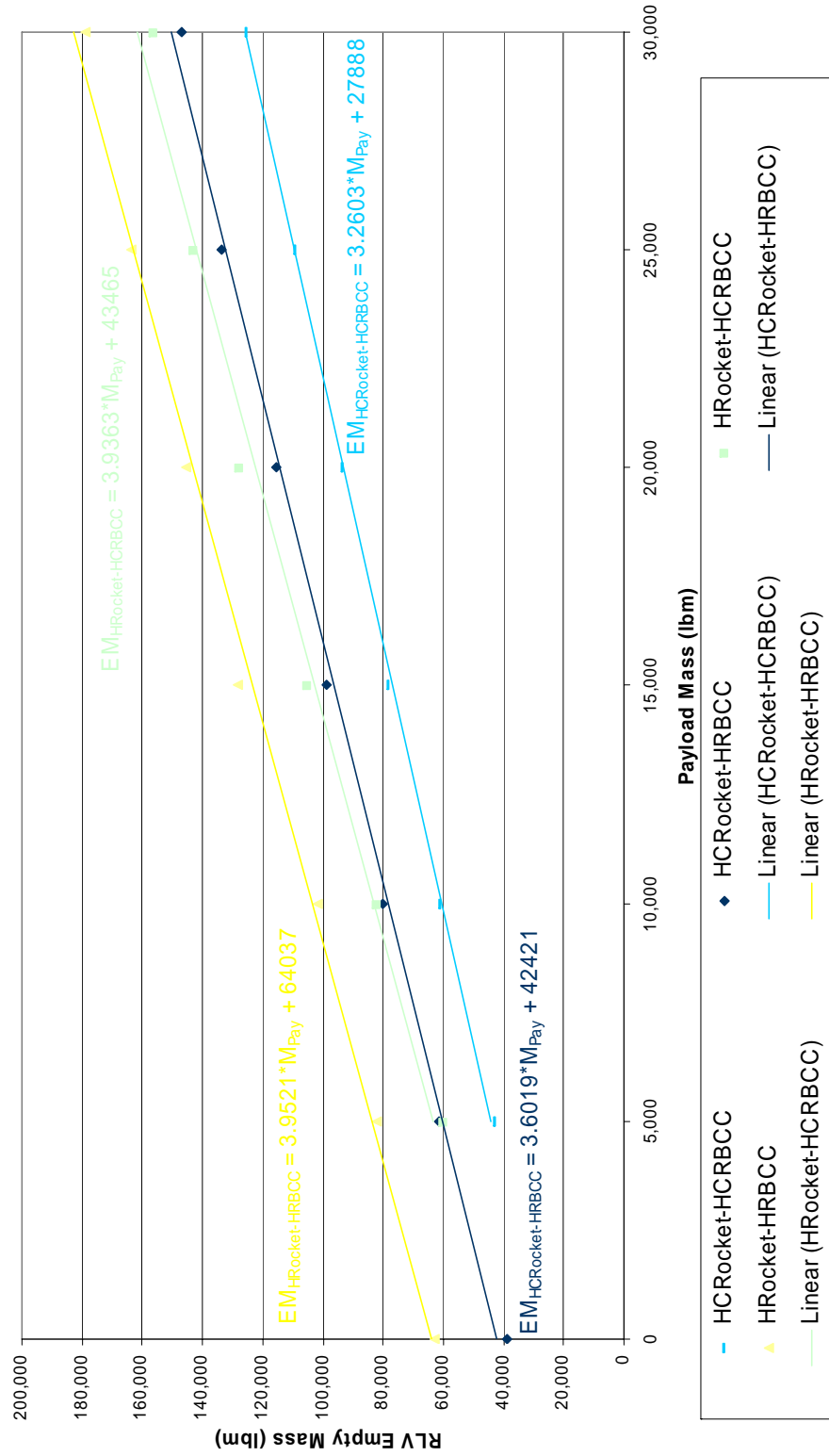




Payload Growth: RBCC-Rocket (VTHL) Empty Mass Comparison



Payload Growth: Rocket-RBCC (VTHL) Empty Mass Comparison



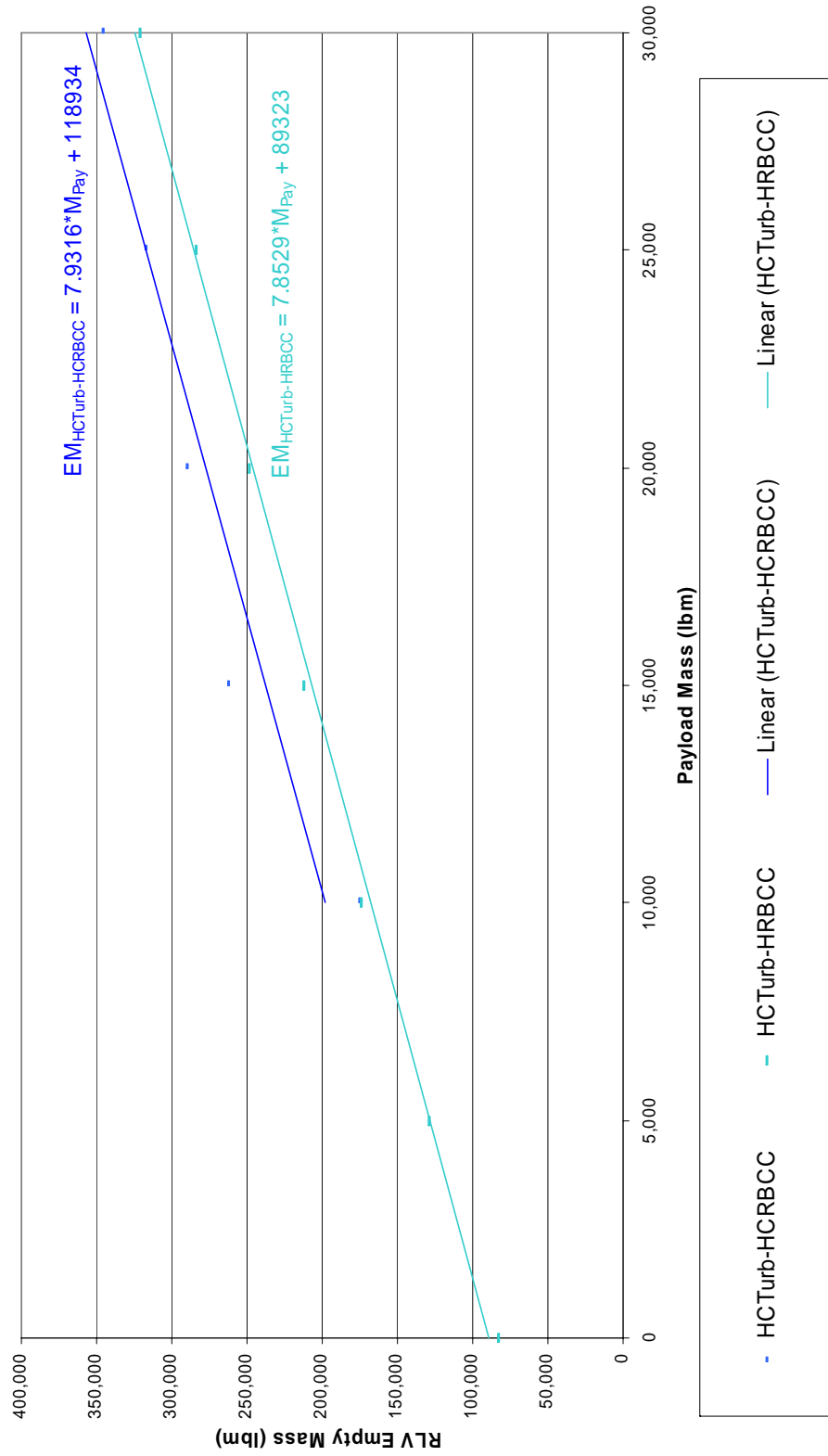
Payload Growth: RBCC-Rocket (HTHL) Empty Mass Comparison

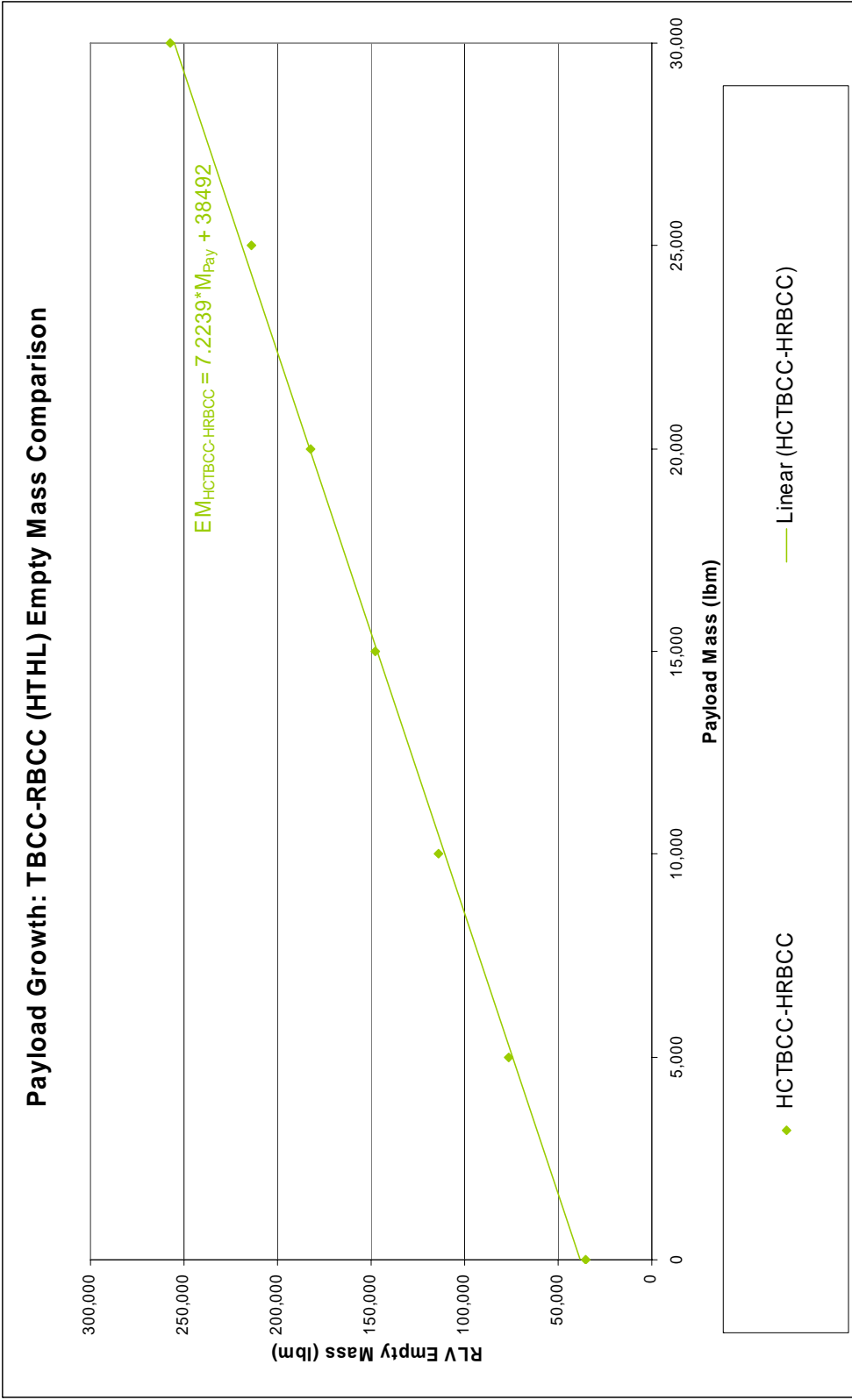


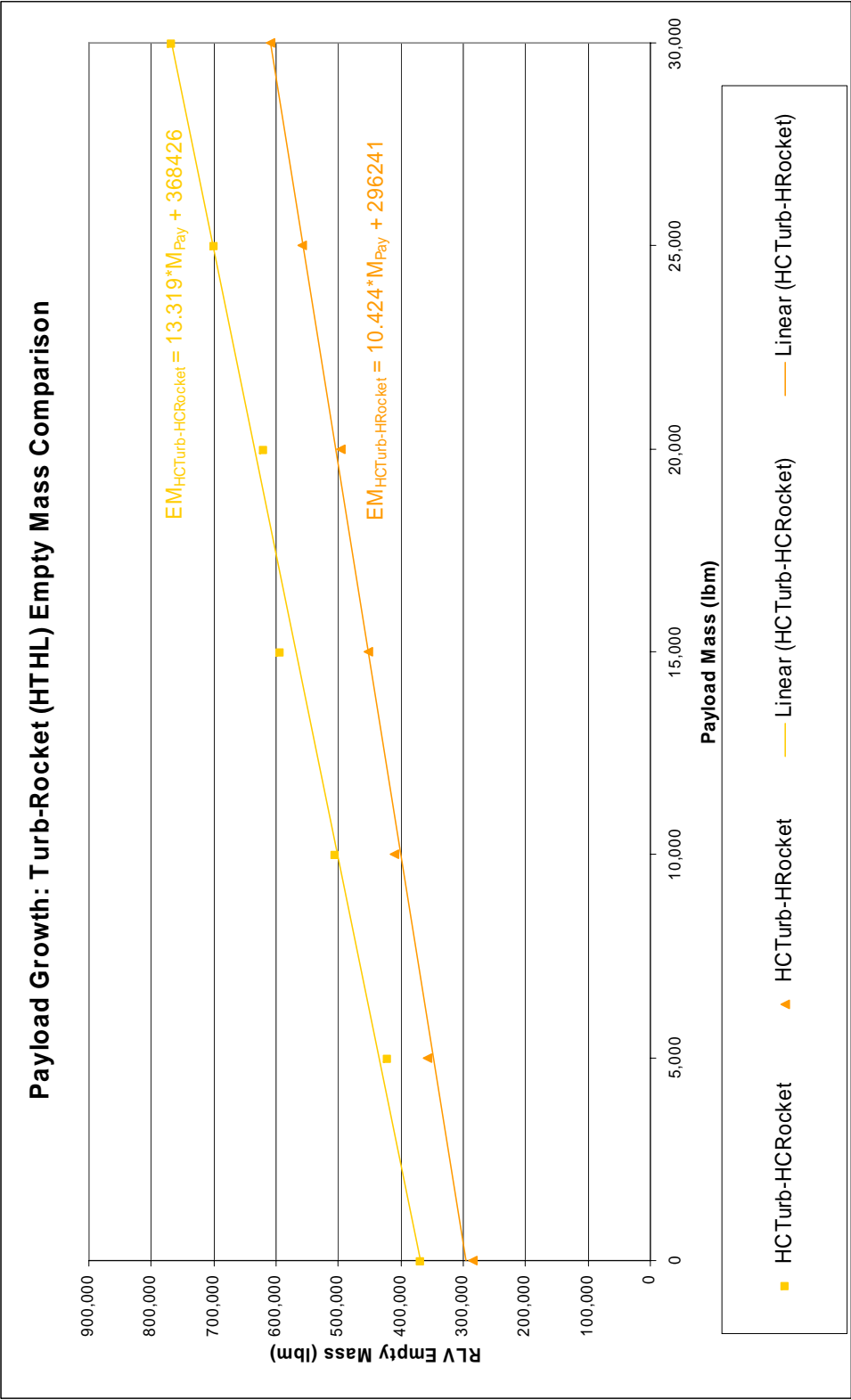
Payload Growth: TBCC-Rocket (HTHL) Empty Mass Comparison

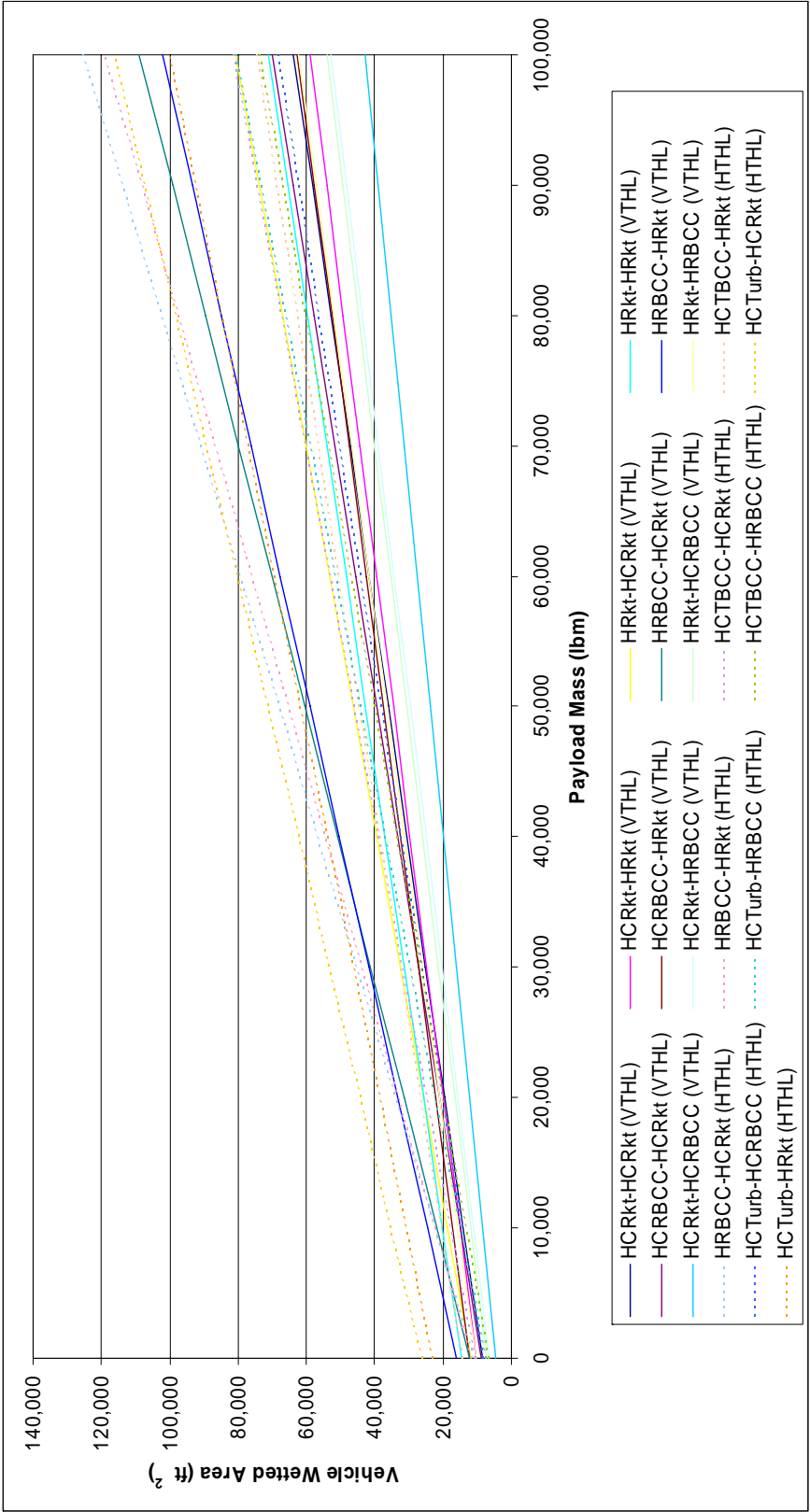


Payload Growth: Turb-RBCC (HTHL) Empty Mass Comparison





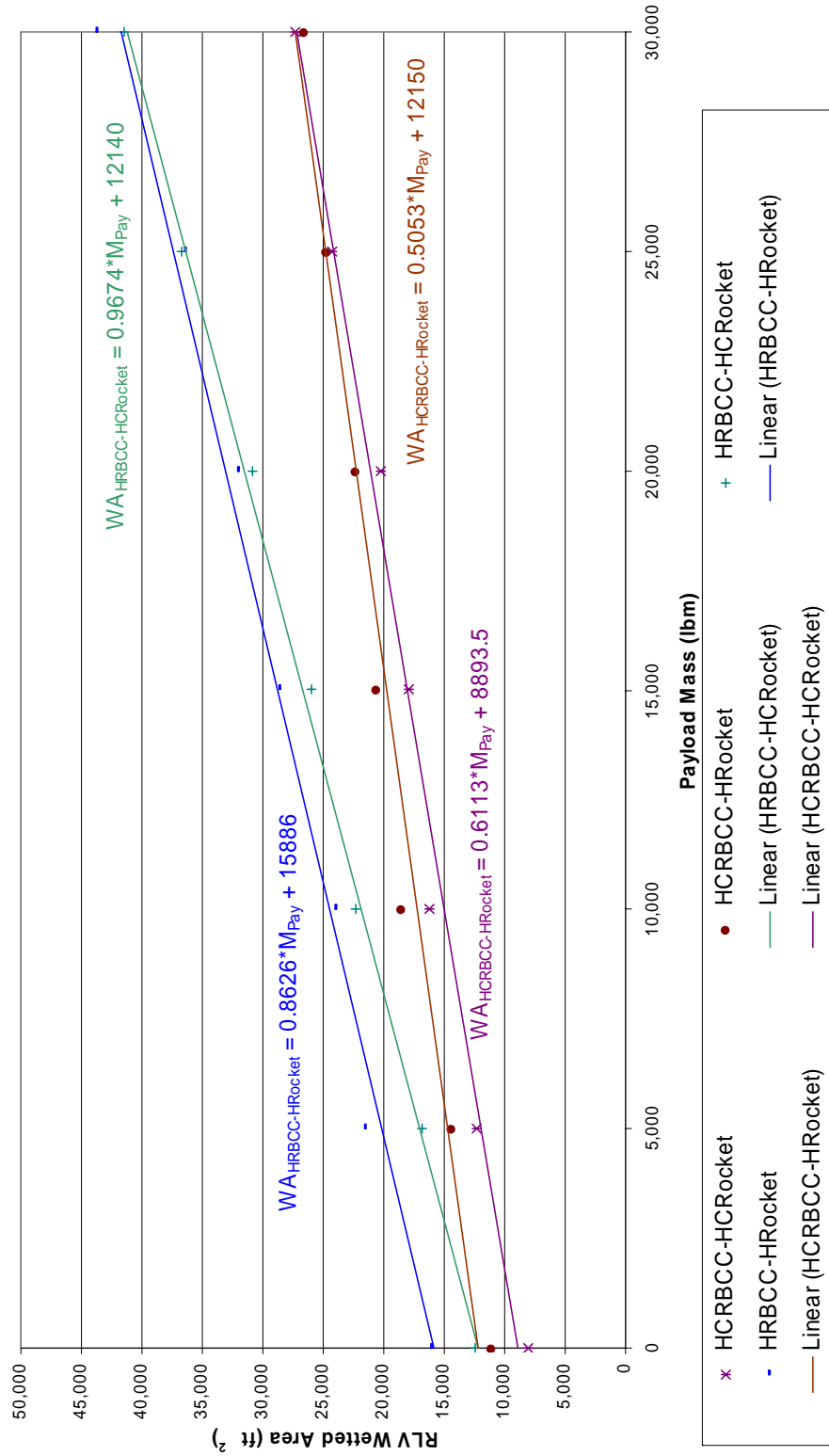




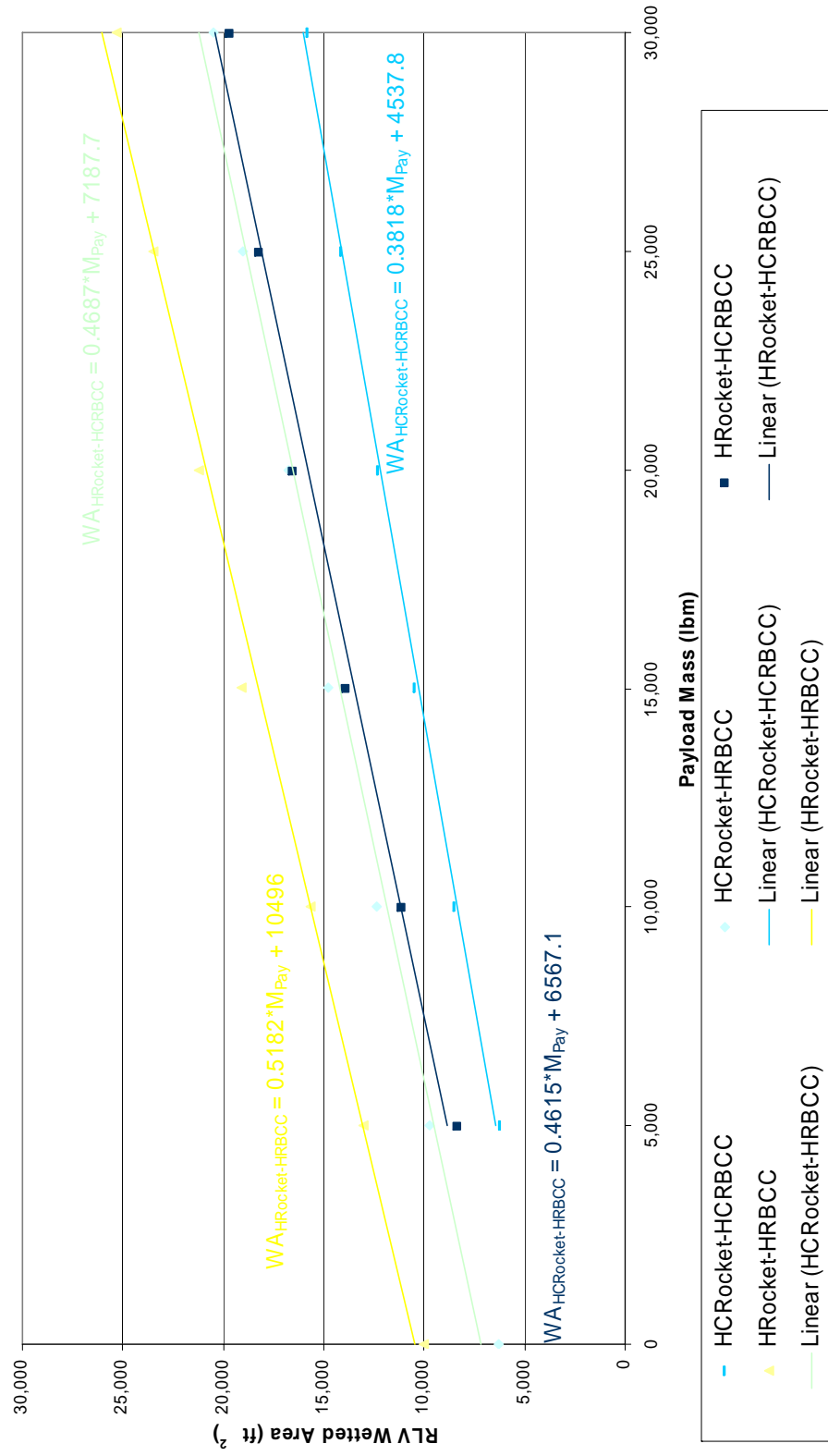
Payload Growth: Rocket-Rocket (VTHL) Wetted Area Comparison



Payload Growth: RBCC-Rocket (VTHL) Wetted Area Comparison



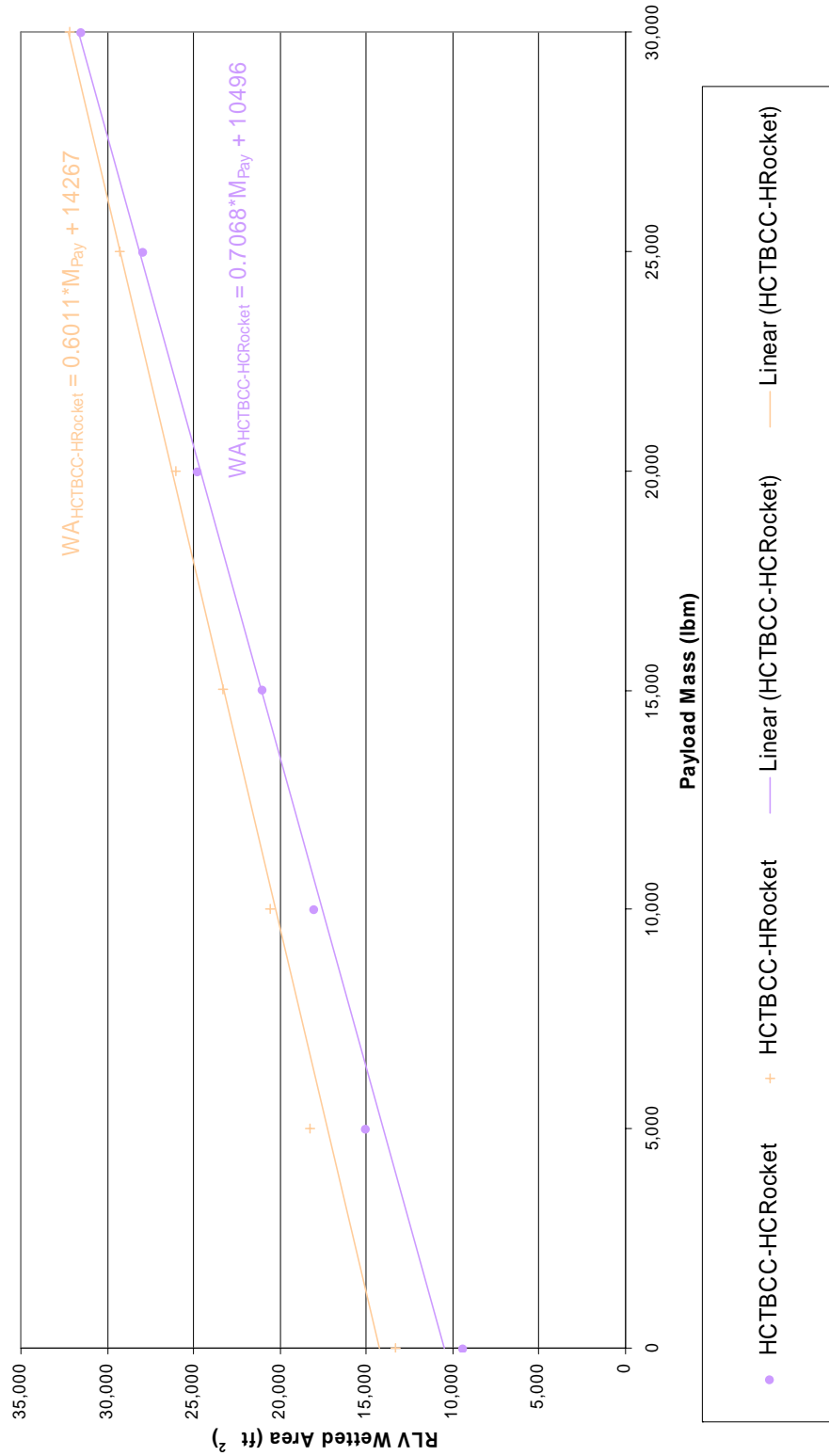
Payload Growth: Rocket-RBCC (VTHL) Wetted Area Comparison

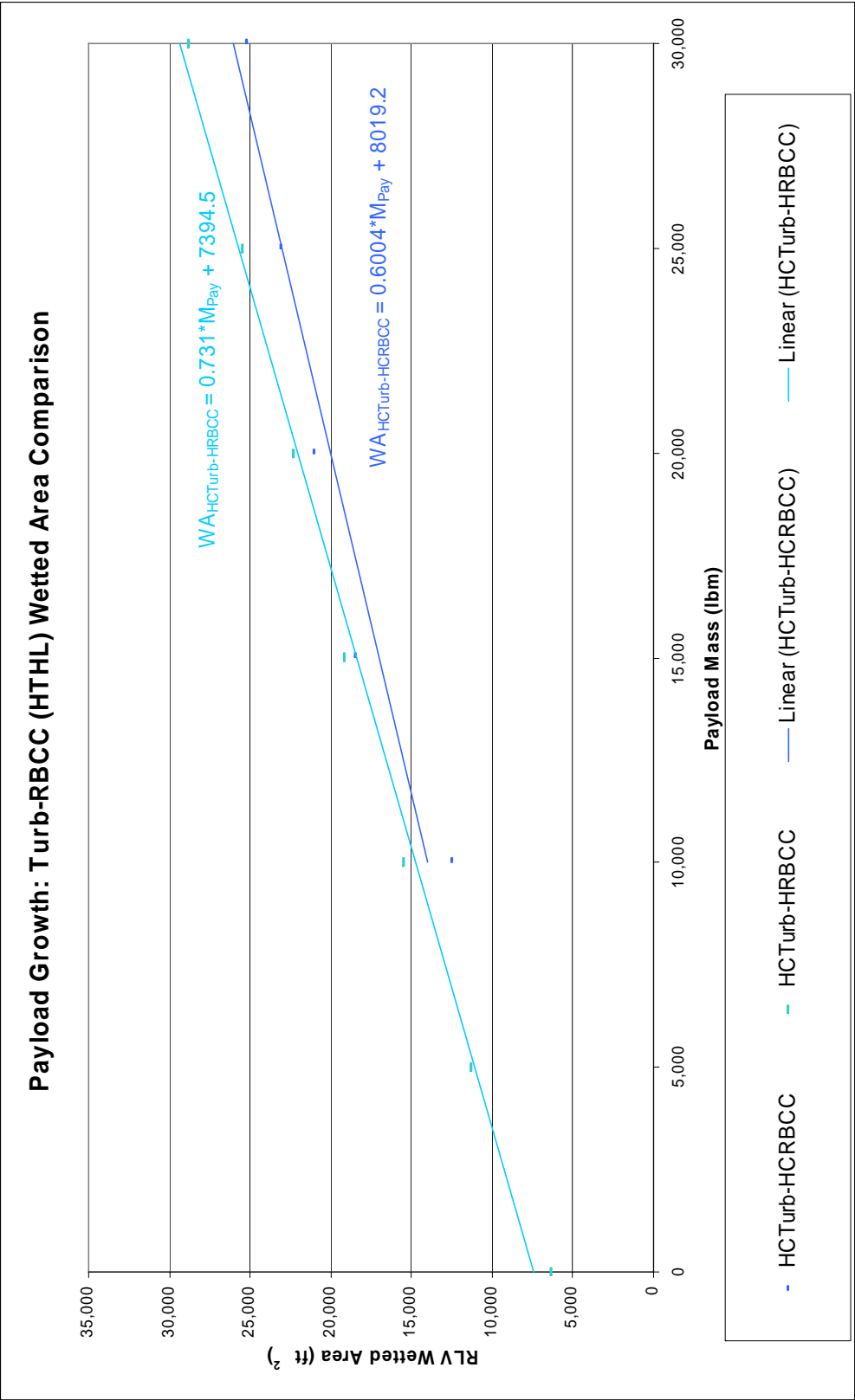


Payload Growth: RBCC-Rocket (HTHL) Wetted Area Comparison



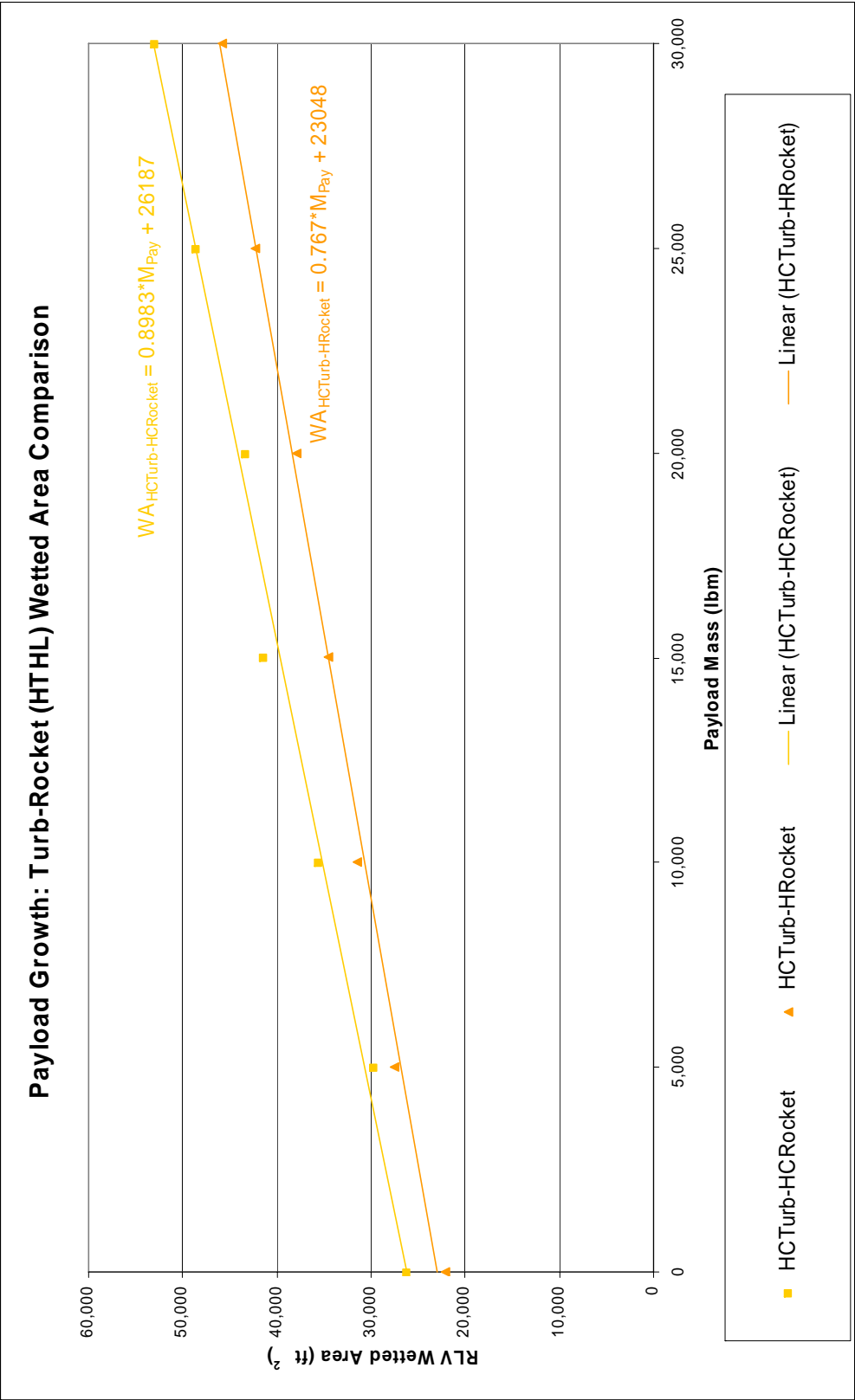
Payload Growth: TBCC-Rocket (HTHL) Wetted Area Comparison





Payload Growth: TBCC-RBCC (HTHL) Wetted Area Comparison

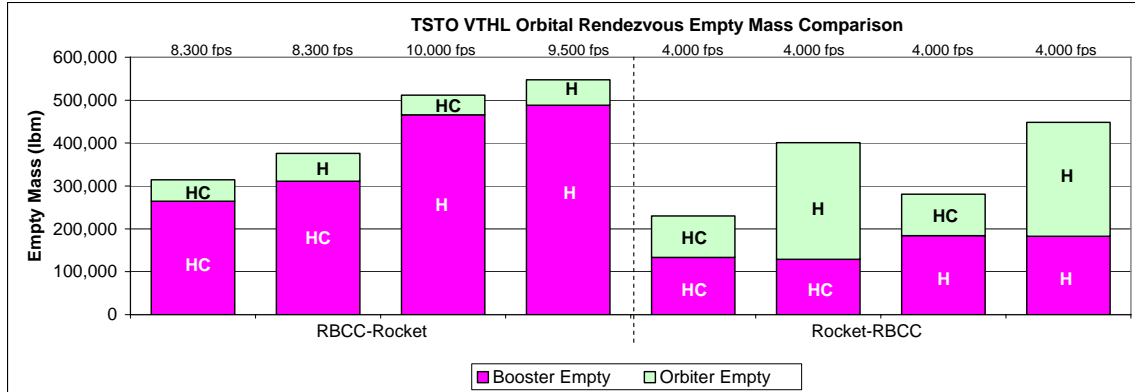
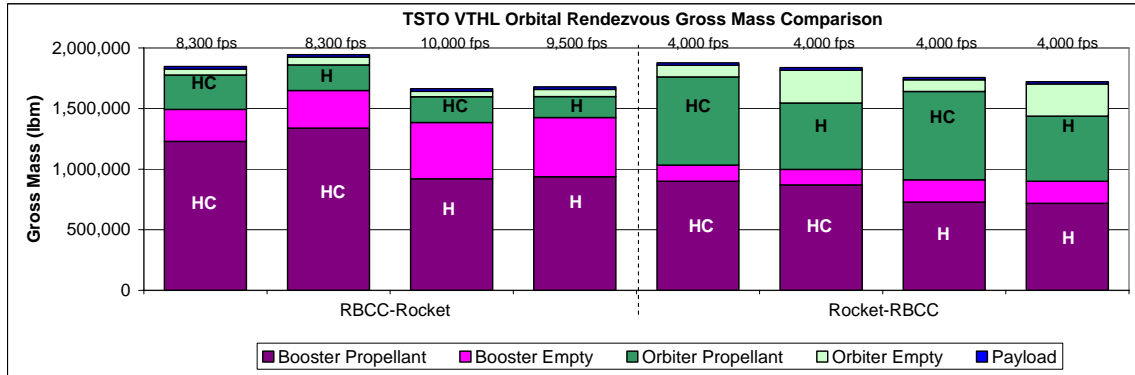




Appendix I. Orbital Rendezvous Results

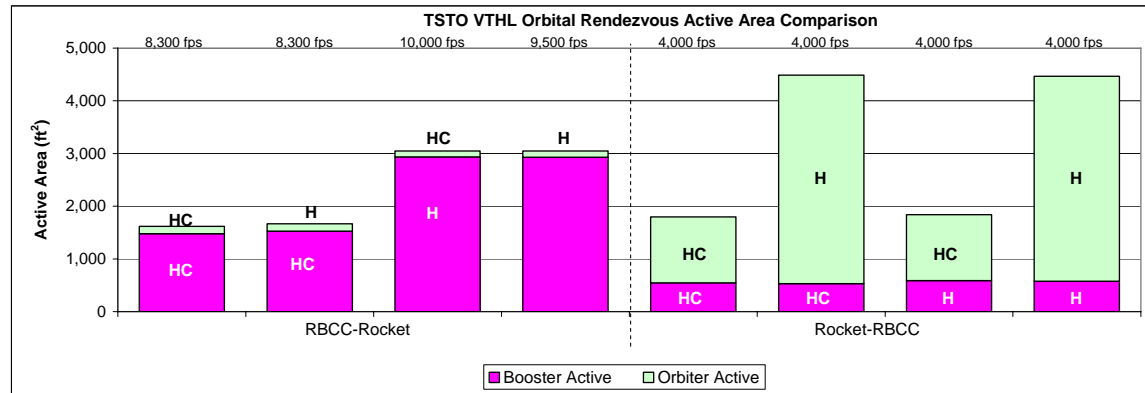
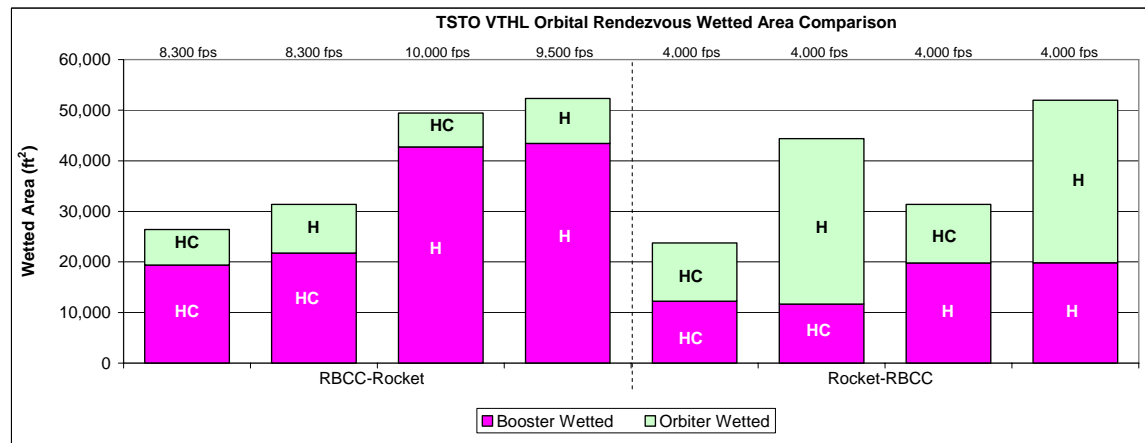
Orbital Rendezvous VTHL Models

	HCRBCC-HCRkt	HCRBCC-HRkt	HRBCC-HCRkt	HRBCC-HRkt	HCRkt-HCRBCC	HCRkt-HRBCC	HRkt-HCRBCC	HRkt-HRBCC
Design Mach #	M7/M20	M7/M20	M8/M20	M8/M20	M4/M7	M4/M12	M4/M7	M4/M12
Staging Velocity	8,300 fps	8,300 fps	10,000 fps	9,500 fps	4,000 fps	4,000 fps	4,000 fps	4,000 fps
Metric (SI)	HCRBCC-HCRkt	HCRBCC-HRkt	HRBCC-HCRkt	HRBCC-HRkt	HCRkt-HCRBCC	HCRkt-HRBCC	HRkt-HCRBCC	HRkt-HRBCC
Orbiter Propellant	127,964.27 kg	95,988.25 kg	96,032.29 kg	79,010.66 kg	330,029.73 kg	248,404.50 kg	330,030.04 kg	243,404.65 kg
Orbiter Empty	22,704.16 kg	29,390.74 kg	20,610.13 kg	27,013.55 kg	43,737.09 kg	123,355.22 kg	43,737.04 kg	120,572.65 kg
Booster Propellant	558,123.42 kg	607,110.71 kg	417,128.72 kg	425,243.34 kg	408,349.78 kg	394,340.57 kg	330,452.98 kg	325,754.16 kg
Booster Empty	119,895.66 kg	141,002.51 kg	211,354.83 kg	221,323.16 kg	60,536.37 kg	58,619.91 kg	83,645.69 kg	82,851.87 kg
Payload	9,071.85 kg	9,071.85 kg	9,071.85 kg	9,071.85 kg	9,071.85 kg	9,071.85 kg	9,071.85 kg	9,071.85 kg
GTOM	837,759 kg	882,564 kg	754,198 kg	761,663 kg	851,725 kg	833,792 kg	796,938 kg	781,655 kg
Empty Mass	142,600 kg	170,393 kg	231,965 kg	248,337 kg	104,273 kg	181,975 kg	127,383 kg	203,425 kg
English	HCRBCC-HCRkt	HCRBCC-HRkt	HRBCC-HCRkt	HRBCC-HRkt	HCRkt-HCRBCC	HCRkt-HRBCC	HRkt-HCRBCC	HRkt-HRBCC
Orbiter Propellant	282,113 lb	211,618 lb	211,715 lb	174,189 lb	727,591 lb	547,638 lb	727,592 lb	536,615 lb
Orbiter Empty	50,054 lb	64,795 lb	45,438 lb	59,555 lb	96,424 lb	271,952 lb	96,424 lb	265,817 lb
Booster Propellant	1,230,452 lb	1,338,450 lb	919,611 lb	937,501 lb	900,257 lb	869,372 lb	728,524 lb	718,165 lb
Booster Empty	264,325 lb	310,857 lb	465,958 lb	487,934 lb	133,460 lb	129,235 lb	184,407 lb	182,657 lb
Payload	20,000 lb	20,000 lb	20,000 lb	20,000 lb	20,000 lb	20,000 lb	20,000 lb	20,000 lb
GTOM	1,846,943 lb	1,945,721 lb	1,662,722 lb	1,679,179 lb	1,877,732 lb	1,838,197 lb	1,756,947 lb	1,723,255 lb
Empty Mass	314,379 lb	375,653 lb	511,395 lb	547,489 lb	229,884 lb	401,186 lb	280,831 lb	448,474 lb



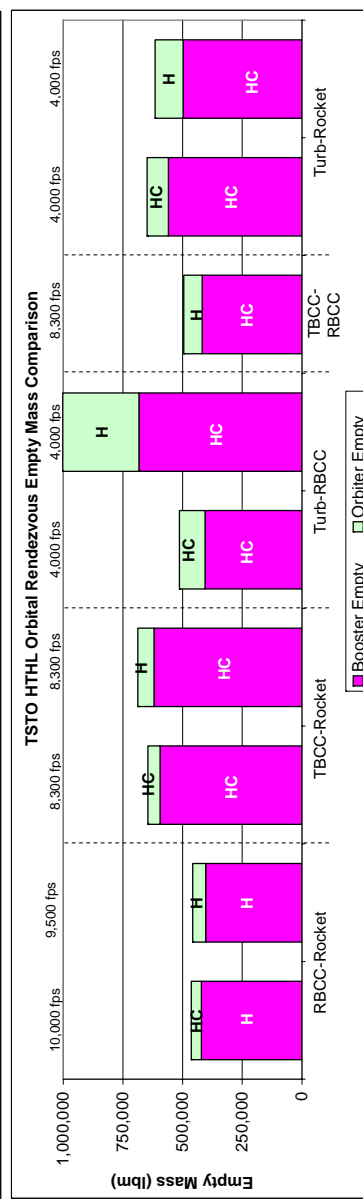
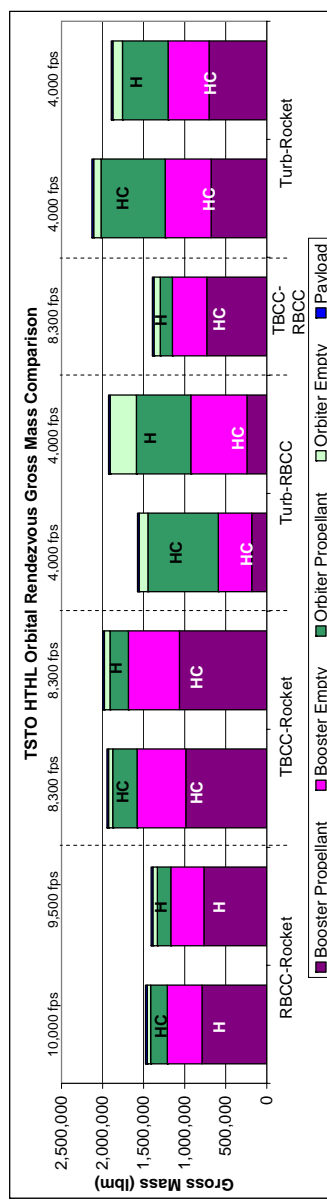
Orbital Rendezvous VTHL Models

	HCRBCC-HCRkt	HCRBCC-HRkt	HRBCC-HCRkt	HRBCC-HRkt	HCRkt-HCRBCC	HCRkt-HRBCC	HRkt-HCRBCC	HRkt-HRBCC
Design Mach #	M7/M20	M7/M20	M8/M20	M8/M20	M4/M7	M4/M12	M4/M7	M4/M12
Staging Velocity	8,300 fps	8,300 fps	10,000 fps	9,500 fps	4,000 fps	4,000 fps	4,000 fps	4,000 fps
Metric (SI)	HCRBCC-HCRkt	HCRBCC-HRkt	HRBCC-HCRkt	HRBCC-HRkt	HCRkt-HCRBCC	HCRkt-HRBCC	HRkt-HCRBCC	HRkt-HRBCC
Orbiter Wetted	656.65 m ²	890.11 m ²	622.52 m ²	825.78 m ²	1,073.45 m ²	3,040.92 m ²	1,073.44 m ²	2,985.35 m ²
Orbiter Active	13.11 m ²	12.78 m ²	10.32 m ²	10.94 m ²	116.18 m ²	367.3 m ²	116.18 m ²	360.92 m ²
Booster Wetted	1,799.02 m ²	2,023.91 m ²	3,969.01 m ²	4,033.89 m ²	1,135.41 m ²	1,082.58 m ²	1,841.86 m ²	1,842.60 m ²
Booster Active	137.25 m ²	142.04 m ²	272.73 m ²	272.13 m ²	50.75 m ²	49.61 m ²	54.71 m ²	53.66 m ²
Wetted Area	2,456 m ²	2,914 m ²	4,592 m ²	4,860 m ²	2,209 m ²	4,124 m ²	2,915 m ²	4,828 m ²
Active Area	150 m ²	155 m ²	283 m ²	283 m ²	167 m ²	417 m ²	171 m ²	415 m ²
English	HCRBCC-HCRkt	HCRBCC-HRkt	HRBCC-HCRkt	HRBCC-HRkt	HCRkt-HCRBCC	HCRkt-HRBCC	HRkt-HCRBCC	HRkt-HRBCC
Orbiter Wetted	7,068 ft ²	9,581 ft ²	6,701 ft ²	8,889 ft ²	11,555 ft ²	32,733 ft ²	11,555 ft ²	32,135 ft ²
Orbiter Active	141 ft ²	138 ft ²	111 ft ²	118 ft ²	1,251 ft ²	3,954 ft ²	1,251 ft ²	3,885 ft ²
Booster Wetted	19,365 ft ²	21,786 ft ²	42,723 ft ²	43,422 ft ²	12,222 ft ²	11,653 ft ²	19,826 ft ²	19,834 ft ²
Booster Active	1,477 ft ²	1,529 ft ²	2,936 ft ²	2,929 ft ²	546 ft ²	534 ft ²	589 ft ²	578 ft ²
Wetted Area	26,433 ft ²	31,367 ft ²	49,424 ft ²	52,311 ft ²	23,777 ft ²	44,386 ft ²	31,381 ft ²	51,969 ft ²
Active Area	1,619 ft ²	1,667 ft ²	3,047 ft ²	3,047 ft ²	1,797 ft ²	4,488 ft ²	1,840 ft ²	4,463 ft ²



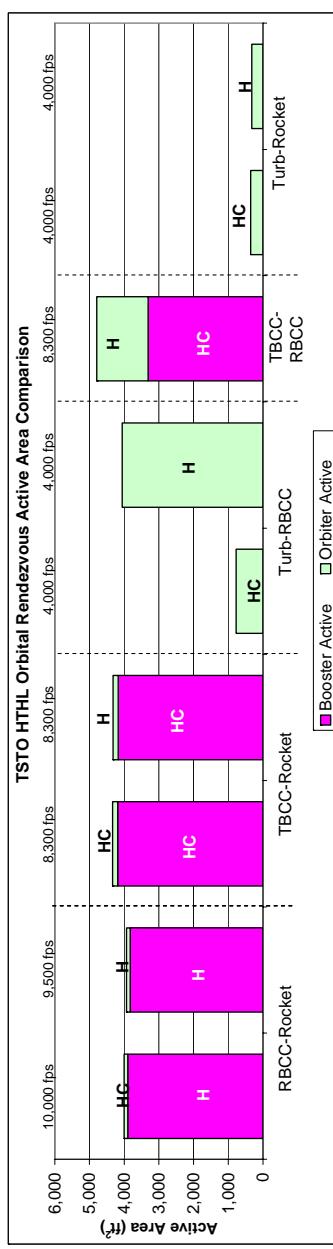
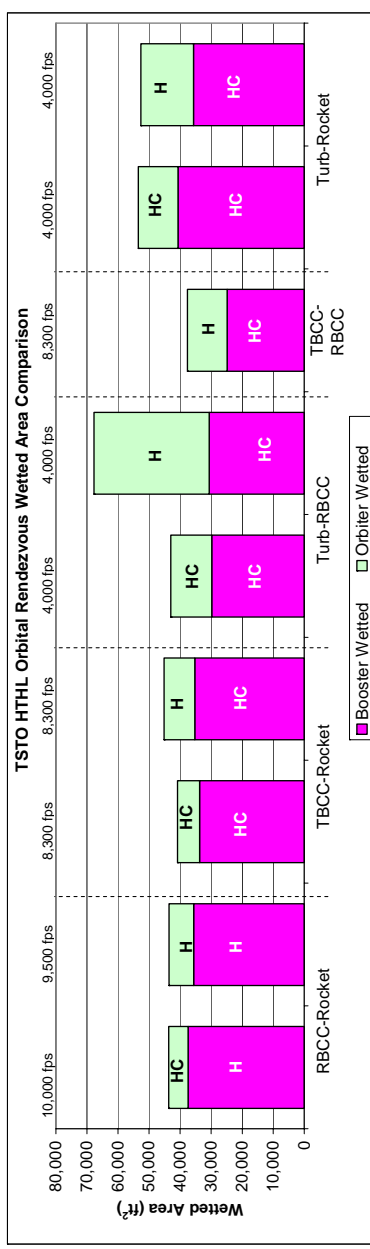
Orbital Rendezvous HTHL Models

Design Mach # Staging Velocity	HRBCC-HCRkt M8/M20 10,000 fps	HRBCC-HRkt M8/M20 9,500 fps	HCTBCC-HCRkt M7/M20 8,300 fps	HCTBCC-HRkt M7/M20 8,300 fps	HCTurb-HCRBCC M4/M7 4,000 fps	HCTurb-HRBCC M4/M12 4,000 fps	HCTurb-HCRkt M4/M20 4,000 fps	HCTurb-HRkt M4/M20 4,000 fps
Metric (SI)	HRBCC-HCRkt M8/M20 10,000 fps	HRBCC-HRkt M8/M20 9,500 fps	HCTBCC-HCRkt M7/M20 8,300 fps	HCTBCC-HRkt M7/M20 8,300 fps	HCTurb-HCRBCC M4/M7 4,000 fps	HCTurb-HRBCC M4/M12 4,000 fps	HCTurb-HCRkt M4/M20 4,000 fps	HCTurb-HRkt M4/M20 4,000 fps
Orbiter Propellant	92,004.52 kg	74,208.37 kg	134,010.96 kg	101,575.78 kg	389,289.99 kg	300,095.04 kg	353,717.46 kg	252,153.29 kg
Orbiter Empty	19,310.64 kg	24,724.96 kg	22,947.07 kg	30,459.84 kg	48,329.55 kg	144,500.23 kg	40,625.10 kg	53,269.71 kg
Booster Propellant	358,250.30 kg	347,563.63 kg	447,064.46 kg	482,827.36 kg	63,033.37 kg	110,161.79 kg	307,991.14 kg	319,211.46 kg
Booster Empty	191,018.37 kg	182,725.02 kg	269,525.99 kg	281,250.30 kg	184,196.27 kg	309,660.85 kg	253,601.08 kg	225,560.40 kg
Payload	9,071.85 kg	9,071.85 kg	9,071.85 kg	9,071.85 kg	9,071.85 kg	9,071.85 kg	9,071.85 kg	9,071.85 kg
GTO	669,656 kg	638,314 kg	882,620 kg	905,565 kg	713,921 kg	873,494 kg	985,007 kg	869,267 kg
Empty Mass	210,329 kg	207,450 kg	292,473 kg	311,710 kg	232,526 kg	454,161 kg	294,226 kg	278,830 kg
English	HRBCC-HCRkt M8/M20 10,000 fps	HRBCC-HRkt M8/M20 9,500 fps	HCTBCC-HCRkt M7/M20 8,300 fps	HCTBCC-HRkt M7/M20 8,300 fps	HCTurb-HCRBCC M4/M7 4,000 fps	HCTurb-HRBCC M4/M12 4,000 fps	HCTurb-HCRkt M4/M20 4,000 fps	HCTurb-HRkt M4/M20 4,000 fps
Orbiter Propellant	202,835 lb	163,601 lb	295,444 lb	224,818 lb	858,238 lb	661,605 lb	779,814 lb	555,903 lb
Orbiter Empty	42,573 lb	54,509 lb	50,590 lb	67,150 lb	106,548 lb	318,568 lb	89,563 lb	117,440 lb
Booster Propellant	789,807 lb	766,291 lb	985,608 lb	1,064,453 lb	183,057 lb	242,865 lb	679,004 lb	703,741 lb
Booster Empty	421,123 lb	402,840 lb	594,203 lb	620,052 lb	406,083 lb	682,685 lb	417,494 lb	559,095 lb
Payload	20,000 lb	20,000 lb	20,000 lb	20,000 lb	20,000 lb	20,000 lb	20,000 lb	20,000 lb
GTO	1,476,338 lb	1,407,241 lb	1,945,845 lb	1,996,474 lb	1,573,926 lb	1,925,724 lb	2,127,475 lb	1,894,359 lb
Empty Mass	463,666 lb	457,349 lb	644,793 lb	687,202 lb	512,632 lb	1,001,254 lb	648,658 lb	614,715 lb



Orbital Rendezvous HTHL Models

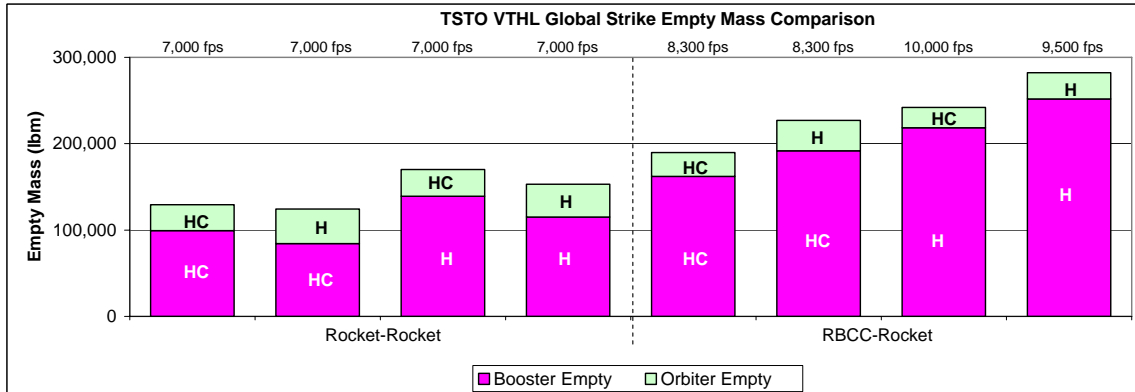
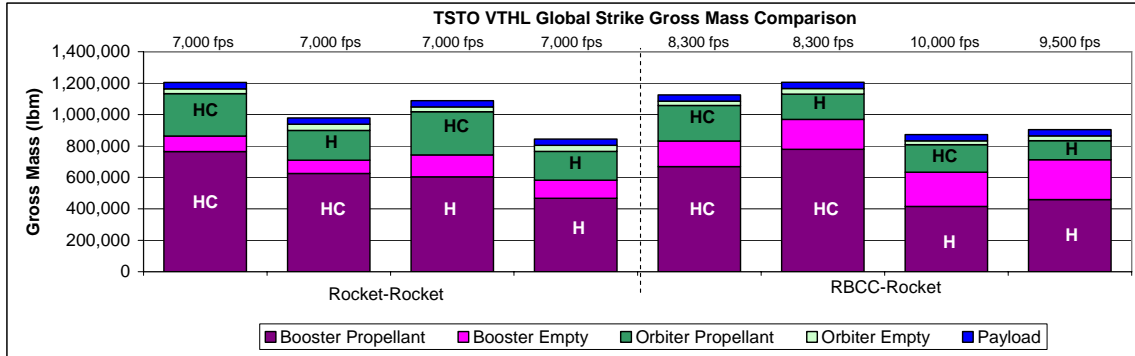
Design Mach # Staging Velocity	HRBCC-HCRkt M8/M20 10,000 fps	HRBCC-HRkt M8/M20 9,500 fps	HCTBCC-HCRkt M7/M20 8,300 fps	HCTBCC-HCRkt M7/M20 8,300 fps	HCTurb-HCRBCC M4/M7 4,000 fps	HCTurb-HRBC M4/M12 4,000 fps	HCTurb-HCRkt M4/M20 4,000 fps
Metric (SI)	HRBCC-HCRkt M8/M20 10,000 fps	HRBCC-HRkt M8/M20 9,500 fps	HCTBCC-HCRkt M7/M20 8,300 fps	HCTBCC-HCRkt M7/M20 8,300 fps	HCTurb-HCRBCC M4/M7 4,000 fps	HCTurb-HRBC M4/M12 4,000 fps	HCTurb-HCRkt M4/M20 4,000 fps
Orbiter Wetted	571.86 m ²	733.67 m ²	660.24 m ²	919.2 m ²	1,226.39 m ²	3,443.32 m ²	1,187.15 m ²
Orbiter Active	9.88 m ²	10.27 m ²	13.63 m ²	13.45 m ²	71.96 m ²	376.97 m ²	33.1 m ²
Booster Wetted	3,480.51 m ²	3,313.02 m ²	3,132.92 m ²	3,277.01 m ²	2,770.00 m ²	2,844.19 m ²	3,778.94 m ²
Booster Active	362.11 m ²	355.44 m ²	389.04 m ²	387.92 m ²	0 m ²	0 m ²	0 m ²
Wetted Area	4,052 m ²	4,047 m ²	3,793 m ²	4,196 m ²	3,996 m ²	6,288 m ²	4,963 m ²
Active Area	372 m ²	366 m ²	403 m ²	401 m ²	72 m ²	377 m ²	33 m ²
English	HRBCC-HCRkt M8/M20 10,000 fps	HRBCC-HRkt M8/M20 9,500 fps	HCTBCC-HCRkt M7/M20 8,300 fps	HCTBCC-HCRkt M7/M20 8,300 fps	HCTurb-HCRBCC M4/M7 4,000 fps	HCTurb-HRBC M4/M12 4,000 fps	HCTurb-HCRkt M4/M20 4,000 fps
Orbiter Wetted	6,156 ft ²	7,897 ft ²	7,107 ft ²	9,895 ft ²	13,201 ft ²	37,065 ft ²	12,750 ft ²
Orbiter Active	108 ft ²	111 ft ²	147 ft ²	145 ft ²	775 ft ²	4,058 ft ²	356 ft ²
Booster Wetted	37,465 ft ²	35,662 ft ²	33,724 ft ²	35,275 ft ²	29,817 ft ²	30,616 ft ²	40,678 ft ²
Booster Active	3,898 ft ²	3,826 ft ²	4,188 ft ²	4,176 ft ²	0 ft ²	0 ft ²	0 ft ²
Wetted Area	43,621 ft ²	43,560 ft ²	40,831 ft ²	45,169 ft ²	43,018 ft ²	67,680 ft ²	53,428 ft ²
Active Area	4,004 ft ²	3,937 ft ²	4,334 ft ²	4,320 ft ²	775 ft ²	4,058 ft ²	356 ft ²



Appendix J. Global Strike Results

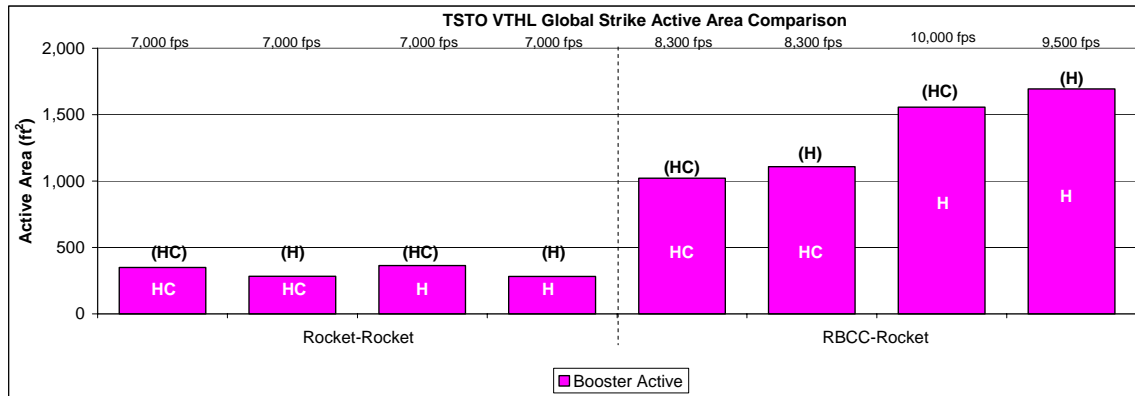
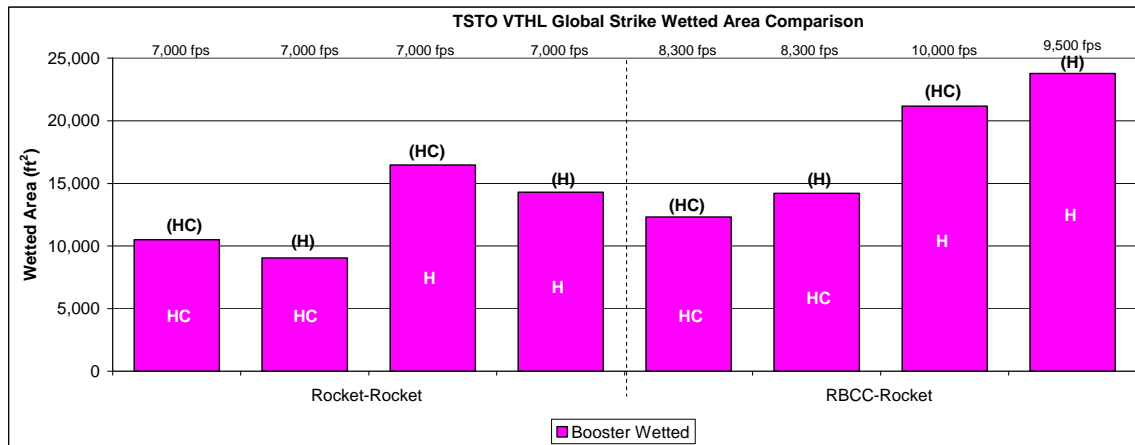
Global Strike VTHL Models

	HCRkt-HCRkt	HCRkt-HRkt	HRkt-HCRkt	HRkt-HRkt	HCRBCC-HCRkt	HCRBCC-HRkt	HRBCC-HCRkt	HRBCC-HRkt
Design Mach #	M7/M20	M7/M20	M7/M20	M7/M20	M7/M20	M7/M20	M8/M20	M8/M20
Staging Velocity	7,000 fps	7,000 fps	7,000 fps	7,000 fps	8,300 fps	8,300 fps	10,000 fps	9,500 fps
Metric (SI)	HCRkt-HCRkt	HCRkt-HRkt	HRkt-HCRkt	HRkt-HRkt	HCRBCC-HCRkt	HCRBCC-HRkt	HRBCC-HCRkt	HRBCC-HRkt
Orbiter Propellant	122,384.00 kg	85,665.91 kg	124,292.12 kg	83,353.41 kg	102,687.84 kg	72,403.55 kg	79,265.49 kg	55,400.55 kg
Orbiter Empty	13,622.22 kg	18,165.26 kg	14,091.13 kg	17,229.21 kg	12,481.02 kg	15,988.08 kg	10,726.73 kg	13,773.25 kg
Booster Propellant	346,887.27 kg	283,853.03 kg	274,135.42 kg	211,997.73 kg	303,586.32 kg	353,197.77 kg	188,566.59 kg	208,753.65 kg
Booster Empty	45,062.01 kg	38,233.85 kg	63,087.59 kg	52,180.26 kg	73,523.31 kg	86,989.33 kg	99,031.08 kg	114,232.51 kg
Payload	18,143.70 kg	18,143.70 kg	18,143.70 kg	18,143.70 kg	18,143.70 kg	18,143.70 kg	18,143.70 kg	18,143.70 kg
GTOM	546,099 kg	444,062 kg	493,750 kg	382,904 kg	510,422 kg	546,722 kg	395,734 kg	410,304 kg
Empty Mass	58,684 kg	56,399 kg	77,179 kg	69,409 kg	86,004 kg	102,977 kg	109,758 kg	128,006 kg
English	HCRkt-HCRkt	HCRkt-HRkt	HRkt-HCRkt	HRkt-HRkt	HCRBCC-HCRkt	HCRBCC-HRkt	HRBCC-HCRkt	HRBCC-HRkt
Orbiter Propellant	269,811 lb	188,861 lb	274,017 lb	183,763 lb	226,388 lb	159,623 lb	174,750 lb	122,137 lb
Orbiter Empty	30,032 lb	40,048 lb	31,066 lb	37,984 lb	27,516 lb	35,248 lb	23,648 lb	30,365 lb
Booster Propellant	764,756 lb	625,789 lb	604,365 lb	467,375 lb	669,293 lb	778,668 lb	415,718 lb	460,223 lb
Booster Empty	99,345 lb	84,291 lb	139,084 lb	115,038 lb	162,091 lb	191,779 lb	218,326 lb	251,840 lb
Payload	40,000 lb	40,000 lb	40,000 lb	40,000 lb	40,000 lb	40,000 lb	40,000 lb	40,000 lb
GTOM	1,203,943 lb	978,989 lb	1,088,532 lb	844,160 lb	1,125,288 lb	1,205,317 lb	872,443 lb	904,565 lb
Empty Mass	129,377 lb	124,339 lb	170,150 lb	153,022 lb	189,607 lb	227,026 lb	241,975 lb	282,204 lb



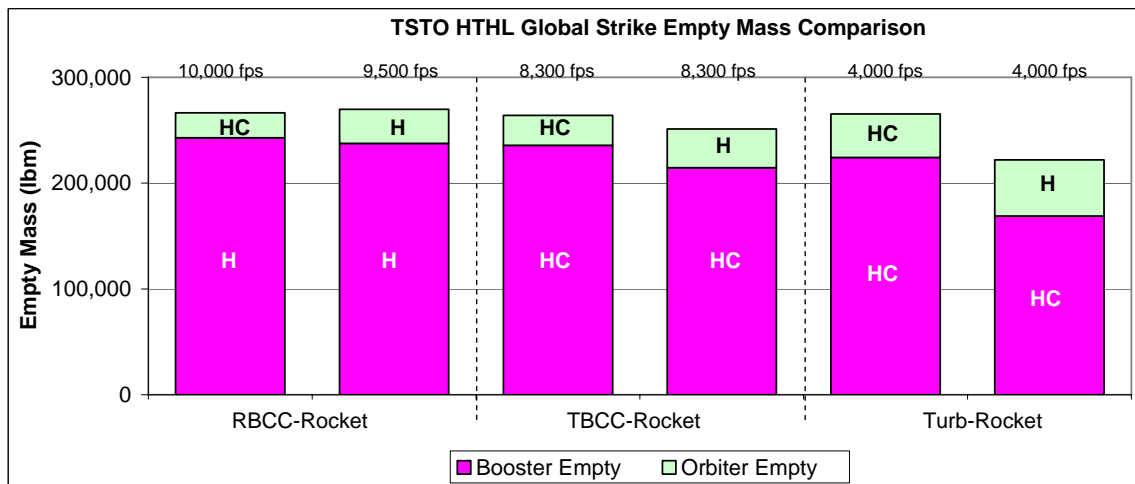
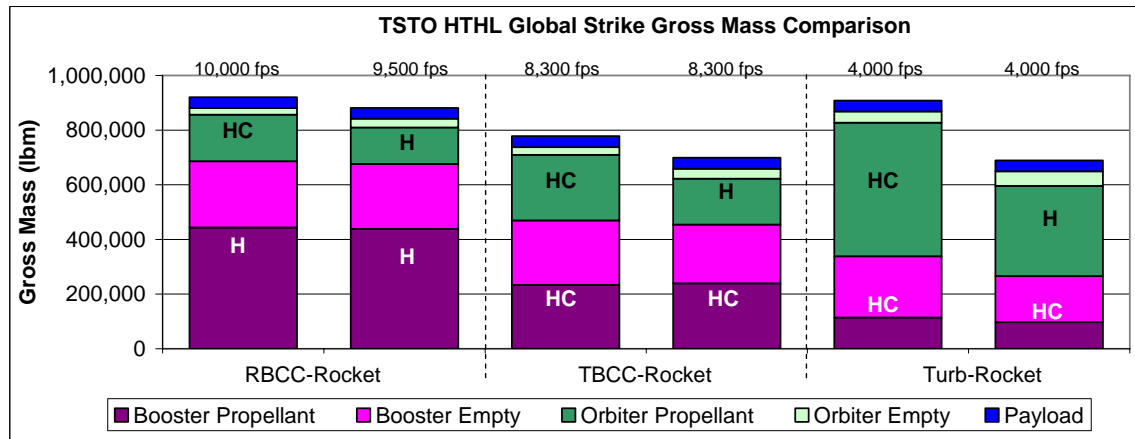
Global Strike VTHL Models

	HCRkt-HCRkt	HCRkt-HRkt	HRkt-HCRkt	HRkt-HRkt	HCRBCC-HCRkt	HCRBCC-HRkt	HRBCC-HCRkt	HRBCC-HRkt
Design Mach #	M7/M20	M7/M20	M7/M20	M7/M20	M7/M20	M7/M20	M8/M20	M8/M20
Staging Velocity	7,000 fps	7,000 fps	7,000 fps	7,000 fps	8,300 fps	8,300 fps	10,000 fps	9,500 fps
Metric (SI)	HCRkt-HCRkt	HCRkt-HRkt	HRkt-HCRkt	HRkt-HRkt	HCRBCC-HCRkt	HCRBCC-HRkt	HRBCC-HCRkt	HRBCC-HRkt
Orbiter Wetted	479.07 m ²	669.94 m ²	483.67 m ²	657.86 m ²	467.46 m ²	623.16 m ²	414.47 m ²	552.98 m ²
Orbiter Active	12.65 m ²	11.6 m ²	12.85 m ²	11.29 m ²	10.94 m ²	10.13 m ²	8.88 m ²	8.3 m ²
Booster Wetted	976.02 m ²	840.16 m ²	1,530.09 m ²	1,329.26 m ²	1,144.95 m ²	1,320.50 m ²	1,967.73 m ²	2,209.61 m ²
Booster Active	32.43 m ²	26.39 m ²	33.82 m ²	26.25 m ²	94.88 m ²	102.96 m ²	144.64 m ²	157.39 m ²
Wetted Area	1,455 m ²	1,510 m ²	2,014 m ²	1,987 m ²	1,612 m ²	1,944 m ²	2,382 m ²	2,763 m ²
Active Area	45 m ²	38 m ²	47 m ²	38 m ²	106 m ²	113 m ²	154 m ²	166 m ²
English	HCRkt-HCRkt	HCRkt-HRkt	HRkt-HCRkt	HCRBCC-HCRkt	HCRBCC-HRkt	HRBCC-HRkt	HCRkt-HCRBCC	HCRkt-HRBCC
Orbiter Wetted	5,157 ft ²	7,211 ft ²	5,206 ft ²	7,081 ft ²	5,032 ft ²	6,708 ft ²	4,461 ft ²	5,952 ft ²
Orbiter Active	136 ft ²	125 ft ²	138 ft ²	122 ft ²	118 ft ²	109 ft ²	96 ft ²	89 ft ²
Booster Wetted	10,506 ft ²	9,044 ft ²	16,470 ft ²	14,309 ft ²	12,325 ft ²	14,214 ft ²	21,181 ft ²	23,785 ft ²
Booster Active	349 ft ²	284 ft ²	364 lb	283 ft ²	1,021 ft ²	1,108 ft ²	1,557 ft ²	1,694 ft ²
Wetted Area	15,663 ft ²	16,255 ft ²	21,677 ft ²	21,390 ft ²	17,356 ft ²	20,922 ft ²	25,643 ft ²	29,737 ft ²
Active Area	485 ft ²	409 ft ²	502 ft ²	404 ft ²	1,139 ft ²	1,217 ft ²	1,653 ft ²	1,784 ft ²



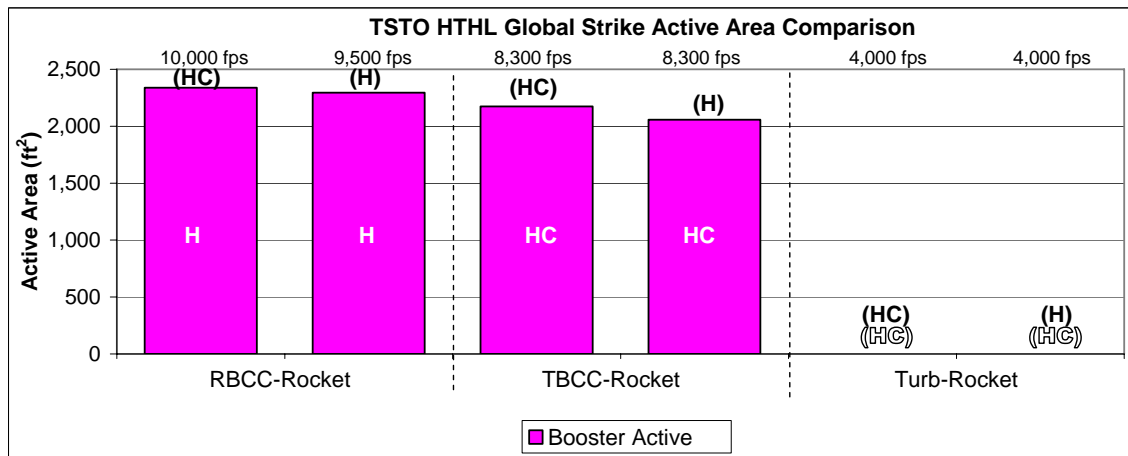
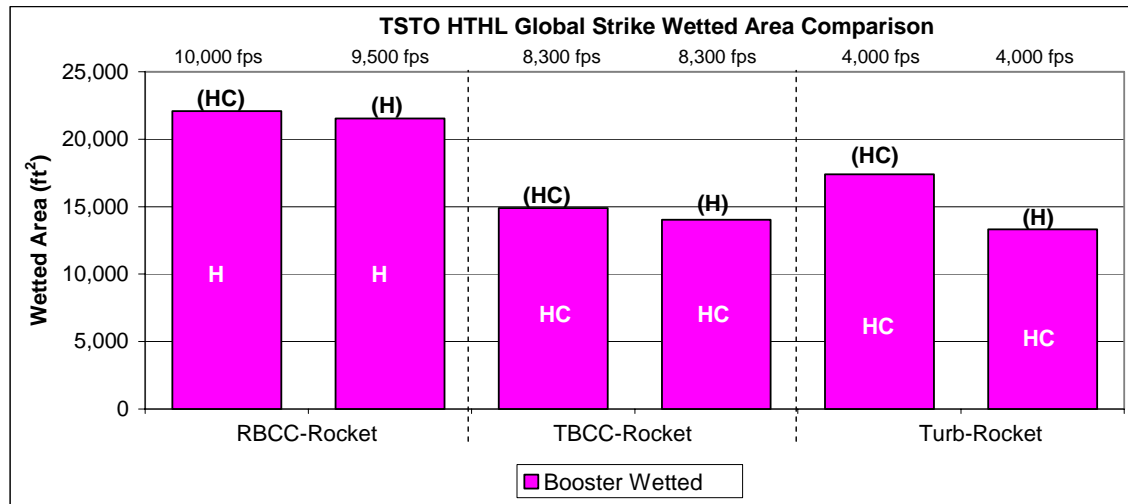
Strike HTHL Models

	HRBCC-HCRkt	HRBCC-HRkt	HCTBCC-HCRkt	HCTBCC-HRkt	HCTurb-HCRkt	HCTurb-HRkt
Design Mach #	M8/M20	M8/M20	M7/M20	M7/M20	M4/M20	M4/M20
Staging Velocity	10,000 fps	9,500 fps	8,300 fps	8,300 fps	4,000 fps	4,000 fps
Metric (SI)	HRBCC-HCRkt	HRBCC-HRkt	HCTBCC-HCRkt	HCTBCC-HRkt	HCTurb-HCRkt	HCTurb-HRkt
Orbiter Propellant	77,358.16 kg	60,487.39 kg	108,740.53 kg	76,367.30 kg	221,720.64 kg	149,847.91 kg
Orbiter Empty	10,724.07 kg	14,576.59 kg	12,882.85 kg	16,558.34 kg	18,608.45 kg	23,982.40 kg
Booster Propellant	200,995.34 kg	198,928.89 kg	106,023.03 kg	108,472.79 kg	51,723.28 kg	43,911.75 kg
Booster Empty	110,147.30 kg	107,761.16 kg	106,958.30 kg	97,372.23 kg	101,721.43 kg	76,688.69 kg
Payload	18,143.70 kg	18,143.70 kg	18,143.70 kg	18,143.70 kg	18,143.70 kg	18,143.70 kg
GTOM	417,369 kg	399,898 kg	352,748 kg	316,914 kg	411,918 kg	312,574 kg
Empty Mass	120,871 kg	122,338 kg	119,841 kg	113,931 kg	120,330 kg	100,671 kg
English	HRBCC-HCRkt	HRBCC-HRkt	HCTBCC-HCRkt	HCTBCC-HRkt	HCTurb-HCRkt	HCTurb-HRkt
Orbiter Propellant	170,546 lb	133,352 lb	239,732 lb	168,361 lb	488,810 lb	330,358 lb
Orbiter Empty	23,643 lb	32,136 lb	28,402 lb	36,505 lb	41,025 lb	52,872 lb
Booster Propellant	443,119 lb	438,563 lb	233,741 lb	239,142 lb	114,030 lb	96,809 lb
Booster Empty	242,833 lb	237,573 lb	235,803 lb	214,669 lb	224,257 lb	169,070 lb
Payload	40,000 lb	40,000 lb	40,000 lb	40,000 lb	40,000 lb	40,000 lb
GTOM	920,140 lb	881,624 lb	777,677 lb	698,677 lb	908,123 lb	689,109 lb
Empty Mass	266,476 lb	269,709 lb	264,205 lb	251,174 lb	265,282 lb	221,942 lb



Global Strike HTHL Models

	HRBCC-HCRkt	HRBCC-HRkt	HCTBCC-HCRkt	HCTBCC-HRkt	HCTurb-HCRkt	HCTurb-HRkt
Design Mach #	M8/M20	M8/M20	M7/M20	M7/M20	M4/M20	M4/M20
Staging Velocity	10,000 fps	9,500 fps	8,300 fps	8,300 fps	4,000 fps	4,000 fps
Metric (SI)	HRBCC-HCRkt	HRBCC-HRkt	HCTBCC-HCRkt	HCTBCC-HRkt	HCTurb-HCRkt	HCTurb-HRkt
Orbiter Wetted	407.41 m ²	573.58 m ²	476.29 m ²	647.8 m ²	654.39 m ²	918.73 m ²
Orbiter Active	8.72 m ²	8.86 m ²	11.47 m ²	10.56 m ²	21.21 m ²	18.25 m ²
Booster Wetted	2,051.62 m ²	2,000.41 m ²	1,383.81 m ²	1,302.64 m ²	1,616.29 m ²	1237.38 m ²
Booster Active	217.31 m ²	213.26 m ²	201.92 m ²	191.21 m ²	0 m ²	0 m ²
Wetted Area	2,459 m ²	2,574 m ²	1,860 m ²	1,950 m ²	2,271 m ²	2,156 m ²
Active Area	226 m ²	222 m ²	213 m ²	202 m ²	21 m ²	18 m ²
English	HRBCC-HCRkt	HRBCC-HRkt	HCTBCC-HCRkt	HCTBCC-HRkt	HCTurb-HCRkt	HCTurb-HRkt
Orbiter Wetted	4,385 ft ²	6,174 ft ²	5,127 ft ²	6,973 ft ²	7,044 ft ²	9,889 ft ²
Orbiter Active	94 ft ²	95 ft ²	123 ft ²	114 ft ²	228 ft ²	196 ft ²
Booster Wetted	22,084 ft ²	21,533 ft ²	14,896 ft ²	14,022 ft ²	17,398 ft ²	13,319 ft ²
Booster Active	2,339 ft ²	2,296 ft ²	2,174 ft ²	2,058 ft ²	0 ft ²	0 ft ²
Wetted Area	26,470 ft ²	27,707 ft ²	20,023 ft ²	20,995 ft ²	24,442 ft ²	23,209 ft ²
Active Area	2,433 ft ²	2,391 ft ²	2,297 ft ²	2,172 ft ²	228 ft ²	196 ft ²



Bibliography

1. Barrère, Marcel, André Jaumotte, Baudouin Fraeijs de Veubeke, and Jean Vandekerckhove. *Rocket Propulsion*. Amsterdam: Elsevier Publishing Company, 1960.
2. Bertin, John J. *Aerodynamics for Engineers* (4th Edition). Upper Saddle River, NJ: Prentice-Hall, Inc., 2002.
3. Bertin, John J, and Russell M. Cummings. "Fifty Years of Hypersonics: Where We've Been, Where We're Going." *Progress in Aerospace Sciences*, Vol 39: 511-536 (2003).
4. Bilardo, V. J., F. M. Curran, J. L. Hunt, N. T. Lovell, G. Maggio, A. W. Wilhite, and L.E. McKinney. "The Benefits of Hypersonic Airbreathing Launch Systems for Access to Space." AIAA 2003-5265, 39th AIAA/ASME/SAE/ASEE Joint Propulsion Conference and Exhibit, Huntsville, AL, 20-23 July 2003.
5. Bowcutt, Kevin, Mark Gonda, Steve Hollowell, and Ted Ralston. "Performance, Operational and Economic Drivers of Reusable Launch Vehicles." AIAA 2002-3901, 38th AIAA/ASME/SAE/ASEE Joint Propulsion Conference and Exhibit, Indianapolis, IN, July 2002.
6. Bradford, John E., A. Charania, J. Wallace, and Dean R. Eklund. "*Quicksat*: A Two-Stage to Orbit Reusable Launch Vehicle Utilizing Air-Breathing Propulsion for Responsive Space Access." AIAA 2004-5950, Space 2004 Conference and Exhibit, San Diego, CA, September 2004.
7. Brock, Marc A. *Performance Study of Two-Stage-to-Orbit Reusable Launch Vehicle Propulsion Alternatives*. MS Thesis, AFIT/GSS/ENY/04-M02. Graduate School of Engineering and Management, Air Force Institute of Technology (AU), Wright-Patterson AFB, OH, March 2004.
8. Caldwell, Richard J. *Weight Analysis of Two-Stage-to-Orbit Reusable Launch Vehicles for Military Applications*. MS Thesis, AFIT/GA/ENY/05-M02. Graduate School of Engineering and Management, Air Force Institute of Technology (AU), Wright-Patterson AFB, OH, March 2005.
9. Chase, Ramon and Ming Tang. "The Quest for Single Stage Earth-to-Orbit: TAV, NASP, DC-X and X-33 Accomplishments, Deficiencies, and Why They Did Not Fly." AIAA 2002-5143, 11th AIAA/AAAF International Space Planes and Hypersonic Systems Technology Conference, Orleans, France, September 2002.

10. Clough, Joshua A., and Mark J. Lewis. "A Comparison of Turbine-Based Combined-Cycle Engine Flowpaths." AIAA 2003-6932, 12th International Space Planes and Hypersonic Systems and Technologies Conference, Norfolk, VA, 15-19 December 2003.
11. Crocker, Andrew M., Jeffery H. Cannon, and Dana G. Andrews. "A Comparison of Horizontal Takeoff RLVs for Next Generation Space Transportation." AIAA 2003-5037, 39th AIAA/ASME/SAE/ASEE Joint Propulsion Conference and Exhibit, Huntsville, AL, 20-23 July 2003.
12. Department of the Air Force. *Mission Need Statement for Operationally Responsive Spacelift*. AFSPC 001-01, HQ AFSPC/DRS, United States Air Force, 20 December 2001.
13. Dissel, Adam F., Ajay P. Kothari, V. Raghavan, and Mark J. Lewis. "Comparison of HTHL and VTHL Air-Breathing and Rocket Systems for Access to Space." AIAA 2004-3988, 40th AIAA/ASME/SAE/ASEE Joint Propulsion Conference and Exhibit, Fort Lauderdale, FL, 11-14 July 2004.
14. Dissel, Adam F. *Comparative System Analysis of Reusable Rocket and Air-breathing Launch Vehicles*. MS Thesis. Department of Aerospace Engineering, University of Maryland, College Park, MD, August 2005.
15. Eklund, Dean R. Aerospace Engineer, Air Force Research Laboratory, Propulsion Directorate, Aerospace Propulsion Division, Wright-Patterson AFB, OH. Personal Correspondence, Phone: 937-255-0632, E-mail: Dean.Eklund@wpafb.af.mil. June 2005-Dec 2005.
16. Fry, Ronald S. "A Century of Ramjet Propulsion Technology Evolution." *Journal of Propulsion and Power*, Vol. 20, No. 1: 27-58 (January-February 2004).
17. Hatekayama, S. J., Keith L. McIver, Jon D. Embler, William G. Gillard, and Lee Jackson. "Operability Sensitivities of Airbreathing and Rocket Propulsion for a Two-Stage-to-Orbit Space Operations Vehicle." AIAA 2002-3903, 38th AIAA/ASME/SAE/ASEE Joint Propulsion Conference and Exhibit, Indianapolis, IN, July 2002.
18. Heiser, William H. and David T. Pratt. *Hypersonic Airbreathing Propulsion*. Washington D.C., American Institute of Aeronautics and Astronautics, Inc., 1994.
19. Hill, Philip, and Carl Peterson. *Mechanics and Thermodynamics of Propulsion* (2nd Edition). New York: Addison-Wesley Publishing Company, 1992.

20. Hueter, Uwe. "Rocket-Based Combined Cycle Propulsion Technology for Access-to-Space Applications." AIAA 99-4925, 9th International Space Planes and Hypersonic Systems and Technologies Conference, Norfolk, VA, 1-5 November 1999.
21. Humble, Ronald W., Gary N. Henry, and Wiley J. Larson. *Space Propulsion Analysis and Design* (Revised). New York: McGraw-Hill Publishing Company, 1995.
22. *Hypersonic System Integrated Design Environment (HySIDE)*. Version 2.11, created using SIDE2000, version 4.0, CD-ROM. Computer Software. ASTROX Corporation, College Park, MD, 2004.
23. Isakowitz, Steven J., Joshua Hopkins, and Joseph P. Hopkins, Jr. *International Reference Guide to Space Launch Systems* (4th Edition). Reston, VA: American Institute of Aeronautics and Astronautics, 2004.
24. Kobayashi, Hiroaki, and Nobuhiro Tanatsugu. "Optimization Method on TSTO Spaceplane System Powered by Airbreather." AIAA 2001-3965, 37th AIAA/ASME/SAE/ASEE Joint Propulsion Conference and Exhibit, Salt Lake City, UT, 8-11 July 2001.
25. Kothari, Ajay P. President, ASTROX Corporation, College Park, MD. Personal Correspondence, Phone: 301-948-4646, E-mail: a.p.kothari@astrox.com. September 2005-January 2006.
26. Kothari, Ajay P., Christopher Tarpley, T.A. McLaughlin, Suresh Babu, and John W. Livingston. "Hypersonic Vehicle Design Using Inward Turning Flowfields." AIAA 96-2552, 32nd AIAA/ASME/SAE/ASME Joint Propulsion Conference, Lake Buena Vista, FL, 1-3 July 1996.
27. Lewis, Mark J. "Significance of Fuel Selection for Hypersonic Vehicle Range." *Journal of Propulsion and Power*, Vol. 17, No.6: 1214-1221 (November-December 2001).
28. Livingston, John W. Systems Design Engineer, Aeronautical Systems Center, Aerospace System Design and Analysis (ASC/XRE), Wright-Patterson AFB, OH. Personal interviews. Phone: 937-255-4550, E-mail: John.Livingston@wpafb.af.mil. October 2004-January 2005.
29. Livingston, John W. "Comparative Analysis of Rocket and Air-breathing Launch Vehicles." AIAA 2004-5948, Space 2004 Conference, San Diego, CA, 28-30 September 2004.
30. Marshall, André W., Ashwani K. Gupta, Thomas Lavelle, and Mark J. Lewis. "Critical Issues in TBCC Modeling." AIAA 2004-3827, 40th

AIAA/ASME/SAE/ASEE Joint Propulsion Conference and Exhibit, Fort Lauderdale, FL, 11-14 July 2004.

31. Miller, Jay. *The X-Planes, X-1 to X-29*. St. Croix, MN: Specialty Press Publishers and Wholesalers, Inc., 1983.
32. Moses, P. L., K. A. Bouchard, R. F. Vause, S. Z. Pinckney, S. M. Ferlemann, C. P. Leonard, L. W. Taylor III, J. S. Robinson, J. G. Martin, D. H. Petley, and J. L. Hunt. "An Airbreathing Launch Vehicle Design with Turbine-Based Low-Speed Propulsion and Dual mode Scramjet High-Speed Propulsion." AIAA 99-4948, 9th International Space Planes and Hypersonic Systems and Technologies Conference, Norfolk, VA, 1-5 November 1999.
33. Powell, O. A., J. T. Edwards, R. B. Norris, K. E. Numbers, and J. A. Pearce. "Development of Hydrocarbon-Fueled Scramjet Engines: The Hypersonic Technology (HyTech) Program." *Journal of Propulsion and Power*, Vol. 17, No.6: 1170-1176 (November-December 2001).
34. Raghavan, V. Research Engineer, ASTROX Corporation, College Park, MD. Personal Correspondence, Phone: 301-948-4646, E-mail: a.p.kothari@astrox.com. September 2005-January 2006.
35. Raymer, Daniel P. *Aircraft Design: A Conceptual Approach* (6th Printing). Reston, VA: American Institute of Aeronautics and Astronautics, 1999.
36. Rooney, Brendan D., and Alicia Hartong. "A Discrete-Event Simulation of Turnaround Time and Manpower of Military RLVs." AIAA 2004-6111, Space 2004 Conference, San Diego, CA, September 28-30, 2004.
37. Serway, Raymond A. *Physics for Scientists and Engineers* (4th edition). Philadelphia: Saunders College Publishing, 1996.
38. Snyder, Lynn E., and Daric W. Escher. "High Mach Turbine Engines for Access to Space Launch Systems." AIAA 2003-5036, 39th AIAA/ASME/SAE/ASEE Joint Propulsion Conference and Exhibit, Huntsville, AL, 20-23 July 2003.
39. Snyder, Lynn E., Daric W. Escher, Rich L. DeFrancesco, Jose L. Gutierrez, and David L. Buckwalter. "Turbine Based Combined Cycle (TBCC) Subsystem Integration." AIAA 2004-3649, 40th AIAA/ASME/SAE/ASEE Joint Propulsion Conference and Exhibit, Fort Lauderdale, FL, 11-14 July 2004.
40. United States Air Force Scientific Advisory Board. *Why and Whither Hypersonics Research in the U. S. Air Force*. SAB-TR-00-03, United States Air Force, December 2003.

41. Wiesel, William E. *Spaceflight Dynamics* (2nd edition). Boston, MA: Irwin/McGraw-Hill, 1997.
42. World Wide Web. http://grin.hq.nasa.gov/BROWSE/space-shuttle_1.html
43. World Wide Web. <http://www.aerospaceweb.org/question/performance/q0146.shtml>
44. World Wide Web. <http://www.af.mil/factsheets/factsheet.asp?id=113>
45. World Wide Web. <http://www.affordablespaceflight.com/nasa2.html>
46. World Wide Web. <http://www.astronautix.com/craft/dynasoar.htm>
47. World Wide Web. <http://www.astronautix.com/craft/tav.htm>
48. World Wide Web. <http://www.astronautix.com/lvs/x30.htm>
49. World Wide Web. http://www.esa.int/SPECIALS/Launchers_Europe_s_Spaceport/ASEVFOI4HNC_0.html
50. World Wide Web. <http://www.fas.org/irp/mystery/nasp.htm>
51. World Wide Web. <http://www.futron.com/pdf/FutronLaunchCostWP.pdf>
52. World Wide Web. <http://www.military-aerospace-technology.com/article.cfm?DocID=93>
53. World Wide Web. http://www.nasa.gov/audience/forstudents/5-8/features/F_HyperX_Greased_Lightning_5_8.html
54. World Wide Web. <http://www.nasa.gov/missions/research/x43-main.html>
55. World Wide Web. http://www.nasm.si.edu/research/aero/aircraft/lockheed_sr71.htm
56. World Wide Web. <http://www.pr.afrl.af.mil/mar/2005/jan2005.pdf>
57. World Wide Web. http://www.pratt-whitney.com/prod_space_rd180.asp
58. World Wide Web. <http://www.sea-launch.com/>

Vita

Capt Joseph M. Hank graduated with honors from Niceville Senior High School in Niceville, Florida in 1994. He entered undergraduate studies at the University of South Alabama in Mobile, Alabama. He graduated summa cum laude with a Bachelor of Science degree in May 1999, majoring in Mechanical Engineering and minoring in Aerospace Studies. He received his commission in the United States Air Force from AFROTC Operating Location 432A, now Detachment 013, at the University of South Alabama. His primary AFSC was 62E (Developmental Engineer), but he was temporarily assigned as 13S (Space and Missile Operations Officer) as part of the Operational Experience Exchange (OPEX) program.

Capt. Hank's first assignment was to Vandenberg AFB, California, as a student in Undergraduate Space and Missile Training, followed by Minuteman-III ICBM Initial Qualification Training. In May 2000, he was assigned to the 740th Missile Squadron, Minot AFB, North Dakota, where he served as a Deputy Missile Combat Crew Member. He upgraded to Missile Combat Crew Commander in October 2001. In May 2002, he transferred to the 91st Operations Support Squadron and became a Missile Combat Crew Instructor Commander. In March 2003, he became section chief of ICBM Training Scenarios, where he served until August 2004. In August 2004, he entered the Graduate School of Engineering and Management, Air Force Institute of Technology, WPAFB, Ohio. Upon graduation, he will be assigned to the Air Force Research Laboratory, Propulsion Directorate, Aerospace Propulsion Division, WPAFB, Ohio.

REPORT DOCUMENTATION PAGE				Form Approved OMB No. 074-0188	
<p>The public reporting burden for this collection of information is estimated to average 1 hour per response, including the time for reviewing instructions, searching existing data sources, gathering and maintaining the data needed, and completing and reviewing the collection of information. Send comments regarding this burden estimate or any other aspect of the collection of information, including suggestions for reducing this burden to Department of Defense, Washington Headquarters Services, Directorate for Information Operations and Reports (0704-0188), 1215 Jefferson Davis Highway, Suite 1204, Arlington, VA 22202-4302. Respondents should be aware that notwithstanding any other provision of law, no person shall be subject to a penalty for failing to comply with a collection of information if it does not display a currently valid OMB control number.</p> <p>PLEASE DO NOT RETURN YOUR FORM TO THE ABOVE ADDRESS.</p>					
1. REPORT DATE (DD-MM-YYYY) 23 Mar 2006		2. REPORT TYPE Master's Thesis		3. DATES COVERED (From – To) August 2004 – March 2006	
4. TITLE AND SUBTITLE Comparative Analysis of Two-Stage-to-Orbit Rocket and Airbreathing Reusable Launch Vehicles for Military Applications				5a. CONTRACT NUMBER	
				5b. GRANT NUMBER	
				5c. PROGRAM ELEMENT NUMBER	
6. AUTHOR(S) Hank, Joseph M., Captain, USAF				5d. PROJECT NUMBER	
				5e. TASK NUMBER	
				5f. WORK UNIT NUMBER	
7. PERFORMING ORGANIZATION NAMES(S) AND ADDRESS(S) Air Force Institute of Technology Graduate School of Engineering and Management (AFIT/EN) 2950 Hobson Way, Building 640 WPAFB OH 45433-8865				8. PERFORMING ORGANIZATION REPORT NUMBER AFIT/GAE/ENY/06-M12	
9. SPONSORING/MONITORING AGENCY NAME(S) AND ADDRESS(ES) AFRL/PRAT Attn: Dr. Dean Eklund 1950 5 th Street Building 18D, Room A-131 Wright-Patterson AFB, OH 45433-7765 DSN: 785- 0632				10. SPONSOR/MONITOR'S ACRONYM(S)	
				11. SPONSOR/MONITOR'S REPORT NUMBER(S)	
12. DISTRIBUTION/AVAILABILITY STATEMENT APPROVED FOR PUBLIC RELEASE; DISTRIBUTION UNLIMITED.					
13. SUPPLEMENTARY NOTES					
14. ABSTRACT <p>The Department of Defense (DoD) has identified operationally responsive, low-cost access to space as vital to maintaining U.S. military supremacy. Reusable Launch Vehicles (RLVs) will allow the U.S. to keep a technological advantage over our adversaries, and advances in airbreathing propulsion technology have made it feasible for use in space launch vehicles. This study considers two-stage-to-orbit (TSTO) RLV configurations, each using combinations of propulsion including pure rocket, pure turbine, rocket-based-combined-cycle (RBCC), and turbine-based-combined-cycle (TBCC) for the both stages. This study explores the advantages of airbreathing propulsion in those key areas when compared to a baseline configuration, using vehicle empty mass and vehicle wetted area as the primary figures of merit. Results show that a vehicle using airbreathing propulsion on the orbiter stage has a lower vehicle empty mass and wetted area than a pure rocket, and allows the RLV to gain the advantages of using airbreathing propulsion. The requirements used for this comparison are: 1) a payload module requirement of 20,000 pounds; 2) a 100x100 nautical mile, 28.5 lat. Easterly orbit and return; 3) use of hydrocarbon fuels (RP-1 and/or JP-7) and liquid hydrogen (LH₂); and 4) use of liquid oxygen and/or air as oxidizers. ASTROX Corporation's Hypersonic System Integrated Design Environment (HySIDE) code is used as the design tool throughout the study.</p>					
15. SUBJECT TERMS Reusable Launch Vehicles, Hypersonic Vehicles, Rocket Propulsion, Jet propulsion, Space Propulsion, Space Launch, Advanced Propulsion Systems					
16. SECURITY CLASSIFICATION OF:			17. LIMITATION OF ABSTRACT UU	18. NUMBER OF PAGES 254	19a. NAME OF RESPONSIBLE PERSON Dr. Milton Franke
a. REPORT U	b. ABSTRACT U	c. THIS PAGE U			19b. TELEPHONE NUMBER (Include area code) (937) 255-6565, ext 4720 E-mail: Milton.Franke@afit.edu